VIRTUAL PLANTS: MODELING PLANT ARCHITECTURE IN CHANGING ENVIRONMENTS

EDITED BY : Katrin Kahlen and Hartmut Stützel

frontiers Research Topics

About Frontiers

Frontiers is more than just an open-access publisher of scholarly articles: it is a pioneering approach to the world of academia, radically improving the way scholarly research is managed. The grand vision of Frontiers is a world where all people have an equal opportunity to seek, share and generate knowledge. Frontiers provides immediate and permanent online open access to all its publications, but this alone is not enough to realize our grand goals.

Frontiers Journal Series

The Frontiers Journal Series is a multi-tier and interdisciplinary set of open-access, online journals, promising a paradigm shift from the current review, selection and dissemination processes in academic publishing. All Frontiers journals are driven by researchers for researchers; therefore, they constitute a service to the scholarly community. At the same time, the Frontiers Journal Series operates on a revolutionary invention, the tiered publishing system, initially addressing specific communities of scholars, and gradually climbing up to broader public understanding, thus serving the interests of the lay society, too.

Dedication to Quality

Each Frontiers article is a landmark of the highest quality, thanks to genuinely collaborative interactions between authors and review editors, who include some of the world's best academicians. Research must be certified by peers before entering a stream of knowledge that may eventually reach the public - and shape society; therefore, Frontiers only applies the most rigorous and unbiased reviews.

Frontiers revolutionizes research publishing by freely delivering the most outstanding research, evaluated with no bias from both the academic and social point of view.

By applying the most advanced information technologies, Frontiers is catapulting scholarly publishing into a new generation.

What are Frontiers Research Topics?

Frontiers Research Topics are very popular trademarks of the Frontiers Journals Series: they are collections of at least ten articles, all centered on a particular subject. With their unique mix of varied contributions from Original Research to Review Articles, Frontiers Research Topics unify the most influential researchers, the latest key findings and historical advances in a hot research area! Find out more on how to host your own Frontiers Research Topic or contribute to one as an author by contacting the Frontiers Editorial Office: **researchtopics@frontiersin.org**

VIRTUAL PLANTS: MODELING PLANT ARCHITECTURE IN CHANGING ENVIRONMENTS

Topic Editors:
Katrin Kahlen, Hochschule Geisenheim University, Germany
Hartmut Stützel, Leibniz Universität Hannover, Germany

Insight view of a greenhouse grown cucumber canppy
Katrin Kahlen took the picture in summer 2006 in a greenhouse at Leibniz Universität Hannover.

Plant architecture is a major determinant of the resource use efficiency of crops. The architecture of a plant shows ontogenetic structural changes which are modified by multiple environmental factors: Plant canopies are exposed to natural fluctuations in light quantity and the dynamically changing canopy architecture induces local variations in light quality. Changing temperature conditions or water availability during growth additionally affect plant architecture and thus crop productivity, because plants have various options to adapt their architecture to the available resources. Meeting the challenge of ensuring food security we must understand the plant's mechanisms for integrating and responding to an orchestra of environmental factors.

'Virtual plants' describe plant architecture in silico. Virtual plants have the potential to help us understanding the complex feedback processes between canopy architecture, multiple environmental factors and crop productivity. As a research tool, they have become increasingly popular within the last decade due to their great power of realistically visualizing the plant's architecture. This Research Topic highlights current research carried out on modeling plant architecture in changing environments.

Table of Contents

Editorial: Virtual Plants: Modeling Plant Architecture in Changing Environments

Hartmut Stützel[1]* and Katrin Kahlen[2]

[1] Institute of Horticultural Production Systems, Leibniz Universität Hannover, Hannover, Germany, [2] Institute of Vegetable Crops, Hochschule Geisenheim University, Geisenheim, Germany

Editorial on the Research Topic

Virtual Plants: Modeling Plant Architecture in Changing Environments

There is increasing awareness that crop productivity is not only a function of the interaction between plants and their environment, but is also determined by the interplay between form and function. The need to better understand and even quantify this complex interaction has led to a new category of models of plant growth and development, often named virtual plants or functional-structural plant models (FSPM, Room et al., 1996; Prusinkiewicz, 2004; DeJong et al., 2011). In contrast to most traditional plant growth models, virtual plants explicitly describe the three-dimensional structure of plants.

This issue is essentially about new approaches to quantify, explain, predict and eventually manipulate the trilateral interaction between plant function, structure and environment. Renton in his opinion paper relates these factors to the first three of the Aristotelian "causes," his framework for explaining why things are as they are: function, Aristotle's "causa materialis," describes the change of matter through transport and transformation, structure, Aristotle's "causa formalis" the change in form, and the effects of the environment, his "causa efficientis." Renton adds Aristotle's fourth cause, the "causa finalis," asking the "why" question, fundamental in science, and sees FSPMs as heuristic tools in an evolutionary sense.

Central in this respect are **morphogenetic processes** on the organ level, like leaf expansion or internode elongation as presented in the paper of Demotes-Mainard et al. who analyze the inter-plant variation of a rose variety with respect to these processes. In cereals, the formation of side shoots, i.e., tillers, is an important mechanism to regulate stem and ear density, and senescence of individual tillers determines their productive phase. Evers and Vos review approaches to model tillering based on environmental cues or physiological conditions and show how architectural models can also serve to test hypotheses about the effects of signaling chemicals and substrate transport. The architecture of the vascular system of the vascular system determines water and solute transport. Hölttä et al. show in their model analysis that the Münch hypothesis explains phloem transport across organs and even over long distances in tall trees. Beyer et al. also leave the level of the individual organ and model canopy development based on local leaf density. Their simulations of crown growth dynamics demonstrate the inherent dynamic properties of self-organization and adaptation of the proposed framework of partial differential equations. In addition, Shapiro et al. provided insight on plant morphodynamics at the cellular level. Their computational framework can be used for simulations of plant tissue including cell growth and cell division.

Morphogenetic processes directly affect **light interception** at the organ and canopy level. Hofmann et al. show how a simple Monte Carlos-based model of radiation partitioning in vineyards

can be used together with a water balance as a component of a growth model to evaluate the risks of climate change to grape production. Light is also the driving force in interplant competition reviewed in the article of Ford. His review assesses the role of plant architecture in interplant competition for light by focusing on both, the dynamics of stands undergoing competitions and the single plant as competitor. He develops a theory for the effects of plant architecture on competition and highlights the role of functional-structural plant models for simulating interplant competition. De Visser et al. analyze the effects of different plant morphologies and light regimes on light interception and light use efficiency, giving an example of the application of an FSPM approach not only for systems understanding, but also for systems control. Buck-Sorlin and Delaire widen the picture and analyze the prospects of FSPM in horticulture, a section of agriculture with a wide spectrum of crops and production systems where manipulation of growth through changing plant morphology by training and pruning is common practice.

Models are by definition simplified representations of reality with simplicity and parsimony being guiding principles in modeling. Models of plant structure and functions are usually detailed and complex. As Renton puts it: "...the strength of FSPMs, their dynamic realism, is also their weakness, because it makes them relatively complex...". Indeed, a more systematic understanding of the relationships between increasing model complexity and scientific gain would be desirable.

AUTHOR CONTRIBUTIONS

The editorial for the topic "Virtual plants: Modeling plant architecture in changing environments" was jointly written by KK and HS.

REFERENCES

DeJong, T. M., Da Silva, D., Vos, J., and Escobar-Gutierrez, A. J. (2011). Using functional-structural plant models to study, understand and integrate plant development and ecophysiology. *Ann. Bot.* 108, 987–989. doi: 10.1093/aob/mcr257

Prusinkiewicz, P. (2004). Modeling plant growth and development. *Curr. Opin. Plant Biol.* 7, 79–81. doi: 10.1016/j.pbi.2003.11.007

Room, P., Hanan, J. S., and Prusinkiewicz, P. (1996). Virtual plants: new perspectives for ecologists, pathologists and agricultural scientists. *Trends Plant Sci.* 1, 33–36. doi: 10.1016/S1360-1385(96)80021-5

Aristotle and adding an evolutionary perspective to models of plant architecture in changing environments

Michael Renton *

School of Plant Biology, The University of Western Australia, Perth, WA, Australia
*Correspondence: michael.renton@uwa.edu.au

Why do plants grow the way that they do? According to Aristotle, there are four kinds of causes, or four fundamentally different ways of answering "why" questions such as this (Aristotle, 1984; Falcon, 2012). In reductionist science, answers to "why" questions typically relate to one of the first three of Aristotle's causes, regarding changes in substances (material cause), in form (formal cause) and in the effects of external influences (efficient cause). This is reflected in much functional-structural pant modeling (FSPM), where "structural" aspects of plant architecture are clearly concerned with formal causes and internal "functional" aspects, such as hormones and transported nutrient are clearly concerned with material causes (Sievänen et al., 2000; Prusinkiewicz, 2004; Yan et al., 2004; Godin and Sinoquet, 2005; Fourcaud et al., 2008; Hanan and Prusinkiewicz, 2008; Vos et al., 2010). The environmental aspects, such as light, soil water and nutrients, pests and pathogens that are also often included in such FSPM and interact with both function and structure are clearly concerned with efficient causes. However, Aristotle's fourth kind of cause, final cause, seems to be less considered in reductionist science in general, and in FSPM in particular.

Final causes concern the aim or purpose being served by the object of interest, a plant in our case. In other words, discussion of final causes concerns answering the question of why a plant grows the way it does by reference to the purpose of that growth. Such answers could take the form of "The plant is growing like that because it is trying to maximize its light interception," for example. In science, such a response may lead to accusations of anthropomorphism, which can be defined as the attribution of human qualities to

things other than humans, with a connotation that such attribution is erroneous and problematic (Horowitz, 2007). If Pavlov (1927) wrote that animals should be "studied as purely physiological facts, without any need to resort to fantastic speculations as to the existence of any possible subjective state in the animal which may be conjectured on analogy with ourselves," then it would seem an even greater sin to explain the behavior of plants as "purposeful," or in terms of what they are trying to achieve with that behavior? However, evolutionary theory provides a clear rationale for the value of explanations of behavior in terms of the purpose of that behavior, as long as it can be seen as having an evolutionary advantage, and thus having been selected for by evolutionary processes. So we can rephrase our "final cause" response more carefully, "The plant is growing like that because that is an ecological strategy that has evolved over time due to the fact that it tends to maximize the plant's light interception." But how can we know whether a growth strategy has indeed evolved over time to maximize light interception (or any other function that contributes to evolutionary success)?

The dynamic structural development of a plant can be seen as a strategy for exploiting the limited resources available within its environment, such as light, soil water and nutrients, and we would expect that evolution would lead to efficient growth strategies that reduce resource costs while maximizing resource acquisition. No one growth strategy will be optimal in all environments; which strategies of structural development are most effective will depend on how the resources on which the plant depends are distributed through both time and space. The relative advantage of a plant's growth strategies

will also depend on how its architecture influences factors such as dispersal of seeds and pollen, the impacts of herbivoury and drought stress, the efficiency of water transport, biomechanical support, and resistance to wind, along with how much it costs to produce and maintain the structures that comprise its architecture (Küppers, 1989; Gartner, 1995). Therefore, if we are to shed light on Aristotle's final cause and start to understand why plants have evolved different strategies of structural development, we need to understand the various costs and benefits of different growth strategies in different environments (Farnsworth and Niklas, 1995; Lynch, 1995).

There is a long history of modeling plants in order to investigate the costs and benefits of different structural growth strategies (e.g., Shinozaki et al., 1964; Honda and Fisher, 1979; Johnson and Thornley, 1987; Niklas, 1999; West et al., 1999; Takenaka et al., 2001; Falster and Westoby, 2003; King et al., 2003). However, many potentially important aspects of plant growth and function have not been represented in these models, largely due to computational constraints and limitations in modeling technology. As simplifications of reality, no model can possibly include all aspects of reality. Nonetheless, recent years have seen the development of a new generation of plant models that include more of these previously neglected aspects, such as the explicit topology and spatial geometry of the plant structure; the way that the plant architecture develops dynamically over time by changes in existing components and the addition of new ones; the feedbacks between plant structure, function, and environment that also change with time as the plant grows and the environment

changes; the way that the distribution of resources within a plant's environment varies with time and space; and competition between individuals within plant populations and communities. It is this "new generation" of models that are often known as functional-structural plant models (FSPMs) or "virtual plants" (Sievänen et al., 2000; Prusinkiewicz, 2004; Yan et al., 2004; Godin and Sinoquet, 2005; Fourcaud et al., 2008; Hanan and Prusinkiewicz, 2008; Vos et al., 2010).
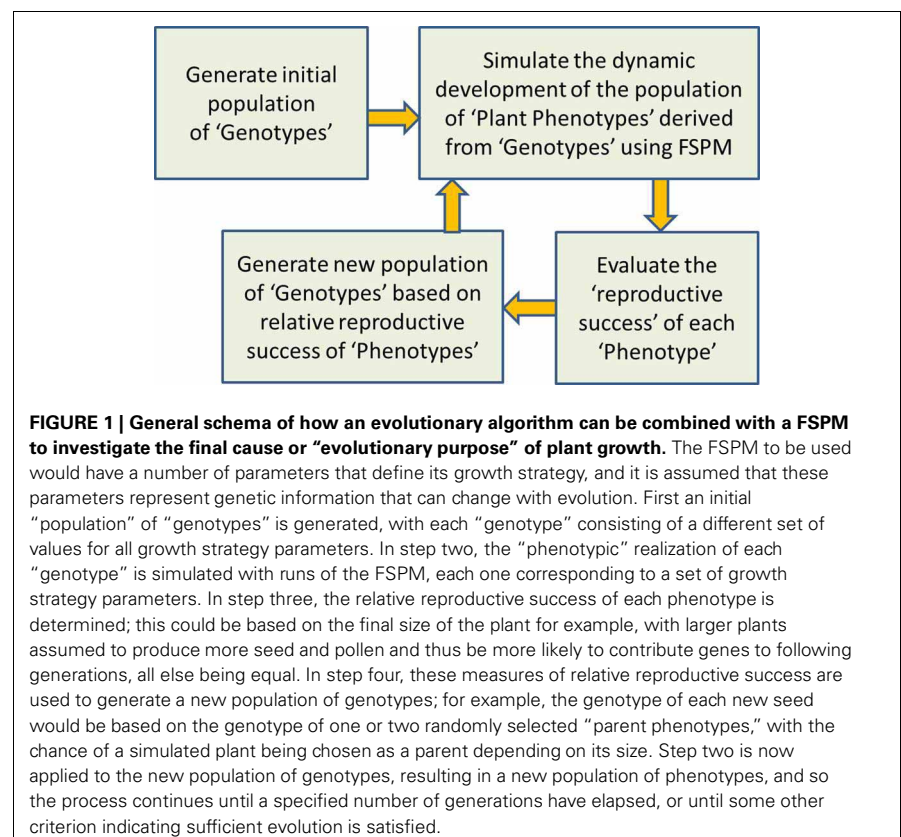
The fact that FSPMs represent a large number of potentially-important interacting processes in a dynamic way and at a high degree of detail would seem to make them a perfect tool for investigating the costs and benefits of different structural growth strategies, and thus providing insight into the final cause of plant growth strategies. Indeed many models that could be termed FSPMs have been employed to investigate the relative advantages of varying below- and above-ground structural growth strategies (e.g., Pearcy and Yang, 1996; Colasanti and Hunt, 1997; Dunbabin et al., 2003; Pearcy et al., 2005; Sterck et al., 2005; Clark and Bullock, 2007; Pagès, 2011). However, the strength of FSPMs, their dynamic realism, is also their weakness, because it makes them relatively complex and computationally demanding. It can take a relatively long time to run even a single FSPM growth simulation, and an FSPM typically contains a large number of growth-strategy-defining parameters, meaning that to run simulations for all combinations of all values of all parameters of interest becomes a major computational challenge. One approach is to use a relatively complex and realistic FSPM but only attempt to evaluate a limited subset of all possible strategies (e.g., Dunbabin et al., 2003; Pagès, 2011), and the other is to use a simpler FSPM but explore a more comprehensive set of strategies (e.g., Niklas, 1994, 1999). However, probably neither of these would really satisfy Aristotle in his search for a final cause of real plant growth; for that we need a thorough and comprehensive search through a wide range of growth strategies with a model that is flexible and detailed enough to capture the most important aspects of real plant growth.

A promising option for moving forward is to employ evolutionary optimization algorithms (Fogel, 1994; Ashlock, 2006). Such algorithms provide a computationally efficient means of exploring a wide range of possibilities in search of optimal solutions. In addition, marrying evolutionary algorithms with FSPMs would also appear to be a perfect way to explore the optimality of plant structures and growth strategies from an evolutionary perspective, in order to deepen our understanding of the relationships between evolution, ecosystems, individual plants, and genes (Prusinkiewicz, 2000). Earlier use of evolutionary algorithms with models of plant structure were aimed at evolving better above-ground plant forms based on aesthetic criteria (McCormack, 1993; Jacob, 1994; Traxler and Gervautz, 1996; McCormack, 2004); these representations of plant structure were relatively simple and abstract and contained little realistic representation of biological processes. In more recent times, more biologically-motivated questions of ecological theory and above-ground plant competition at the level of individual plants and plant populations have been tackled with a combination of structural plant models and evolutionary computation, but still at a relatively abstract level (Bornhofen and Lattaud, 2006, 2007, 2009; Kennedy, 2010; Bornhofen et al., 2011). These examples only highlight the huge potential for using sophisticated evolutionary computation with more detailed and realistic FSPMs. While the potential focus of such FSPMs is almost limitless (above-ground, below-ground, herbs, shrubs, trees…), the way that an evolutionary algorithm can be combined with a FSPM to investigate the final cause of plant growth can be explained in quite general terms (**Figure 1**).

In a recent study illustrating the potential of this approach, we explored below-ground plant structural optimality by linking an evolutionary optimization algorithm with a dynamic root growth FSPM (Renton et al., 2012; Renton and Poot, 2013, unpublished) in a Tool for Analysis of Root Structures Incorporating Evolution of Rooting Strategies (TARSIERS). This study extended on previous studies by including a relatively detailed representation of root structure and spatial and

FIGURE 1 | General schema of how an evolutionary algorithm can be combined with a FSPM to investigate the final cause or "evolutionary purpose" of plant growth. The FSPM to be used would have a number of parameters that define its growth strategy, and it is assumed that these parameters represent genetic information that can change with evolution. First an initial "population" of "genotypes" is generated, with each "genotype" consisting of a different set of values for all growth strategy parameters. In step two, the "phenotypic" realization of each "genotype" is simulated with runs of the FSPM, each one corresponding to a set of growth strategy parameters. In step three, the relative reproductive success of each phenotype is determined; this could be based on the final size of the plant for example, with larger plants assumed to produce more seed and pollen and thus be more likely to contribute genes to following generations, all else being equal. In step four, these measures of relative reproductive success are used to generate a new population of genotypes; for example, the genotype of each new seed would be based on the genotype of one or two randomly selected "parent phenotypes," with the chance of a simulated plant being chosen as a parent depending on its size. Step two is now applied to the new population of genotypes, resulting in a new population of phenotypes, and so the process continues until a specified number of generations have elapsed, or until some other criterion indicating sufficient evolution is satisfied.

temporal variations in resource distributions, applied to a realistic case study situation—perennial plants growing on shallow soils in seasonally dry environments. The approach was able to simulate reasonable patterns of evolution of structural growth strategies that converged toward the specialized root system morphologies that have been observed in species restricted to these types of habitats, and which are likely to enhance access to water resources in cracks in the underlying rock (Poot and Lambers, 2003a,b, 2008; Poot et al., 2008, 2012). The study showed how adding an evolutionary perspective to FSPMs could provide insights into both evolutionary processes and the ecological costs and benefits of different plant growth strategies.

As computing technology and modeling methodologies continue to advance, the computational difficulties of applying comprehensive and realistic evolutionary algorithms to detailed and realistic models of plant structure and function will continue to be overcome. While the realm of possibilities will keep expanding, the challenge will continue to be to design plant models that are simple enough for evolutionary optimization to be computationally feasible, yet flexible enough to allow a range of structural development strategies to be explored and realistic enough to capture the essential characteristics of interest. Within current FSPMs, the representation of the interactions between functional processes and structural development can be relatively simple and empirical (Renton et al., 2005a,b, 2007) or more mechanistic, realistic, detailed, and thus complex (Allen et al., 2005; Costes et al., 2008; Lopez et al., 2008); it is likely that relatively simple approaches will be of most use for integration into evolutionary simulations in the foreseeable future, although the use of "super-computing" facilities could potentially allow evolutionary optimization to be applied to even very complex and detailed FSPMs. The approaches developed will give insights into both evolutionary processes and the ecological costs and benefits of different plant growth strategies. The strategies considered could include both fixed strategies, which do not depend on the environment encountered by an individual plant, and plastic strategies, that do adapt to the encountered environment. By showing how plant architectural strategies have evolved to meet the requirements of certain specific environments, they will also help understand and predict how these strategies are likely to function or adapt as environments change in the future. If, as Dobzhansky (1973) wrote, "nothing in biology makes sense except in the light of evolution," then it is essential to add an evolutionary perspective to FSPM, which addresses Aristotle's fourth and final cause in addition to his first three causes addressed by the structural, functional, and environmental perspectives already commonly used in FSPM. This will help to provide a more complete answer to the question of why plants grow the way they do.

ACKNOWLEDGMENTS

REFERENCES

Allen, M. T., Prusinkiewicz, P., and DeJong, T. M. (2005). Using L-systems for modeling source-sink interactions, architecture and physiology of growing trees: the L-PEACH model. *New Phytol.* 166, 869–880. doi: 10.1111/j.1469-8137.2005.01348.x

Aristotle. (1984). *Complete Works of Aristotle, Vol. 1. The Revised Oxford Translation*. Princeton, NJ: Princeton University Press.

Ashlock, D. (2006). *Evolutionary Computation for Modeling and Optimization*. New York, NY: Springer-Verlag.

Bornhofen, S., and Lattaud, C. (2006). Life history evolution of virtual plants: trading off between growth and reproduction. *Lect. Notes Comput. Sci.* 4193, 808–817. doi: 10.1007/11844297_82

Bornhofen, S., and Lattaud, C. (2007). "Evolution of virtual plants interacting with their environment," in *Proceedings of the 9th International Conference on Virtual Reality (VRIC'07)*, (Laval), 172–176.

Bornhofen, S., and Lattaud, C. (2009). Competition and evolution in virtual plant communities: a new modeling approach. *Nat. Comput.* 8, 349–438. doi: 10.1007/s11047-008-9089-5

Bornhofen, S., Barot, S., and Lattaud, C. (2011). The evolution of CSR life-history strategies in a plant model with explicit physiology and architecture. *Ecol. Model.* 222, 1–10. doi: 10.1016/j.ecolmodel.2010.09.014

Clark, B., and Bullock, S. (2007). Shedding light on plant competition: modelling the influence of plant morphology on light capture (and vice versa). *J. Theor. Biol.* 244, 208–217. doi: 10.1016/j.jtbi.2006.07.032

Colasanti, R. L., and Hunt, R. (1997). Resource dynamics and plant growth: a self-assembling model for individuals, populations and communities. *Funct. Ecol.* 11, 133–145. doi: 10.1046/j.1365-2435.1997.00088.x

Costes, E., Smith, C., Renton, M., Guédon, Y., Prusinkiewicz, P., and Godin, C. (2008). MAppleT: simulation of apple tree development using mixed stochastic and biomechanical models. *Funct. Plant Biol.* 35, 936–950. doi: 10.1071/FP08081

Dobzhansky, T. (1973). Nothing in biology makes sense except in the light of evolution. *Am. Biol. Teach.* 35, 125–129. doi: 10.2307/4444260

Dunbabin, V., Diggle, A., and Rengel, Z. (2003). Is there an optimal root architecture for nitrate capture in leaching environments? *Plant. Cell. Environ.* 26, 835–844. doi: 10.1046/j.1365-3040.2003.01015.x

Falcon, A. (2012). "Aristotle on Causality," in *The Stanford Encyclopedia of Philosophy (Winter 2012 Edn.)*, ed E. N. Zalta. Available online at: http://plato.stanford.edu/archives/win2012/entries/aristotle-causality/. (Accessed June 26, 2013).

Falster, D. S., and Westoby, M. (2003). Plant height and evolutionary games. *Trends Ecol. Evol.* 18, 337–343. doi: 10.1016/S0169-5347(03)00061-2

Farnsworth, K. D., and Niklas, K. J. (1995). Theories of optimization, form and function in branching architecture in plants. *Funct. Ecol.* 9, 355. doi: 10.2307/2389997

Fogel, D. B. (1994). An introduction to simulated evolutionary optimization. *IEEE Trans. Neural Netw.* 5, 3–14. doi: 10.1109/72.265956

Fourcaud, T., Zhang, X., Stokes, A., Lambers, H., and Korner, C. (2008). Plant growth modelling and applications: the increasing importance of plant architecture in growth models. *Ann. Bot.* 101, 1053–1063. doi: 10.1093/aob/mcn050

Gartner, B. L. (ed.). (1995). *Plant Stems: Physiology and Functional Morphology*. London: Academic Press.

Godin, C., and Sinoquet, H. (2005). Functional-structural plant modelling. *New Phytol.* 166, 705–708. doi: 10.1111/j.1469-8137.2005.01445.x

Hanan, J., and Prusinkiewicz, P. (2008). Foreword: studying plants with functional-structural models. *Funct. Plant Biol.* 35, i–iii. doi: 10.1071/FPv35n10_FO

Honda, H., and Fisher, J. B. (1979). Ratio of tree branch lengths: the equitable distribution of leaf clusters on branches. *PNAS* 76, 3875–3879. doi: 10.1073/pnas.76.8.3875

Horowitz, A. (2007). "Anthropomorphism," in *Encyclopedia of Human-Animal Relationships: A Global Exploration of Our Connections With Animals*, ed M. Bekoff (Westport, CT: Greenwood Publishing Group Incorporated), 60–66.

Jacob, C. (1994). "Genetic L-System programming," in *Parallel Problem Solving from Nature – PPSN III Lecture Notes in Computer Science*, eds Y. Davidor, H.-P. Schwefel, and R. Männer (Springer: Berlin; Heidelberg), 333–343. Available online at: http://link.springer.com/chapter/10.1007/3-540-58484-6_277. (Accessed January 29, 2013).

Johnson, I. R., and Thornley, J. H. M. (1987). A model of shoot: root partitioning with optimal growth. *Ann. Bot.* 60, 133–142.

Kennedy, M. C. (2010). Functional-structural models optimize the placement of foliage units for

multiple whole-canopy functions. *Ecol. Res.* 25, 723–732. doi: 10.1007/s11284-009-0658-6

King, J., Gay, A., Sylvester-Bradley, R., Bingham, I., Foulkes, J., Gregory, P., et al. (2003). Modelling cereal root systems for water and nitrogen capture: towards an economic optimum. *Ann. Bot.* 91, 383–390. doi: 10.1093/aob/mcg033

Küppers, M. (1989). Ecological significance of above-ground architectural patterns in woody plants: a question of cost-benefit relationships. *Trends Ecol. Evol.* 4, 375–379. doi: 10.1016/0169-5347(89)90103-1

Lopez, G., Favreau, R. R., Smith, C., Costes, E., Prusinkiewicz, P., and DeJong, T. M. (2008). Integrating simulation of architectural development and source-sink behaviour of peach trees by incorporating Markov chains and physiological organ function submodels into L-PEACH. *Funct. Plant Biol.* 35, 761–771. doi: 10.1071/FP08039

Lynch, J. (1995). Root architecture and plant productivity. *Plant Physiol.* 109, 7.

McCormack, J. (2004). "Aesthetic evolution of L-Systems revisited," in *Applications of Evolutionary Computing Lecture Notes in Computer Science*, eds G. R. Raidl, S. Cagnoni, J. Branke, D. W. Corne, R. Drechsler, Y. Jin et al., (Springer: Berlin; Heidelberg), 477–488. Available online at: http://link.springer.com/chapter/10.1007/978-3-540-24653-4_49. (Accessed January 24, 2013).

McCormack, J. (1993). "Interactive evolution of L-system grammars for computer graphics modelling," in *Complex Systems: From Biology to Computation*, eds D. G. Green, and T. R. J. Bossomaier (Amsterdam: IOS Press), 118–130.

Niklas, K. J. (1994). Morphological evolution through complex domains of fitness. *Proc. Natl. Acad. Sci. U.S.A.* 91, 6772–6779. doi: 10.1073/pnas.91.15.6772

Niklas, K. J. (1999). Evolutionary walks through a land plant morphospace. *J. Exp. Bot.* 50, 39–52.

Pagès, L. (2011). Links between root developmental traits and foraging performance. *Plant Cell Environ.* 34, 1749–1760. doi: 10.1111/j.1365-3040.2011.02371.x

Pavlov, I. P. (1927). "Lecture II," in *Conditioned Reflexes: An Investigation of the Physiological Activity of the Cerebral Cortex* (Courier Dover Publications). Available online at: http://psychclassics.yorku.ca/Pavlov/lecture2.htm

Pearcy, R. W., Muraoka, H., and Valladares, F. (2005). Crown architecture in sun and shade environments: assessing function and trade-offs with a three-dimensional simulation model. *New Phytol.* 166, 791–800. doi: 10.1111/j.1469-8137.2005.01328.x

Pearcy, R. W., and Yang, W. (1996). A three-dimensional crown architecture model for assessment of light capture and carbon gain by understory plants. *Oecologia* 108, 1–12. doi: 10.1007/BF00333208

Poot, P., Bakker, R., and Lambers, H. (2008). Adaptations to winter-wet ironstone soils: a comparison between rare ironstone Hakea (Proteaceae) species and their common congeners. *Aust. J. Bot.* 56, 574–582. doi: 10.1071/BT08155

Poot, P., Hopper, S. D., and van Diggelen, J. M. H. (2012). Exploring rock fissures: does a specialized root morphology explain endemism on granite outcrops? *Ann. Bot.* 110, 291–300. doi: 10.1093/aob/mcr322

Poot, P., and Lambers, H. (2003a). Are trade-offs in allocation pattern and root morphology related to species abundance? A congeneric comparison between rare and common species in the south-western Australian flora. *J. Ecol.* 91, 58–67. doi: 10.1046/j.1365-2745.2003.00738.x

Poot, P., and Lambers, H. (2003b). Growth responses to waterlogging and drainage of woody Hakea (Proteaceae) seedlings, originating from contrasting habitats in south-western Australia. *Plant Soil* 253, 57–70. doi: 10.1023/A:1024540621942

Poot, P., and Lambers, H. (2008). Shallow-soil endemics: adaptive advantages and constraints of a specialized root-system morphology. *New Phytol.* 178, 371–381. doi: 10.1111/j.1469-8137.2007.02370.x

Prusinkiewicz, P. (2000). Simulation modeling of plants and plant ecosystems. *Commun. ACM* 43, 84–93. doi: 10.1145/341852.341867

Prusinkiewicz, P. (2004). Modeling plant growth and development. *Curr. Opin. Plant Biol.* 7, 79–83. doi: 10.1016/j.pbi.2003.11.007

Renton, M., Hanan, J., and Burrage, K. (2005a). Using the canonical modelling approach to simplify the simulation of function in functional-structural plant models. *New Phytol.* 166, 845–857. doi: 10.1111/j.1469-8137.2005.01330.x

Renton, M., Kaitaniemi, P., and Hanan, J. (2005b). Functional-structural plant modelling using a combination of architectural analysis, L-systems and a canonical model of function. *Ecol. Model.* 184, 277–298. doi: 10.1016/j.ecolmodel.2004.10.008

Renton, M., and Poot, P. (2013). "Simulating the evolution of optimal rooting strategies in shallow soils and extreme climates," in *Proceedings of the 7th International Conference on Functional-Structural Plant Models*, eds R. Sievänen, E. Nikinmaa, C. Godin, A. Lintunen, and P. Nygren (Saariselkä; Vantaa: Finnish Society of Forest Science). Available online at: http://www.metla.fi/fspm2013/proceedings

Renton, M., Poot, P., and Evers, J. B. (2012). "Simulation of optimal rooting strategies: what's the best way to find a wet crack?" in *Proceedings of the Fourth International Symposium on Plant Growth Modeling and Applications (PMA12)* (Shanghai: IEEE Computer Society).

Renton, M., Thornby, D., and Hanan, J. (2007). "Canonical modelling: An approach for intermediate-level simulation of carbon allocation in functional-structural plant models," in *Functional-Structural Plant Modelling in Crop Production*, eds J. Vos, L. Marcelis, P. Visser, and J. Struik (Wageningen University, The Netherlands: Frontis/Springer), 151–164.

Shinozaki, K., Yoda, K., Hozumi, K., and Kira, T. (1964). A quantitative analysis of plant form-the pipe model theory: I. basic analyses. *Japan. J. Ecol.* 14, 97–105.

Sievänen, R., Nikinmaa, E., Nygren, P., Ozier-Lafontaine, H., Perttunen, J., and Hakula, H. (2000). Components of functional-structural tree models. *Ann. For. Sci.* 57, 399–412. doi: 10.1051/forest:2000131

Sterck, F. J., Schieving, F., Lemmens, A., and Pons, T. L. (2005). Performance of trees in forest canopies: explorations with a bottom-up functional-structural plant growth model. *New Phytol.* 166, 827–843. doi: 10.1111/j.1469-8137.2005.01342.x

Takenaka, A., Takahashi, K., and Kohyama, T. (2001). Optimal leaf display and biomass partitioning for efficient light capture in an understorey palm, *Licuala arbuscula*. *Func. Ecol.* 15, 660–668. doi: 10.1046/j.0269-8463.2001.00562.x

Traxler, C., and Gervautz, M. (1996). "Using genetic algorithms to improve the visual quality of fractal plants generated with csg-pl-systems," in *Proceedings of the Fourth International Conference in Central Europe on Computer Graphics and Virtual Worlds*, 367–376. Available online at: http://www.cg.tuwien.ac.at/research/rendering/csg-graphs/Papers/GeneticAlgorithms.pdf. (Accessed January 24, 2013).

Vos, J., Evers, J. B., Buck-Sorlin, G. H., Andrieu, B., Chelle, M., and de Visser, P. H. B. (2010). Functional-structural plant modelling: a new versatile tool in crop science. *J. Exp. Bot.* 61, 2101–2115. doi: 10.1093/jxb/erp345

West, G. B., Brown, J. H., and Enquist, B. J. (1999). A general model for the structure and allometry of plant vascular systems. *Nature* 400, 664–667. doi: 10.1038/23251

Yan, H.-P., Kang, M. Z., Reffye, P. D., and Dingkuhn, M. (2004). A dynamic, architectural plant model simulating resource-dependent growth. *Ann. Bot.* 93, 591–602. doi: 10.1093/aob/mch078

Rose bush leaf and internode expansion dynamics: analysis and development of a model capturing interplant variability

Sabine Demotes-Mainard[1,2,3,4]*, **Jessica Bertheloot**[1,2,3,4], **Rachid Boumaza**[1,2,3,4],
Lydie Huché-Thélier[1,2,3,4], **Gaëlle Guéritaine**[1,2,3,4], **Vincent Guérin**[1,2,3,4] **and Bruno Andrieu**[5,6]

[1] Institut National de la Recherche Agronomique, UMR1345 IRHS, Beaucouzé, France
[2] Agrocampus-Ouest, UMR1345 IRHS , Angers, France
[3] Université d'Angers, UMR1345 IRHS, Angers, France
[4] SFR4207 QUASAV, Angers, France
[5] Institut National de la Recherche Agronomique, UMR1091 EGC, Thiverval-Grignon, France
[6] AgroParisTech, UMR1091 EGC, Thiverval-Grignon, France

Rose bush architecture, among other factors, such as plant health, determines plant visual quality. The commercial product is the individual plant and interplant variability may be high within a crop. Thus, both mean plant architecture and interplant variability should be studied. Expansion is an important feature of architecture, but it has been little studied at the level of individual organs in rose bushes. We investigated the expansion kinetics of primary shoot organs, to develop a model reproducing the organ expansion of real crops from non-destructive input variables. We took interplant variability in expansion kinetics and the model's ability to simulate this variability into account. Changes in leaflet and internode dimensions over thermal time were recorded for primary shoot expansion, on 83 plants from three crops grown in different climatic conditions and densities. An empirical model was developed, to reproduce organ expansion kinetics for individual plants of a real crop of rose bush primary shoots. Leaflet or internode length was simulated as a logistic function of thermal time. The model was evaluated by cross-validation. We found that differences in leaflet or internode expansion kinetics between phytomer positions and between plants at a given phytomer position were due mostly to large differences in time of organ expansion and expansion rate, rather than differences in expansion duration. Thus, in the model, the parameters linked to expansion duration were predicted by values common to all plants, whereas variability in final size and organ expansion time was captured by input data. The model accurately simulated leaflet and internode expansion for individual plants (RMSEP = 7.3 and 10.2% of final length, respectively). Thus, this study defines the measurements required to simulate expansion and provides the first model simulating organ expansion in rosebush to capture interplant variability.

Keywords: *Rosa hybrida* L., individual plant, phytomer, model, elongation kinetics, leaflet size, internode length, growth

INTRODUCTION

Plant architecture constitutes the interface by which the plant gathers resources and perceives signals from its environment, which in turn modify plant architecture. In ornamental crops, such as rose bush, plant architecture is important in its own right, because it conditions plant visual quality, largely accounting for consumer choice (Boumaza et al., 2010). The management of plant architecture, by manipulation of the environment, in particular, is therefore an important issue for rose bush growers. The development of plant architecture should be studied at two levels: that of the crop, the level at which management operates and interactions occur between neighbors, and the individual plant level, as it is individual plants that are sold. A knowledge of mean values for a crop is therefore not sufficient; the variability between plants within a crop should also be characterized. To investigate the relationships between rose bush architecture and

its environment, a functional-structural plant model (FSPM) of rose bush would be a powerful tool. Firstly, FSPMs account for plant architecture at the individual plant level; secondly, when coupled with phylloclimate models, FSPMs enable to estimate the physical environment actually perceived by aerial organs, which is heterogeneous within and between plants (Chelle, 2005).

Plant architecture firstly depends on bud fate, which determines the number and location of shoots; furthermore on the initiation, expansion and (re)orientation of internodes and leaves, and on floral transition, which determines the time of flowering and the number of flowers. All these traits have a potential impact on the visual quality of rose bush. The architectural traits that we wished to model in this study relate to the expansion of the main organs of the aerial vegetative apparatus: the stems and leaves. In addition to their physiological functions, the stems determine the shape of the plant (top-sided shape, symmetry). Together with the

leaves, they determine the compactness of the plant. Both these traits are thus important elements of visual quality (Boumaza et al., 2009). The expansion of an individual organ is characterized by the time of organ expansion, the expansion rate and expansion duration. Within a shoot, these traits follow gradients according to organ position which need to be characterized.

Expansion features vary between species, and specific studies are therefore required. The kinetics of leaf and internode expansion at the phytomer level have never been described for rose. Several models describing architectural variables have been developed for cut-flower roses. A first group of models predicts variables at the level of the whole shoot, such as total stem length and basal stem diameter (Hopper et al., 1994; Costa and Heuvelink, 2003; Oki et al., 2006) or morphological quality classes (Morisot, 1996). Structural descriptions have been refined further in more mechanistic models (Lieth and Pasian, 1991; Dayan et al., 2004), mostly with a view to predicting the harvest of rose flowers more accurately. Considerable effort has thus gone into modeling photosynthesis and assimilate partitioning, but the kinetics of expansion of individual organs and its variation with respect to organ position have not been described. The FSPM of Buck-Sorlin et al. (2011) for cut-flower roses included the expansion kinetics of individual organs, but the paper focuses on simulating the local light climate and photosynthesis and does not present results for organ expansion. In rose bush, Demotes-Mainard et al. (2009) have described the coordination of leaflet and internode expansion kinetics as a function of position along the primary shoot. However, these preliminary results were obtained for only one set of growth conditions and relate exclusively to the behavior of an average 11-phytomer plant. With a view to developing a FSPM for rose bush one step consists in modeling organ expansion. Therefore, additional knowledge of the kinetics of individual organs must be obtained.

As in many species, organ size in rose is influenced by environmental factors, such as water (Demotes-Mainard et al., 2013), or nitrogen (Ashok and Rengasamy, 2000; Huché-Thélier et al., 2011) availability, light quality (Rajapakse and Kelly, 1994; Maas and Bakx, 1995) and intensity (Hopper and Hammer, 1991; Bredmose, 1993; Maas and Bakx, 1995), mechanical stimulation (Morel et al., 2012), and genotype (Morel et al., 2009). Current knowledge of the effects of environmental factors is not sufficient to predict internode or leaf size in a range of environments. However, one way to reconstruct the plant architecture of experimental crops accurately for the investigation of plant functioning involves using a model that simulates architecture with data obtained from experimental crops. These experimental data must capture the variability induced by the environment and not predicted by the model. This approach has been applied successfully in several studies [for example in Baccar et al. (2011), to study the effect of wheat architecture on *Septoria tritici* epidemics; Kahlen and Stützel (2011), to study the photo-modulation of cucumber internode elongation]. The input data used to reconstruct architecture are generally the means obtained for plant samples. We suggest that the use of data from individual plants should make it possible to explain and reproduce not only the mean plant characteristics, but also the interplant variability. Using individual data would not increase the time required for

data acquisition, because architectural data are necessarily measured at the individual plant and organ level. For the correct reproduction of individual plants, the input data should capture interplant variability. This requires good knowledge of variations of the expansion kinetics of individual organs between plants.

The aim of this work was (i) to investigate the expansion kinetics of rose bush primary shoot internodes and leaves and its variation between phytomer positions and between plants and (ii) to propose an empirical model reproducing organ expansion kinetics that accounts for interplant variability and makes use of non-destructive, easy-to-measure input variables.

MATERIALS AND METHODS
PLANT MATERIAL AND GROWING CONDITIONS
Rosa hybrida "Radrazz" rose bushes were grown in Angers, France, in three experiments. Experiment 1 took place in spring 2007 (2007-Sp), experiment 2 in summer 2007 (2007-Su), and experiment 3 in spring 2010, with a low (2010-LD) or high (2010-HD) plant density. Single-node cuttings bearing a five- or seven-leaflet leaf were harvested from the medial part of mother plant stems and grown for 4–5 weeks in humid conditions until rooting was achieved. Well rooted cuttings were planted in individual pots containing a mixture of neutral peat, coconut fibers and perlite. Plants were transferred to a greenhouse before bud break and grown, with a border row, at a density of 23 plants m^{-2} in experiments 1 and 2, and at a density of 21 or 100 plants m^{-2} in experiment 3. The bud from the cutting produced the primary axis. After floral bud and last leaf appearance, a variable number of lateral buds burst and developed in secondary shoots. These shoots were let to grow but not measured. Plants were subirrigated, with tensiometer monitoring to ensure an absence of water stress. Mineral nutrition was provided by fertigation (5.0 mM KNO_3, 2.0 mM $Ca(NO_3)_2$, 2.0 mM NH_4NO_3, 2.0 mM KH_2PO_4, 2.0 mM $MgSO_4$, 0.25 mM NaOH; trace elements (Kanieltra 6-Fe,0.1 ml.l^{-1},Hydro Azote, Nanterre, France); pH 5.6; EC 1.77 mS.cm^{-1}). Air temperature was measured above the canopy, in a ventilated shelter, with a platinum sensor. Leaf temperature was measured in experiment 3 on the abaxial surface of leaves, at about the height of the apex, with copper-constantan thermocouples. Photosynthetically active radiation (PAR) was continuously measured above each canopy, with a line quantum sensor (LI-191 LI-COR, Lincoln, Neb. USA). It was also measured with line quantum sensors at both the base and the top of the canopy, at various locations, at solar noon, under a cloudy sky, on three dates during primary shoot expansion in experiment 3, for the calculation of intercepted PAR. The climatic conditions prevailing during the period of primary shoot expansion are presented in **Table 1**.

PLANT MEASUREMENTS
Destructive measurements of leaf dimensions
Groups of 62, 17, and 18 plants were selected at random from the 2007-Sp, 2010-LD, and 2010-HD crops, respectively, and destructively sampled at various times (5–11 times, according to the crop), beginning when the basal leaves were expanding and ending when all the leaves were fully expanded. We determined the number of leaflets per leaf for all leaves (197, 201,

Table 1 | Prevailing climatic conditions and PAR interception during shoot expansion, at high and low plant density, in each experiment.

Experiment	2007 spring	2007 summer		2010 spring	
				High plant density	Low plant density
Incident PAR (mol.m^{-2}.day^{-1})	8.0 ± 1.6	11.7 ± 1.1		7.7 ± 1.1	
			Days after bud break		
Intercepted PAR (%)			15	72.3 ± 3.1	8.5 ± 0.2
			30	93.9 ± 1.0	37.8 ± 2.6
			36	95.0 ± 0.1	47.0 ± 2.1
Air temperature (daily mean, °C)	20.2 ± 1.9	21.7 ± 1.3		20.2 ± 0.9	
Leaf temperature (daily mean, °C)				22.3 ± 1.6	22.8 ± 1.4
Humidity (%)	57.1 ± 6.5	75.6 ± 4.5		56.1 ± 7.7	

Each value is the mean ± standard deviation.

199 leaves for 2007-Sp, 2010-LD, and 2010-HD, respectively), the length and width of all leaflets and leaf length (measured with a ruler in 2007-Sp and by image analysis (ImageJ 1.43m, Wayne Rasband National Institute of Health, USA) in 2010-LD and 2010-HD). For 2010-LD and 2010-HD, we also determined the area of each leaflet by image analysis. For lateral leaflets, there was no significant difference between opposite leaflets for length, width or area, thus, for data analysis we used the mean value of length, width or area of each pair of opposite leaflets of an individual leaf.

Time-course measurements of visible leaf number, internode and terminal leaflet lengths

We randomly selected 33, 28, and 22 plants from the 2007-Su, 2010-LD, and 2010-HD crops, respectively. These plants were not those used for destructive measurements. The time of bud break of the cutting (referred to simply as bud break hereafter), marking the start of primary shoot development, was noted for each plant. Five times per week for 2007-Su and six times per week for 2010-LD and 2010-HD, we counted the number of visible leaves on each plant, including the scaly and stipular leaves located at the base of the shoot. A leaf was counted as visible as soon as its tip emerged. On primary shoots, we measured the length of the terminal leaflet of each leaf and the length of each internode with a ruler, from the first day on which the organ was fully visible until the end of organ expansion. A terminal leaflet was fully visible when its insertion on the rachis was visible, and an internode was fully visible when the node at its base was visible. Phytomer position of the organ was specified. The total number N_p of phytomers, including the peduncle, of the primary shoot of the plant p was determined at the end of shoot expansion.

DATA ANALYSIS

Convention for phytomer position

For data analysis, organ position along the shoot was expressed in terms of the relative rank of the phytomer (i), such that the most basal or apical phytomers could be compared regardless of the number of phytomers per shoot. Relative rank was calculated as:

$$i = (r - 1)/(N_p - 1) \quad (1)$$

where r is the absolute rank numbered from the base ($r = 1$) to the top ($r = N_p$) of the shoot. The relative rank of the peduncle is therefore 1. For the figures, the rounded phytomer relative rank, the relative rank of the phytomer rounded to the nearest tenth (0.1), was used for the sake of clarity. A phytomer consists of an internode, the leaf at the top of the internode and its axillary bud.

Time of leaf appearance

We calculated thermal time from air temperature above the crop, using a base temperature of 2.1°C. This base temperature was determined for *Rosa hybrida* "Radrazz" in a previous experiment (Guerin, pers. com.) according to Yang et al. (1995). All variables defining the time of an event are expressed in degree days (°Cd) since cutting bud break.

The thermal time of leaf appearance $t_p^a(i)$ for relative rank i of plant p could not be directly assessed by measurement, because the times at which the measurements were made did not correspond exactly to the time of leaf appearance. Thus, time $t_p^a(i)$ was estimated from the parameters of a piecewise linear function fitted to the time of the first observation of each leaf (with or without leaflets) of plant p (**Figure 1**):

$$t_p^a(i) = \begin{cases} \alpha_p + \beta_p i & \text{if } i \le c_p \\ \alpha_p + \beta_p i_p + \gamma_p (i - c_p) & \text{if } c_p < i \le 1 \end{cases} \quad (2)$$

where c_p is the relative rank at which the two lines intersect, defining the transition between a phase of rapid leaf appearance and a phase of slow appearance, α_p is the thermal time at which the first leaf appeared, β_p and γ_p the phyllochrons (°Cd) for the leaves of relative ranks below and above c_p, respectively. Peduncles do not bear leaves, but a date of "virtual leaf" appearance was calculated by linear extrapolation for the peduncle ($i = 1$).

Fitting of organ expansion

Each organ on the shoot was characterized by its kind (k, with $k = lea$ for terminal leaflets and $k = int$ for internodes) and relative rank i. If the final organ length exceeded 12 mm, the time course of length $L_{p,k}(t, i)$, expressed in mm, was fitted with a logistic

FIGURE 1 | Time (in degree days since budbreak) at which a leaf was observed for the first time (symbols) plotted against relative phytomer rank for an individual plant. The lines correspond to the fitting of a piecewise linear function, as in Equation (2), to the experimental data.
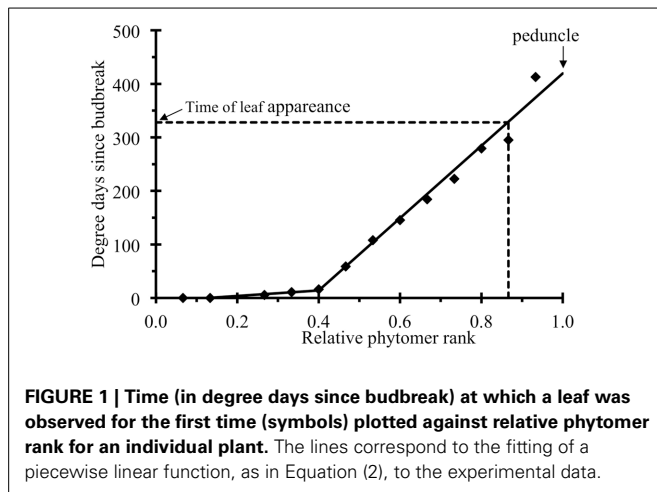
function of the thermal time (t) since bud break of plant p:

$$L_{p,k}(i, t) = \frac{L^m_{p,k}(i)}{1 + \exp\left(4\frac{v^m_{p,k}(i)}{L^m_{p,k}(i)}\left(t^0_{p,k}(i) - t\right)\right)} \quad (3)$$

where $L^m_{p,k}(i)$ is the maximal length of the organ, $t^0_{p,k}(i)$ is thermal time at the inflexion point, referred to as time at mid-expansion hereafter, and $v^m_{p,k}(i)$ is the expansion rate (mm °Cd^{-1}) at the inflexion point (maximal expansion rate). The ratio $w^m_{p,k}(i) = v^m_{p,k}(i)/L^m_{p,k}(i)$ is the maximal expansion rate when organ size is normalized, *i.e.*, the maximal expansion rate of the ratio $L_{p,k}(i, t)/L^m_{p,k}(i)$. If final organ length was lower than 12 mm, which includes the internodes at the very base of the shoot for most plants and the internode just below the peduncle for a few plants, the thermal time course of organ length was not fitted with any function, because of a lack of accuracy, and the organ was discarded from the analyses using the fitting data.

For each individual organ whose final length exceeded 12 mm, we used the values of the parameters of the logistic function to calculate the duration of expansion, defined as the time required for the organ to expand from 10 to 90% of its final length. Duration of expansion of an organ is inversely proportional to the value of $w^m_{p,k}(i)$ for this organ.

Modeling time of the inflexion point of the expansion function

The time $t^0_{p,k}(i)$ of the inflexion point of the time course function of the organ k (*lea* for terminal leaflet, *int* for internode) at relative rank i of plant p was estimated from observed data as described in Fitting of Organ Expansion. We also aimed to predict the time of the inflexion point $t^0_{p,k}(i)$ from the time of leaf appearance $t^a_p(i)$, therefore $t^0_{p,k}(i)$ was calculated as polynomials of the time of leaf appearance $t^a_p(i)$ of the corresponding phytomer:

$$t^0_{p,lea}(i) = \delta_{lea,0} + \delta_{lea,1}\, t^a_p(i) + \delta_{lea,2}\, t^a_p(i)^2 \quad (4.1)$$

$$t^0_{p,int}(i) = \begin{cases} \delta_{int,0} + \delta_{int,1}\, t^a_p(i) & \text{if } i < 1 \\ \delta_{ped,0} + \delta_{ped,1}\, t^a_p(i) & \text{if } i = 1 \end{cases} \quad (4.2)$$

The reasons for using such polynomials are given in the results section.

MODEL DESCRIPTION
Overview
The data analysis was used to develop a model reproducing the organ expansion kinetics of individual plants from a real crop of rose bush primary shoots, from input data. Organ length was simulated as a logistic function of thermal time since bud beak. In the reference scenario (S_0), the input variables were chosen so as to capture variability in both final length and the time of organ expansion. Two other scenarios (S_1 and S_2), differing in the number of input variables, were compared with the reference scenario. In these three scenarios, the input variables selected were both easy to measure and non-destructive.

Reference scenario S_0
Scenario inputs. The input variables for each plant p are:

- (I1) The number N_p of phytomers of p from which we derived the set of the relative ranks $0, 1/(N_p - 1), \ldots, (N_p - 2)/(N_p - 1), 1$, using Equation (1).
- (I2) The time $t^{a,\,\mathrm{obs}}_p(i)$ when the leaf of relative rank i ($i = 0, \ldots, (N_p - 2)/(N_p - 1)$) of p was observed for the first time.
- (I3) The final length $L^{m,\,\mathrm{obs}}_{p,lea}(i)$ of the terminal leaflet of relative rank i ($i = 0, \ldots, (N_p - 2)/(N_p - 1)$) of p.
- (I4) The final length $L^{m,\,\mathrm{obs}}_{p,int}(i)$ of the internode of relative rank i ($i = 0, \ldots, 1$) of p.

Scenario outputs. The outputs of the model consist of predicted functions. For each plant p of N_p phytomers, the predicted length of its organ k ($k = lea$ for terminal leaflet and $k = int$ for internode) at relative rank i, expressed in thermal time t since bud break of p is

$$L^{\mathrm{pred}}_{p,k}(i, t) = \frac{L^{m,\,\mathrm{obs}}_{p,k}(i)}{1 + \exp\left(4w^m_k(i)\left(t^{0,\,\mathrm{pred}}_{p,k}(i) - t\right)\right)} \quad (5)$$

where the parameters $t^{0,\,\mathrm{pred}}_{p,k}(i)$ and $w^m_k(i)$ are specified in the next paragraph.

Parameter computations. From the observed times $t^{a,\,\mathrm{obs}}_p(i)$, we estimated the parameters α_p, β_p, γ_p, and c_p of Equation (2), then we deduced the adjusted times ($t^{a,\,\mathrm{adj}}_p(i)$) of leaf appearance. These appearance times were used to compute the predicted times $t^{0,\,\mathrm{pred}}_{p,k}(i)$ corresponding to the inflexion points, using Equations (4.1) and (4.2).

First, we estimated the parameters $w^m_{p,k}(i) = \frac{v^m_{p,k}(i)}{L^m_{p,k}(i)}$ using the fitting procedure introduced in the paragraph Fitting of Organ Expansion for each organ kind, relative rank, and plant. Then, using these estimations for all plants, we estimated $w^m_k(i)$ for each relative rank i with the LOESS method of SAS. In the model, the estimated value of $w^m_k(i)$ thus depends on kind of organ and its relative rank, but not on the individual plant.

Scenario 1

Scenario input. The time of leaf appearance is the most demanding of the input variables to measure, because it requires a series of observations to be taken at particular times, with little flexibility in timing possible. We therefore, decided to eliminate this observation from scenario S_1. So the input variables of each plant p are (I1), (I3), and (I4).

Scenario outputs. The output functions of the scenario S_1

$$L_{p,k}^{\text{pred}}(i, t) = \frac{L_{p,k}^{m,\text{obs}}(i)}{1 + \exp\left(4w_k^m(i)\left(t_k^0(i) - t\right)\right)} \qquad (6)$$

are similar to the outputs of the scenario S_0 Equation (5), except that the thermal time at mid-expansion is independent of the plant and depends only on relative rank. The parameter $w_k^m(i)$ is specified in the paragraph Reference Scenario S_0 Parameter Computations and the parameter $t_k^0(i)$ is specified in the next paragraph.

Parameter computations. In S_1, the value $t_k^0(i)$ was estimated by relating the values $t_{p,k}^0(i)$, estimated with the fitting procedure introduced in the paragraph Fitting of Organ Expansion, with relative rank i by the LOESS method of SAS.

Scenario 2

Scenario input. Scenario S_2 simulates the kinetics of expansion of plants differing only in phytomer number. The comparison of S_0 with S_2 was designed to estimate the gain in accuracy with the use of a model using n different individual plants to simulate expansion (S_0) rather than a model reproducing n mean plants differing only in phytomer number (S_2). In S_2, the only input variable is the number of phytomers per primary shoot (I1), which is used to calculate relative ranks.

Scenario output. The output of the scenario S_2 is independent of the plant in the sense that the organ lengths of plants with the same number of phytomers are similar:

$$L_k^{\text{pred}}(i, t) = \frac{L_k^m(i)}{1 + \exp\left(4w_k^m(i)\left(t_k^0(i) - t\right)\right)} \qquad (7)$$

where the parameters $w_k^m(i)$ and $t_k^0(i)$ are previously specified and the parameter $L_k^m(i)$ is specified in the next paragraph.

Parameter computations. The final organ length $L_k^m(i)$ was estimated by relating the measured values of $L_{p,k}^m(i)$ to i, with the LOESS method of SAS.

MODEL EVALUATION

The three scenarios were evaluated by the leave-one-out cross-validation method (Linhart and Zucchini, 1986).

For each plant p of the original data set consisting of n plants:

– We removed plant p and estimated the model parameters from the $n - 1$ remaining plants.

– We computed the expansion curves for each terminal leaflet and each internode of plant p, using the scenario output, and calculated the mean square error of prediction:

$$MSEP_{p,k}(i) = \frac{\sum_{t=1}^{n_{p,k}(i)} \left(L_{p,k}^{\text{obs}}(i, t) - L_{p,k}^{\text{pred}}(i, t)\right)^2}{n_{p,k}(i)} \qquad (8)$$

where $n_{p,k}(i)$ is the number of observations for an organ of kind k of plant p of relative rank i, $L_{p,k}^{\text{obs}}(t, i)$ is the observed organ length at time t and $L_{p,k}^{\text{pred}}(i, t)$ (or $L_k^{\text{pred}}(i, t)$ for S_2) is the predicted organ length at time t computed from one of the functions given in Equations (5–7). For $MSEP_{p,k}(i)$ calculations, we retained only four values for the plateau, defined as the time at which organ length exceeded 0.97 times the final length, to avoid giving too much weight to the plateau.

Mean $MSEP_{p,k}(i)$ was then calculated for all plants, both per rounded relative rank and for all phytomer relative ranks pooled together. The square root of MSEP (RMSEP) was then calculated.

STATISTICAL ANALYSES

Principal component analyses were performed with SPAD software (V7.4, Coheris, Suresnes, France). All other statistical analyses were performed with SAS software (V 9.3, SAS Institute). For the fitting of logistic functions Equation (3) and of piecewise linear functions Equation (2), we used the NLIN procedure. For the establishment of relationships between relative rank i on the one hand and $w_k^m(i)$, $t_k^0(i)$, or $L_k^m(i)$ on the other, we used non-parametric methods and the LOESS procedure.

RESULTS

We will first present the variability present in the datasets used for expansion studies. We will then propose a simplified representation of rose compound leaves for studies of the kinetics of expansion, and describe the principal features of organ expansion kinetics: global pattern, origin and amplitude of the variability and how this variability can be captured through relationships. Finally, we will present a model based on this analysis that simulates leaflet and internode expansion kinetics from non-destructive input data.

ARCHITECTURAL VARIABLES WERE HIGHLY VARIABLE BOTH BETWEEN PHYTOMER POSITIONS AND BETWEEN PLANTS

High levels of variation were observed in all three crops used for time-course measurements. Primary shoots comprised between 10 and 16 phytomers on the plants used for time-course measurements (**Table 2**). The rate of leaf appearance was highly variable, with the phyllochron during the phase of slow leaf appearance varying from 20.6 to 53.4°Cd between plants within a crop, resulting in considerable variation of the dates of leaf appearance at equivalent phytomer positions (e.g., at rank 10, leaf appearance on the first plant occurred 172°Cd before that on the last plant within a crop). Final lengths were between 6.5 and 87.5 mm for terminal leaflets and between 1.0 and 63.5 mm for internodes, considering all ranks together. At a given phytomer position, final lengths also varied considerably between plants. For example,

Table 2 | Mean values and variability of architectural variables for the three crops used for the expansion study.

	Phytomers per shoot	Phyllochron during the phase of slow leaf appearance (°Cd)	Time of leaf appearance at rank 10 (°Cd since bud break)	Final lengths (mm), all ranks together		Final lengths (mm) at relative rank 0.8	
				Terminal leaflet	Internode	Terminal leaflet	Internode
2007-Su							
Mean ± std	12.0 ± 0.9 c[a]	35.0 ± 7.8 b	198.0 ± 28.3 a	60.6 ± 12.2 ab	21.0 ± 12.8 b	71.5 ± 5.4 b	27.8 ± 6.7 b
Min-max	10–13	21.2–50.7	152.3–264.3	18.0–83.0	1.0–62.0	58.0–80.0	9.0–40.0
2010-LD							
Mean ± std	14.4 ± 1.0 a	35.5 ± 5.9 b	127.1 ± 24.4 c	62.4 ± 16.7 a	23.9 ± 14.1 a	77.5 ± 5.1 a	36.0 ± 5.5 a
Min-max	13–16	24.5–46.8	79.0–173.4	6.5–87.5	3.5–61.5	63.0–86.0	22.5–48.0
2010-HD							
Mean ± std	13.5 ± 1.4 b	39.7 ± 7.9 a	159.5 ± 47.6 b	58.2 ± 16.0 b	24.5 ± 16.0 a	71.0 ± 6.2 b	34.9 ± 7.7 a
Min-max	10–16	20.6–53.4	87.0–258.6	6.5–82.0	3.0–63.5	59.0–82.0	16.0–49.5

[a]*Mean values with the same letters do not differ significantly between crops at P < 0.05, in One-Way ANOVA followed by LSD tests. Variability was assessed by determining both the standard deviation and the minimal and maximal values within each crop.*

at a rounded relative rank of 0.8, the range of final lengths was 58.0–86.0 mm for terminal leaflets and 9.0–49.5 mm for internodes. Differences in mean values between crops, for phytomer numbers, timing of leaf appearance and final lengths, were significant.

TERMINAL LEAFLET LENGTH CAN BE USED TO SIMULATE THE DIMENSIONS OF ALL LEAFLETS WITHIN A LEAF

Rose leaves have generally odd numbers of leaflets, with between one and nine leaflets per leaf, except at the base of the shoot, where leaves are reduced to scales or stipules. Principal component analysis (PCA) was performed on the lengths, widths and square roots of the areas of all individual leaflets of both growing and mature leaves collected from the 2007-Sp, 2010-LD, and 2010-HD crops. The percentage of the variance explained by the first principal component was 97, 79, 79, and 80% for 1-, 3-, 5-, and 7-leaflet leaves, respectively (no nine-leaflet leaf sampled in these experiments). These very high values for a single component indicate that all the dimensions (lengths, widths and square roots of areas) of all the leaflets were correlated within a given leaf, for both growing and mature leaves. Consequently, we were able to simplify the study of leaf expansion by focusing on a single dimension. We chose to study terminal leaflet length, because all leaves composed of leaflets have a terminal leaflet and this dimension is easily measured earlier in expansion than the other possible dimensions.

Terminal leaflet length (L) can be used to calculate whole leaf area (A) at any growth stage, given the number of leaflets of the leaf (N_L), from the following equation:

$$A = 0.287\, L^2\, N_L^{0.746} \quad (n = 201,\ R^2 = 0.93) \qquad (9)$$

With a multiplicative model for terminal leaflet length and leaflet number per leaf, the residual distribution did not depend on leaflet number per leaf as with a linear model. The two parameter values (0.287 and 0.746) were adjusted so as to maximize R^2.
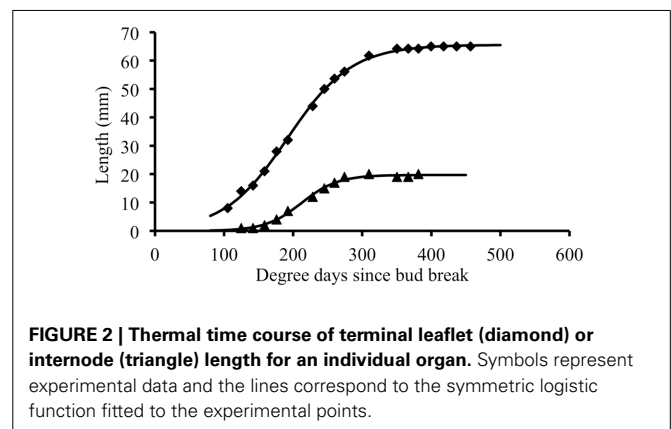
FIGURE 2 | Thermal time course of terminal leaflet (diamond) or internode (triangle) length for an individual organ. Symbols represent experimental data and the lines correspond to the symmetric logistic function fitted to the experimental points.

EXPANSION FOLLOWS A SIGMOIDAL PATTERN THAT CAN BE FITTED BY LOGISTIC FUNCTION

In individual organs, changes in terminal leaflet or internode length as a function of thermal time followed a sigmoidal pattern (**Figure 2**). This pattern of change was well fitted by a logistic function (**Table 3**): R^2 close to 1 and RMSEP around 1 mm. For all phytomers, the period of internode expansion was included within the expansion period of the terminal leaflet of the same phytomer (**Figure 2**). Terminal leaflets reached 10% of their final size a mean of 31°Cd before the corresponding internodes reached 10% of their final size, and the leaflets reached 90% of their final size a mean of 35°Cd after the internodes.

DIFFERENCES IN EXPANSION KINETICS ARE LARGELY DUE TO DIFFERENCES IN THE TIME AT WHICH EXPANSION OCCURS AND TO MAXIMAL EXPANSION RATE
Between plants at a given phytomer position
Within each relative rank, the variability of terminal leaflet expansion kinetics was high, as shown for relative rank 0.7 in **Figure 3A**. This variability resulted from high variability of

Table 3 | Goodness-of-fit of logistic functions to expansion curves of individual terminal leaflets and internodes: number of fitted curves, mean values of R^2, root mean square error (RMSE), and mean number of observations per curve.

	Terminal leaflets	Internodes
Number of organs for which expansion curves were fitted	622	711
R^2	0.99	0.98
RMSE (mm)	1.2	0.81
Number of observations per curve	19	16

FIGURE 3 | Elongation of individual organs positioned at relative rounded rank 0.7, as a function of thermal time since bud break, for terminal leaflets (A) or internodes (C). (B,D) show the same data for normalized length (length at any time divided by final length) and for thermal time counted since the inflexion point of the expansion curve of each individual organ. The crops 2007-Su, 2010-LD, and 2010 HD are represented by different symbols and colors. Each point corresponds to the measurement of an individual organ. Examples of individual curves are given for three plants (plants 11, 34, and 76).

FIGURE 4 | Final length (A,C), maximum expansion rate (B,D, closed symbols) and expansion duration (B,D, open symbols) plotted against rounded relative phytomer rank for terminal leaflets (A,B) and internodes (C,D). The 2007-Su, 2010-LD, and 2010-HD crops are represented by different symbols and colors: black triangles for 2007-Su, blue circles for 2010-LD and red squares for 2010-HD. Error bars represent the standard deviation, with 33, 28, and 22 plants in the 2007-Su, 2010-LD, and 2010-HD crops, respectively.

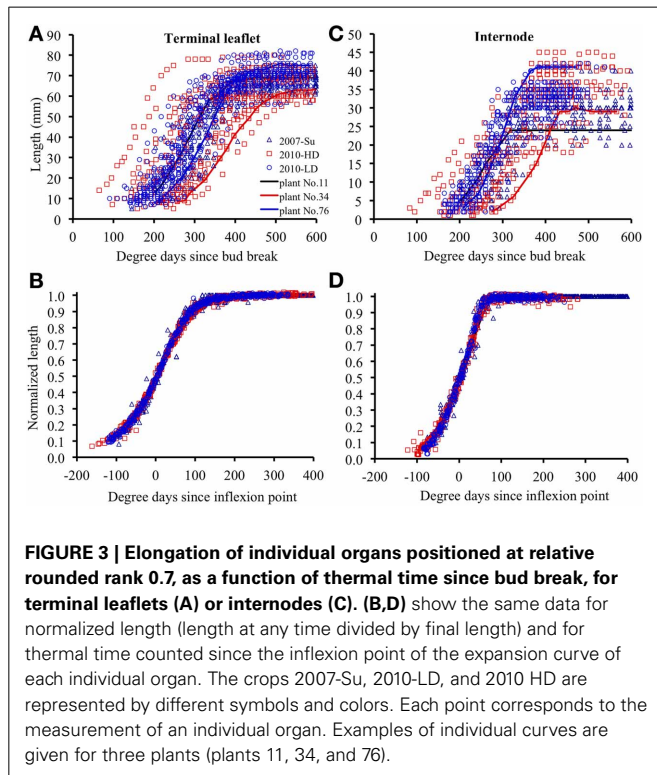both size and the time at which expansion occurred (265°Cd separating the times at mid- expansion of the first and last plants). All individual observations were almost superimposable if the length of each organ at a given time was normalized by dividing by its final length, and if the time was expressed as time since mid-expansion of individual organ ($t_{p,k}^0(i)$; **Figure 3B**). Thus, the differences in organ size between plants essentially resulted from differences in maximal expansion rate, rather than differences in expansion duration. This was true for all relative ranks, for both terminal leaflets and internodes (**Figures 3C,D**).

Between phytomer positions

For terminal leaflets, the variations of final length and maximal expansion rate with phytomer position followed the same tendencies for all three crops: a strong increase in the basal part of the shoot (up to relative ranks 0.4–0.5), then a more moderate increase up to relative rank 0.8, followed by a
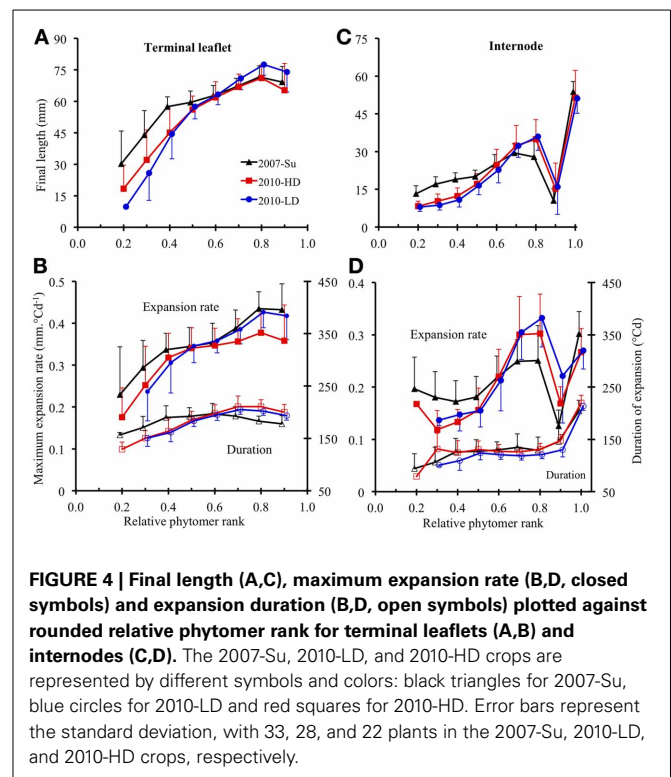
slight decrease or stability (**Figures 4A,B**). Expansion duration increased moderately from the base to relative rank 0.4 (2007-Su) or 0.7 (2010-LD and 2010-HD) and then stabilized and decreased for upper ranks (**Figure 4B**).

For internodes, final length (**Figure 4C**) increased up to relative ranks 0.8 then strongly decreased for relative rank 0.9 and increased strongly for relative rank 1.0 (peduncle). The variations of maximal expansion rate followed an essentially similar pattern to final length, except at the base of the axis (**Figure 4D**). By contrast, variations of expansion duration along the shoot (**Figure 4D**) were characterized by stability from relative ranks 0.3–0.9, with a lower duration at relative rank 0.2 and a much greater duration (×1.7) for the peduncle.

For both terminal leaflets and internodes, absolute values of final length, maximal expansion rate and expansion duration differed between the crops; in addition, the ranking of the three crops for these variables differed between different zones of the shoot. However, for all crops, the amplitude of variation between phytomer relative ranks was much higher for final length and maximal expansion rate than for expansion duration.

Within each crop, plants with a high leaflet or internode final length at a particular phytomer position did not necessarily also have a greater length at the next phytomer (not shown); the same was true for low leaflet or internode final lengths.

TIME OF LEAF APPEARANCE CAN BE USED TO ESTIMATE TIME AT MID-EXPANSION

Figure 5 shows the mid-expansion times for individual leaflets ($n = 629$) and internodes ($n = 584$) plotted against time of leaf appearance. These relationships integrate both the rate at which

expansion occurs on successive phytomers and the duration of expansion, because the predicted variable is the time at the middle and not at the beginning of expansion. For terminal leaflets, the relationship between time at mid-expansion and time of leaf appearance gradually curves, because expansion duration changes gradually with phytomer relative rank (**Figure 4B**). We therefore decided to use second-order polynomials to adjust the relationship for terminal leaflets. For the internodes, expansion duration was almost stable for vegetative internodes and much longer for peduncles (**Figure 4D**). We therefore, used first-order polynomials to adjust the relationship between time at mid-expansion and time of leaf appearance, using different parameters for vegetative internodes and peduncles. Estimates for the parameters of the relationships defined in the Equations (4.1) and (4.2) are given in **Table 4**.

The intercepts $\delta_{lea,0}$ and $\delta_{int,0}$ correspond, for phytomers whose leaf appears at bud break, to the time lag between leaf appearance and organ (leaflet or internode, respectively) maximal expansion rate. The other parameters of Equations (4.1) and (4.2) have no direct biological meaning. The adjusted determination coefficients were $R^2_{adj} = 0.97$ ($n = 627$) for terminal leaflets, $R^2_{adj} = 0.96$ ($n = 525$) for vegetative internodes and $R^2_{adj} = 0.86$ ($n = 59$) for peduncles. These high R^2 indicate that time of leaf appearance can be used to estimate time at mid-expansion for individual leaflets and internodes, because these relationships capture the variability between crops, between individual plants and between phytomer positions.

A MODEL OF LEAFLET AND INTERNODE EXPANSION REPRODUCES INTERPLANT VARIABILITY

From the results presented above, we developed a model reproducing the terminal leaflet and internode expansion of a crop of rose bush primary shoots. The three scenarios of the model, differing in the number of input variables, were evaluated by cross-validation.

In the reference scenario (S_0), input variables accounted for interplant variability in both organ final lengths and time of leaf appearance. The term $w_k^m(i)$ depends only on phytomer position and does not vary between individual plants. This term represents the maximal expansion rate for a normalized expansion curve and is inversely proportional to expansion duration. The parameters of S_0 are given in **Table 4** and the values of $w_k^m(i)$ estimated by the LOESS method are given in **Table 5**. S_0 correctly reproduced the expansion kinetics of the different terminal leaflets and internodes of an individual plant (**Figures 6A,C**) and of different plants within a given crop (**Figures 6B,D**). The RMSEP for all ranks together was 4.5 mm for leaflets and 2.5 mm for internodes, corresponding to 7.3 and 10.2%, respectively, of organ final lengths. The accuracy of the model was similar for the
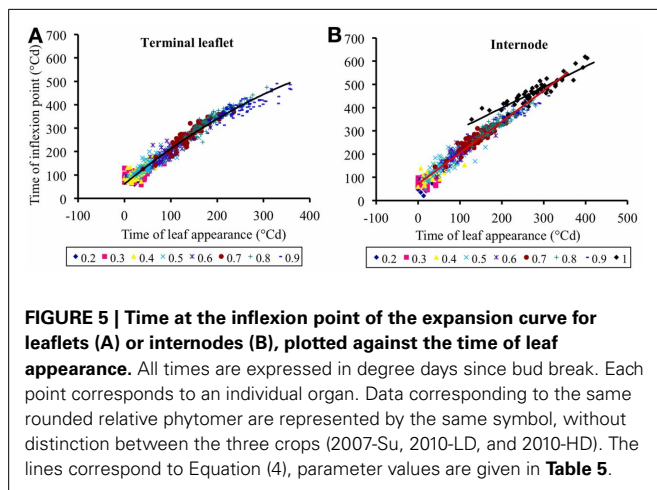

FIGURE 5 | Time at the inflexion point of the expansion curve for leaflets (A) or internodes (B), plotted against the time of leaf appearance. All times are expressed in degree days since bud break. Each point corresponds to an individual organ. Data corresponding to the same rounded relative phytomer are represented by the same symbol, without distinction between the three crops (2007-Su, 2010-LD, and 2010-HD). The lines correspond to Equation (4), parameter values are given in **Table 5**.

Table 4 | Values of the model parameters used in the reference scenario (S_0) other than those obtained by the LOESS method (see Table 5).

Parameter	Equation	Value
$\delta_{lea,0}$ (°Cd)	4.1	61.5
$\delta_{lea,1}$	4.1	1.62
$\delta_{lea,2}$ (°Cd^{-1})	4.1	−0.00113
$\delta_{int,0}$ (°Cd)	4.2	70.6
$\delta_{int,1}$	4.2	1.34
$\delta_{ped,0}$ (°Cd)	4.3	220
$\delta_{ped,1}$	4.3	0.893

Table 5 | Model parameters: values of $w_k^m(i)$, $t_k^0(i)$, and $L_k^m(i)$ estimated from the experimental data by the LOESS method.

Relative rank	Terminal leaflets			Internodes		
	$w_{lea}^m(i) \times 10^3$ (°Cd)	$t_{lea}^0(i)$ (°Cd)	$L_{lea}^m(i)$ (mm)	$w_{int}^m(i) \times 10^3$ (°Cd)	$t_{int}^0(i)$ (°Cd)	$L_{int}^m(i)$ (mm)
0.0						5.9
0.05						7.0
0.1					23.7	9.0
0.15	7.39	74.7	19.6		38.8	10.4
0.2	7.16	82.4	27.1	11.72	54.9	11.7
0.25	6.94	89.7	34.3	10.99	70.5	12.5
0.3	6.72	97.1	41.5	10.35	86.1	13.0
0.35	6.53	105.0	46.9	9.76	100.4	13.3
0.4	6.31	116.6	52.5	9.27	118.8	14.6
0.45	6.11	132.9	55.3	8.88	138.8	16.1
0.5	5.93	154.3	57.8	8.66	162.6	17.9
0.55	5.78	180.7	60.1	8.76	189.4	20.4
0.6	5.66	211.6	62.7	8.86	217.7	23.4
0.65	5.56	250.3	65.9	8.95	250.3	28.2
0.7	5.53	281.9	68.4	8.97	277.0	31.7
0.75	5.54	313.6	71.1	8.94	306.1	33.6
0.8	5.60	340.2	73.1	8.77	334.8	32.4
0.85	5.70	362.6	73.4	8.43	363.9	26.1
0.9	5.79	381.4	72.2	7.94	394.6	14.4
0.93	5.84	393.3	71.4	7.34	414.2	8.0
1.0				5.19	457.6	52.7

$w_k^m(i)$ is used in scenarios S_0, S_1 and S_2; $t_k^0(i)$ is used in scenarios S_1 and S_2; $L_k^m(i)$ is used in scenario S_2.

different phytomer positions, for both leaflets (**Figure 7A**) and internodes (**Figure 7B**).

Scenario 1 was designed to assess model accuracy assuming that the time at which expansion occurred depended only on phytomer position, rather than being estimated, as in S_0, from an input variable. The parameters of S_1 are given in **Table 5**. In S_1, the RMSEP for all ranks together was 8.6 mm for leaflets and 4.5 mm for internodes (14.2 and 18.2% of final lengths, respectively). The RMSEP calculated for each phytomer position increased from the base to the top of the shoot (**Figure 7**). This was due to an increase in variability between plants for mid-expansion time, from the base to the top of the shoot (**Figure 5**). The optimal scenario would thus involve estimating the time at mid-expansion from a value dependent only on relative rank for basal phytomer positions and from measurements of leaf appearance time for more central and apical positions. In practical terms, this would decrease measurement time with respect to S_0, because the leaf-like structures at the base of the shoot are the most difficult to observe.
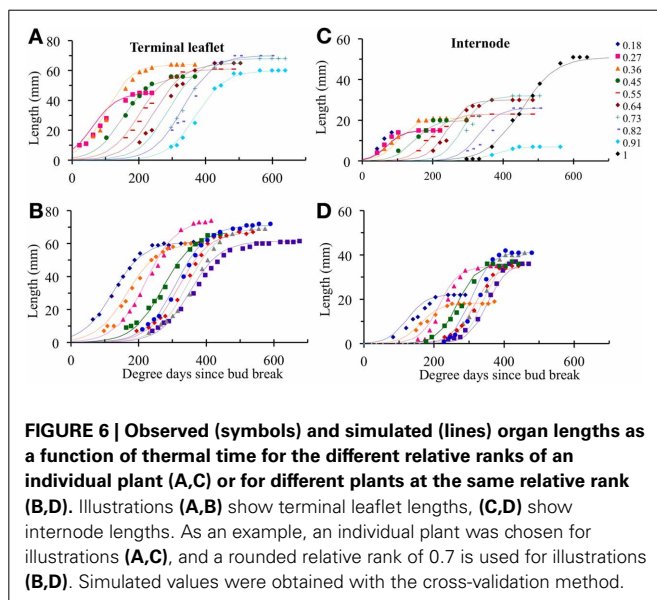

FIGURE 6 | Observed (symbols) and simulated (lines) organ lengths as a function of thermal time for the different relative ranks of an individual plant (A,C) or for different plants at the same relative rank (B,D). Illustrations **(A,B)** show terminal leaflet lengths, **(C,D)** show internode lengths. As an example, an individual plant was chosen for illustrations **(A,C)**, and a rounded relative rank of 0.7 is used for illustrations **(B,D)**. Simulated values were obtained with the cross-validation method.
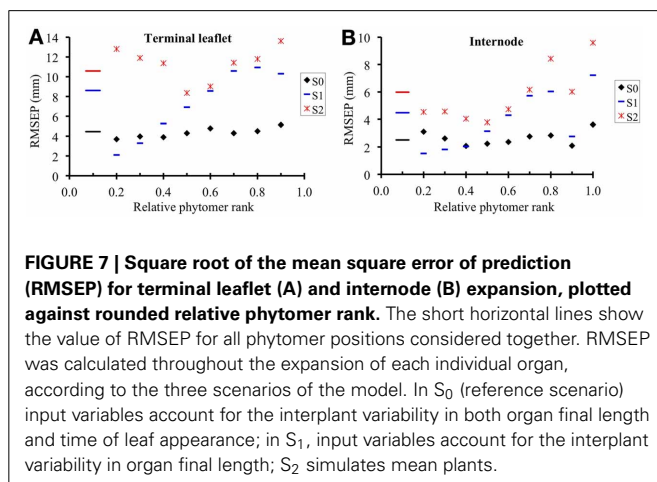

FIGURE 7 | Square root of the mean square error of prediction (RMSEP) for terminal leaflet (A) and internode (B) expansion, plotted against rounded relative phytomer rank. The short horizontal lines show the value of RMSEP for all phytomer positions considered together. RMSEP was calculated throughout the expansion of each individual organ, according to the three scenarios of the model. In S_0 (reference scenario) input variables account for the interplant variability in both organ final length and time of leaf appearance; in S_1, input variables account for the interplant variability in organ final length; S_2 simulates mean plants.

Scenario 2 simulates the kinetics of expansion of plants differing only in terms of phytomer number. The parameters of S_2 are given in **Table 5**. For S_2, RMSEP was calculated by plant, so the comparison of the RMSEP values for S_0 and S_2 provides an estimate of the gain in accuracy when a scenario accounting for interplant variability (S_0) is used to simulate the expansion kinetics of a heterogeneous crop over a scenario reproducing n mean plants. In S_2, RMSEP for all ranks together was 10.6 mm (17.4 %) for leaflets and 6.0 mm (24.2%) for internodes, these values being 2.4 times higher than those for S_0. This loss of accuracy for S_2 with respect to S_0 concerned all phytomer positions (**Figure 7**). It should be borne in mind that the method used to calculate MSEP does not aim to assess the ability of S_2 to simulate a mean plant, because simulated lengths were not compared with mean observed lengths.

DISCUSSION

The aim of this study was to assess the kinetics of expansion of rose bush primary shoot internodes and leaves and to propose an empirical model reproducing organ expansion kinetics from non-destructive, easy-to-measure variables. Bush roses are ornamental and are sold as individual plants. We therefore, paid particular attention to interplant variability in expansion kinetics and to the ability of the model to simulate this variability.

GROWING CONDITIONS AND INTER- AND INTRA-CROP VARIABILITY

We studied expansion in three crops (2007-Su, 2010-LD, and 2010-HD) subjected to different growing conditions, contrasting in terms of incident PAR, humidity and plant density in particular, to ensure that we obtained robust results. Contrasted experimental conditions were used to find regularities in expansion kinetics, but not to establish quantitative relationships between architectural traits and environmental factors, such as density, light intensity or quality. This would require specific experiments. The large differences in PAR interception between densities in 2010 (**Table 1**) suggest that light quality in the canopies, including the red-far red ratio in particular, differs between plant densities. These differences in growing conditions resulted in significant differences between crops in terms of the mean values of architectural variables. Within each growing condition, the plants also displayed considerable variability. This level of interplant variability is typical of rose bush crops. This variability was observed although we selected cuttings to reduce heterogeneity due to topophysis (Bredmose et al., 2001) and differences in cutting leaf area (Costa and Heuvelink, 2003).

AT ANY TIME DURING EXPANSION, THE DIMENSIONS OF THE WHOLE LEAF CAN BE RECONSTITUTED FROM TERMINAL LEAFLET LENGTH

Our results show that it is possible to reconstitute the dimensions of the different leaflets of a rose leaf from a single dimension at any time during leaf expansion, given the number of leaflets per leaf. These results generalize those of Gao et al. (2012), who established that, for fully expanded leaves, total leaf area could be inferred from one leaf dimension and number of leaflets, within a genotype. The allometric relationships using terminal leaflet length as a predictor of either whole leaf area (presented here, section Terminal Leaflet Length can be Used to Simulate the Dimensions

of all Leaflets Within a Leaf) or leaflet dimensions (Demotes-Mainard et al., 2009) should probably be established for each genotype. Indeed, only relationships based on the product of length by width have been found to be stable across a range of genotypes, both at the leaflet level (Rouphael et al., 2010) and the leaf level (Gao et al., 2012), because the shape of leaflets and their insertion position along the rachis (loose or close) vary between genotypes.

STABILITY OF ORGAN EXPANSION DURATION AND VARIABILITY OF FINAL ORGAN SIZE

Differences in organ final size between phytomer positions and between plants at a given position resulted mainly from differences in maximal expansion rate, rather than expansion duration. This is similar to the behavior of other species. For example, whereas final leaf and internode size widely varies between phytomers along the main shoot, organ expansion duration little varies in narrow-leafed lupin (Dracup and Kirby, 1993) and is stable in arabidopsis (Mündermann et al., 2005). At a given phytomer position, expansion duration is stable in thermal time between plants grown in contrasted growing conditions for sunflower leaves (Granier and Tardieu, 1998; Dosio et al., 2003), sorghum leaves (Lafarge and Tardieu, 2002) and internodes (Xue et al., 2012). In tall fescue and wheat, expansion duration is more stable if expressed in phyllochronic time (thermal time divided by the phyllochron) than if expressed in thermal time (Fournier et al., 2005). This stability in phyllochronic time has been interpreted as an emerging property of a self-regulated system, in which the appearance of an organ triggers changes in expansion (Fournier et al., 2005; Verdenal et al., 2008). Under this hypothesis, the link between phyllochron and duration results from a large proportion of expansion occurring when the leaf is still in the whorl generated by previous leaves.

In rose bush, as in many other species (for example lupin, Dracup and Kirby, 1993; wheat, Evers et al., 2005; cucumber, Kahlen, 2006; sorghum, Xue et al., 2012), there was a general gradient of final organ length with phytomer relative rank common to all three crops and plants. This gradient can be used to model a mean plant, as in scenario S_2. However, this gradient varied between individual plants: a plant with a high (or low) leaflet or internode final length at a particular phytomer position did not systematically present a high (or low) length at the next phytomer. This was unexpected, at least for basal phytomer positions. Indeed, during their expansion basal phytomers depend on the cutting, both for nitrogen, which is provided by remobilization (Cabrera, 2003) and for photosynthesis (Costa and Heuvelink, 2003). In addition, on average eight phytomers closest to the base of the plant are preformed in the bud in the variety studied here (Girault et al., 2008), suggesting that they may be influenced similarly by the physiological state of the mother stem. We therefore, assume that the differences in leaflet or internode final size between plants may reflect differences in the phylloclimate perceived by the organs during their expansion. Indeed, final size is dependent, in several species, on phylloclimate (or climate) at the time of organ expansion (Granier and Tardieu, 1999, for sunflower leaves; Gautier et al., 2000, for white clover internodes, petioles and leaves; Andrieu et al., 2004, for maize leaves; Kahlen

and Stützel, 2011, for cucumber internodes). Our model could be used to test this hypothesis, by accurately defining the timing of individual organ expansion.

MODELING THE EXPANSION OF INDIVIDUAL PRIMARY SHOOTS

We developed a model reproducing the kinetics of leaflet and internode expansion on rose bush primary shoots, based on non-destructive and easy-to-measure input variables. The comparison of the three scenarios showed that, to reproduce accurately the variability of expansion within a crop, it was necessary to measure the final lengths of terminal leaflets and internodes and to count the number of phytomers per shoot and of leaflets per leaf, all of which can be done after the final primary shoot has ceased to elongate. The timing of leaf appearance must also be established, at least for leaves in the middle and upper part of the shoot, as fixed values of time at mid-expansion can be used for the basal phytomers. These data are easy to acquire, but their acquisition is labor-intensive. The model based on these input variables satisfactorily simulated the diversity of individual plants. For eco-physiological studies, this model will make it possible to relate traits of interest measured on specific plants to features of expansion for the same plants, which is important for experimental crops with high levels of interplant variability.

In order to represent architectural development, our model of organ expansion can be easily integrated in a FSPM of rose bush using L-systems. The addition of a three-dimensional structure to the expansion model implies to model organs' shape and spatial position, as done for FSPMs of other species (e.g., Evers et al., 2005; Mündermann et al., 2005; Kahlen et al., 2008). This 3D model would provide essential information to study the environmental regulation of bud break, which strongly influences plant architecture and still remains a major research area (Domagalska and Leyser, 2011). Indeed, when coupled with a light model, the model will give information about light phylloclimate, which is a key factor controlling bud break through carbohydrate availability (Girault et al., 2010; Henry et al., 2011; Rabot et al., 2012), and light quality (Mor and Halevy, 1984; Girault et al., 2008). In rose bush, there is considerable interplant variability in the number and position of buds breaking along the primary shoot (for instance, in 2007-Su between 2 and 8 buds outgrew on primary shoots with the same number of axillary buds). It may therefore, be particularly relevant to be able to investigate the relationships between light phylloclimate and bud break at the level of individual plants.

The differences in organ expansion kinetics between plants within a relative rank resulted mainly from differences in maximal expansion rate, rather than differences in expansion duration. This had two related implications, which were used in the model. Firstly, variations in organ final size were sufficient to capture interplant variability in size at any time during expansion, within a relative rank, as in scenarios S_0 and S_1. Secondly, in the model, the term $w_k^m(i)$, which is inversely proportional to expansion duration, can be predicted from a single value common to all plants within a relative rank with little loss of accuracy (all scenarios). In the model the term $w_k^m(i)$ depends on relative rank. However, the variations of expansion duration

between phytomer positions were moderate for terminal leaflets and for vegetative internodes. In scenario S_0, if $w_k^m(i)$ was replaced by only three values, one common to all terminal leaflets ($w_{lea}^m = 5.96 \times 10^{-3}\,°\text{Cd}$), one common to all vegetative internodes ($w_{int}^m = 9.04 \times 10^{-3}\,°\text{Cd}$) and one for peduncles ($w_{ped}^m = 5.17 \times 10^{-3}\,°\text{Cd}$), the accuracy of the model remained the same (RMSEP = 7.4 and 10.2% of final length, for terminal leaflets and internodes, respectively, data not shown) as with $w_k^m(i)$. Thus, if the model has to be calibrated for a new genotype, this process could be simplified by estimating the model parameters from a limited number of phytomer positions.

The time of leaf appearance has been used in several architectural models for the prediction of ontogenic development (for example in wheat: Fournier et al., 2003; Evers et al., 2005; in cucumber: Kahlen, 2006; in ryegrass: Verdenal et al., 2008). In our model, we used this parameter in the reference scenario S_0 to predict the mid-expansion time for both leaflets and internodes. This coordinates expansion between different phytomer positions for the same kind of organ, and between leaflets and internodes.

CONCLUSION

This work provides insight into the kinetics of expansion at the level of individual organs that was lacking for rose bush. It is original in that it considers interplant variability, which has been little studied, in any plant species. This variability is important for rose bushes, because crops display high levels of interplant variability for architecture and the commercial product is the individual plant. On the basis of these results, we propose an empirical model that accurately reproduces, for individual plants, the expansion kinetics of primary shoots from non-destructive input variables. Even in its current state, this model already provides a useful tool for studying ecophysiological processes, such as bud break response to light phylloclimate, because a primary shoot constitutes an interesting model of the whole plant, with simple interactions between organs. With a view to studying rose bush architecture, these results can be used as a grid for analyzing the expansion of shoots resulting from branching, and for investigating genotype differences.

ACKNOWLEDGMENTS

REFERENCES

Andrieu, B., Moulia, B., Maddonni, G., Birch, C., Sonohat, G., Sohbi, Y., et al. (2004). "Plasticity of plant architecture in response to density: using maize as a model," in *IV International Workshop on Functional Structural Plant Models (FSMP04)*, ed C. Godin (Montpellier: UMR AMAP), 141–145.

Ashok, A. D., and Rengasamy, P. (2000). Effect of nitrogen fertigation at different levels and sources on the growth of cut rose cv. First Red under greenhouse conditions. *South Indian Hortic.* 48, 139–141.

Baccar, R., Fournier, C., Dornbusch, T., Andrieu, B., Gouache, D., and Robert, C. (2011). Modelling the effect of wheat canopy architecture as affected by sowing density on Septoria tritici epidemics using a coupled epidemic-virtual plant model. *Ann. Bot.* 108, 1179–1194. doi: 10.1093/aob/mcr126

Boumaza, R., Demotes-Mainard, S., Huché-Thellier, L., and Guérin, V. (2009). Visual characterization of the esthetic quality of the rosebush. *J. Sens. Stud.* 24, 774–796. doi: 10.1111/j.1745-459X.2009.00238.x

Boumaza, R., Huche-Thelier, L., Demotes-Mainard, S., Le Coz, E., Leduc, N., Pelleschi-Travier, S., et al. (2010). Sensory profiles and preference analysis in ornamental horticulture: the case of the rosebush. *Food Qual. Prefer.* 21, 987–997. doi: 10.1016/j.foodqual.2010.05.003

Bredmose, N. (1993). Effects of year-round supplementary lighting on shoot development, flowering and quality of two glasshouse rose cultivars. *Sci. Hortic.* 54, 69–85. doi: 10.1016/0304-4238(93)90084-4

Bredmose, N., Hansen, J., and Nielsen, J. (2001). "Topophysic influences on rose bud and shoot growth and flower development are determined by endogenous axillary bud factors," in *III International Symposium on Rose Research and Cultivation*, eds N. Zieslin and H. Agbaria (Herzliya: International Society Horticultural Science), 177–183.

Buck-Sorlin, G., De Visser, P. H., Henke, M., Sarlikioti, V., van der Heijden, G. W., Marcelis, L. F., et al. (2011). Towards a functional-structural plant model of cut-rose: simulation of light environment, light absorption, photosynthesis and interference with the plant structure. *Ann. Bot.* 108, 1121–1134. doi: 10.1093/aob/mcr190

Cabrera, R. I. (2003). Nitrogen balance for two container-grown woody ornamental plants. *Sci. Hortic.* 97, 297–308. doi: 10.1016/S0304-4238(02)00151-6

Chelle, M. (2005). Phylloclimate or the climate perceived by individual plant organs: what is it? How to model it? What for? *New Phytol.* 166, 781–790. doi: 10.1111/j.1469-8137.2005.01350.x

Costa, J. M., and Heuvelink, E. (2003). "Modelling growth of the primary shoot of rose," in *Proceedings of the International Workshop on Models for Plant Growth and Control of Product Quality in Horticultural Production*, eds M. Fink and C. Feller (Postdam: International Society Horticultural Science), 279–285.

Dayan, E., Presnov, E., and Fuchs, M. (2004). Prediction and calculation of morphological characteristics and distribution of assimilates in the ROSGRO model. *Math. Comput. Simul.* 65, 101–116. doi: 10.1016/j.matcom.2003.09.021

Demotes-Mainard, S., Guéritaine, G., Boumaza, R., Favre, P., Guérin, V., Huché-Thellier, L., et al. (2009). "Coordinated development of the architecture of the primary shoot in bush rose," in *PMA09: The Third International Symposium on Plant Growth Modeling, Simulation, Visualization and Applications*, IEEE Computer Society, eds B. Li, M. Jaeger, and Y. Guo (Beijing: IEEE), 214–221. doi: 10.1109/PMA.2009

Demotes-Mainard, S., Huché-Thélier, L., Morel, P., Boumaza, R., Guérin, V., and Sakr, S. (2013). Temporary water restriction or light intensity limitation promotes branching in rose bush. *Sci. Hortic.* 150, 432–440. doi: 10.1016/j.scienta.2012.12.005

Domagalska, M. A., and Leyser, O. (2011). Signal integration in the control of shoot branching. *Nat. Rev. Mol. Cell Biol.* 12, 211–221. doi: 10.1038/nrm3088

Dosio, G. A., Rey, H., Lecoeur, J., Izquierdo, N. G., Aguirrezabal, L. A., Tardieu, F., et al. (2003). A whole-plant analysis of the dynamics of expansion of individual leaves of two sunflower hybrids. *J. Exp. Bot.* 54, 2541–2552. doi: 10.1093/jxb/erg279

Dracup, M., and Kirby, E. J. M. (1993). Patterns of growth and development of leaves and internodes of narrow-leafed lupin. *Field Crops Res.* 34, 209–225. doi: 10.1016/0378-4290(93)90008-B

Evers, J., Vos, J., Fournier, C., Andrieu, B., Chelle, M., and Struik, P. (2005). Towards a generic architectural model of tillering in Gramineae, as exemplified by spring wheat (Triticum aestivum). *New Phytol.* 166, 801–812. doi: 10.1111/j.1469-8137.2005.01337.x

Fournier, C., Andrieu, B., Ljutovac, S., and Saint-Jean, S. (2003). "ADEL-Wheat: a 3D Architectural model of wheat development,"

in *International Symposium on Plant Growth Modeling, Simulation, Visualization and Their Applications*, eds B.G. Hu and M. Jaeger (Beijing: Tsinghua University Press, Springer Verlag), 54–63.

Fournier, C., Durand, J., Ljutovac, S., Schäufele, R., Gastal, F., and Andrieu, B. (2005). A functional-structural model of elongation of the grass leaf and its relationships with the phyllochron. *New Phytol.* 166, 881–894. doi: 10.1111/j.1469-8137.2005.01371.x

Gao, M., van der Heijden, G. W. A. M., Vos, J., Eveleens, B. A., and Marcelis, L. F. M. (2012). Estimation of leaf area for large scale phenotyping and modeling of rose genotypes. *Sci. Hortic.* 138, 227–234. doi: 10.1016/j.scienta.2012.02.014

Gautier, H., Mech, R., Prusinkiewicz, P., and Varlet-Grancher, C. (2000). 3D architectural modelling of aerial photomorphogenesis in white Clover (*Trifolium repens* L.) using L-systems. *Ann. Bot.* 85, 359–370. doi: 10.1006/anbo.1999.1069

Girault, T., Abidi, F., Sigogne, M., Pelleschi-Travier, S., Boumaza, R., Sakr, S., et al. (2010). Sugars are under light control during bud burst in Rosa sp. *Plant Cell Environ.* 33, 1339–1350. doi: 10.1111/j.1365-3040.2010.02152.x

Girault, T., Bergougnoux, V., Combes, D., Viemont, J. D., and Leduc, N. (2008). Light controls shoot meristem organogenic activity and leaf primordia growth during bud burst in Rosa sp. *Plant Cell Environ.* 31, 1534–1544. doi: 10.1111/j.1365-3040.2008.01856.x

Granier, C., and Tardieu, F. (1998). Is thermal time adequate for expressing the effects of temperature on sunflower leaf development? *Plant Cell Environ.* 21, 695–703. doi: 10.1046/j.1365-3040.1998.00319.x

Granier, C., and Tardieu, F. (1999). Leaf expansion and cell division are affected by reducing absorbed light before but not after the decline in cell division rate in the sunflower leaf. *Plant Cell Environ.* 22, 1365–1376. doi: 10.1046/j.1365-3040.1999.00497.x

Henry, C., Rabot, A., Laloi, M., Mortreau, E., Sigogne, M., Leduc, N., et al. (2011). Regulation of RhSUC2, a sucrose transporter, is correlated with the light control of bud burst in Rosa sp. *Plant Cell Environ.* 34, 1776–1789. doi: 10.1111/j.1365-3040.2011.02374.x

Hopper, D. A., and Hammer, P. A. (1991). Regression models describing *Rosa hybrida* response to day/night temperature and photosynthetic photon flux. *J. Am. Soc. Hortic. Sci.* 116, 609–617.

Hopper, D. A., Hammer, P. A., and Wilson, J. R. (1994). A simulation model of *Rosa hybrida* growth response to constant irradiance and day and night temperatures. *J. Am. Soc. Hortic. Sci.* 119, 903–914.

Huché-Thélier, L., Boumaza, R., Demotes-Mainard, S., Canet, A., Symoneaux, R., Douillet, O., et al. (2011). Nitrogen deficiency increases basal branching and modifies visual quality of the rose bushes. *Sci. Hortic.* 130, 325–334. doi: 10.1016/j.scienta.2011.07.007

Kahlen, K. (2006). "3D architectural modelling of greenhouse cucumber (Cucumis sativus L.) using L-systems," in *Proceedings of the IIIrd International Symposium on Models for Plant Growth, Environmental Control and Farm Management in Protected Cultivation Hortimodel 2006, International Society Horticultural Science*, eds L. F. M. Marcelis, G. Van Straten, C. Stanghellini, and E. Heuvelink (Wageningen), 51–58.

Kahlen, K., and Stützel, H. (2011). Modelling photo-modulated internode elongation in growing glasshouse cucumber canopies. *New Phytol.* 190, 697–708. doi: 10.1111/j.1469-8137.2010.03617.x

Kahlen, K., Wiechers, D., and Stuetzel, H. (2008). Modelling leaf phototropism in a cucumber canopy. *Funct. Plant Biol.* 35, 876–884. doi: 10.1071/FP08034

Lafarge, T., and Tardieu, F. (2002). A model co-ordinating the elongation of all leaves of a sorghum cultivar was applied to both Mediterranean and Sahelian conditions. *J. Exp. Bot.* 53, 715–725. doi: 10.1093/jexbot/53.369.715

Lieth, J. H., and Pasian, C. C. (1991). A simulation model for the growth and development of flowering rose shoots. *Sci. Hortic.* 46, 109–128. doi: 10.1016/0304-4238(91)90097-I

Linhart, H., and Zucchini, W. (1986). *Model Selection*. New York, NY: John Wiley and Sons.

Maas, F. M., and Bakx, E. J. (1995). Effects of light on growth and flowering of *Rosa hybrida* 'Mercedes'. *J. Am. Soc. Hortic. Sci.* 120, 571–576.

Mor, Y., and Halevy, A. H. (1984). Dual effect of light on flowering and sprouting of rose shoots. *Physiol. Plant.* 61, 119–124. doi: 10.1111/j.1399-3054.1984.tb06110.x

Morel, P., Crespel, L., Galopin, G., and Moulia, B. (2012). Effect of mechanical stimulation on the growth and branching of garden rose. *Sci. Hortic.* 135, 59–64. doi: 10.1016/j.scienta.2011.12.007

Morel, P., Galopin, G., and Dones, N. (2009). Using architectural analysis to compare the shape of two hybrid tea rose genotypes. *Sci. Hortic.* 120, 391–398. doi: 10.1016/j.scienta.2008.11.039

Morisot, A. (1996). 'PP.Rose': an empirical model to predict the potential yield of cut roses. *Acta Hortic.* 424, 87–93.

Mündermann, L., Erasmus, Y., Lane, B., Coen, E., and Prusinkiewicz, P. (2005). Quantitative modeling of arabidospsis development. *Plant Physiol.* 139, 960–968. doi: 10.1104/pp.105.060483

Oki, L. R., Mattson, N. S., and Lieth, J. H. (2006). "Predicting stem length of cut flower roses at harvest using stem elongation rates in relationship to developmental events," in *III International Symposium on Models for Plant Growth, Environmental Control and Farm Management in Protected Cultivation (HortiModel 2006)*, eds L. F. M. Marcelis, G. Van Straten, C. Stanghellini, and E. Heuvelink (Wageningen: International Society for Horticultural Science), 113–120.

Rabot, A., Henry, C., Ben Baaziz, K., Mortreau, E., Azri, W., Lothier, J., et al. (2012). Insight into the role of sugars in bud burst under light in the rose. *Plant Cell Physiol.* 53, 1068–1082. doi: 10.1093/pcp/pcs051

Rajapakse, N. C., and Kelly, J. W. (1994). Influence of spectral filters on growth and postharvest quality of potted miniatures roses. *Sci. Hortic.* 56, 245–255. doi: 10.1016/0304-4238(94)90006-X

Rouphael, Y., Mouneimne, A. H., Ismail, A., Mendoza-De Gyves, E., Rivera, C. M., and Colla, G. (2010). Modeling individual leaf area of rose (*Rosa hybrida* L.) based on leaf length and width measurement. *Photosynthetica* 48, 9–15. doi: 10.1007/s11099-010-0003-x

Verdenal, A., Combes, D., and Escobar-Gutierrez, A. J. (2008). A study of ryegrass architecture as a self-regulated system, using functional-structural plant modelling. *Funct. Plant Biol.* 35, 911–924. doi: 10.1071/FP08050

Xue, S., Han, D. Q., Yu, Y. J., Steinberger, Y., Han, L. P., and Xie, G. H. (2012). Dynamics in elongation and dry weight of internodes in sweet sorghum plants. *Field Crops Res.* 126, 37–44. doi: 10.1016/j.fcr.2011.09.014

Yang, S., Logan, J., and Coffey, D. L. (1995). Mathematical formulae for calculating the base temperature for growing degree days. *Agric. For. Meteorol.* 74, 61–74. doi: 10.1016/0168-1923(94)02185-M

Modeling branching in cereals

Jochem B. Evers* and Jan Vos

Centre for Crop Systems Analysis, Wageningen University, Wageningen, Netherlands

Cereals and grasses adapt their structural development to environmental conditions and the resources available. The primary adaptive response is a variable degree of branching, called tillering in cereals. Especially for heterogeneous plant configurations the degree of tillering varies per plant. Functional–structural plant modeling (FSPM) is a modeling approach allowing simulation of the architectural development of individual plants, culminating in the emergent behavior at the canopy level. This paper introduces the principles of modeling tillering in FSPM, using (I) a probability approach, forcing the dynamics of tillering to correspond to measured probabilities. Such models are particularly suitable to evaluate the effect structural variables on system performance. (II) Dose–response curves, representing a measured or assumed response of tillering to an environmental cue. (III) Mechanistic approaches to tillering including control by carbohydrates, hormones, and nutrients. Tiller senescence is equally important for the structural development of cereals as tiller appearance. Little study has been made of tiller senescence, though similar concepts seem to apply as for tiller appearance.

Keywords: functional–structural plant modeling, cereal, grass, branching, tillering, tillering probability, dose–response curve, mechanistic modeling

INTRODUCTION

Production of branches (tillering) is an important trait of many cereal plants such as wheat (*Triticum aestivum*) and rice (*Oryza* species). Cereal plants are able to maximize total plant light capture and grain production through processes such as bud dormancy break, tiller development, and tiller senescence. These processes are highly plastic: the growing conditions a cereal plant experiences strongly influence the tillering characteristics of the plant (e.g., Casal et al., 1990; Rodríguez et al., 1999; Lafarge and Hammer, 2002; Evers et al., 2006; Sparkes et al., 2006). At high population densities, bud break is generally low and tiller mortality is relatively high (Darwinkel, 1978).

Most crop growth models of cereals, which aim at predicting grain production on an area basis, do not take into consideration the plant's response to environmental conditions in terms of tiller production (Jamieson et al., 1998). For many scenarios this is not a problem, since within a common range of agronomical practice (population density, row distance) leaf area and ear production is rather predictable and stable when expressed per unit of ground area. However, accurate prediction of variables such as light interception and ear production becomes more difficult in the case of more heterogeneous canopy configurations, such as in intercropping systems (Li et al., 2001), wide-row crop systems (Winter and Welch, 1987), and in crops that show erratic emergence and establishment. Such non-uniform leaf area distribution is difficult to represent in most crop models, leading to inaccuracies in predictions of crop growth.

Here, we review the possibilities to simulate branch production in cereals using a plant architectural modeling technique: functional–structural plant modeling (FSPM; Vos et al., 2010; DeJong et al., 2011; Evers et al., 2011). Using FSPM, tiller production and senescence can be evaluated for every individual plant in the canopy. This results in an accurate three-dimensional representation of canopy development over time. In this paper, we show how tiller appearance and senescence can be represented in FSPM and how internal and environmental regulation of tillering can be implemented.

MODELING CEREAL ARCHITECTURE

Leaves are provided with tiller buds in their axils, which only produce a branch if circumstances are favorable. Therefore, the composition of the vegetative cereal phytomer is always the same: an internode, a leaf (sheath and lamina), and an axillary bud (McMaster, 2005; Forster et al., 2007). Modeling cereal architecture starts with the phytomer which, in classic L-system notation (Prusinkiewicz and Lindenmayer, 1990), can be represented by a string of characters B (tiller bud), I (internode), N (node), S (sheath) and L (lamina):

$$[B] I N [S L]$$

where the brackets represent structures forking off the main axis such as leaves and branches. A typical L-system rewriting rule (Prusinkiewicz and Lindenmayer, 1990) that represents the creation of new phytomers by the apical meristem (A) is:

$$A \Rightarrow [B] I N [S L] A \qquad (1)$$

Starting with only A, and applying the rewriting rule three times will result in a stem segment consisting of three phytomers and a shoot apical meristem at the top, represented by the string:

$$[B] I N [S L][B] I N [S L][B] I N [S L] A$$

which could be represented graphically as shown in **Figure 1A**. As the shoot develops and under favorable conditions, cereal shoots

FIGURE 1 | (A) Graphical representation of an L-system string containing three vegetative cereal phytomers with an apical meristem on top and **(B)** three vegetative cereal phytomers the lower two of which have grown a two-phytomer and one-phytomer tiller, respectively. L, lamina; S, sheath; I, internode; N, node; B, bud; A, apical

meristem. In **(B)**, sheaths and laminae (connected at the dashed lines) have been omitted for clarity. **(C,D)** Cereal architecture simulated using L-systems, using functional–structural plant modeling (FSPM): cereal plant in flowering stage with no tillers **(C)** and with four tillers **(D)**.

produce tillers in acropetal direction. An L-system rewriting rule that represents the change from a dormant bud to an actively developing shoot could simply look like:

$$B \Rightarrow A \qquad (2)$$
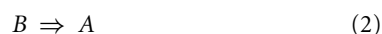
after which rule 1 could be applied to the newly created apex, to make the tiller develop like its parent shoot. In most cases tillering starts from the bottom-most phytomer, which is represented in **Figure 1B** for the case of a developing four-phytomer shoot with two developing tillers. In turn, the buds present on the first-order tillers can potentially produce tillers themselves. In this way higher-order tillers, which frequently occur in cereals, can be generated.

The representation of tillering above only considers the network of interconnected organs, i.e., the topology of the plant. To be able to simulate regulation of tiller appearance and senescence by internal and/or environmental factors, organ geometry needs to be considered as well. Geometrical characteristics such as internode length, blade size, shape and angle, shoot and leaf orientation determine factors like transport of compounds throughout the plant, and interception and scattering of light by the plant's organs. In FSPM, organ geometry can be taken into account explicitly, which, together with plant topology, allows for accurate three-dimensional representation of plant architecture (**Figures 1C,D**).

MODELING REGULATION OF TILLERING
PROBABILITY DISTRIBUTIONS
The number of tillers formed and senesced can be represented in an FSP model using a purely statistical, descriptive approach. To this end, each bud represented in the model is typically provided with a value for the probability it will break and form a

tiller, and the probability it will senesce before reaching maturity. At initiation of each bud the values for these parameters are chosen randomly from a distribution of values obtained experimentally. Typically, such distributions are determined for a range of population densities, nutrition levels or light levels. As such conditions are normally model input, an appropriate number of tillers will emerge upon model execution, mimicking tillering in real canopies (Watanabe et al., 2005; Evers et al., 2007b). This is fine in those cases where plant stands experiencing one certain set of conditions is being simulated, for example, for a particular population density or climate. Such simulated copies of real plant stands can subsequently be used, e.g., to assess the impact of cultivar leaf angle on rate soil covering, the light climate within the canopy during cereal crop development, the dispersion of fungi within a crop canopy, etc.

However, modeling of tillering using probability distributions becomes more cumbersome and less useful in case canopy configuration or environmental conditions are not uniform on an area basis. Such models based on single parameter distributions cannot represent tillering characteristics of border plants, especially in intercropping and wide-row systems. A solution could be to determine the local conditions per plant and provide the model with parameter distributions for all sets of local conditions occurring. A more elegant and simple solution to this problem is to use dose–response curves directly relating environment to tillering.

DOSE–RESPONSE CURVES
Tiller bud break and tiller senescence are known to directly depend on environmental conditions, such as soil phosphorus (e.g., Rodríguez et al., 1999; Dingkuhn et al., 2006) and nitrogen (Zhong et al., 2003; Alzueta et al., 2012), and the red/far-red ratio (R:FR) of the light within the canopy (e.g., Casal et al., 1987; Sparkes et al., 2006). To accurately describe the tillering response

of cereal plants to local light or nutrient conditions in an FSP model of cereal development, dose–response curves can be implemented. In FSPM such curves relate an environmental variable such as R:FR (Evers et al., 2007a) or multiple environmental variables such as both R:FR and light intensity (Gautier et al., 2000) to the probability of a tiller to start growing or to senesce. The shape of such a curve depends on the response observed experimentally. Dose–response curves may have diverse shapes (**Figure 2**).

In the case of light, an essential difference between models using probability distributions and those using response curves relating light to tillering is that the latter allow for tiller-environment feedback. Newly formed tillers and tillers that just senesced affect the light environment, possibly affecting appearance and senescence of other tillers on the same or neighboring plants. This feedback between tillering and the light climate in a canopy gives interesting opportunities for research questions in the domain of plant manipulation or other processes affecting plant architecture. Processes such as defoliation, thinning, or (partial) plant death due to diseases can be implemented in the FSP model, and the resulting effects on tillering behavior can be studied.

Dose–response curves enable the simulated plants to make their tillering behavior depend on local conditions. Plants at the border of a simulated plot will experience a different nutritional status of the soil (less belowground competition) and/or a different light climate (higher radiation intensity, higher R:FR), and will consequently produce more tillers compared to plants in the middle of the plot. Depending on which type of response curve was chosen, simulated tillering behavior may or may not realistically mimic actual observations (Evers et al., 2007a). Nevertheless, models simulating tiller appearance and senescence using response curves still merely *describe* tillering behavior rather than *explain* it. For research questions that focus on understanding how tillering is regulated, and what processes are involved and are interacting to result in the tillering patterns observed, another level of detail needs to be added.
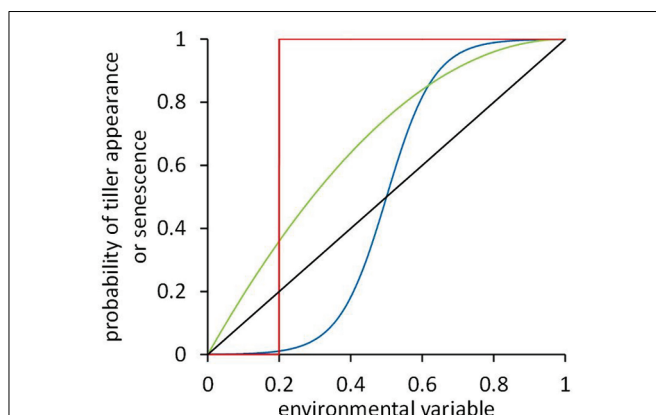

FIGURE 2 | Dose–response curves representing the response of tiller appearance or senescence probability to some environmental variable. Four hypothetical curves are shown: unit-step response with a threshold value of 0.2 (red line), a curvilinear response (green line), a sigmoidal response with an inflection point at 0.5 (blue line), and a linear response (black line).

MECHANISTIC MODELING OF TILLER APPEARANCE

The term mechanistic modeling is used for those models that incorporate mechanisms on one level of integration, and provide output at a higher level of integration. Such models aim at explaining the output based on the underlying mechanisms. Therefore, mechanistic models are usually capable of predicting also outside the ranges they were originally calibrated for. Tillering is controlled through many different mechanisms (Tomlinson and O'Connor, 2004; McSteen, 2009; Assuero and Tognetti, 2010). Here, we will consider three main groups of processes related to tillering control (regulation by carbohydrate availability, by hormones, and by macronutrients) to discuss mechanistic modeling of tillering.

Carbohydrate control

A bud needs carbohydrates to grow out into a tiller, making it a strong sink for carbohydrates. In case a plant experiences low light levels, or has many sink organs simultaneously, the ratio between the supply and demand for carbohydrates (the source/sink ratio) may be low. In such a case only a fraction of the buds will have the opportunity to grow a tiller. As a new tiller develops, it gradually changes its role from sink to source for carbohydrates, influencing the source/sink ratio of the whole plant. Next to their role as substrates for growth, carbohydrates have also been identified as signaling molecules for a host of physiological processes (sugar signaling; Rolland et al., 2006) which may affect tillering. Although most evidence of tillering control by carbohydrates either as growth substrates or as physiological signals is of correlative nature (Assuero and Tognetti, 2010), carbohydrates are undeniably needed for branch growth, so the source/sink ratio has been implemented widely in simulation models as a determinant of tillering and branching (Luquet et al., 2006; Tomlinson et al., 2007; Mathieu et al., 2009; Evers et al., 2010).

To implement carbohydrate control of tillering in an FSP model, processes related to carbohydrate supply and demand need to be incorporated. Carbohydrates supply is usually captured by implementing light absorption and photosynthesis routines at the level of the plant organ (Wernecke et al., 2007; Evers et al., 2010; Xu et al., 2011). Light absorption can be calculated using various approaches such as radiosity or ray-tracing (Chelle and Andrieu, 1999), which take into account reflection, transmission, and absorption of photosynthetically active radiation by all organs in the simulated canopy. The most popular photosynthesis submodel in FSPM and many other types of plant and crop model is the Farquhar–von Caemmerer–Berry (FvCB) biochemical photosynthesis model (Farquhar et al., 1980). The FvCB model can be calibrated easily using data from gas-exchange measurements. In FSPM, light absorption and photosynthesis simulation give carbohydrate supply at the organ level, which may differ between organs depending on their local light environment. A frequently used approach to modeling carbohydrate demand at the organ scale is the relative sink-strength approach (Heuvelink, 1996) which dictates that substrates are allocated to growing organs according to their relative sink strength, i.e., their potential growth rate (in units of substrate demanded per unit of time) proportional to the potential growth rate of the whole plant. The ratio between the total plant supply of carbohydrates as calculated from organ photosynthesis, and the total plant demand for carbohydrates calculated

as the sum of the potential growth rates of all organs requiring carbohydrates, is the source/sink ratio.

Instead of attempting to estimate the sink strength of individual buds, a threshold value of the source/sink ratio is often determined above which buds are allowed to form a tiller. Such a threshold may represent a physiological state analogous to sugar signaling (Luquet et al., 2006). A threshold value of 1.0 means that a tiller may develop in case the carbohydrate supply exceeds the demand. Lower or higher values may represent more opportunistic or conservative strategies toward tiller development, respectively.

Hormonal control

A complex system of hormonal interactions controls branch formation in general (Leyser, 2009; Domagalska and Leyser, 2011; Dun et al., 2012). To a large extent tillering is governed by the same processes, although there are small differences compared to dicots (McSteen, 2009; Assuero and Tognetti, 2010). Processes in branching control concern (long-distance) signaling by plant hormones auxin, strigolactone (both branching suppressors), and cytokinin (branching promotor) and are conserved between mono- and dicots. In grasses, ethylene and gibberellins also play a role (Rajala and Peltonen-Sainio, 2001; Frantz et al., 2004; Kebrom et al., 2013).

In order to simulate hormonal control of tillering using FSPM, processes such as hormone biosynthesis, transport, and decay need to be implemented. In their pioneering work, Prusinkiewicz et al. (2009) associated biosynthesis of auxin with modules representing the apex and the buds in a simple FSP model, and incorporated routines to calculate active (i.e., transporter-protein mediated) transport of auxin through the developing plant structure. Bud activation and subsequent branch development was an emerging property of the model, driven by auxin levels in the bud and the adjacent stem and by the feedback between the dynamics of auxin and transport-protein levels. This approach was adopted and extended to simulate R:FR control of hormone-regulated branching in *Arabidopsis* (Evers and Van der Krol, 2012). Similar approaches could be used to simulate cereal tillering as well. The current discussion on which hormonal factors are involved for branching control in grasses and dicots (Dun et al., 2012; Renton et al., 2012; Shinohara et al., 2013) provide good opportunities for FSPM to test hypotheses on branching and tillering control.

Nutrient control

Both soil nitrogen and phosphorus affect tillering in cereals (Rodríguez et al., 1999; Zhong et al., 2003; Dingkuhn et al., 2006; Alzueta et al., 2012). Soil nitrogen limitation can suppress branch growth directly (McIntyre, 2001) and through an effect on production of cytokinin (Tomlinson and O'Connor, 2004). Soil phosphorus limitation results in decreased branching (Kohlen et al., 2011) acting through hormone signaling by stimulating strigolactone production and transport within the plant.

Analogous to control by carbohydrates, simulation of tillering control by nutrients requires definition of nutrient supply, nutrient demand, and allocation of nutrients to demanding organs. Simulation of nutrient supply, i.e., uptake by the root system, itself can be done at various levels of detail. The simplest approach is to provide the simulated plant with nutrients each time step according to measured values of uptake. A far more elaborate

approach is to include the soil environment and development and growth of the root system architecture, making nutrient uptake dependent on root architecture, rooting depth and horizontal distribution, heterogeneity in soil nutrient distribution, uptake processes, etc. (Dunbabin et al., 2004; Pagès et al., 2004). In principle, nutrient demand and allocation can be included similar to carbohydrates, which would allow for simulation of both tiller production and tiller senescence.

MECHANISTIC MODELING OF TILLER SENESCENCE

Upon cessation of appearance of new tillers a phase sets in of cessation of growth and onset of senescence of part of the tillers. The number of appeared tillers represents an adaptation to the environment. A variable fraction of survival is another adaptation option, occurring somewhat later in the life cycle than cessation of tiller appearance. As mentioned, the same modeling paradigms can be applied to tiller senescence as to cessation of tiller appearance, i.e., from probability distributions, dose–response curves up to mechanistic modeling. Sparkes et al. (2006) associated the onset of tiller senescence with the drop below a critical value of R:FR ratio at the base of the canopy. Interestingly, this critical R:FR threshold was suggested to interact with leaf nitrogen content – where leaf nitrogen content is higher, the critical R:FR is lower. In other words, when more nitrogen is available, the canopy is allowed to grow larger before tiller death starts and vice versa. The carbohydrate source/sink ratio may proof to be a suitable concept to simulate tiller senescence but to our knowledge this has not been studied. Similar remarks apply to hormonal and nutrient control. For good reasons research has addressed mechanisms governing branching and tillering but for realistic modeling of the architectural dynamics of plants it is equally important to develop our understanding of the processes that govern senescence of tillers and branches.

CONCLUDING REMARKS

FSP models provide excellent opportunities to address questions related to tillering in cereals, its regulation, environmental response, and consequences at plant and canopy level. Explicitly including tillering in a model may improve predictions of leaf area development especially in non-uniform canopies such as those in intercropping or wide-row systems. The choice whether to simulate tillering using probabilities, driven by dose–response relationships or by underlying processes depends very much on the purpose of the modeling exercise. If the goal is to mimic the three-dimensional structure of a cereal canopy, to be used for instance in a light-interception study, modeling of tiller appearance and senescence using probabilities may be sufficient. When studying the dynamics of tillering itself, it is essential to include the feedback between environment and tillering in the model. In such cases dose–response curves or more mechanistic approaches are required, which have disadvantages of additional data requirement and computational costs. In any case, FSP models are capable of simulating tillering and the consequences for cereal architecture at a high level of detail using well-established and straightforward modeling techniques. As such, FSP models can seamlessly complement experimental studies on plant and canopy development.

REFERENCES

Alzueta, I., Abeledo, L. G., Mignone, C. M., and Miralles, D. J. (2012). Differences between wheat and barley in leaf and tillering coordination under contrasting nitrogen and sulfur conditions. *Eur. J. Agron.* 41, 92–102. doi: 10.1016/j.eja.2012.04.002

Assuero, S. G., and Tognetti, J. A. (2010). Tillering regulation by endogenous and environmental factors, and its agricultural management. *Am. J. Plant Sci. Biotechnol.* 4, 35–48.

Casal, J. J., Sánchez, R. A., and Deregibus, V. A. (1987). Tillering responses of *Lolium multiflorum* plants to changes of red/far-red ratio typical of sparse canopies. *J. Exp. Bot.* 38, 1432–1439. doi: 10.1093/jxb/38.9.1432

Casal, J. J., Sánchez, R. A., and Gibson, D. (1990). The significance of changes in the red/far-red ratio, associated with either neighbour plants or twilight, for tillering in *Lolium multiflorum* Lam. *New Phytol.* 116, 565–572. doi: 10.1111/j.1469-8137.1990.tb00540.x

Chelle, M., and Andrieu, B. (1999). Radiative models for architectural modelling. *Agronomie* 19, 225–240. doi: 10.1051/agro:19990304

Darwinkel, A. (1978). Patterns of tillering and grain production of winter wheat at a wide range of plant densities. *Neth. J. Agric. Sci.* 26, 383–398.

DeJong, T. M., Da Silva, D., Vos, J., and Escobar-Gutiérrez, A. J. (2011). Using functional–structural plant models to study, understand and integrate plant development and ecophysiology. *Ann. Bot.* 108, 987–989. doi: 10.1093/aob/mcr257

Dingkuhn, M., Luquet, D., Kim, H., Tambour, L., and Clement-Vidal, A. (2006). EcoMeristem, a model of morphogenesis and competition among sinks in rice. 2. Simulating genotype responses to phosphorus deficiency. *Funct. Plant Biol.* 33, 325–337. doi: 10.1071/FP05267

Domagalska, M. A., and Leyser, O. (2011). Signal integration in the control of shoot branching. *Nat. Rev. Mol. Cell Biol.* 12, 211–221. doi: 10.1038/nrm3088

Dun, E. A., De Saint Germain, A., Rameau, C., and Beveridge, C. A. (2012). Antagonistic action of strigolactone and cytokinin in bud outgrowth control. *Plant Physiol.* 158, 487–498. doi: 10.1104/pp.111.186783

Dunbabin, V., Rengel, Z., and Diggle, A. J. (2004). Simulating form and function of root systems: efficiency of nitrate uptake is dependent on root system architecture and the spatial and temporal variability of nitrate

supply. *Funct. Ecol.* 18, 204–211. doi: 10.1111/j.0269-8463.2004.00827.x

Evers, J. B., and Van der Krol, A. R. (2012). "Capturing hormonal and light interactions in a simulation model of shoot branching," in *Plant Growth Modelling, Simulation, Visualization and Applications - PMA12*, eds M. Kang, Y. Dumont, and Y. Guo (Beijing: IEEE), 101–108.

Evers, J. B., Van Der Krol, A. R., Vos, J., and Struik, P. C. (2011). Understanding shoot branching by modelling form and function. *Trends Plant Sci.* 16, 464–467. doi: 10.1016/j.tplants.2011.05.004

Evers, J. B., Vos, J., Andrieu, B., and Struik, P. C. (2006). Cessation of tillering in spring wheat in relation to light interception and red:far-red ratio. *Ann. Bot.* 97, 649–658. doi: 10.1093/aob/mcl020

Evers, J. B., Vos, J., Chelle, M., Andrieu, B., Fournier, C., and Struik, P. C. (2007a). Simulating the effects of localized red:far-red ratio on tillering in spring wheat (*Triticum aestivum*) using a three-dimensional virtual plant model. *New Phytol.* 176, 325–336. doi: 10.1111/j.1469-8137.2007.02168.x

Evers, J. B., Vos, J., Fournier, C., Andrieu, B., Chelle, M., and Struik, P. C. (2007b). An architectural model of spring wheat: evaluation of the effects of population density and shading on model parameterization and performance. *Ecol. Model.* 200, 308–320. doi: 10.1016/j.ecolmodel.2006.07.042

Evers, J. B., Vos, J., Yin, X., Romero, P., Van Der Putten, P. E. L., and Struik, P. C. (2010). Simulation of wheat growth and development based on organ-level photosynthesis and assimilate allocation. *J. Exp. Bot.* 61, 2203–2216. doi: 10.1093/jxb/erq025

Farquhar, G. D., von Caemmerer, S., and Berry, J. A. (1980). A biochemical model of photosynthetic CO_2 assimilation in leaves of C_3 species. *Planta* 149, 78–90. doi: 10.1007/BF00386231

Forster, B. P., Franckowiak, J. D., Lundqvist, U., Lyon, J., Pitkethly, I., and Thomas, W. T. B. (2007). The barley phytomer. *Ann. Bot.* 100, 725–733. doi: 10.1093/aob/mcm183

Frantz, J. M., Pinnock, D., Klassen, S., and Bugbee, B. (2004). Characterizing the environmental response of a gibberellic acid-deficient rice for use as a model crop. *Agron. J.* 96, 1172–1181. doi: 10.2134/agronj2004.1172

Gautier, H., Mĕch, R., Prusinkiewicz, P., and Varlet-Grancher, C. (2000). 3D architectural modelling of aerial

photomorphogenesis in white clover (*Trifolium repens* L.) using L-systems. *Ann. Bot.* 85, 359–370. doi: 10.1006/anbo.1999.1069

Heuvelink, E. (1996). Dry matter partitioning in tomato: validation of a dynamic simulation model. *Ann. Bot.* 77, 71–80. doi: 10.1006/anbo.1996.0009

Jamieson, P. D., Porter, J. R., Goudriaan, J., Ritchie, J. T., Van Keulen, H., and Stol, W. (1998). A comparison of the models AFRCWHEAT2, CERES-Wheat, Sirius, SUCROS2 and SWHEAT with measurements from wheat grown under drought. *Field Crops Res.* 55, 23–44. doi: 10.1016/S0378-4290(97)00060-9

Kebrom, T. H., Spielmeyer, W., and Finnegan, E. J. (2013). Grasses provide new insights into regulation of shoot branching. *Trends Plant Sci.* 18, 41–48. doi: 10.1016/j.tplants.2012.07.001

Kohlen, W., Charnikhova, T., Liu, Q., Bours, R., Domagalska, M. A., Beguerie, S., et al. (2011). Strigolactones are transported through the xylem and play a key role in shoot architectural response to phosphate deficiency in non-AM host *Arabidopsis thaliana*. *Plant Physiol.* 155, 974–987. doi: 10.1104/pp.110.164640

Lafarge, T. A., and Hammer, G. L. (2002). Tillering in grain sorghum over a wide range of population densities. Modelling dynamics of tiller fertility. *Ann. Bot.* 90, 99–110. doi: 10.1093/aob/mcf153

Leyser, O. (2009). The control of shoot branching: an example of plant information processing. *Plant Cell Environ.* 32, 694–703. doi: 10.1111/j.1365-3040.2009.01930.x

Li, L., Sun, J., Zhang, F., Li, X., Yang, S., and Rengel, Z. (2001). Wheat/maize or wheat/soybean strip intercropping: I. Yield advantage and interspecific interactions on nutrients. *Field Crops Res.* 71, 123–137. doi: 10.1016/S0378-4290(01)00156-3

Luquet, D., Dingkuhn, M., Kim, H., Tambour, L., and Clement-Vidal, A. (2006). EcoMeristem, a model of morphogenesis and competition among sinks in rice. 1. Concept, validation and sensitivity analysis. *Funct. Plant Biol.* 33, 309–323. doi: 10.1071/FP05266

Mathieu, A., Cournede, P. H., Letort, V., Barthelemy, D., and De Reffye, P. (2009). A dynamic model of plant growth with interactions between development and functional mechanisms to study plant structural plasticity related

to trophic competition. *Ann. Bot.* 103, 1173–1186. doi: 10.1093/aob/mcp054

McIntyre, G. I. (2001). Control of plant development by limiting factors: a nutritional perspective. *Physiol. Plant.* 113, 165–175. doi: 10.1034/j.1399-3054.2001.1130203.x

McMaster, G. S. (2005). Phytomers, phyllochrons, phenology and temperate cereal development. *J. Agric. Sci.* 143, 137–150. doi: 10.1017/S0021859605005083

McSteen, P. (2009). Hormonal regulation of branching in grasses. *Plant Physiol.* 149, 46–55. doi: 10.1104/pp.108.129056

Pagès, L., Vercambre, G., Drouet, J.-L., Lecompte, F., Collet, C., and Le Bot, J. (2004). Root Typ: a generic model to depict and analyse the root system architecture. *Plant Soil* 258, 103–119. doi: 10.1023/B:PLSO.0000016540.47134.03

Prusinkiewicz, P., Crawford, S., Smith, R. S., Ljung, K., Bennett, T., Ongaro, V., et al. (2009). Control of bud activation by an auxin transport switch. *Proc. Natl. Acad. Sci. U.S.A.* 106, 17431–17436. doi: 10.1073/pnas.0906696106

Prusinkiewicz, P., and Lindenmayer, A. (1990). *The Algorithmic Beauty of Plants*. New York: Springer-Verlag. doi: 10.1007/978-1-4613-8476-2

Rajala, A., and Peltonen-Sainio, P. (2001). Plant growth regulator effects on spring cereal root and shoot growth. *Agron. J.* 93, 936–943. doi: 10.2134/agronj2001.934936x

Renton, M., Hanan, J., Ferguson, B. J., and Beveridge, C. A. (2012). Models of long-distance transport: how is carrier-dependent auxin transport regulated in the stem? *New Phytol.* 194, 704–715. doi: 10.1111/j.1469-8137.2012.04093.x

Rodríguez, D., Andrade, F. H., and Goudriaan, J. (1999). Effects of phosphorus nutrition on tiller emergence in wheat. *Plant Soil* 209, 283–295. doi: 10.1023/A:1004690404870

Rolland, F., Baena-Gonzalez, E., and Sheen, J. (2006). Sugar sensing and signaling in plants: conserved and novel mechanisms. *Annu. Rev. Plant Biol.* 57, 675–709. doi: 10.1146/annurev.arplant.57.032905.105441

Shinohara, N., Taylor, C., and Leyser, O. (2013). Strigolactone can promote or inhibit shoot branching by triggering rapid depletion of the auxin efflux protein PIN1 from the plasma membrane. *PLoS Biol.* 11:e1001474. doi: 10.1371/journal.pbio.1001474

Sparkes, D. L., Holme, S. J., and Gaju, O. (2006). Does light

quality initiate tiller death in wheat? *Eur. J. Agron.* 24, 212–217. doi: 10.1016/j.eja.2005.08.003

Tomlinson, K. W., Dominy, J. G., Hearne, J. W., and O'Connor, T. G. (2007). A functional–structural model for growth of clonal bunchgrasses. *Ecol. Model.* 202, 243–264. doi: 10.1016/j.ecolmodel.2006.11.002

Tomlinson, K. W., and O'Connor, T. G. (2004). Control of tiller recruitment in bunchgrasses: uniting physiology and ecology. *Funct. Ecol.* 18, 489–496. doi: 10.1111/j.0269-8463.2004.00873.x

Vos, J., Evers, J. B., Buck-Sorlin, G. H., Andrieu, B., Chelle, M., and De Visser, P. H. B. (2010). Functional–structural plant modelling: a new versatile tool in crop science. *J. Exp. Bot.* 61, 2102–2115. doi: 10.1093/jxb/erp345

Watanabe, T., Hanan, J. S., Room, P. M., Hasegawa, T., Nakagawa, H., and Takahashi, W. (2005). Rice morphogenesis and plant architecture: measurement, specification and the reconstruction of structural development by 3D architectural modelling. *Ann. Bot.* 95, 1131–1143. doi: 10.1093/aob/mci136

Wernecke, P., Müller, J., Dornbusch, T., Wernecke, A., and Diepenbrock, W. (2007). "The virtual crop-modelling system "VICA" specified for barley," in *Functional–Structural Plant Modelling in Crop Production*, eds J. Vos, L. F. M. Marcelis, P. H. B. De Visser, P. C. Struik, and J. B. Evers (Dordrecht: Springer), 53–64.

Winter, S. R., and Welch, A. D. (1987). Tall and semidwarf wheat response to dryland planting systems. *Agron. J.* 79, 641–645. doi: 10.2134/agronj1987.00021962007900040012x

Xu, L., Henke, M., Zhu, J., Kurth, W., and Buck-Sorlin, G. (2011). A functional–structural model of rice linking quantitative genetic information with morphological development and physiological processes. *Ann. Bot.* 107, 817–828. doi: 10.1093/aob/mcq264

Zhong, X., Peng, S., Sanico, A. L., and Liu, H. (2003). Quantifying the interactive effect of leaf nitrogen and leaf area on tillering of rice. *J. Plant Nutr.* 26, 1203–1222. doi: 10.1081/PLN-120020365

Conflict of Interest Statement: The authors declare that the research was conducted in the absence of any commercial or financial relationships that could be construed as a potential conflict of interest.

Scaling of xylem and phloem transport capacity and resource usage with tree size

Teemu Hölttä*, Miika Kurppa and Eero Nikinmaa

Department of Forest Sciences, University of Helsinki, Helsinki, Finland

Xylem and phloem need to maintain steady transport rates of water and carbohydrates to match the exchange rates of these compounds at the leaves. A major proportion of the carbon and nitrogen assimilated by a tree is allocated to the construction and maintenance of the xylem and phloem long distance transport tissues. This proportion can be expected to increase with increasing tree size due to the growing transport distances between the assimilating tissues, i.e., leaves and fine roots, at the expense of their growth. We formulated whole tree level scaling relations to estimate how xylem and phloem volume, nitrogen content and hydraulic conductance scale with tree size, and how these properties are distributed along a tree height. Xylem and phloem thicknesses and nitrogen contents were measured within varying positions in four tree species from Southern Finland. Phloem volume, nitrogen amount and hydraulic conductance were found to be concentrated toward the branch and stem apices, in contrast to the xylem where these properties were more concentrated toward the tree base. All of the species under study demonstrated very similar trends. Total nitrogen amount allocated to xylem and phloem was predicted to be comparable to the nitrogen amount allocated to the leaves in small and medium size trees, and to increase significantly above the nitrogen content of the leaves in larger trees. Total volume, hydraulic conductance and nitrogen content of the xylem were predicted to increase faster than that of the phloem with increasing tree height in small trees ($< \sim 10$ m in height). In larger trees, xylem sapwood turnover to heartwood, if present, would maintain phloem conductance at the same level with xylem conductance with further increases in tree height. Further simulations with a previously published xylem-phloem transport model demonstrated that the Münch pressure flow hypothesis could explain phloem transport with increasing tree height even for the tallest trees.

Keywords: carbon allocation, metabolic scaling, nitrogen allocation, phloem transport, pipe model, xylem transport

INTRODUCTION

Structural-functional tree models describe formation and growth of new stem and branch axes as a function of their local environment and topological position within a tree (e.g., Sievänen et al., 2000). This approach has been shown to be a powerful tool in reproducing realistic tree architectures (Prusinkiewicz, 2004). Scaling rules, such as the pipe model (Shinozaki et al., 1964), have been used to quantify secondary growth to analyse tree mass balance during growth (e.g., Perttunen et al., 1996). While these empirical rules work well to describe average tree growth, they actually describe fundamental functional properties of trees related to material uptake and their long distance transport (e.g., West et al., 1999; McCulloh et al., 2003; Hölttä et al., 2011; Nikinmaa et al., 2013). Simultaneously, axial and secondary growth patterns determine the resource allocation within trees. Understanding the functional implications of axial scaling patterns is thus an essential feature of structural-functional tree models.

The long distance transport capacity of tree xylem has to be high enough to be able to deliver water from soil to leaves at the rate that it is transpired. Similarly, the long distance transport capacity of phloem has to match the production rate of carbon compounds assimilated in photosynthesis in the leaves. In addition, water and carbon exchange rates are strongly coupled as both occur through the same stomatal pores in leaves, although water use efficiency, i.e., the ratio of plant photosynthetic production to plant transpiration rate, may somewhat vary across tree species, climatic conditions and tree size (Cernusak et al., 2007). It is therefore reasonable to expect that the xylem and phloem transport capacities, i.e., conductance per leaf area, must also be coupled, but they may vary within species and tree sizes. It is well-recognized that xylem transport capacity will ultimately limit the photosynthetic production rate of a tree (Tyree and Sperry, 1988; Jones and Sutherland, 1991). Similarly, when the transport rate of photosynthates through the phloem is not able to keep up with the rate of photosynthesis, carbohydrates will start accumulating in the leaves and will cause down-regulation of photosynthesis and/or stomatal closure (e.g., Paul and Foyer, 2001; Nikinmaa et al., 2013).

The allometric relationships concerning the xylem have been under rigorous study for centuries [(Leonardo's notes MacCurdy, 2002; Huber, 1928; Zimmermann, 1983)]. Scaling

relationships for xylem hydraulic conductance have been developed from theoretical basis and also tested empirically. Xylem sapwood cross-sectional area has been found to be conserved in branching, and also to be approximately linearly proportional to leaf area (Shinozaki et al., 1964; Berninger et al., 2005). Xylem conduit radius and conductivity has been found to increase from tree apex downwards, and also to increase with tree size (West et al., 1999; McCulloh et al., 2003) to compensate for the increased transport distance from soil to leaves. However, these changes in conductance compensate only partially the increased tree size (e.g., Mäkelä and Valentine, 2006).

Allometric relations of xylem have been of great interest not only from the water transport point of view, but also because the xylem construction and maintenance consumes a major proportion of the carbon budget of a tree (Mäkelä, 1986; Nikinmaa, 1992). The thick lignified xylem cell walls require large amounts of carbon over the long transport path in trees (Hacke et al., 2001). Xylem transport physiology and its connection with structure are relatively well-understood. The allometric relations concerning phloem transport have received much less attention. Anatomical and physiological measurements are much more difficult to conduct on the phloem, which is a more heterogeneous tissue and sensitive to external perturbations caused by direct measurements. Also, the transport rate of fluids, and therefore the required transport capacity, in the xylem typically exceeds that of the phloem by more than an order of magnitude (Hölttä et al., 2009). The few studies which have measured phloem dimensions report increased phloem allocation and decreased conduit dimensions, i.e., cross-sectional area (Quilhó et al., 2000), toward the tree apex. Phloem conduit size at tree base has also been found to increase with increases in tree height (Jensen et al., 2011, 2012; Mencuccini et al., 2011).

Although at static evaluation, the phloem comprises only a minor proportion of the carbon allocated to the tree, the yearly difference in allocation compared to xylem is not as large as functional phloem structures do not accumulate in the stem at the same extent as the xylem sapwood does. Further, phloem contains significant amounts of nitrogen since it is metabolically more active tissue with high protein content. Nitrogen is the most significant limitation of tree growth in boreal forests (Chapin et al., 1987; Bergh et al., 1999). Unlike total leaf area, which saturates to a rather stable value with increasing tree size at least at the stand level, e.g., Vanninen and Mäkelä (1999), the amount of xylem and phloem tissue should increase with tree height. Consequently, a growing proportion of tree's nitrogen could be expected to be found in the trunk and branches of a tree with increasing tree size (Helmisaari, 1995).

It has been suggested that, as a growth limiting substance, nitrogen is allocated optimally among leaves in tree crowns (Mooney and Gulmon, 1979; Field, 1983). The attention has focused especially on optimizing photosynthetic N-use efficiency (PNUE), the ratio of photosynthesis to leaf nitrogen content. In the optimal solution PNUE should be maximal and the same for all leaves independently of their position in the canopy (Mooney and Gulmon, 1979; Field, 1983). Yet, observed nitrogen allocation to leaves typically deviates from theoretical expectations (Field, 1983; Hirose and Werger, 1987; Evans, 1993; Hollinger, 1996; Kull, 2002; Wright et al., 2004). One overlooked aspect that may contribute to this deviation is that while foliar photosynthetic capacity depends on foliar nitrogen content, balanced structural design requires that there has to be sufficient capacity to transport photosynthates from the leaves as well. One should therefore consider also the nitrogen required for transporting substances to and from the leaves (in addition to the nitrogen needed for leaf functions) to understand the optimal within tree allocation of nitrogen.

We set out to determine allometric relations for the amounts of xylem and phloem, and their hydraulic conductances and nitrogen concentrations as a function of tree stem/branch diameters. We studied whether these relations were similar in four different species co-occurring in Southern Finland; birch (*Betula pendula*), aspen (*Populus tremula*), pine (*Pinus sylvestris*), and spruce (*Picea abies*). In general, the same biophysical constraints with respect to both xylem and phloem transport (in terms of mass flow driven by pressure gradient in a medium where the transport resistance is characterized by the transport distance and the cross-section area of the conducting tissues and the radius of the conduits within these tissues) have to apply to all of these species which are living in the same environmental conditions. We were interested whether the species specific differences, from e.g., differences in water use efficiency, phenological development, nitrogen requirements, and growth rates, would be large enough to reflect on these allometric relations despite the common driving gradients. Based on the allometric relations derived from the measurements, we derived scaling relations to estimate how whole tree xylem sapwood and phloem volume, nitrogen content and hydraulic conductance change as a function of tree size and how these properties are axially distributed within a tree. We also set out to estimate how much nitrogen was allocated to the xylem and phloem in comparison to the leaves. Then, using a previously published xylem and phloem transport model, we set out to answer whether the Münch pressure flow hypothesis would be a consistent explanation of phloem transport of photosynthates with increasing tree size.

MATERIALS AND METHODS
DERIVATION OF SCALING RELATIONSHIPS AS A FUNCTION OF STEM/BRANCH DIAMETER

We expressed stem/branch diameter (d) as a power law function of distance from apex (x) Equation (1a). Xylem and phloem cross-sectional areas (A_x and A_p), nitrogen concentrations ($\rho_{N,\,x}$ and $\rho_{N,\,p}$), conduit sizes (r_x, r_p), and the fraction of xylem and phloem cross-sectional areas occupied by conduits ($\rho_{c,\,x}$ and $\rho_{c,\,p}$) were expressed as power law functions of stem/branch diameter Equations (1b–i). The power function form was used since it is generally used to describe allometric variation in biological properties (e.g., Brown et al., 2004). See **Table 1** for the list of symbols used in the manuscript.

Table 1 | Symbols used in the manuscript.

A_b	Cross-sectional area of bark
A_{leaf}	Leaf area
A_p	Phloem (living bark) cross-sectional area
$A_{p, tot}$	Phloem cross-sectional area summed across all branches of a given diameter
A_x	Xylem cross-sectional area
$A_{x, tot}$	Xylem cross-sectional area summed across all branches of a given diameter
A_{sw}	Xylem sapwood cross-sectional area
A_{hw}	Xylem heartwood cross-sectional area
d	Branch/stem diameter
$K_{tot, p}$	Total phloem conductance over the whole path-length (over whole tree)
$K_{tot, x}$	Total xylem conductance over the whole path-length (over whole tree)
k_p	Phloem hydraulic conductivity summed across all branches of a given diameter
k_x	Xylem hydraulic conductivity summed across all branches of a given diameter
L	Tree height
L_0	Distance from apex at which integration of whole tree properties are started from
$N_{p, tot}$	Total amount of nitrogen in the phloem of a tree
$N_{x, tot}$	Total amount of nitrogen in the xylem of a tree
n	Number of branches, i.e., furcations at a given height or stem/branch diameter
$R_{tot, p}$	Total phloem resistance over the whole path-length (over whole tree)
$R_{tot, x}$	Total xylem resistance over the whole path-length (over whole tree)
r_p	Phloem conduit radius
$r_{sw, max}$	Maximum sapwood radius (in cases where heartwood was taken into account)
r_x	Xylem conduit radius
$V_{p, tot}$	Total phloem volume in a tree
$V_{x, tot}$	Total xylem volume in a tree
x	Distance from leaf apex
$\rho_{c, p}$	Fraction of phloem occupied by the conducting sieve tubes
$\rho_{c, x}$ l	Fraction of xylem occupied by the conducting sieve tubes
$\rho_{N, phloem}$	Nitrogen concentration of phloem
$\rho_{N, bark}$	Nitrogen concentration of outer bark
$\rho_{N, xylem}$	Nitrogen concentration of xylem
γ, α_i	Bases for scaling relations
δ, β_i	Exponents for scaling relations

$$d = \gamma x^{\delta}. \tag{1a}$$

$$A_x = \alpha_1 * d_1^{\beta} = \alpha_1 * \left(\gamma x^{\delta}\right)_1^{\beta} = \alpha_1 \gamma_1^{\beta} x_1^{\delta\beta} \tag{1b}$$

$$A_p = \alpha_2 * d_2^{\beta} = \alpha_2 * \left(\gamma x^{\delta}\right)_2^{\beta} = \alpha_2 \gamma_2^{\beta} x_2^{\delta\beta} \tag{1c}$$

$$\rho_{N, x} = \alpha_3 * d_3^{\beta} = \alpha_3 * \left(\gamma x^{\delta}\right)_3^{\beta} = \alpha_3 \gamma_3^{\beta} x_3^{\delta\beta} \tag{1d}$$

$$\rho_{N, p} = \alpha_4 * d_4^{\beta} = \alpha_4 * \left(\gamma x^{\delta}\right)_4^{\beta} = \alpha_4 \gamma_4^{\beta} x_4^{\delta\beta} \tag{1e}$$

$$r_x = \alpha_5 * d_5^{\beta} = \alpha_5 * \left(\gamma x^{\delta}\right)_5^{\beta} = \alpha_5 \gamma_5^{\beta} x_5^{\delta\beta} \tag{1f}$$

$$r_p = \alpha_6 * d_6^{\beta} = \alpha_6 * \left(\gamma x^{\delta}\right)_6^{\beta} = \alpha_6 \gamma_5^{\beta} x_6^{\delta\beta} \tag{1g}$$

$$\rho_{c, x} = \alpha_7 * d_7^{\beta} = \alpha_7 * \left(\gamma x^{\delta}\right)_7^{\beta} = \alpha_7 \gamma_7^{\beta} x_7^{\delta\beta} \tag{1h}$$

$$\rho_{c, p} = \alpha_8 * d_8^{\beta} = \alpha_8 * \left(\gamma x^{\delta}\right)_8^{\beta} = \alpha_8 \gamma_8^{\beta} x_8^{\delta\beta} \tag{1i}$$

We also took into account that xylem hydraulic conductance decreases radially inwards to the xylem tissue due to heartwood formation and/or decrease in the conduit size and connectivity to transpiring foliage (e.g., Melcher et al., 2003). For this, we assumed two extreme scenarios where (A) all of the xylem was conducting sapwood and (B) where conducting sapwood was restricted only to the outermost 2 cm of the xylem ($r_{sw, max} = 2$ cm) (e.g., Sellin, 1994). We reason that the actual amount of conducting sapwood, and thus xylem hydraulic conductance, must be in between these two extreme scenarios, and exploring the space between these two extremes describes how sensitive the scaling predictions are to changes in the radial profile of xylem hydraulic conductance. In addition, we assumed two extreme scenarios for xylem heartwood nitrogen content, where (A) heartwood nitrogen concentration was the same as in sapwood and (B) where heartwood nitrogen content was zero. Again, the actual amount of nitrogen in the xylem must lie in between these two extreme scenarios. A literature review by Meerts (2002) done on 71 angiosperm and 22 gymnosperm species reported that the nitrogen concentration of the heartwood was on average 76% of the nitrogen content of the sapwood, but varied a lot between species and studies.

We made an assumption that the cross-sectional area of the xylem sapwood is conserved at branching junctions. This assumption is from the pipe model theory formulated originally by Shinozaki et al. (1964). The pipe model assumption has been shown to hold reasonably well for the tree species used in our measurements (Kaufmann and Troendle, 1981; Ilomaki et al., 2003; Kantola and Mäkelä, 2004; Berninger et al., 2005), and also to result from maximizing the carbon use efficiency of xylem structure (Hölttä et al., 2011). Note that the original pipe model assumption, presented e.g., in Shinozaki et al. (1964), does not necessarily imply that xylem conduit radius is constant within a tree. We further assumed leaf area to be proportional to xylem cross-sectional sapwood area. This assumption is also from the Pipe model theory (Shinozaki et al., 1964) and is supported by experimental evidence (Berninger et al., 2005). Note that scaling of phloem and leaf properties are affected by the assumptions made about sapwood turnover to heartwood. This behavior stems from the pipe model assumption. The amount of heartwood affects the number of furcations [i.e., n in Equation (A18)], which in turn affects phloem properties [see Equations (A20), (A22), and (A24)]. The more heartwood there is, the higher the furcation number (n) is at any given height, and the more phloem tissue there is. The coefficients $\alpha_i, \beta_i, \gamma,$ and δ in Equation (1) were derived from measurements or from literature estimates. We used the allometric relations in Equation (1) to scale whole tree xylem and phloem volume, conductance and nitrogen amount with tree height for two of the measured species (one gymnosperm and one angiosperm); pine and aspen.

TREE MEASUREMENTS

We harvested six birch (*Betula pendula*), aspen (*Populus tremula*), pine (*Pinus sylvestris*), and spruce (*Picea abies*) trees from forests surrounding Hyytiälä Forestry Field Station (61° 51′ N, 24° 17′ E, 180 m a.s.l.) and two from Ruotsinkylä research forests (60° 22′ N, 25° 00′ E) so that there were two trees of each species. Trees varied between 6.7 and 24.9 m in height and between 4.6 and 30.6 cm in breast height diameter and they grew in even-aged stands whose density varied between 8.6 and 28.3 m^2/ha in basal area. The trees were harvested between May and October 2010. In addition, two additional pine trees were harvested in September 2013 for some additional nitrogen content measurements. All harvested trees were healthy. The cardinal points were marked to the sample trees before felling. Stem diameters were measured from various relative locations within the stem (1.0; 2.5; 5.0; 7.5; 10.0; 15.0; 20.0; 30.0; 40.0; 50.0; 60.0; 70.0; 80.0; 85.0, and 90.0%) in East to West and North to South directions. Bark thickness measurement were made from tree trunk at breast height and at 6 m height. We numbered all living branches from the base of the crown to the top of the tree and measured their heights from the tree base and marked their compass direction, length, and base diameters. Branch diameters were measured beyond noticeable basal swelling and the distance from tree trunk and apex were measured. The crown was divided into segments of height and compass directions and a total of 10–15 sample branches were selected from each tree from different heights and sides of the tree so that the branch size distribution was evenly represented in the sample. Only healthy appearing and non-damaged branches entered the sample.

We measured the length of sample branches from the cut surface to branch apex and measured over and under bark diameters from the base of the branch. Subsequently we divided each branch into segments. The first segment was from the base to the first fork and the following segments were between subsequent forking points. The length and one to three diameters were measured from each segment at 10, 50, and 90% of length along with the bark-less diameters. Thickness of the bark was calculated as the difference between under bark and over bark diameter divided by two. Altogether, we measured 4379 branch or stem diameters with and without bark between 0.9 and 276.2 mm with average and median diameter of 6.5 and 4.2 mm, respectively.

For measurements of the dimensions of the living bark we cut 85 stem disks from different heights of each tree (2.5–276.2 mm in diameter). The cut surfaces were sanded and scanned, and the thicknesses of the periderm and living bark were measured using a self-made image analyzer program. We used 62 samples from stem and branch disks (3.6–276 mm in diameter) for nitrogen the content measurements. The bark was removed from xylem. The periderm of bark was then removed, and the rest of the bark was termed as living bark, which consisted of the primary and secondary phloem, and vascular cambium. We dried the periderm and living bark samples at 60°C for 72 h and xylem samples for 120 h and ground all dried parts with an oscillating mill (Retsch MM400). The total nitrogen concentration in samples was determined by an element analyzer (Vario MAX CN) at the Department of Forest Sciences at the University of Helsinki.

Allometric equations were fitted to the measured data using non-linear regression between sample diameter and xylem and bark properties with Sigmaplot (Sigmaplot for Windows version 11.0). We used ANCOVA to compare similarities/differences amongst the different species in the above regressions with lm function of R version 2.13.0 after the data had been ln-transformed to correspond with the assumption of the test and verified the correspondence with the assumptions from residual plots.

ESTIMATION OF THE NON-MEASURED SCALING RELATIONS FROM THE LITERATURE

Xylem conduit radius (r_x) was estimated to scale as $r_x \alpha x^{0.25}$ (e.g., West et al., 1999; Anfodillo et al., 2006). There are different estimates in the literature for the scaling of phloem conduit radius with tree height. We used a scaling relation of $r_p \alpha x^{0.25}$, i.e., the same as for the xylem. This is an intermediate scaling between the scaling exponent of 0.15 reported by Mencuccini et al. (2011), and 1/3 reported by Jensen et al. (2011). As distance to leaf apex is scaled from stem diameter, xylem and phloem conduit radius and conductance thus scale with stem/branch diameter, as has been found to be the case for xylem conduits (e.g., Zimmermann, 1983; Olson and Rosell, 2013). We assumed that a constant fraction of the xylem and phloem cross-sectional area was conducting lumen volume (the rest being conduit walls, parenchyma, etc.), i.e., β_7 and β_8 (exponents for the scaling equations for $\rho_{c, x}$ and $\rho_{c, p}$) were equal to zero. This is in agreement with a formulation described e.g., in Savage et al. (2010).

SENSITIVITY ANALYSIS FOR THE SCALING RELATIONS

To demonstrate the sensitivity of the scaling of xylem and phloem volume, nitrogen content, and hydraulic conductance to the values of the measured/estimated scaling exponents we conducted simulations where the scaling exponents β_1, β_2, β_3, β_4, β_5, β_6, and δ were varied simultaneously in random (from a linear distribution) between 75 and 125% of the values in comparison to values presented in **Table 2**. Simultaneously, the maximum sapwood depth ($r_{sw, max}$) was varied between 2 and 200 cm.

SIMULATIONS OF XYLEM AND PHLOEM TRANSPORT WITH A NUMERICAL MODEL

Xylem and phloem transport and the resulting within tree pressure gradients were simulated using the scaling relations obtained and a previously published xylem and phloem transport model (Hölttä et al., 2009). The model calculates xylem and phloem pressure and sugar concentrations and their within tree axial gradients in steady state. Pressure differences drive xylem and phloem transport, i.e., flow is proportional to pressure gradient, and water potential equilibrium is maintained between the xylem and phloem. Phloem sap viscosity was made to be sugar concentration dependent. Transpiration rate, phloem loading (made equal to photosynthesis rate) and unloading rates and soil water potential were given as boundary conditions, and xylem and phloem hydraulic conductance and tree height were given as structural parameters. The position of phloem unloading could be varied in the transport model so that we ran simulations where phloem unloading was made to occur either evenly along the

Table 2 | Measured properties as a function of stem/branch diameter for each species from the measurements: $P = B * d^E$, where P is the property under consideration, B is the base, and E is the exponent.

Quantity	Corresponding scaling coefficient (intercept and slope)	Species	Intercept (units)	Slope	R^2	P	n
Bark cross-sectional area	–	Birch	$0.45\,mm^2$	1.60	0.98	***	553
		Pine	$0.38\,mm^2$	1.61	0.88	***	2050
		Spruce	$0.52\,mm^2$	1.59	0.97	***	1371
		Aspen	$0.61\,mm^2$	1.53	0.97	***	399
		All	$0.31\,mm^2$	1.69	0.90	***	4377
Xylem cross-sectional area	α_1 and β_1	Birch	$0.67\,mm^2$	2.01	0.999	***	555
		Pine	$0.82\,mm^2$	1.98	0.999	***	2052
		Spruce	$0.55\,mm^2$	2.05	0.999	***	1372
		Aspen	$0.71\,mm^2$	2.00	0.999	***	401
		All	$0.69\,mm^2$	2.00	0.999	***	4379
Phloem cross-sectional area	α_2 and β_2	Birch	$0.32\,mm^2$	1.59	0.99	***	10
		Pine	$0.75\,mm^2$	1.27	0.98	***	62
		Spruce	$0.0086\,mm^2$	2.35	0.93	***	10
		Aspen	$0.99\,mm^2$	1.3	0.94	***	37
		All	$1.97\,mm^2$	1.11	0.94	***	130
Xylem nitrogen content	α_3 and β_3	Birch	0.11%	0.21	0.099	NS	4
		Pine	2.02%	−0.61	0.86	***	27
		Spruce	0.15%	−0.021	0.0033	NS	8
		Aspen	0.68%	−0.34	0.80	**	9
		All	1.92%	−0.59	0.85	***	48
Phloem nitrogen content	α_4 and β_4	Birch	7.1%	−0.59	0.86	***	12
		Pine	1.4%	−0.22	0.73	***	28
		Spruce	0.87%	−0.10	0.0387	NS	9
		Aspen	22 %	−0.79	0.90	***	13
		All	1.48%	−0.20	0.38	***	62
Distance from apex	γ and δ	Birch	115 mm	1.00	0.97	***	370
		Pine	61 mm	1.029	0.97	***	1168
		Spruce	85 mm	0.98	0.96	***	1144
		Aspen	73 mm	1.05	0.97	***	483
		All	87 mm	0.98	0.94	***	3165

Stem/branch diameter (d) is in units of millimeters (mm). Significance levels $^{***}P < 0.001$, $^{**}P < 0.01$, $NS = P > 0.05$.

phloem transport pathway or exclusively in the roots. We did three simulations with the model. (1) We used the model to calculate the axial xylem and phloem pressure and sugar concentration gradients taking into account the axial distribution of xylem and phloem tissue and their specific conductivity. We used a 10 m pine with a maximum sapwood depth of 2 cm as an example, and took the axial distribution of xylem and phloem conductivity from the equations shown in the Appendix A3 and demonstrated in **Figure 7.** (2) We modeled how phloem tissue should be distributed axially in order to minimize turgor pressure difference between the leaves and roots, i.e., source and sink, for a fixed phloem volume at the whole tree level. In other words, the total amount of phloem tissue was preserved, but was distributed unevenly as a function of axial position. (3) We

simulated how phloem turgor pressure difference between the leaves and roots would change as a function of increasing tree height, and whether phloem transport would be able to function according to the Münch pressure flow hypothesis when trees become taller. For this, we used the scaling relations for whole tree xylem and phloem hydraulic conductance as a function of tree height derived in Appendixes A1 and A2 (and demonstrated in **Figure 4** and **Table 4**) for the case of pine. In this simulation, leaf gas exchange rates (i.e., transpiration and photosynthesis rates) were determined for each tree height so that leaf xylem water potential always remained at a constant value, i.e., we assumed isohydric behavior. Leaf water potential was held at −2.0 MPa, which is a typical value for Scots Pine in Hyytiälä Forestry Field Station in summer conditions (Martinez-Vilalta et al., 2009).

Photosynthesis rate was made to be proportional to transpiration rate. Water use efficiency was set to 250, a typical value for Scots Pine in Hyytiälä Forestry Field Station (e.g., Hari and Mäkelä, 2003). The absolute value for phloem conductance was chosen so that the turgor pressure difference between the leaves and roots obtained a reasonable value, ~0.7 MPa for the case of unloading in the soil for a 10 m tree. Note that this resulted in different initial values for phloem conductance between the cases where no heartwood was assumed and the case where the maximum sapwood depth was set at 2 cm. We also varied the initial value of phloem conductive and distribution of phloem unloading to see their effects on the results.

RESULTS

SCALING OF WHOLE TREE PROPERTIES FROM ALLOMETRIC EQUATIONS

The equations obtained for the scaling of xylem and phloem properties as a function of tree height (L) (starting from a distance L_0 from leaf apex) are as follows

$$n(x) = \left(\frac{L}{x}\right)^{\delta\beta_1} \tag{2a}$$

$$V_{x,\,tot} = \alpha_1 \gamma^{\beta_1} \left(L^{\delta\beta_1 + 1} - L_0^{\delta\beta_1 + 1} \right) \tag{2b}$$

$$V_{p,\,tot} = \frac{L^{\delta\beta_1} \alpha_2 \gamma^{\beta_2}}{\delta\beta_2 - \delta\beta_1 + 1} \left(L^{\delta\beta_2 - \delta\beta_1 + 1} - L_0^{\delta\beta_2 - \delta\beta_1 + 1} \right) \tag{2c}$$

$$N_{x,\,tot} = \frac{\alpha_1 \gamma^{\beta_1} \alpha_3 \gamma^{\beta_3} \rho_x}{\delta\beta_3 + 1} \left(L^{\delta\beta_1 + \delta\beta_3 + 1} - L_0^{\delta\beta_1 + \delta\beta_3 + 1} \right) \tag{2d}$$

$$N_{p,\,tot} = \frac{L^{\delta\beta_1} \alpha_2 \gamma^{\beta_2} \alpha_4 \rho_N \gamma^{\beta_4}}{\delta\beta_4 + \delta\beta_2 - \delta\beta_1 + 1}$$
$$\left(L^{\delta\beta_4 + \delta\beta_2 - \delta\beta_1 + 1} - L_0^{\delta\beta_4 + \delta\beta_2 - \delta\beta_1 + 1} \right) \tag{2e}$$

$$N_{leaf,\,tot} = \frac{\alpha_1 \gamma^{\beta_1} \left(L^{\delta\beta_1 + 1} - L_0^{\delta\beta_1 + 1} \right)}{L} C_{ls} \rho_{SLA} \rho_{N,\,leaf} \tag{2f}$$

$$K_{x,\,tot}^{-1} = \left(L^{\delta\beta_1} \alpha_1 \alpha_7 \alpha_5^2 \gamma^{\beta_1 + \beta_7 + 2\beta_5} \right)^{-1} \frac{1}{-\delta\beta_7 - 2\delta\beta_5 + 1}$$
$$\left(L^{-\delta\beta_7 - 2\delta\beta_5 + 1} - L_0^{-\delta\beta_7 - 2\delta\beta_5 + 1} \right) \tag{2g}$$

$$K_{p,\,tot}^{-1} = \left(L^{\delta\beta_1} \alpha_2 \alpha_8 \alpha_6^2 \gamma^{\beta_2 + \beta_8 + 2\beta_6} \right)^{-1}$$
$$\frac{1}{-\delta\beta_2 + \delta\beta_1 - \delta\beta_8 - 2\delta\beta_6 + 1}$$
$$\left(L^{-\delta\beta_2 + \delta\beta_1 - \delta\beta_8 - 2\delta\beta_6 + 1} - L_0^{-\delta\beta_2 + \delta\beta_1 - \delta\beta_8 - 2\delta\beta_6 + 1} \right) \tag{2h}$$

where n is the number of branches, i.e., furcations, at a distance x from the leaf apex, $V_{x,\,tot}$ is the total xylem volume in a tree, $V_{x,\,tot}$ is the total xylem volume in a tree, $N_{x,\,tot}$ is the total amount of nitrogen in the xylem in a tree, $N_{p,\,tot}$ is the total amount of nitrogen in the phloem in a tree, $N_{leaf,\,tot}$ is the total amount of

nitrogen in the leaves of a tree, $K_{x,\,tot}$ is the whole tree hydraulic conductance of the xylem, $K_{x,\,tot}$ is the whole tree hydraulic conductance of the phloem. The derivation of the equations is presented in the Appendix A1. These equations apply only to the case without heartwood. The numerical equations for the whole tree scaling relations including sapwood to heartwood turnover are shown in Appendix A2. L_0 was set to 0.1 m, except in the case of aspen phloem nitrogen content, in which L_0 was set to 1.0 m. The values of 0.1 m and 1 m for L_0 correspond to branch diameter of ~2 and 20 mm, respectively (see **Figure 2C**). Xylem and phloem properties were given constant values at branches than smaller than this. The values for L_0 were chosen large enough so that we had measurements from branches of corresponding diameter.

TREE MEASUREMENTS

Whole bark vs. diameter

The cross-sectional area of the whole bark (A_b), i.e., inner plus outer bark, increased with stem/branch diameter following a relationship $A_b = 0.31d^{1.68}$ when all the data was pooled together (**Figure 1A**). The scaling exponent ranged from 1.5344 in aspen to 1.59–1.61 in spruce, birch and pine with all relations being highly significant (see **Table 2**). The scaling exponents were rather close to each other across the species. When testing the difference, the logarithmic transformation changed the exponents somewhat (1.45, 1.50, 1.52, and 1.60 in pine, birch, aspen, and spruce,
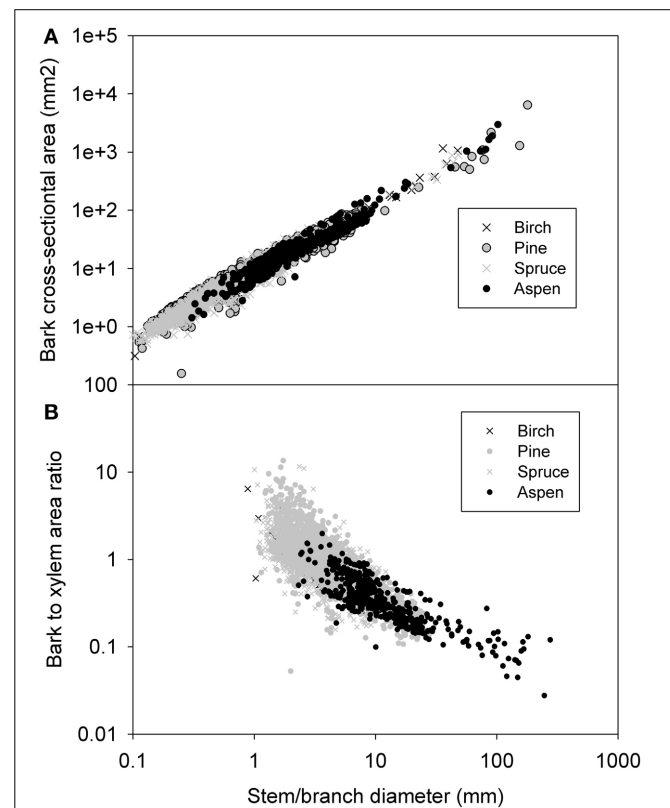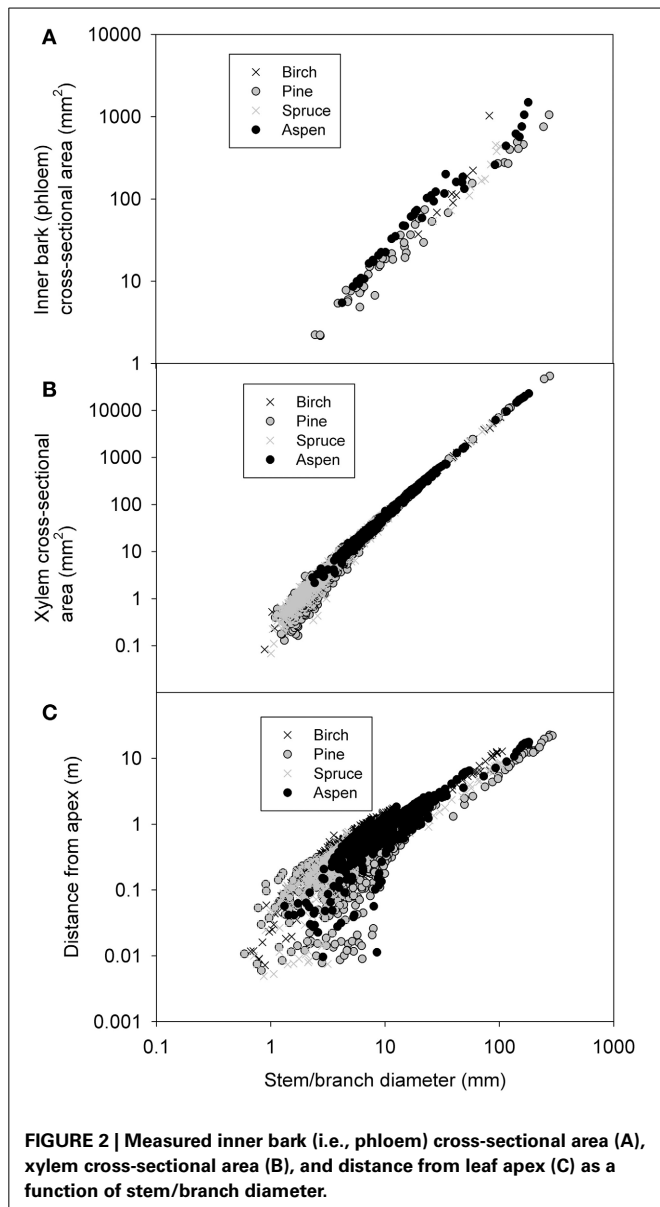

FIGURE 1 | Measured bark cross-sectional (A) and the ratio of bark to xylem cross-sectional area (B) as a function of stem/branch diameter.

FIGURE 2 | Measured inner bark (i.e., phloem) cross-sectional area (A), xylem cross-sectional area (B), and distance from leaf apex (C) as a function of stem/branch diameter.

respectively). Out of these values, only the spruce exponent was very significantly different ($p < 0.001$) from the birch exponent. The ratio of whole bark to xylem diameter showed a consistent trend of decreasing with increases in stem/branch diameter, following a relationship $A_b/A_x = 3.32d^{-0.94}$ (**Figure 1B**). The relation of whole bark diameter against stem/branch diameter was not used in the scaling predictions since it does no. Instead, the bark was divided into outer and inner bark, and the latter represents the functional phloem tissue.

Inner bark and xylem cross-sectional area vs. diameter and stem taper

For inter-species comparison of inner bark thickness there was sufficient data for aspen and pine. Their exponents were not significantly different from each other in the ln-transferred data. Pooling all species data together for the non-linear regression yielded $A_p = 1.2d^{1.286}$ for the relation between bark and
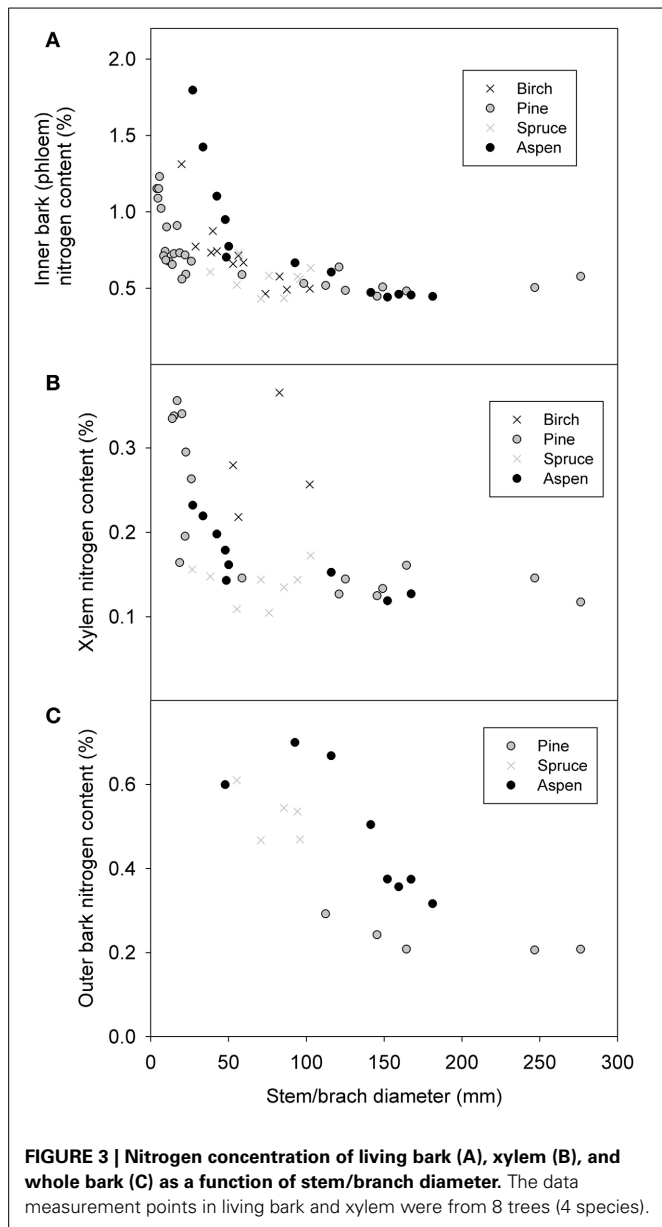
branch/stem diameter (**Figure 2A**, **Table 2**). The cross-sectional area of the xylem (A_x) increased with stem/branch diameter in slightly different manner between the species (see **Table 2**). Pooling the data together yields $A_x = 0.68d^{2.009}$ for the relation between xylem tissue and branch/stem diameter (**Table 2**, **Figure 2B**). When all data was pooled together, the cross-sectional areas of xylem and phloem were equal at branch diameters of $\sim$2.5 mm. Phloem thickness resulted in saturating to a very constant value (phloem thickness $= 0.88 * d^{0.082}$, all species combined together, not shown). When data from the main stems plus the first order branches was pooled together, the distance from leaf apex was found to scale with stem/branch diameter following $\alpha\, d^{0.98}$ (**Figure 2C**).

Nitrogen content

Nitrogen content increased clearly with decreasing stem diameter in both the living bark and the whole bark, but remained fairly constant for the xylem (**Figure 3**). When all species were pooled together relations of $\rho_{N,\,phloem} = 0.0148\ d^{-0.20}$ for the inner bark, and $\rho_{N,\,xylem} = 0.0192\ d^{-0.59}$ for xylem (**Table 2**). As there were only four birch values that differed clearly from the rest we also calculated the relationship without birch yielding $\rho_{N,\,xylem} = 0.0021\ d^{-0.64}$. While all species seemed to follow similar pattern for the living bark, there seemed to be a level difference for the whole bark so that there was the most nitrogen in the aspen bark and least in pine bark for the same diameter. The phloem nitrogen concentrations in the smallest branch diameters were found to be very close to the nitrogen concentration found in the foliage of the corresponding species in pine and aspen (compare **Figure 2A** to $\rho_{N,\,leaf}$ in **Table 3**).

Whole tree scaling relations

Whole tree scaling relation predictions were made for two example species: pine and aspen. The allometric relations used in the scaling of whole tree xylem and phloem volume, nitrogen content and hydraulic conductance are presented in **Table 3**. Some of the parameter values ($\alpha_{1-4}, \beta_{1-5}, \gamma,$ and δ) used in the scaling were taken from the measurements, while the rest ($\alpha_5 - \alpha_8, \beta_6 - \beta_9, C_{ls}, \rho_{SLA},$ and $\rho_{N,\,leaf}$) were estimated from literature. **Figure 4** shows the scaling relations for phloem and leaf properties in relation to the xylem properties, and **Figure 5** shows the absolute values for xylem, phloem and leaf properties. Whole tree phloem volume and hydraulic conductance decreased more sharply in comparison to whole tree xylem sapwood volume and hydraulic conductance with increases in tree height in small tree heights ($<$10 m in height), and also in larger trees in the absence of xylem heartwood formation (**Figures 4A,B, 5A–D,G,H**). However, at trees larger than $\sim$10 m in height, xylem heartwood formation according to the maximum 2 cm sapwood depth scenario was found to maintain phloem conductance and volume at approximately a constant proportion of the xylem sapwood with increases in tree height. Aspen had a larger amount of phloem and higher phloem to xylem ratio in relation to pine. Leaves were the largest sink of nitrogen in small trees, but xylem and phloem exceeded the leaves as a nitrogen sink with increases in tree height (**Figures 4C,D, 5E,F**). The total nitrogen content of the phloem was smaller than that of the xylem in pine and large aspen trees. The total nitrogen content of the phloem exceeded the

FIGURE 3 | Nitrogen concentration of living bark (A), xylem (B), and whole bark (C) as a function of stem/branch diameter. The data measurement points in living bark and xylem were from 8 trees (4 species).

Sensitivity analysis for the scaling relations

Figure 6 shows the minimum and maximum xylem and phloem volume, nitrogen content and conductance in relation to a 10 m tree obtained from the sensitivity analysis done with 1000 parameter combinations. The general trends within remained unchanged, although the xylem, phloem and leaf properties overlapped with each other. Xylem and leaf properties seemed to be more sensitive to parameter combination than those of phloem.

Axial distribution within a tree

Within a 10 m tree (taken as an example here) phloem cross-section (and volume) was distributed very much toward the apex, whereas xylem sapwood cross-section was evenly distributed axially, following from our pipe model assumption (**Figure 7A**). Xylem and phloem nitrogen content were more concentrated toward the apex (**Figure 7B**), but this relation was much stronger for the phloem, especially for aspen. Xylem conductivity was more concentrated ($k_x \alpha\ x^{0.5}$) toward the base, whereas phloem conductivity was concentrated toward the apex when no heartwood formation was assumed (**Figure 7C**). Assuming maximum sapwood depth to be 2 cm caused phloem conductance to be distributed more evenly within the transport axis. The axial distribution of xylem and phloem properties was very similar in pine and aspen for cross-sectional area and conductance, but differed greatly for nitrogen content.

Simulations for the pressure and sugar gradients within the xylem and phloem, simulation 1

The xylem pressure (water potential) drop was predicted to occur more steeply close to the apex, while phloem pressure drop was predicted to occur more at the tree base in (**Figures 8A,B**), particularly when phloem unloading occurred in the soil. Phloem pressure gradients were sensitive to heartwood assumptions. In the absence of heartwood formation, phloem hydraulic conductivity was more concentrated toward the apex (see **Figure 7C**), which resulted in the phloem turgor pressure drop to concentrate more toward the base of the tree (**Figure 8B**). Phloem osmotic concentration gradient, which results from the interplay between both xylem and phloem transport properties, was predicted to be more evenly distributed over the transport axes. The normalized pressure and concentration gradients shown in the figure were not very sensitive to parameterization of the model, but the absolute values naturally were (not shown).

Simulations for "optimal" allocation of axial phloem transport capacity, simulation 2

When all of the sugar unloading occurred in the roots, the lowest turgor pressure difference between source and sink was obtained when phloem cross-sectional area scaled by $A_p \alpha\ x^{-0.17}$ (x is distance from apex). When phloem unloading was made to occur evenly within the stem, a scaling relation of $A_p \alpha\ x^{-0.33}$ yielded the lowest turgor pressure difference. Importantly, the optimal axial allocation of phloem tissue predicted by the model was never as large as in the scaling results from the measurements, i.e., $A_p \alpha\ x^{-0.69}$ for pine and $A_p \alpha\ x^{-0.67}$ for aspen for a 10 m tree without heartwood and $A_p \alpha\ x^{-0.45}$ for both pine and aspen when a maximum sapwood depth of 2 cm was assumed.

xylem nitrogen content in small aspen trees (**Figures 4C,D, 5E,F**). Assumptions on heartwood proportions and nitrogen content of the heartwood caused the relative nitrogen contents between the tissues to vary strongly. When heartwood nitrogen concentration was low ("hw N 0%" in **Figure 4C**), phloem remained an important nitrogen sink relative to xylem even in large trees. However, when there was no heartwood, or the nitrogen content of heartwood was assumed to be same as that of the sapwood, then the role of the phloem as a nitrogen sink decreased in relation to xylem with increases in tree size. **Table 4** present the absolute values for scaling of tree xylem and phloem volume, nitrogen content, conductance, and leaf area-specific conductance as a function of tree size. Note that scaling is not strictly allometric [see Equation (2) and Appendix A2], although very close to it, for each case.

Table 3 | The scaling coefficients of xylem and phloem properties as a function of stem/branch diameter used in the scaling Equation (1).

Scaling coefficient	Symbol	Value used for pine	Value used for aspen	Measured/estimated from literature*
Base for stem/branch diameter as a function of distance from leaf apex (mm)	γ	15.8 mm	15.6 mm	Measured
Base for xylem cross-sectional area as a function of stem/branch diameter	α_1	0.82	0.71	Measured
Base for phloem cross-sectional area as a function of stem/branch diameter	α_2	0.75	0.99	Measured
Base for xylem nitrogen concentration as a function of stem/branch diameter	α_3	2.02	0.68	Measured
Base for phloem nitrogen concentration as a function of stem/branch diameter	α_4	1.4	22.1	Measured
Base for xylem conduit radius as a function of stem/branch diameter	α_5	1 unit less	1 unit less	Irrelevant as only relative values are shown
Base for phloem conduit radius as a function of stem/branch diameter	α_6	1 unit less	1 unit less	Irrelevant as only relative values are shown
Base for xylem conduit density (ratio of conduit cross-sectional area to tissue cross-section area) as a function of stem/branch diameter	α_7	1 unit less	1 unit less	Irrelevant as only relative values are shown
Base for phloem conduit density (ratio of conduit cross-sectional area to tissue cross-section area) as a function of stem/branch diameter	α_8	1 unit less	1 unit less	Irrelevant as only relative values are shown
Exponent for stem/branch diameter as a function of distance from leaf apex	δ	0.97	0.97	Measured
Exponent for xylem cross-sectional area as a function of stem/branch diameter	β_1	1.98	2.00	Measured
Exponent for phloem cross-sectional area as a function of stem/branch diameter	β_2	1.27	1.31	Measured
Exponent for xylem nitrogen concentration as a function of stem/branch diameter	β_3	−0.61	−0.34	Measured
Exponent for phloem nitrogen concentration as a function of stem/branch diameter	β_4	−0.22	−0.80	Measured
Exponent for xylem conduit radius as a function of stem/branch diameter	β_5	0.25	0.25	West et al., 1999
Exponent for phloem conduit radius as a function of stem/branch diameter	β_6	0.25	0.25	West et al., 1999; Jensen et al., 2011; Mencuccini et al., 2011
Exponent for xylem conduit density (ratio of conduit cross-sectional area to tissue cross-section area) as a function of stem/branch diameter	β_7	0	0	Savage et al., 2010
Exponent for phloem conduit density (ratio of conduit cross-sectional area to tissue cross-section area) as a function of stem/branch diameter	β_8	0	0	Assumed to be the same as for the xylem
Leaf to sapwood area ratio C_{ls}	C_{ls}	3400 m^2/m^2	2700 m^2/m^2	Hoffmann and Usoltsev, 2002; Martinez-Vilalta et al., 2009
Specific leaf area	ρ_{SLA}	300 g/m^2	80 g/m^2	Niinemets, 1997; Martinez-Vilalta et al., 2009
Leaf nitrogen content	$\rho_{N, leaf}$	1.2%	2.4%	Niinemets, 1997; Martinez-Vilalta et al., 2009

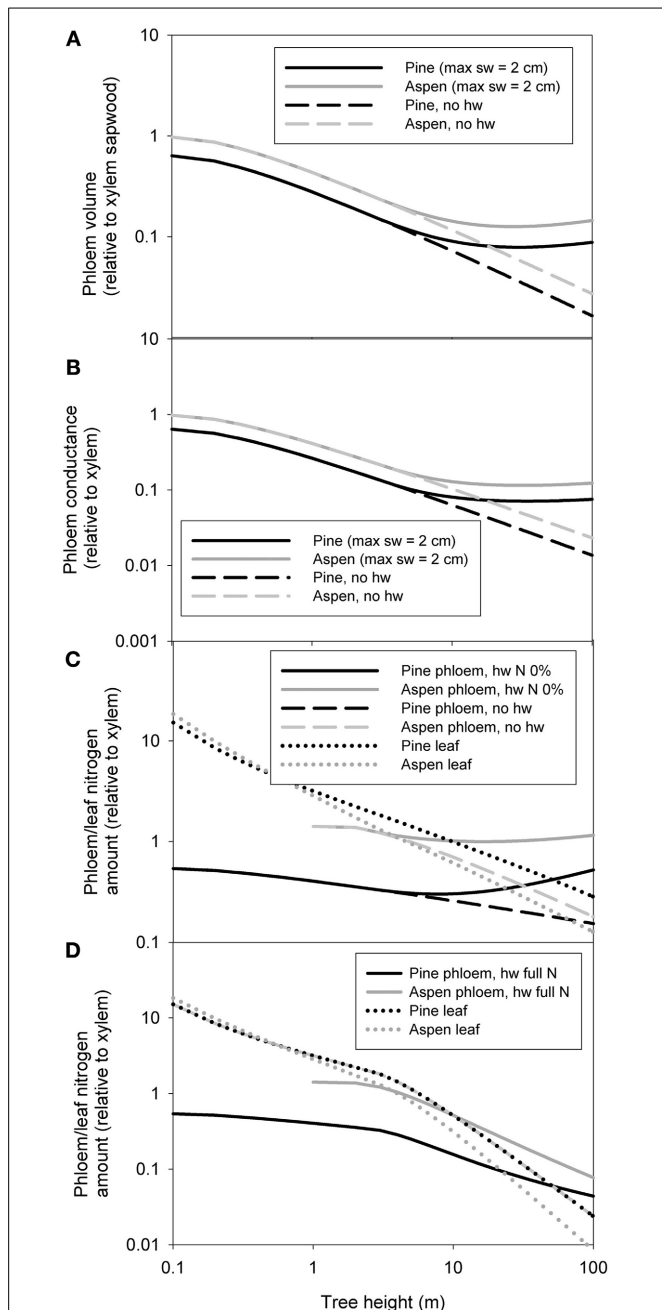*Stem/branch diameter (d) is in units of millimeters (mm).*

FIGURE 4 | The predictions for the whole tree phloem volume in relation to xylem sapwood volume (A), phloem hydraulic conductance in relation xylem hydraulic conductance (B), total phloem and leaf nitrogen content in relation to xylem hydraulic content for the scenarios in which the heartwood has the same nitrogen content as the sapwood and for the case of no heartwood (C), and phloem and leaf nitrogen content in relation to xylem hydraulic content for the case where the heartwood has the same nitrogen content as the sapwood (D). "sw = 2 cm" refers to a scenario where maximum sapwood depth was assumed to be 2 cm and the heartwood did not contain any nitrogen, "no hw" to a scenario of no heartwood formation, i.e., all of the xylem was assumed to be conducting, and "hw full N" a scenario where maximum sapwood depth was assumed to be 2 cm and the heartwood nitrogen content was the same as that of the sapwood. In **(B)** the same area-specific conductivity was assumed for xylem and phloem.

Simulated whole tree phloem turgor pressure differences, simulation 3

Finally, in simulation 3, we analyzed how the whole tree level turgor pressure difference varies as a function of tree height using the predicted structural scaling of whole tree xylem and phloem hydraulic conductance. Phloem turgor pressure was predicted generally to increase slightly with increases in tree height when no heartwood formation was assumed, and to decrease slightly when maximum sapwood depth was limited to 2 cm (**Figure 9**). As the actual amount of sapwood can be predicted to lie in between these extreme scenarios, the turgor pressure differences between the leaves and roots could thus be expected to remain rather stable with increases in tree height. Phloem became unable to transport all of the assimilated sugars in trees larger than 15 m only in the case of low initial phloem conductivity and the assumption of no heartwood formation. In this case phloem sap viscosity experienced a sharp build up preventing an increase in the phloem transport despite an increase in the turgor pressure gradient. The increase in turgor pressure difference with increasing tree size was more pronounced when sugar unloading occurred exclusively in the roots (**Figure 9A**) in comparison to phloem unloading occurring evenly along the stem (**Figure 9B**). In many of the cases presented, phloem turgor pressure difference increased with increasing tree height for small trees, but then started to decline again. This was due to gravity which started become important for taller tree. Gravity aids phloem transport while decreasing the capacity of the xylem to transport water to the leaves. According to the isohydric scenario presented here, the decrease in xylem transport led to lower leaf exchange rates and thus also for a smaller transport need for the phloem. Increase in the initial value for phloem conductivity decreased the turgor pressure gradient for all tree sizes, as would be expected. Importantly, the turgor pressure difference between the leaves and roots required to drive the phloem transport of the assimilated sugars was predicted not to increase linearly with increases in tree height.

Pine was used as an example species in all of the simulations done with the xylem and phloem transport model, but the corresponding simulations for at least aspen would yield similar results as the scaling relations for the xylem and phloem volumes and hydraulic conductances are quite similar amongst the species (see **Figure 4** and **Table 4**).

DISCUSSION
The equations constructed in this study make it possible to estimate whole tree level xylem and phloem properties (volume, hydraulic conductivity, nitrogen content). The equations require relations for xylem and phloem thicknesses/cross-sectional areas, conduit sizes and densities, and the nitrogen content across stem/branch samples of different diameters, and on the shape of the stem taper. Predictions can be made on how whole tree level properties scale with tree size assuming that the measured relationships do not change with tree height. This was supported by the data presented here on trees that varied in size measured for four different species. Phloem, bark, and xylem cross-sectional areas, and nitrogen content could be predicted with minimal deviation from stem/branch diameter alone using allometric, i.e., power law, relationships. The approach presented here can also
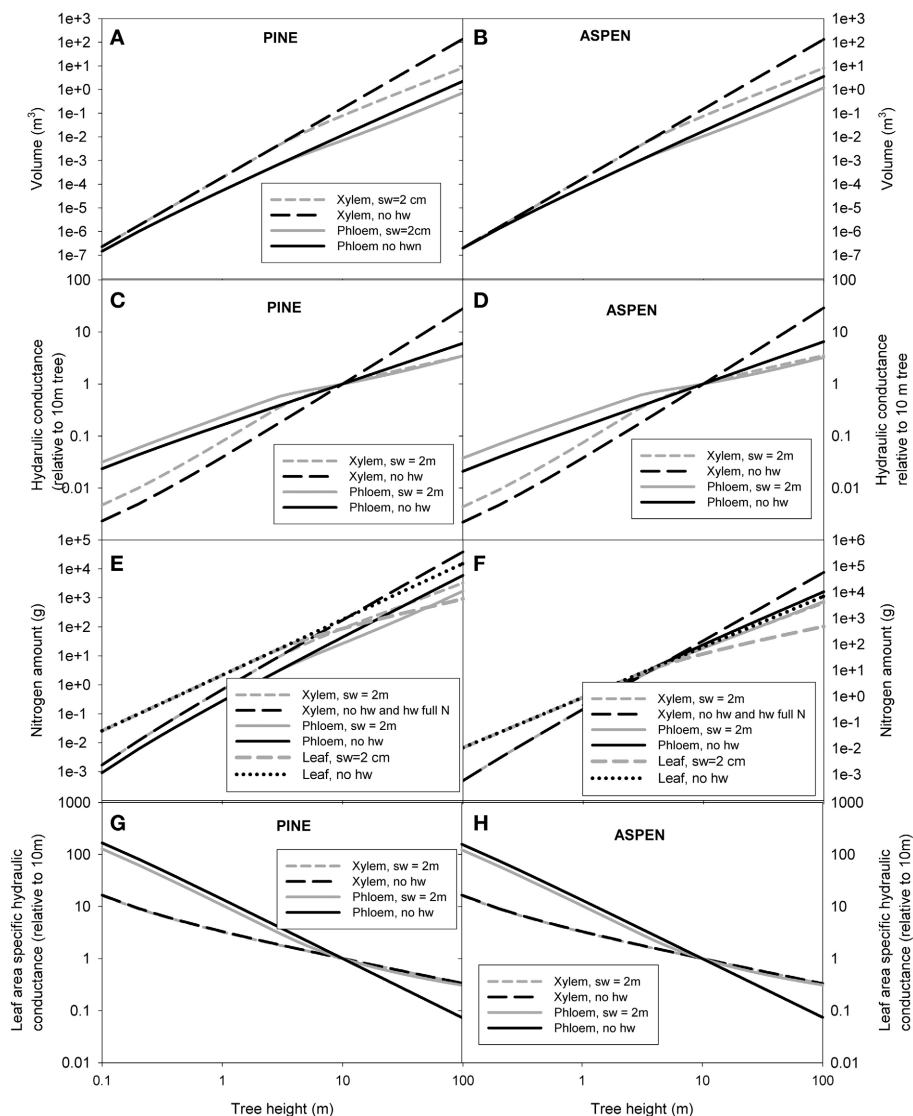
FIGURE 5 | The predictions for the absolute values for whole tree volume of xylem and phloem (A,B), hydraulic conductance of xylem and phloem (C,D), nitrogen content of xylem, phloem and leaves (E,F), and hydraulic conductance of xylem and phloem per leaf area (G,H) as a function of tree height. "sw = 2 cm" refers to a scenario where maximum sapwood depth was assumed to be 2 cm and the heartwood did not contain any nitrogen, "no hw" to a scenario of no heartwood formation, i.e., all of the xylem was assumed to be conducting, and "hw full N" a scenario where maximum sapwood depth was assumed to be 2 cm and the heartwood nitrogen content was the same as that of the sapwood.

be connected to functional-structural tree models that often provide detailed description of tree axes and their dimensions (e.g., Sievänen et al., 2000).

Phloem volume and nitrogen content were predicted to be concentrated heavily toward the tree apex, in contrast to the xylem, whose properties were more evenly distributed within a tree (**Figure 7**). Partially the latter was due to the pipe model assumption for the xylem. However, the pipe model assumption has been shown to work quite well for all the species analyzed in the measurements (Kaufmann and Troendle, 1981; Ilomaki et al., 2003; Kantola and Mäkelä, 2004; Berninger et al., 2005). Also phloem transport capacity (hydraulic conductance) was concentrated more toward the apex, especially if heartwood formation was limited. In contrast, xylem conductance was concentrated toward the base. In both cases the translocation capacity is thus largest closest to the source of the principal transported substance. Our measurements on the axial profile of the phloem thickness and cross-sectional area confirm the findings of Quilhó et al. (2000) who found that the thickness of conducting phloem cells is approximately constant along the stem height, while the cross-sectional area of water conducting xylem increases clearly from stem top toward base. The highly uneven axial distribution of nitrogen in both the xylem and phloem (**Figure 3**) signifies that nitrogen sampling must be done from varying branch sizes and/or tree heights in order to get an appropriate estimate for whole tree level xylem and phloem nitrogen content. For example, if

Table 4 | The results for scaling of tree properties as a function of tree height (*L*).

Property	Pine xylem	Pine phloem	Aspen xylem	Aspen phloem
Volume (no hw)	$2*10^{-5}*L^{2.93}$	$6.5*10^{-5}*L^{2.27}$	$2*10^{-5}*L^{2.94}$	$9.0*10^{-5}*L^{2.31}$
Volume (sw = 2 cm)	$9*10^{-5}*L^{1.99}$[†]	$4.4*10^{-5}*L^{2.11}$	$9*10^{-5}*L^{1.99}$[†]	$6.2*10^{-5}*L^{2.14}$
Nitrogen content (no hw)	$0.79*L^{2.3467}$	$0.35*L^{2.11}$	$0.34*L^{2.61}$	$1.0488*L^{1.9954}$
Nitrogen content (sw = 2 cm, hw full N)	$0.79*L^{2.3467}$	$0.30*L^{1.88}$	$0.34*L^{2.61}$	$1.03*L^{1.82}$
Nitrogen content (sw = 2 cm, hw N 0%)	$2.52*L^{1.56}$	$0.30*L^{1.88}$	$1.54*L^{1.70}$	$1.03*L^{1.82}$
Conductance (sw = 2 cm)	$\alpha\, L^{0.54}$	$\alpha\, L^{0.56}$	$\alpha\, L^{0.55}$	$\alpha\, L^{0.53}$
Conductance (no hw)	$\alpha\, L^{1.45}$	$\alpha\, L^{0.78}$	$\alpha\, L^{1.47}$	$\alpha\, L^{0.81}$
Conductance/leaf area (no hw)	$\alpha\, L^{-0.64}$	$\alpha\, L^{-1.07}$	$\alpha\, L^{-0.64}$	$\alpha\, L^{-1.06}$
Conductance/leaf area (sw = 2 cm)	$\alpha\, L^{-0.63}$	$\alpha\, L^{-1.06}$	$\alpha\, L^{-0.63}$	$\alpha\, L^{-1.05}$
Leaf nitrogen content, no hw	$2.14*L^{1.93}$		$0.91*L^{1.94}$	
Leaf nitrogen content sw = 2 cm	$9.40*L^{1.00}$		$4.57*L^{1.01}$	

Only the exponents were estimated for the conductances. "(sw = 2 cm, hw N 0%)" refers to a scenario where maximum sapwood depth was assumed 2 cm and heartwood was assumed not to contain any nitrogen, "sw = 2 cm, hw full N" a scenario where maximum sapwood depth was assumed to be 2 cm and the heartwood nitrogen content was the same as that of the sapwood, and "no hw" refers to a scenario of no heartwood formation, i.e., all of the xylem was assumed to be conducting.
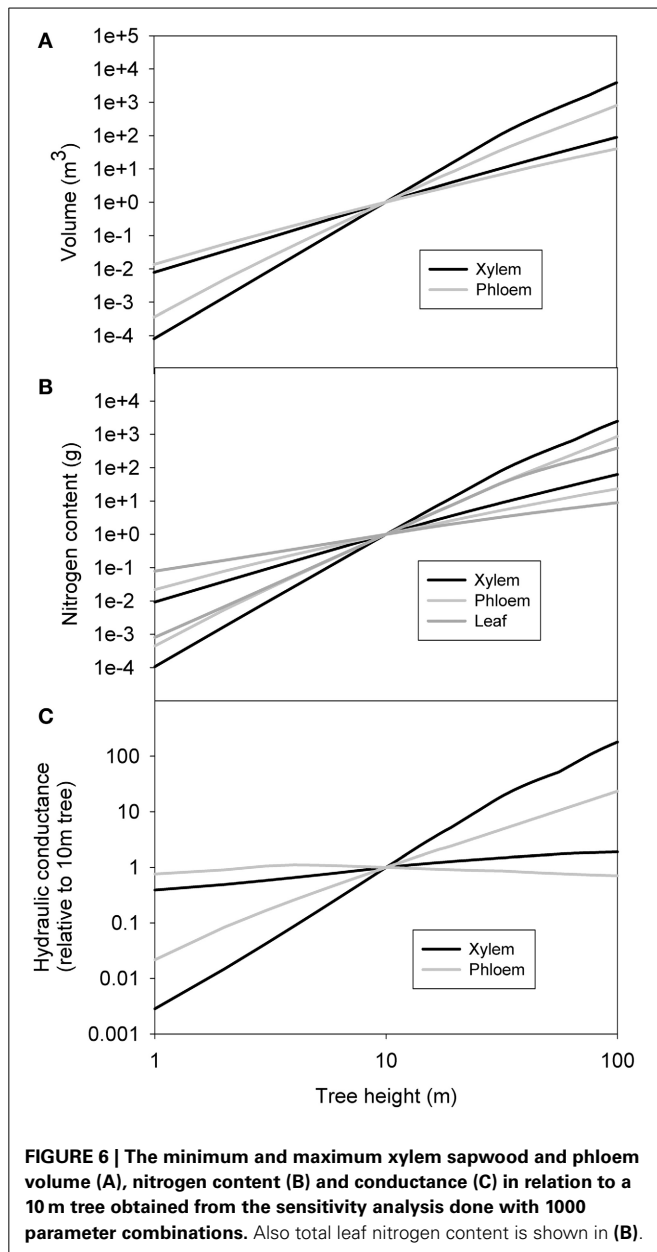
[†]*Sapwood volume*

nitrogen content sampling was done exclusively from larger stem and branch parts, then the total amount of nitrogen allocated to the vascular tissues would be grossly underestimated. This result has also direct implications to forest management where bioenergy harvesting is becoming more popular with the need for boosting the use of renewable energy sources. Our results imply that removal of distal parts of the crown from the growing site will deplete the ecosystem nitrogen pool as efficiently as the removal of leaves.

The relations between xylem sapwood and phloem volumes and conductances at the whole tree level were found to be sensitive to the assumption made about sapwood turnover to heartwood. When no heartwood formation was assumed, whole phloem conductance could not keep up with xylem conductance with increase in tree height. However, when a maximum sapwood radius of 2 cm was assumed, whole tree xylem and phloem conductances were predicted to change at approximately the same rates with tree growth, and xylem sapwood to phloem ratio was predicted to saturate approximately to a value of 10 (**Figure 4A**). This is approximately the same ratio as Hölttä et al. (2009) predicted based on the ratio of typical water to CO_2 exchange rate the leaves and ranges of xylem and phloem pressure gradients typically observed.

It seems clear that the xylem and phloem become increasingly larger sinks of nitrogen in relation to foliage with increases in tree height, and that the nitrogen requirements of the vascular tissues could be a major limiting factor to tree growth in the Boreal region. In trees larger than ∼10 m (**Figures 4C,D**; the exact height was depend on the species and the assumptions made about heartwood), xylem had the highest nitrogen content. Also some previous studies have reported large amounts of nitrogen in the stems of large trees (e.g., Helmisaari, 1995). Aspen had a larger proportion of nitrogen in the phloem in comparison to xylem and leaf than pine. Also the proportion of nitrogen in the xylem in comparison to the leaves was smaller in aspen in relation to pine. The case of nitrogen allocation between

phloem and foliage is particularly interesting as there is a clear tradeoff between the nitrogen used to assimilation or assimilate transport. Already Mooney and Gulmon (1979) and Field (1983) suggested on theoretical grounds that optimal nitrogen allocation within tree crowns should yield constant photosynthetic nitrogen use efficiency. However, such distribution has rarely been found, probably owing to various other factors that influence photosynthetic production rate of foliage in the crown apart from nitrogen (e.g., Posada et al., 2012). In reality, the proportion of nitrogen allocated to the leaves could decline even more strongly with height than our analysis suggests as the leaf to sapwood ratio typically decreases with increases in tree height (e.g., McDowell et al., 2002a,b), which was not taken into account in our analysis. However, not all of the nitrogen found in the xylem and phloem is necessarily bound to the tissue structure, but it could also be in temporary storage there (Wetzel et al., 1989). Our study was conducted in the boreal environment where soil water availability is hardly ever restricting tree function and growth, while nitrogen is the main resource limitation for tree growth. It would be interesting to see if the allometric relations observed here diverge if trees from different environments would be added to the comparison.

The phloem transport capacity was predicted to decline more strongly than the xylem transport capacity when a tree grows in height, although the scenario of rapid xylem sapwood to heartwood turnover led to the ratio of phloem to xylem to phloem to stabilize at tree heights larger than 10 m. Theoretically, xylem and phloem transport conductances should scale almost equally with growth in height, if the ratios between water and carbon exchange and the driving forces for xylem and phloem transport are to be maintained. How is it then possible that leaf specific phloem transport capacity will decrease more in proportion to xylem transport capacity? We can hypothesize several explanations for this; (A) Gravity will increase the flow rate in the phloem and decrease the flow rate in the xylem for a given pressure gradient with increasing tree height. (B) A large proportion of the photosynthates might be consumed close to the apex in tall trees, so that

FIGURE 6 | The minimum and maximum xylem sapwood and phloem volume (A), nitrogen content (B) and conductance (C) in relation to a 10 m tree obtained from the sensitivity analysis done with 1000 parameter combinations. Also total leaf nitrogen content is shown in **(B)**.

FIGURE 7 | The axial distribution of xylem sapwood and phloem cross-sectional area (A), nitrogen content (B) and hydraulic conductivity in a 10-m tree (C). Values are expressed in relation to tree base in each case. "sw = 2 cm" refers to a scenario where maximum sapwood depth was assumed to be 2 cm, and "no hw" refers to a scenario of no heartwood formation, i.e., all of the xylem was assumed to be conducting.

phloem conductance can be allowed to decline at lower heights in the tree. This is in contrast to the xylem where practically all of the water is transported all the way from soil to the foliage. (C) Trees compensate for the decreased leaf area specific phloem conductance by increasing the turgor and osmotic pressure gradient in the phloem as a tree grows in height. Our simulations with the coupled xylem and phloem transport model revealed that the factors given above could explain the functioning of phloem transport by the Münch pressure flow hypothesis with increasing tree height even when phloem conductance decreases slightly in relation to xylem conductance with increasing tree height. The simulations also revealed that in most of the scenarios explored the turgor pressure difference between the leaves and roots remained rather constant with increases in tree height. This result is line with a recent review (Turgeon, 2010) which stated
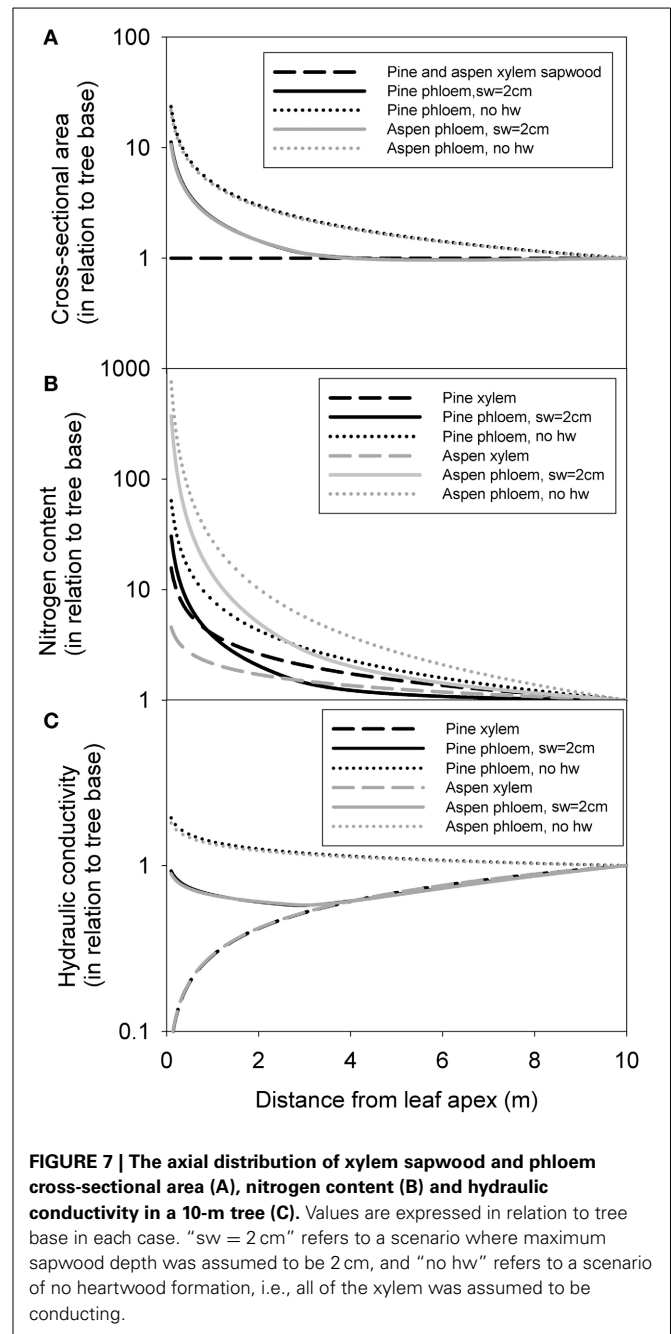
that there are indications that the turgor pressure differences between the sources and sink would not increase with tree size.

The xylem and phloem transport model also predicted that concentrating phloem volume more toward the leaf apex yielded lower turgor pressure difference between leaves and roots, especially if part of the sugars transported in the phloem are utilized along the stem. However, the actual increase in phloem volume toward the apex (based on the measurements and the scaling presented in this study) was found to be even larger than that predicted by the transport model. Also the within tree gradients of turgor pressure and osmotic concentration can be predicted from the axial distribution of xylem sapwood and phloem volumes and

FIGURE 8 | Simulated xylem water potential, phloem turgor pressure and phloem osmotic concentration axial profiles for cases of phloem unloading in sink and phloem unloading along the stem for pine with an assumption of maximum sapwood depth of 2 cm (A) and no heartwood formation (B).

FIGURE 9 | Simulated turgor pressure difference between leaf and root phloem as a function of tree height with varying parameterization for a case where all phloem unloading occurs in the root (A) and evenly along the stem (B) for pine. "sw = 2 cm" refers to a scenario where maximum sapwood depth was assumed to be 2 cm, and "no hw" refers to a scenario of no heartwood formation, i.e., all of the xylem was assumed to be conducting. "$K_{p,tot}*2$," and "$K_{p,tot}*0.5$" refer cases where the absolute phloem conductance has been multiplied by a factor of 2 and 0.5, respectively.

area-specific conductivities using a transport model (**Figure 8**). One can hypothesize a feedback loop between local pressure and osmotic concentration mediated by xylem and phloem conductances, and the local growth rate of new xylem and phloem tissue. This feedback loop, spanning several growing seasons, could be explained by the direct link between cell division, expansion, and cell wall synthesis on the local water and carbon status (e.g., De Schepper and Steppe, 2010; Hölttä et al., 2010; Pantin et al., 2012) providing a structural-functional automata for vascular development in trees.

Xylem conductance also decreases with growth in height, but not nearly as sharply as phloem conductance. Xylem conductance decreases at the rate of square root of tree height, which stems from two simple empirical observations: the cross-sectional area of xylem sapwood over branching is conserved (Shinozaki et al., 1964) and the increase in xylem conduit radius with tree height ($r_x \alpha\ x^{1/4}$) (West et al., 1999). Various findings also support the notion that tree transpiration and photosynthesis rates decrease with tree height as either stomatal conductance and/or leaf to sapwood area decrease (McDowell et al., 2002a,b, 2005; Martínez-Vilalta et al., 2007). The strong decrease of phloem conducting capacity toward the tree base stems from the observation that the phloem width does not change very much from tree top
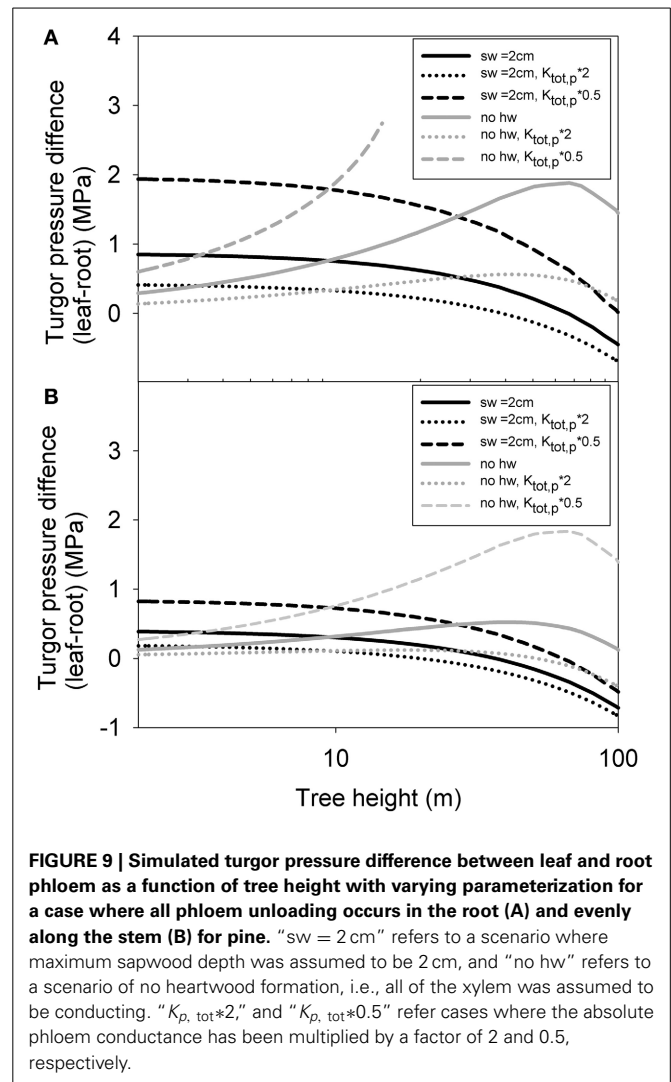
to the base (see also Quilhó et al., 2000). One possible explanation for this is that it follows from the limitations of cambium activity. Unlike the sapwood, which accumulates over several years, phloem apparently needs to be renewed practically yearly (Ewers, 1982). Secondary growth results from rate of cell division and their subsequent enlargement. These are constrained by the length of the growth period and temperature during the period but also by the water status and sugar supply to the growth location (e.g., De Schepper and Steppe, 2010; Hölttä et al., 2010). While it seems that the vigor of the tree may influence the extension of growth period (Rathgeber et al., 2011) it is ultimately influenced by the duration of the favorable conditions, particularly in boreal environment. The water status and available sugars are influenced by the tree size such that there is less foliage, and presumably sugars, relative to stem the bigger the trees. For these reasons, the annual width of phloem growth could be limited, and although the relatively constant phloem width in axial direction means that phloem width increases relative to yearly tree ring width from top to base, it is not able to compensate for the different functional longevities of the tissues. The increasing girth of

the trees, however, will help to balance the difference. We could even hypothesize that the need to balance the amounts of phloem and xylem tissue would be behind the stem diameter growth and sapwood turnover. With a given sapwood requirement, its higher turnover would necessarily mean faster thickness growth, which would have a large impact also on resource allocation and tree development (Nikinmaa, 1992). All these functional-structural interactions impose strong boundary conditions for the tree development and function.

CONCLUSIONS

The study showed that important understanding of whole tree functions can be gained by dimensional analysis across tree axes. The observed regularities in xylem and phloem structure, and the Münch- pressure flow hypothesis seem to provide a feasible explanation of phloem transport even in the largest trees. Sapwood turnover to heartwood seems to have an important functional role in affecting the scaling relations for xylem and phloem hydraulic conductances and nitrogen allocation. Xylem and phloem tissues are clearly a larger sink of nitrogen than the foliage as trees grow in height becoming an important and an often overlooked factor in the forest nitrogen cycle particularly in the nitrogen limited boreal forest where the slow nitrogen turnover rate is often the reason for growth limitation.

ACKNOWLEDGMENTS

REFERENCES

Anfodillo, T., Carraro, V., Carrer, M., Fior, C., and Rossi, S. (2006). Convergent tapering of xylem conduits in different woody species. *New Phytol.* 169, 279–290. doi: 10.1111/j.1469-8137.2005.01587.x

Bergh, B., Linder, S., Lundmark, T., and Elfving, B. (1999). The effect of water and nutrient availability on the productivity of Norway spruce in northern and southern Sweden. *For. Ecol. Manage.* 119, 51–62. doi: 10.1016/S0378-1127(98)00509-X

Berninger, F., Coll, L., Vanninen, P., Mäkelä, A., Palmroth, S., and Nikinmaa, E. (2005). Effects of tree size and position on pipe model ratios in Scots pine. *Can. J. For. Res.* 35, 1294–1305. doi: 10.1139/x05-055

Brown, J. H., Gillooly, J. F., Allen, A. P., Savage, V. M., and West, G. B. (2004). Toward a metabolic theory of ecology. *Ecology* 85, 1771–1789. doi: 10.1890/03-9000

Cernusak, L. A., Aranda, J., Marshall, J. D., and Winter, K. (2007). Large variation in whole-plant water-use efficiency among tropical tree species. *New Phytol.* 173, 294–305. doi: 10.1111/j.1469-8137.2006.01913.x

Chapin, F. S. III, Bloom, A. J., and Field, C. B. (1987). Plant responses to multiple environmental factors. *Bioscience* 37, 49–57. doi: 10.2307/1310177

De Schepper, V., and Steppe, K. (2010). Development and verification of a water and sugar transport model using measured stem diameter variations. *J. Exp. Bot.* 61, 2083–2099. doi: 10.1093/jxb/erq018

Evans, J. R. (1993). Photosynthetic acclimation and nitrogen partitioning within a lucerne canopy. II. Stability through time and comparison with a theoretical optimum. *Aust. J. Plant Physiol.* 20, 69–82. doi: 10.1071/PP9930069

Ewers, F. W. (1982). Secondary growth in needle leaves of pinus longaeva (bristlecone pine) and other conifers: quantitative data. *Am. J. Bot.* 69, 1552–1559. doi: 10.2307/2442909

Field, C. (1983). Allocating leaf nitrogen for the maximization of carbon gain: leaf age as a control on the allocation program. *Oecologia* 56, 341–347. doi: 10.1007/BF00379710

Hacke, U. G., Sperry, J. S., Pockman, W. P., Davis, S. D., and McCulloh, K. A. (2001). Trends in wood density and structure are linked to prevention of xylem implosion by negative pressure. *Oecologia* 126, 457–461. doi: 10.1007/s004420100628

Hari, P., and Mäkelä, A. (2003). Annual pattern of photosynthesis in Scots pine in the boreal zone. *Tree Physiol.* 23, 145–155. doi: 10.1093/treephys/23.3.145

Helmisaari, H. S. (1995). Nutrient cycling in *Pinus sylvestris* stands in eastern Finland. *Plant Soil.* 168–169, 327–336. doi: 10.1007/BF00029345

Hirose, T., and Werger, M. J. A. (1987). Maximizing daily canopy photosynthesis with respect to the leaf nitrogen allocation pattern in the canopy. *Oecologia* 72, 520–526. doi: 10.1007/BF00378977

Hoffmann, C. W., and Usoltsev, V. A. (2002). Tree-crown biomass estimation in forest species of the Ural and of Kazakhstan. *For. Ecol. Manage.* 158, 59–69. doi: 10.1016/S0378-1127(00)00669-1

Hollinger, D. Y. (1996). Optimality and nitrogen allocation in a tree canopy. *Tree Physiol.* 16, 627–634. doi: 10.1093/treephys/16.7.627

Hölttä, T., Mäkinen, H., Nöjd, P., Mäkelä, A., and Nikinmaa, E. (2010). A physiological model of softwood cambial growth. *Tree Physiol.* 30, 1235–1252. doi: 10.1093/treephys/tpq068

Hölttä, T., Mencuccini, M., and Nikinmaa, E. (2009). Linking phloem function to structure: analysis with a coupled xylem–phloem transport model. *J. Theor. Biol.* 259, 325–337. doi: 10.1016/j.jtbi.2009.03.039

Hölttä, T., Mencuccini, M., and Nikinmaa, E. (2011). A carbon cost-gain model explains the observed patterns of xylem safety and efficiency. *Plant Cell Environ.* 34, 1819–1834. doi: 10.1111/j.1365-3040.2011.02377.x

Huber, B. (1928). Weitere quantitative untersuchungen über das wasserleitungssystem der Pflanzen. *Jahrb. Wiss. Bot.* 67, 877–959.

Ilomaki, S., Nikinmaa, E., and Makela, A. (2003). Crown rise due to competition drives biomass allocation in silver birch (*Betula pendula L.*). *Can. J. For. Res.* 33, 2395–2404. doi: 10.1139/x03-164

Jensen, K. H., Lee, J., Bohr, T., Bruus, H., Holbrook, N. M., and Zwieniecki, M. A. (2011). Optimality of the Münch mechanism for translocation of sugars in plants. *J. R. Soc. Interface* 8, 1155–1165. doi: 10.1098/rsif.2010.0578

Jensen, K. H., Liesche, J., Bohr, T., and Schulz, A. (2012). Universality of phloem transport in seed plants. *Plant Cell Environ.* 35, 1065–1076. doi: 10.1111/j.1365-3040.2011.02472.x

Jones, H. G., and Sutherland, R. A. (1991). Stomatal control of xylem embolism. *Plant Cell Environ.* 14, 607–612. doi: 10.1111/j.1365-3040.1991.tb01532.x

Kantola, A., and Mäkelä, A. (2004). Crown development in Norway spruce (*Picea Abies* [L.]Karst.) *Trees* 18, 408–421. doi: 10.1007/s00468-004-0319-x

Kaufmann, M. R., and Troendle, C. A. (1981). The relationship of leaf area and foliage biomass to sapwood conducting area in four subalpine forest tree species. *For. Sci.* 27, 477–482.

Korhonen, J. F. J., Pihlatie, M., Pumpanen, J., Aaltonen, H., Hari, P., Levula, J., et al. (2013). Nitrogen balance of a boreal Scots pine forest. *Biogeosciences* 10, 1083–1095. doi: 10.5194/bg-10-1083-2013

Kull, O. (2002). Acclimation of photosynthesis in canopies: models and limitations. *Oecologia* 133, 267–279. doi: 10.1007/s00442-002-1042-1

Lusk, C. H., Wright, I., and Reich, P. (2003). Photosynthetic differences contribute to competitive advantage of evergreen angiosperm trees over evergreen conifers in productive habitats. *New Phytol.* 160, 329–336. doi: 10.1046/j.1469-8137.2003.00879.x

MacCurdy, E. (ed.). (2002). *The Notebooks of Leonardo Da Vinci. Definitive edition in one volume.* Old Saybrook, CT; Konecky and Konecky.

Mäkelä, A. (1986). Implications of the pipe model theory on dry matter partitioning and height growth of trees. *J. Theor. Biol.* 123, 103–120. doi: 10.1016/S0022-5193(86)80238-7

Mäkelä, A., and Valentine, H. T. (2006). The quarter-power scaling model does not imply size-invariant hydraulic resistance in plants. *J. Theor. Biol.* 243, 283–285. doi: 10.1016/j.jtbi.2006.06.006

Martinez-Vilalta, J., Cochard, H., Mencuccini, M., Sterck, F., Herrero, A., Korhonen, J. F. J., et al. (2009). Hydraulic adjustment of Scots pine across Europe. *New Phytol.* 184, 353–364. doi: 10.1111/j.1469-8137.2009.02954.x

Martínez-Vilalta, J., Vanderklein, D., and Mencuccini, M. (2007). Tree height and age-related decline in growth in Scots pine

(*Pinus sylvestris* L.). *Oecologia* 150, 529–544. doi: 10.1007/s00442-006-0552-7

McCulloh, K. A., Sperry, J. S., and Adler, F. R. (2003). Water transport in plants obeys Murray's law. *Nature* 421, 939–942. doi: 10.1038/nature01444

McDowell, N. G., Licata, J., and Bond, B. (2005). Environmental sensitivity of gas exchange in different-sized trees. *Oecologia* 145, 9–20. doi: 10.1007/s00442-005-0104-6

McDowell, N. G, Phillips, N, Lunch, C, Bond, B. J, and Ryan, M. G. (2002a). An investigation of hydraulic limitation and compensation in large, old Douglas-fir trees. *Tree Physiol.* 22, 763–774. doi: 10.1093/treephys/22.11.763

McDowell, N. G, Barnard, H., Bond, B., Hinckley, T., Hubbard, R., Ishii, H., et al. (2002b). The relationship between tree height and leaf area: sapwood area ratio. *Oecologia* 132, 12–20. doi: 10.1007/s00442-002-0904-x

Meerts, P. (2002). Mineral nutrient concentrations in sapwood and heartwood: a literature review. *Ann. For. Sci.* 59, 713–722. doi: 10.1051/forest:2002059

Melcher, P. J., Zwieniecki, M. A., and Holbrook, N. M. (2003). Vulnerability of xylem vessels to cavitation in sugar maple. Scaling from individual vessels to whole branches. *Plant Physiol.* 131, 1775–1780. doi: 10.1104/pp.102.012856

Mencuccini, M., Hölttä, T., and Martinez-Vilalta, J. (2011). "Design criteria for models of the transport systems of tall trees," in *Size- and age-related changes in tree structure and function. Volume in Springer Tree Physiology Series*, eds F. C. Meinzer, T. Dawson, and B. Lachenbruch (New York, NY: Springer-Verlag), 309–339. doi: 10.1007/978-94-007-1242-3_12

Mooney, H. A., and Gulmon, S. L. (1979). "Environmental and evolutionary constraints on the photosynthetic characteristics of higher plants," in *Topics in Plant Population Biology*, eds O. T. Solbrig, S. Jain, G. B. Johnson, and P. H. Raven (New York, NY: Columbia University Press), 316–337.

Niinemets, Ü. (1997). Role of foliar nitrogen in light harvesting and shade tolerance of four temperate deciduous woody species. *Funct. Ecol.* 11, 518–531. doi: 10.1046/j.1365-2435.1997.00109.x

Nikinmaa, E. (1992). Analyses of the growth of Scots pine; matching structure with function. *AFF* 235, 68.

Nikinmaa, E., Hölttä, T., Hari, P., Kolari, P., Mäkelä, A., Sevanto, S., et al. (2013). Assimilate transport in phloem sets conditions for leaf gas exchange. *Plant Cell Environ.* 36, 655–669. doi: 10.1111/pce.12004

Olson, M. E., and Rosell, J. A. (2013). Vessel diameter–stem diameter scaling across woody angiosperms and the ecological causes of xylem vessel diameter variation. *New Phytol.* 197, 1204–1213. doi: 10.1111/nph.12097

Pantin, F., Simonneau, T., and Muller, B. (2012). Coming of leaf age: control of growth by hydraulics and metabolics during leaf ontogeny. *New Phytol.* 196, 349–366. doi: 10.1111/j.1469-8137.2012.04273.x

Paul, M. J., and Foyer, C. H. (2001). Sink regulation of photosynthesis. *J. Exp. Bot.* 52, 1383–1400. doi: 10.1093/jexbot/52.360.1383

Perttunen, J., Sievänen, R., Nikinmaa, E., Salminen, H., Saarenmaa, H., and Väkevä, J. (1996). LIGNUM: a tree model based on simple structural units. *Ann. Bot.* 77, 87–98. doi: 10.1006/anbo.1996.0011

Posada, J. M., Sievänen, R., Messier, C., Perttunen, J., Nikinmaa, E., and Lechowicz, M. J. (2012). Contributions of leaf A_{max}, leaf angle and self-shading to the maximization of net photosynthesis in Acer saccharum: a modeling assessment. *Ann. Bot.* 110, 731–741. doi: 10.1093/aob/mcs106

Prusinkiewicz, P. (2004). Modeling plant growth and development. *Curr. Opin. Plant Biol.* 7, 79–83. doi: 10.1016/j.pbi.2003.11.007

Quilhó, T., Pereira, H., and Richter, H. G. (2000). Within-tree variation in phloem cell dimensions and proportions in Eucalyptus globulus. *IAWA J.* 21, 31–40. doi: 10.1163/22941932-90000234

Rathgeber, C. B. K., Rossi, S., and Bontemps, J. D. (2011). Cambial activity related to tree size in a mature silver-fir plantation. *Ann. Bot.* 108, 429–438. doi: 10.1093/aob/mcr168

Reich, P. B., Walters, M. B., Ellsworth, D. S., Vose, J. M., Volin, J. C., Gresham, C., et al. (1998). Relationships of leaf dark respiration to leaf nitrogen, specific leaf area and leaf life-span: a test across biomes and functional groups. *Oecologia*, 114, 471–482. doi: 10.1007/s004420050471

Savage, V. M., Bentley, L. P., Enquist, B. J., Sperry, J. S., Smith, D. D., Reich, P. B., et al. (2010). Hydraulic trade-offs and space filling enable better predictions of vascular structure and function in plants. *Proc. Natl. Acad. Sci. U.S.A.* 107, 22722–22727. doi: 10.1073/pnas.1012194108

Sellin, A. (1994). Sapwood-heartwood proportion related to tree diameter, age, and growth rate in Picea abies. *Can. J. For. Res.* 24, 1022–1028. doi: 10.1139/x94-133

Shinozaki, K., Yoda, K., Hozumi, K., and Kira, T. A. (1964). Quantitative analysis of plant form- the pipe model theory: I. Basic analysis. *Jap. J. Ecol.* 14, 97–105.

Sievänen, R., Nikinmaa, E., Nygren, P., Ozier-Lafontaine, H, Perttunen, J., and Hakula, H. (2000). Components of functional-structural tree models. *Ann. For. Sci.* 57, 399–412. doi: 10.1051/forest:2000131

Turgeon, R. (2010). The Puzzle of phloem pressure. *Plant Physiol.* 154, 578–581. doi: 10.1104/pp.110.161679

Tyree, M. T, and Sperry, J. S. (1988). Do woody plants operate near the point of catastrophic xylem dysfunction caused by dynamic water stress? *Plant Physiol.* 88, 574–580. doi: 10.1104/pp.88.3.574

Vanninen, P., and Mäkelä, A. (1999). Fine root biomass of Scots pine stands differing in age and soil fertility in southern Finland. *Tree Physiol.* 19, 823–830. doi: 10.1093/treephys/19.12.823

West, G. B., Brown, J. H., and Enquist, B. J. (1999). A general model for the structure and allometry of plant vascular systems. *Nature* 400, 664–667. doi: 10.1038/23251

Wetzel, S., Demmers, C., and Greenwood, J. S. (1989). Seasonally fluctuating bark proteins are a potential form of nitrogen storage in three temperate hardwoods. *Planta* 178, 275–281. doi: 10.1007/BF00391854

Wright, I. J., Reich, P. B., Westoby, M., Ackerly, D. D., Baruch, Z., Bongers, F., et al. (2004). The worldwide leaf economics spectrum. *Nature* 428, 821–827. doi: 10.1038/nature02403

Zimmermann, M. H. (1983). *Xylem Structure and The Ascent of Sap*. Berlin: Springer-Verlag. doi: 10.1007/978-3-662-22627-8

Conflict of Interest Statement: The authors declare that the research was conducted in the absence of any commercial or financial relationships that could be construed as a potential conflict of interest.

APPENDIX

A1. DERIVATION OF THE ANALYTIC SCALING FUNCTIONS FOR XYLEM AND PHLOEM PROPERTIES AS A FUNCTION OF TREE SIZE

The number of furcations at distance of x from the leaf apex is (assuming pipe model relations, i.e., nAx is preserved)

$$n(x) = \frac{n_{\text{ref}} A_{x,\text{ref}}}{A_x(x)} = \frac{n_{\text{ref}} \alpha_1 \gamma^{\beta_1} L^{\delta\beta_1}}{\alpha_1 \gamma^{\beta_1} x^{\delta\beta_1}} = \frac{L^{\delta\beta_1}}{x^{\delta\beta_1}} = \left(\frac{L}{x}\right)^{\delta\beta_1} \quad (A1)$$

where n_{ref} is the number of furcations at the base of tree ($n_{\text{ref}} = 1$) is and L is total tree height.

Total amount of xylem in a tree as a function of tree height (starting from a distance L_0 away from leaf apex) is

$$V_{x,\text{tot}} = \int_0^L nA_x dx = \int_0^L \left(\frac{L}{x}\right)^{\delta\beta_1} \alpha_1 \gamma^{\beta_1} x^{\delta\beta_1} dx$$

$$= \int_0^L L^{\delta\beta_1} \alpha_1 \gamma^{\beta_1} x^{\delta\beta_1} x^{-\delta\beta_1} dx = \int_0^L L^{\delta\beta_1} \alpha_1 \gamma^{\beta_1} dx =$$

$$= L^{\delta\beta_1} \alpha_1 \gamma^{\beta_1} L = \alpha_1 \gamma^{\beta_1} L^{\delta\beta_1+1} - \alpha_1 \gamma^{\beta_1} L_0^{\delta\beta_1+1} \quad (A2)$$

If the distance L_0 is more than zero (e.g., if measurements only exist starting from a distance L_0 from the apex as in our measurements) and if the xylem properties are assumed to remain constant between distance 0 and L_0, the amount xylem between 0 and L_0 (0.1 m in this case) must be added to the sum. Xylem properties were assumed to be constant (the same as at a distance L_0 from the apex = in this range. The amount of xylem between 0 and 0.1 m is

$$V_{x,0-L_0} = nA_x dx = \left(\frac{L}{L_0}\right)^{\delta\beta_1} \alpha_1 \gamma^{\beta_1} L_0^{\delta\beta_1} L_0$$

$$= \left(\frac{L}{0.1\,\text{m}}\right)^{\delta\beta_1} \alpha_1 \gamma^{\beta_1} 0.1\,\text{m}^{\delta\beta_1} * 0.1\,\text{m} \quad (A3)$$

Total amount of phloem in tree as a function of tree height is

$$V_{p,\text{tot}} = \int_{L_0}^L nA_p dx = \int_{L_0}^L \left(\frac{L}{x}\right)^{\delta\beta_1} \alpha_2 \gamma^{\beta_2} x^{\delta\beta_2} dx$$

$$= \int_{L_0}^L L^{\delta\beta_1} \alpha_2 \gamma^{\beta_2} x^{\delta\beta_2} x^{-\delta\beta_1} dx = \int_{L_0}^L L^{\delta\beta_1} \alpha_2 \gamma^{\beta_2} x^{\delta\beta_2 - \delta\beta_1} dx =$$

$$= \frac{L^{\delta\beta_1} \alpha_2 \gamma^{\beta_2}}{\delta\beta_2 - \delta\beta_1 + 1} \left(L^{\delta\beta_2 - \delta\beta_1 + 1} - L_0^{\delta\beta_2 - \delta\beta_1 + 1}\right)$$

$$= \frac{L^{\delta\beta_1} \alpha_2 \gamma^{\beta_2}}{\delta\beta_2 - \delta\beta_1 + 1} \left(L^{\delta\beta_2 - \delta\beta_1 + 1} - L_0^{\delta\beta_2 - \delta\beta_1 + 1}\right) \quad (A4)$$

where L_0 is the height (distance from apex) from which the integration is started from. The integration could not be started from $L_0 = 0$ as the phloem volume approaches infinity when L_0 approaches 0.

Also, the amount of phloem between 0 and L_0 must be added to the sum. Phloem properties were assumed to be constant in

this range. The amount of phloem between 0 and 0.1 m is

$$V_{p,0-L_0} = nA_p dx = \left(\frac{L}{L_0}\right)^{\delta\beta_1} \alpha_2 \gamma^{\beta_2} L_0^{\delta\beta_2} L_0$$

$$= \left(\frac{L}{0.1\,\text{m}}\right)^{\delta\beta_1} \alpha_2 \gamma^{\beta_2} 0.1\,\text{m}^{\delta\beta_2} * 0.1\,\text{m} \quad (A5)$$

Total amount of nitrogen in xylem as a function of tree height is

$$N_{x,\text{tot}} = \int_{L_0}^L nA_x \rho_{N,x} \rho_x dx$$

$$= \int_{L_0}^L \left(\frac{L}{x}\right)^{\delta\beta_1} \alpha_1 \gamma^{\beta_1} x^{\delta\beta_1} \alpha_3 \gamma^{\beta_3} x^{\delta\beta_3} \rho_x dx$$

$$= \int_{L_0}^L L^{\delta\beta_1} \alpha_1 \gamma^{\beta_1} \alpha_3 \gamma^{\beta_3} x^{\delta\beta_1} x^{-\delta\beta_1} x^{\delta\beta_3} \rho_x dx =$$

$$\int_{L_0}^L L^{\delta\beta_1} \alpha_1 \gamma^{\beta_1} \alpha_3 \gamma^{\beta_3} x^{\delta\beta_3} \rho_x dx = \frac{L^{\delta\beta_1} \alpha_1 \gamma^{\beta_1} \alpha_3 \gamma^{\beta_3} \rho_x L^{\delta\beta_3 + 1}}{\delta\beta_3 + 1}$$

$$= \frac{\alpha_1 \gamma^{\beta_1} \alpha_3 \gamma^{\beta_3} \rho_x}{\delta\beta_3 + 1} L^{\delta\beta_1 + \delta\beta_3 + 1}$$

$$- \frac{\alpha_1 \gamma^{\beta_1} \alpha_3 \gamma^{\beta_3} \rho_x}{\delta\beta_3 + 1} L_0^{\delta\beta_1 + \delta\beta_3 + 1} \quad (A6)$$

where ρ_x is the density of the xylem tissue (gm^{-3}). We assume ρ_N to be $0.5 * 10^{-6}$ gm^{-3}.

Also, the amount nitrogen in the xylem between 0 and L_0 must be added to the sum. Phloem properties were assumed to be constant in this range. The amount of phloem between 0 and 1 m is

$$N_{x,0-L_0} = nA_x \rho_x \rho_x dx = \left(\frac{L}{L_0}\right)^{\delta\beta_1} \alpha_1 \gamma^{\beta_1} L_0^{\delta\beta_1} \alpha_3 \gamma^{\beta_3} \rho_N L_0^{\delta\beta_3} L_0$$

$$= \left(\frac{L}{1\,\text{m}}\right)^{\delta\beta_1} \alpha_1 \gamma^{\beta_1} (1\,\text{m})^{\delta\beta_1} \alpha_3 \gamma^{\beta_3} \rho_N 1\,\text{m}^{\delta\beta_3} * 1\,\text{m} \quad (A7)$$

Total amount of nitrogen in phloem as a function of tree height is

$$N_{p,\text{tot}} = \int_0^L nA_p \rho_p \rho_N dx = \int_0^L \left(\frac{L}{x}\right)^{\delta\beta_1} \alpha_2 \gamma^{\beta_2} x^{\delta\beta_2} \alpha_4 \gamma^{\beta_4} \rho_N x^{\delta\beta_4} dx$$

$$= \int_0^L L^{\delta\beta_1} \alpha_2 \gamma^{\beta_2} \alpha_4 \gamma^{\beta_4} \rho_N x^{\delta\beta_2} x^{-\delta\beta_1} x^{\delta\beta_4} dx =$$

$$= \int_0^L L^{\delta\beta_1} \alpha_2 \gamma^{\beta_2} \alpha_4 \gamma^{\beta_4} \rho_N x^{\delta\beta_4 + \delta\beta_2 - \delta\beta_1} dx$$

$$= \frac{L^{\delta\beta_1} \alpha_2 \gamma^{\beta_2} \alpha_4 \rho_N \gamma^{\beta_4}}{\delta\beta_4 + \delta\beta_2 - \delta\beta_1 + 1} \left(L^{\delta\beta_4 + \delta\beta_2 - \delta\beta_1 + 1} - L_0^{\delta\beta_4 + \delta\beta_2 - \delta\beta_1 + 1}\right) \quad (A8)$$

ρ_N is the density of the phloem tissue (g m^{-3}). We assume ρ_N to be $0.5 * 10^{-6}$ gm^{-3}, i.e., the same as for the xylem tissue.

Also, the amount nitrogen in the phloem between 0 and L_0 must be added to the sum. Phloem properties were assumed

to be constant in this range. The amount of phloem between 0 and 1 m is

$$
N_{p,\,0-L_0} = nA_p\rho_p\rho_N dx = \left(\frac{L}{L_0}\right)^{\delta\beta_1}\alpha_2\gamma^{\beta_2}L_0^{\delta\beta_2}\alpha_4\gamma^{\beta_4}\rho_N L_0^{\delta\beta_4}L_0
$$

$$
= \left(\frac{L}{1\,\mathrm{m}}\right)^{\delta\beta_1}\alpha_2\gamma^{\beta_2}(1\,\mathrm{m})^{\delta\beta_2}\alpha_4\gamma^{\beta_4}\rho_N 1\,\mathrm{m}^{\delta\beta_4}*1\,\mathrm{m} \quad (A9)
$$

Total hydraulic conductance of the xylem is

$$
K_{x,\,\mathrm{tot}}^{-1} = \int_0^L \left(nA_x\rho_{c,x}r_x^2\right)^{-1}dx
$$

$$
= \int_0^L \left(\left(\frac{L}{x}\right)^{\delta\beta_1}\alpha_1\gamma^{\beta_1}x^{\delta\beta_1}\alpha_7\gamma^{\beta_7}x^{\delta\beta_7}\alpha_5^2\gamma^{2\beta_5}x^{2\delta\beta_5}\right)^{-1}dx
$$

$$
= \int_0^L \left(L^{\delta\beta_1}\alpha_1\alpha_7\alpha_5^2\gamma^{\beta_1+\beta_7+2\beta_5}\right)^{-1}x^{-\delta\beta_7-2\delta\beta_5}dx
$$

$$
= \left(L^{\delta\beta_1}\alpha_1\alpha_7\alpha_5^2\gamma^{\beta_1+\beta_7+2\beta_5}\right)^{-1}
$$

$$
\frac{1}{-\delta\beta_7-2\delta\beta_5+1}\left(L^{-\delta\beta_7-2\delta\beta_5+1}-L_0^{-\delta\beta_7-2\delta\beta_5+1}\right) \quad (A10)
$$

Also, the xylem resistance between 0 and L_0 must be added to the sum. Xylem properties were assumed to be constant in this range. Xylem conductance between 0 and L_0 is

$$
K_{x,\,0-L_0}^{-1} = \left(nA_x\rho_{c,x}r_x^2\right)^{-1}dx
$$

$$
= \left(\left(\frac{L}{L_0}\right)^{\delta\beta_1}\alpha_1\gamma^{\beta_1}L_0^{\delta\beta_1}\alpha_7\gamma^{\beta_7}L_0^{\delta\beta_7}\alpha_5^2\gamma^{2\beta_5}L_0^{2\delta\beta_5}\right)^{-1}L_0
$$

$$
= \left(\left(\frac{L}{L_0}\right)^{\delta\beta_1}\alpha_1\alpha_7\alpha_5^2\gamma^{\beta_1+\beta_7+2\beta_5}L_0^{\delta\beta_1+\delta\beta_7+2\delta\beta_5}\right)^{-1}L_0 \quad (A11)
$$

Total hydraulic conductance of the phloem is

$$
K_{p,\,\mathrm{tot}}^{-1} = \int_0^L \left(nA_p\rho_{c,p}r_p^2\right)^{-1}dx
$$

$$
= \int_0^L \left(L^{\delta\beta_1}\alpha_2\alpha_8\alpha_6^2\gamma^{\beta_2+\beta_8+2\beta_6}\right)^{-1}x^{-\delta\beta_2+\delta\beta_1-\delta\beta_8-2\delta\beta_6}dx =
$$

$$
= \left(L^{\delta\beta_1}\alpha_2\alpha_8\alpha_6^2\gamma^{\beta_2+\beta_8+2\beta_6}\right)^{-1}\frac{1}{-\delta\beta_2+\delta\beta_1-\delta\beta_8-2\delta\beta_6+1}
$$

$$
\left(L^{-\delta\beta_2+\delta\beta_1-\delta\beta_8-2\delta\beta_6+1}-L_0^{-\delta\beta_2+\delta\beta_1-\delta\beta_8-2\delta\beta_6+1}\right) \quad (A12)
$$

Also, the amount phloem between 0 and L_0 must be added to the sum. Phloem properties were assumed to be constant in this range. The amount of phloem between 0 and L_0 is

$$
K_{p,\,0-L_0}^{-1} = \left(nA_p\rho_{c,p}r_p^2\right)^{-1}dx
$$

$$
= \left(\left(\frac{L}{L_0}\right)^{\delta\beta_1}\alpha_2\gamma^{\beta_2}L_0^{\delta\beta_2}\alpha_8\gamma^{\beta_8}L_0^{\delta\beta_8}\alpha_6^2\gamma^{2\beta_6}L_0^{2\delta\beta_6}\right)^{-1}L_0
$$

$$
= \left(\left(\frac{L}{0.1\,\mathrm{m}}\right)^{\delta\beta_1}\alpha_2\alpha_8\alpha_6^2\gamma^{\beta_2+\beta_8+2\beta_6}(0.1\,\mathrm{m})^{\delta\beta_2+\delta\beta_8+2\delta\beta_6}\right)
$$

$$
-1*0.1\,\mathrm{m}
$$

$$
\tag{A13}
$$

Nitrogen in leaves

Assuming that leaf area scales with xylem sapwood cross-sectional area and that leaf nitrogen content is constant, total amount of nitrogen in leaves can be estimated to be

$$
A_{\mathrm{leaf}} = A_x * C_{ls} \quad (A14)
$$

where C_{ls} is the leaf to sapwood ratio

$$
N_{\mathrm{leaf,\,tot}} = A_{\mathrm{leaf}}\rho_{\mathrm{SLA}}\rho_{N,\,\mathrm{leaf}} = A_{x,\,\mathrm{ref}}C_{ls}\rho_{\mathrm{leaf}}\rho_{N,\,\mathrm{leaf}} \quad (A15)
$$

In accordance with the pipe model prediction, xylem cross-sectional area equals total xylem volume divided by tree height. Total leaf nitrogen content can then be written as

$$
N_{\mathrm{leaf,\,tot}} = \frac{\alpha_1\gamma^{\beta_1}\left(L^{\delta\beta_1+1}-L_0^{\delta\beta_1+1}\right)}{L}C_{ls}\rho_{\mathrm{SLA}}\rho_{N,\,\mathrm{leaf}} \quad (A16)
$$

The parameters used in the calculations are shown in **Table 3**. The values for leaf-to-sapwood area ratio, specific leaf area, and leaf nitrogen content were taken for pine from the Supplementary material in Martinez-Vilalta et al. (2009) in which these values are reported for the SMEAR II Hyytiälä research station in Hyytiälä Southern Finland, the same place from where most of the trees were taken for our measurements. Korhonen et al. (2013) reported a very similar value, 1.2%, for leaf nitrogen content of 1.2% at the same site. The corresponding values for aspen could not be obtained for the same site, and the values are taken studies of Niinemets (1997), and Hoffmann and Usoltsev (2002). Values for both pine and aspen are in line with values from metastudies containing several species: McDowell et al. (2002a,b) compiled data of leaf to sapwood area from 14 different studies containing conifer and broadleaved trees. The average of the species was ~2700 m^2 (leaf area)/m^2 (sapwood). Lusk et al. (2003) compiled data average for 23 evergreen angiosperm and 20 conifer populations from six sites in American continent and found an SLA of 150 g/m^2 and nitrogen content of 1.14% on average. Reich et al. (1998) compiled data from 69 species from four functional groups (forbs, broad-leafed trees and shrubs, and needle-leafed conifers) in six sites in American continent and found an average SLA 140 g/m^2 and nitrogen content 1.7%.

A2. DERIVATION OF THE SCALING FUNCTIONS WITH HEARTWOOD INCLUDED

In additional calculations, we also took into account that part of the xylem is heartwood. We assumed that there is a maximum sapwood radius $r_{sw,\,\mathrm{max}}$, and that any xylem tissue radial inwards to the maximum sapwood depth was heartwood. We assumed that heartwood did not contain any nitrogen and did not contribute to xylem conductance. We did not find analytical solutions to the scaling in the case of heartwood inclusion. Results shown

are from the following numerical integration, using a numerical integration interval (dx) of 1 mm.

$$A_{sw} = A_x - A_{hw} = \alpha_1 \gamma^{\beta_1} x^{\delta\beta_1} - \pi \left(r_{xyl} - r_{sw,\,max}\right)^2$$

$$= \alpha_1 \gamma^{\beta_1} x^{\delta\beta_1} - \pi \left(\alpha_1 \gamma^{\beta_1} x^{\delta\beta_1} - r_{sw,\,max}\right)^2 \mathrm{if} r_{xyl} > r_{sw,\,max} \tag{A17}$$

The number of furcations at distance of x from the leaf apex is then

$$n(x) = \frac{n_{ref} A_{sw,\,ref}}{A_{sw}(x)} = \frac{\left(\alpha_1 \gamma^{\beta_1} L^{\delta\beta_1} - \pi (r_{xyl}(L) - r_{sw,\,max})^2\right)}{\left(\alpha_1 \gamma^{\beta_1} x^{\delta\beta_1} - \pi (r_{xyl}(x) - r_{sw,\,max})^2\right)} \tag{A18}$$

Total amount of xylem sapwood is then

$$V_{x,\,tot} = \int_0^L nA_x dx = \int_0^L \frac{\left(\alpha_1 \gamma^{\beta_1} L^{\delta\beta_1} - \pi (r_{xyl}(L) - r_{sw,\,max})^2\right)}{\left(\alpha_1 \gamma^{\beta_1} x^{\delta\beta_1} - \pi (r_{xyl}(x) - r_{sw,\,max})^2\right)}$$

$$\left(\alpha_1 \gamma^{\beta_1} x^{\delta\beta_1} - \pi (r_{xyl}(x) - r_{sw,\,max})^2\right) dx$$

$$= \int_0^L \left(\alpha_1 \gamma^{\beta_1} x^{\delta\beta_1} - \pi (r_{xyl}(x) - r_{sw,\,max})^2\right) dx \tag{A19}$$

Total amount of phloem is then

$$V_{p,\,tot} = \int_0^L nA_p dx$$

$$= \int_0^L \frac{\left(\alpha_1 \gamma^{\beta_1} L^{\delta\beta_1} - \pi (r_{xyl}(L) - r_{sw,\,max})^2\right)}{\left(\alpha_1 \gamma^{\beta_1} x^{\delta\beta_1} - \pi (r_{xyl}(x) - r_{sw,max})^2\right)} \alpha_2 \gamma^{\beta_2} x^{\delta\beta_2} dx \tag{A20}$$

Total amount of nitrogen in the xylem is then

$$N_{x,\,tot} = \int_0^L nA_x \rho_{N,\,x} \rho_x dx$$

$$= \int_0^L \frac{\left(\alpha_1 \gamma^{\beta_1} L^{\delta\beta_1} - \pi (r_{xyl}(L) - r_{sw,\,max})^2\right)}{\left(\alpha_1 \gamma^{\beta_1} x^{\delta\beta_1} - \pi (r_{xyl}(x) - r_{sw,\,max})^2\right)}$$

$$\left(\alpha_1 \gamma^{\beta_1} x^{\delta\beta_1} - \pi (r_{xyl}(x) - r_{sw,\,max})^2\right) \alpha_3 \gamma^{\beta_3} x^{\delta\beta_3} \rho_x dx \tag{A21}$$

Total amount of nitrogen in the phloem is then

$$N_{p,\,tot} = \int_0^L nA_p \rho_p \rho_N dx$$

$$= \int_0^L \frac{\left(\alpha_1 \gamma^{\beta_1} L^{\delta\beta_1} - \pi (r_{xyl}(L) - r_{sw,\,max})^2\right)}{\left(\alpha_1 \gamma^{\beta_1} x^{\delta\beta_1} - \pi (r_{xyl}(x) - r_{sw,\,max})^2\right)} \alpha_2 \gamma^{\beta_2} x^{\delta\beta_2} \alpha_4 \gamma^{\beta_4} \rho_N x^{\delta\beta_4} dx \tag{A22}$$

Xylem hydraulic conductance is then

$$K_{x,\,tot}^{-1} = \int_0^L \left(nA_x \rho_{c,\,x} r_x^2\right)^{-1} dx =$$

$$= \int_0^L \left(\frac{\left(\alpha_1 \gamma^{\beta_1} L^{\delta\beta_1} - \pi (r_{xyl}(L) - r_{sw,\,max})^2\right)}{\left(\alpha_1 \gamma^{\beta_1} x^{\delta\beta_1} - \pi (r_{xyl}(x) - r_{sw,\,max})^2\right)}\right.$$

$$\left.\left(\alpha_1 \gamma^{\beta_1} x^{\delta\beta_1} - \pi (r_{xyl}(x) - r_{sw,\,max})^2\right) \alpha_7 \alpha_5^2 \gamma^{\beta_7 + 2\beta_5} x^{\delta\beta_7 + 2\delta\beta_5}\right)^{-1} dx \tag{A23}$$

Phloem hydraulic conductance is then

$$K_{p,\,tot}^{-1} = \int_0^L \left(nA_p \rho_{c,\,p} r_p^2\right)^{-1} dx$$

$$= \int_0^L \left(\frac{\left(\alpha_1 \gamma^{\beta_1} L^{\delta\beta_1} - \pi (r_{xyl}(L) - r_{sw,\,max})^2\right)}{\left(\alpha_1 \gamma^{\beta_1} x^{\delta\beta_1} - \pi (r_{xyl}(x) - r_{sw,\,max})^2\right)}\right.$$

$$\left.\alpha_2 \alpha_8 \alpha_6^2 \gamma^{\beta_2 + \beta_8 + 2\beta_6} x^{\delta\beta_2 + \delta\beta_8 + 2\delta\beta_6}\right)^{-1} dx \tag{A24}$$

Total leaf area is then proportional to sapwood, instead of whole xylem, cross-sectional area

$$A_{leaf} = A_{sx} * C_{ls} \tag{A25}$$

A3. DERIVATION OF THE ANALYTIC SCALING FUNCTIONS FOR THE AXIAL DISTRIBUTION OF XYLEM AND PHLOEM PROPERTIES FOR A GIVEN TREE SIZE

Axial distribution of xylem volume is

$$V_x(x) = nA_x = \left(\frac{L}{x}\right)^{\delta\beta_1} \alpha_1 \gamma^{\beta_1} x^{\delta\beta_1} = L^{\delta\beta_1} \alpha_1 \gamma^{\beta_1} \tag{A26}$$

Note that the distribution of xylem volume is constant with axial position. This stems from the pipe model hypothesis.

Axial distribution of xylem volume is

$$V_p(x) = nA_p = \left(\frac{L}{x}\right)^{\delta\beta_1} \alpha_2 \gamma^{\beta_2} x^{\delta\beta_2} = L^{\delta\beta_1} \alpha_2 \gamma^{\beta_2} x^{\delta(\beta_2 - \beta_1)} \tag{A27}$$

Axial distribution of nitrogen in the xylem is

$$V_x(x) = nA_x \rho_{N,\,x} = \left(\frac{L}{x}\right)^{\delta\beta_1} \alpha_1 \gamma^{\beta_1} x^{\delta\beta_1} \alpha_3 \gamma^{\beta_3} x^{\delta\beta_3}$$

$$= L^{\delta\beta_1} \alpha_1 \alpha_3 \gamma^{\beta_1 + \beta_3} x^{\delta\beta_3} \tag{A28}$$

Axial distribution of nitrogen in the phloem is

$$V_p(x) = nA_p \rho_{N,\,p} = \left(\frac{L}{x}\right)^{\delta\beta_1} \alpha_2 \gamma^{\beta_2} x^{\delta\beta_2} \alpha_4 \gamma^{\beta_4} x^{\delta\beta_4}$$

$$= L^{\delta\beta_1} \alpha_2 \alpha_4 \gamma^{\beta_2} \gamma^{\beta_4} x^{\delta(\beta_2 - \beta_1 + \beta_4)} \tag{A29}$$

Axial distribution of xylem conductance is

$$V_x(x) = nA_x \rho_{c,\,x} r_x^2 = \left(\frac{L}{x}\right)^{\delta\beta_1} \alpha_1 \gamma^{\beta_1} x^{\delta\beta_1} \alpha_7 \gamma^{\beta_7} x^{\delta\beta_7} \alpha_5^2 \gamma^{2\beta_5} x^{2\delta\beta_5}$$

$$= L^{\delta\beta_1} \alpha_1 \alpha_7 \alpha_5^2 \gamma^{\beta_1 + \beta_7 + 2\beta_5} x^{\delta(\beta_7 + 2\beta_5)} \tag{A30}$$

Axial distribution of phloem conductance is

$$V_p(x) = nA_p \rho_{c,\,p} r_p^2 = \left(\frac{L}{x}\right)^{\delta\beta_1} \alpha_2 \gamma^{\beta_2} x^{\delta\beta_2} \alpha_8 \gamma^{\beta_8} x^{\delta\beta_8} \alpha_6^2 \gamma^{2\beta_6} x^{2\delta\beta_6}$$

$$= L^{\delta\beta_1} \alpha_2 \alpha_8 \alpha_6^2 \gamma^{\beta_2 + \beta_8 + 2\beta_6} x^{\delta(\beta_2 - \beta_1 + \beta_8 + 2\beta_6)} \tag{A31}$$

Modeling tree crown dynamics with 3D partial differential equations

Robert Beyer *, Véronique Letort and Paul-Henry Cournède

Ecole Centrale Paris, Applied Mathematics and Systems Laboratory, Châtenay-Malabry, France

We characterize a tree's spatial foliage distribution by the *local leaf area density*. Considering this spatially continuous variable allows to describe the spatiotemporal evolution of the tree crown by means of 3D partial differential equations. These offer a framework to rigorously take locally and adaptively acting effects into account, notably the growth toward light. Biomass production through photosynthesis and the allocation to foliage and wood are readily included in this model framework. The system of equations stands out due to its inherent dynamic property of self-organization and spontaneous adaptation, generating complex behavior from even only a few parameters. The density-based approach yields spatially structured tree crowns without relying on detailed geometry. We present the methodological fundamentals of such a modeling approach and discuss further prospects and applications.

Keywords: leaf area density, continuity equation, functional-structural plant model, crown plasticity, competition for light, Beer-Lambert's law

1. INTRODUCTION

In terms of model scale, light sensitive functional-structural tree growth modeling has experienced the emergence of various trends. Organ-level approaches bring about a high precision of physiological processes, averting inaccuracies and effects of scale non-invariance, which may arise from simplifications in larger-scale approaches. Moreover, arbitrary small-scale biophysical or biochemical processes can in principle be readily induced. The LIGNUM model (Perttunen et al., 1996; Sievänen et al., 2008), the model by Sterck et al. (2005) or the L-Peach model (Allen et al., 2005) are examples of this model category. Local light interception (cf. also Chelle and Andrieu, 2007 for a methods review) determines the production and allocation of biomass. Their detail of physiological and morphological processes is at the same time the drawback of these models. On the one hand, the large number of organs implies high computational costs—all the more in competition scenarios of multiple trees. On the other hand, their detail can make these models susceptible to the propagation of errors, which could have been compensated for in an averaging rough scale approach.

Other organ-level models like Greenlab (Yan et al., 2004; Cournède et al., 2006) a priori focus on the topology in terms of the plant's structure. This implies the inability of easily taking physiological and structural responses to varying local light conditions into account. As one consequence, the approach cannot be straightforwardly applied to scenarios of competition for light: An additional yet non local competition index provides for this (Cournède et al., 2008). In another context of formal grammars used for tree growth simulation, Kurth and Sloboda (1999) present the 2D concept of the shadow-relevant cone of a shoot in order to take local light conditions into account, which in turn affect the rewriting system. Comparable methods have been used by Purves et al. (2007) and Takenaka (1994).

Sonntag (1996) presents a model in which the spatial motion and allocation of leaf area is based on heuristic rules on a 2D cellular space. Though quite different in terms of formalism, his approach bears conceptual resemblances to ours.

Models with a rougher scale use to impose certain characteristics on the crown shape. For instance, the Balance model Grote and Pretzsch (2002) and the model by Sorrensen-Cothern et al. (1993) describe the crown shape in terms of disk-like horizontal layers. This technique implies advantages with regard to the computational speed as well as a general robustness, compared to small-scale models. Yet it does so at the expense of a thorough plastic spatial crown structure. When applied to competition scenarios, these models often make use of empirically fitted competition indices (e.g., Pretzsch, 1992).

While being affiliated more with the latter forestry models in the attempt to describe crown structure and dynamics macroscopically for applications at the stand level, the present approach attempts a middle course between the fine organ-centered way and the rougher pre-imposition of the crown form. We characterize a tree's spatial foliage distribution via its *local leaf area density*. The focusing on this variable circumvents difficulties in terms of robustness in the geometrically detailed models accounting for individual leaf positions. At the same time, the locality allows for arbitrary spatial structures.

Applying Beer Lambert's law allows to express the local light conditions within a crown as a function of the local leaf area density. Aiming at an increased future light interception, local leaf area density is assumed to tend to move toward the light. This approach, which induces the spatial expansion of the crown, translates directly into a partial differential equation. Details are specified based on mass conservation and optimization considerations. The technique notably allows to account for a local and

spontaneous adaptiveness with regard to changing environmental light conditions.

The mathematical approach of density-based partial differential equations has long established itself in spatial biology and ecology (cf. e.g., Okubo and Levin, 2002). In the context of macroscopic individual plant modeling, so far notably in the form of diffusion equations, it has proven applicable for root growth and proliferation (see Page and Gerwitz, 1974 for the original approach, Reddy and Pachepsky, 2001 for a review of later developments and Dupuy et al., 2010 for a current advance). A 2D diffusion approach for the foliage of crops with the objective to model competition in different field densities, without considering the vertical dimension, was presented by Beyer et al. (2014). Partial differential equations can generate, even from only a few terms, complex self-adapting dynamics, which is indeed present in biological systems. Attempts to reproduce this by simpler terms often requires a larger model framework and set of parameters. The latter, in turn, requires large data sets, which are often not available.

In this article we will exemplify the use of the leaf area density-based partial differential equation approach by means of a simplified model setup presented in section 2. The continuity of the approach suggests embedding into in the context of continuously growing trees sensu (Hallé et al., 1978), i.e., "with no marked endogenous cessation of extension [and] a more or less constant production of leaves and/or shoots throughout the year" (Barthélémy and Caraglio, 2007).

Since merely selected dynamics are presented, without constructing a realistic model, we settle for illustrations of key qualitative properties of the approach instead of quantitative data comparison. Throughout the article, we will point out possibilities of extending and customizing process assumptions while preserving the advantages of the overall methodological framework. Extending future steps are discussed in section 3.

2. MODEL FRAMEWORK

For clarity's sake all recurrently appearing variables and parameters and their definitions are listed in **Table 1**. We describe the spatial foliage distribution of a tree canopy by means of the

Table 1 | Key model variables and parameters.

$\alpha(x, t)$	Leaf area density in x at time t (in $m^2\,m^{-3}$)
$\alpha(\cdot, t)$	The map $\mathbb{R}^3 \to \mathbb{R}$, $x \mapsto \alpha(x, t)$
Λ	Mean leaf transmittance
$\lambda(x, v)$	Cosine of the angle between leaf plane normal and sun ray
S_+^2	Upper half unit sphere $\{x \in \mathbb{R}^3 : \|x\| = 1, x_3 \geq 0\}$
μ	Energetic efficiency (in $g\,MJ^{-1}$)
$PAR(v, t)$	Radiation from direction v at time t (in $MJ\,m^{-2}\,s^{-1}$)
$b(x, t)$	Local biomass production in x at time t (in $g\,s^{-1}$)
SLA	Specific leaf area (in $m^2\,g^{-1}$)
WD	Wood density (in $g\,m^{-3}$)
P	Pipe model theory constant (in $m^2\,m^{-2}$): 1 unit $\alpha \cong P$ Units pipe cross-sectional area
$\|x\|_\Upsilon$	Length of the sapwood pipe leading to x (in m)
$L(x, t)$	Local radiation in x induced by the leaf density $\alpha(t)$ (in $MJ\,m^{-2}$)

(local) leaf area density $\alpha(x, t) \geq 0$ (in $m^2\,m^{-3}$) in a point $x = (x_1, x_2, x_3) \in \mathbb{R}^3$ (each entry in m) at a time $t \geq 0$ (in years), i.e., the spatial density of the total one-sided green leaf area (previously considered e.g., by Sinoquet et al., 2005). The map $\alpha(\cdot, t) : \mathbb{R}^3 \to \mathbb{R}$, $x \mapsto \alpha(x, t)$ is continuous for any t. For brevity, we will use the notion *leaf density* in place of leaf area density.

We aim to describe the evolution $t \mapsto \alpha(\cdot, t)$. To this end we will first determine the biomass production B of a tree, which, along with the senescence S of old biomass, allows to describe the net biomass increment of a tree corresponding to a leaf density $\alpha(\cdot, t)$ at a given time t:

$$\frac{\partial}{\partial t} m(t) = B(t) - S(t)$$

This, in turn, will be distributed among foliage and sapwood according to the pipe model theory (Shinozaki et al., 1964), specified in the subsequent paragraph. The coaction of foliage allocation and senescence in the case of a continuously growing tree induces what we abstractly interpret as a continuous motion of $\alpha(\cdot, t)$, in particular directed toward the light, aiming at an increased future biomass production. This perspective leads to the description of the course of $t \mapsto \alpha(\cdot, t)$ essentially by means of a continuity equation.

Sapwood Associated to a Leaf Density: The pipe model theory by Shinozaki et al. (1964) allows to determine the sapwood mass corresponding to an arbitrary leaf density $\alpha(\cdot, t)$. In the present context, the theory states that for any point $x \in \mathbb{R}^3$ with $\alpha(x, t) > 0$, a sapwood pipe, in charge of the transport of water and nutrients, leads from x down to the roots with a length denoted by $\|x\|_\Upsilon$, its cross-sectional area being proportional to the leaf density $\alpha(x, t)$ at its tip via a constant P. The mass of the pipe leading to x then equals

$$\underbrace{\alpha(x, t) \cdot P}_{\text{cross-sectional area}} \cdot \underbrace{\|x\|_\Upsilon}_{\text{length}} \cdot WD,$$

WD denoting the wood density (in $g\,m^{-3}$).

It is worth mentioning that, motivated by the limitations to the pipe model theory, pointed out e.g., by Tyree (1988), Pouderoux et al. (2001), and Deleuze and Houllier (2002), generalizations have been suggested: A noteworthy approach is the one by Bouchon et al. (1997), who, based on an allocation perspective, reason that the pipe does not necessarily have a constant cross-sectional area along its path, but more generally a one exponentially decreasing toward the stem base. This principle integrates in our context with only minor technical changes. Likewise, the approach by Letort et al. (2008), parametrically combining the pipe model approach and a uniform, common pool sapwood allocation, would be feasible.

As for the pipe's length $\|x\|_\Upsilon$ from x to the root tip, for the sake of simplicity, here we follow the multi-species approach used by Sonntag (1996), based on the branch architecture of coniferous species and the assumption that root length equals branch length, resulting in

$$\|x\|_\Upsilon := |x_3| + 2 \cdot \|(x_1, x_2)\| . \tag{1}$$

A more accurate choice for a particular species can be made by taking specific characteristics of its branching geometry (such as branching angles) and topology into account.

Finally, the sum of foliage and sapwood mass is given by

$$\underbrace{\int_{\mathbb{R}^3} \frac{\alpha(x,t)}{SLA}\,dx}_{\text{foliage mass}} + \underbrace{\int_{\mathbb{R}^3} \alpha(x,t) \cdot P \cdot \|x\|_{\Upsilon} \cdot WD\,dx}_{\text{sapwood mass}} \tag{2}$$

where SLA denotes the specific leaf area (in $m^2\,g^{-1}$).

2.1. BIOMASS PRODUCTION

We determine the amount of biomass produced through photosynthetic activity by a given leaf density. To this, we take direct and diffuse radiation into account, cf. Fu and Rich (1999), using the horizontal celestial coordinate system, with $\mathbb{R}^2 \times \{0\}$ being the local horizon of a tree rooting in $(0,0,0)$, and the vector $(1,0,0)$ pointing north. The unit directional vector $\sigma(t) \in S_+^2 := \{x \in \mathbb{R}^3 : \|x\| = 1, x_3 \geq 0\}$, under which the sun is seen from the tree at daytime t reads $\sigma(t) = (\cos(-Az(t)) \cdot \cos(Alt(t)), \sin(-Az(t)(t)) \cdot \cos(Alt(t)), \sin(Alt(t)))$, where $Alt(t)$ and $Az(t)$ denote the time dependent altitude and azimuth, respectively.

For diffusive radiation, a uniform diffuse model (uniform overcast sky) is applied, in which incoming diffuse radiation is assumed to be the same from all sky directions. Let $PAR_{dir}(t)$ and $PAR_{diff}(t)$ (in $MJ\,m^{-2}$) denote the photosynthetically active direct and diffuse radiation at time t, respectively. Then the total radiation from direction $v \in S_+^2$ at time t is

$$PAR(v,t) := PAR_{diff}(t) + PAR_{dir}(t) \cdot \mathbb{1}_{\{v=\sigma(t)\}}(t),$$

with the indicator function $\mathbb{1}_A(x) := 1$ if $x \in A$ and 0 else.

2.1.1. Isolated Tree

Incoming radiation is partly intercepted by the tree's foliage and partly passes through it. The fraction between 0 and 100% of radiation from direction $v \in S_+^2$ which actually reaches the point $x \in \mathbb{R}^3$ can be determined using Beer-Lambert's law, where foliage characterized by leaf density acts as a light absorbing medium with locally varying α-concentration. This fraction reads

$$\exp\left(-\Lambda \cdot \int_{x+\mathbb{R}_+ v} \lambda(\xi,v) \cdot \alpha(\xi,t)\,d\xi\right) \tag{3}$$

where the extinction coefficient $\Lambda \leq 1$ represents the mean light transmittance of foliage (Monteith, 1969; Nouvellon et al., 2000) and

$$\lambda(x,v) := N(x) \cdot v$$

takes into account the angle between the sun ray and foliage in x, $N(x) \in S_+^2$ denoting the unit normal to the plane in which foliage in x lies. $N(x)$ can be chosen according to leaf angle distribution models without further ado (Wang et al., 2007) provide a review.

Assuming that local biomass production is proportional to the total locally intercepted ratiation via an energy efficiency μ (in

$g\,MJ^{-1}$) (Monteith, 1977), the instantaneous local biomass production $b(x,t)$ (in $g\,m^{-3}\,s^{-1}$) in $x \in \mathbb{R}^3$ at time t for the leaf density $\alpha(\cdot,t)$ reads

$$b(x,t) = \mu \cdot$$
$$\int_{S_+^2} \lambda(x,v) \cdot \alpha(x,t) \cdot \underbrace{\exp\left(-\Lambda \cdot \int_{x+\mathbb{R}_+ v} \lambda(\xi,v) \cdot \alpha(\xi,t)\,d\xi\right) \cdot PAR(v,t)}_{\text{radiation reaching } x \text{ from direction } v}\,dv. \tag{4}$$
$$\underbrace{}_{\text{radiation from direction } v \text{ intercepted in } x}$$

2.1.2. Population of Trees

At a time t, let $\alpha_1(\cdot,t), \ldots, \alpha_n(\cdot,t)$ denote the leaf densities of n trees, shading each other and competing for light. Then the instantaneous local biomass production of tree $i \in \{1, \ldots, n\}$ in x generalizes to

$$b_i(x,t) = \mu \cdot \int_{S_+^2} \frac{\left(\lambda_i(x,v) \cdot \alpha_i(x,t)\right)^2}{\sum_{j=1}^{n} \lambda_j(x,v) \cdot \alpha_j(x,t)} \cdot$$
$$\exp\left(-\Lambda \cdot \int_{x+\mathbb{R}_+ v} \sum_{j=1}^{n} \lambda_j(\xi,v) \cdot \alpha_j(\xi,t)\,d\xi\right) \cdot PAR(v,t)\,dv$$

The fraction $\frac{\lambda_i(x,v) \cdot \alpha_i(x,t)}{\sum_{j=1}^{n} \lambda_j(x,v) \cdot \alpha_j(x,t)}$ is the part of the incoming radiation in x that is attributed to tree i's foliage in x. In particular it reduces to 1 if two trees' crowns do not occupy common space.

2.2. DYNAMICS

2.2.1. Mass balance

We determine the instantaneous change in living mass (conductive sapwood and foliage mass) due to the production of new, and the senescence of old biomass. For convenience we assume that the senescence of leaves as well as the loss of conductivity of sapwood depend on time only. If sapwood and foliage that have existed for τ_W and τ_F years become nonconductive and senescent, respectively, then the living mass at time t reduces by

$$S(t) := \int_{\mathbb{R}^3} \frac{\frac{\partial}{\partial t}\alpha(x, t-\tau_F)}{SLA}\,dx + \int_{\mathbb{R}^3} \frac{\partial}{\partial t}\alpha(x, t-\tau_W) \cdot$$
$$P \cdot \|x\|_{\Upsilon} \cdot WD\,dx.$$

At the same time it increases by the total instantaneous biomass production at t, i.e., $B(t) := \int_{\mathbb{R}^3} b(x,t)\,dx$. Thus we have

$$\frac{\partial}{\partial t}m(t) = B(t) - S(t) \tag{5}$$

for the change in living mass at time t. A priori, the possibility $\frac{\partial}{\partial t}m(t) < 0$ is not excluded for arbitrary parameters. However, since $m(t) > S(t)$, it follows that $m(t) > 0$ and thus $B(t) > 0$ for all $t \geq 0$.

2.2.2. Leaf density dynamics

With this information on the global mass of the tree at hand, we consider the variable

$$\widehat{\alpha}(x, t) = \frac{\alpha(x, t)}{\int_{\mathbb{R}^3} \alpha(x, t) dx},$$

i.e., the leaf density modulo mass, or *(mass-)relative* leaf density, with the property that $\int_{\mathbb{R}^3} \widehat{\alpha}(x, t)\, dx = 1$ for all t, which is understood as an indicator of the spatial structure of the real leaf density $\alpha(\cdot, t)$. Instead of describing the course of $\alpha(\cdot, t)$ directly, we do so for $\widehat{\alpha}(\cdot, t)$ and deduce $\alpha(\cdot, t)$ as $\alpha(x, t) = \lambda(t) \cdot \widehat{\alpha}(x, t)$, where $\lambda(t)$ is chosen such that the living mass corresponding to $\lambda(t) \cdot \widehat{\alpha}(x, t)$ (cf. (2)) equals indeed $m(t)$ yielded by (5). Thus

$$\lambda(t) = \frac{m(t)}{\int_{\mathbb{R}^3} \frac{\widehat{\alpha}(x,t)}{SLA}\, dx + \int_{\mathbb{R}^3} \widehat{\alpha}(x, t) \cdot P \cdot \|x\|_\Upsilon \cdot {}_{WD}\, dx}. \quad (6)$$

The continuity of the growth process of the trees we consider suggests a description of the course of $\widehat{\alpha}(\cdot, t)$ in terms of a (mass-conserving) continuity equation,

$$\frac{\partial}{\partial t} \widehat{\alpha}(x, t) = \nabla_x \cdot \phi(x, t), \quad (7)$$

in which the relative leaf density is subject to a transport motion induced by a continuous flux $\phi : \mathbb{R}^3 \times \mathbb{R}_+ \to \mathbb{R}^3$, itself determined by $\alpha(\cdot, t)$. The idea of this transporting flux ϕ is that it incorporates both the effect of the allocation of new leaves and of the abscission of old ones on the spatial structure of foliage, which in combination, induces what we describe as an abstract motion of leaf density.

A predominant driver in the spatial dispersal of leaf density is the local expansion toward the light, aiming at an increase in future light interception. We formally embed this factor in the above framework, where it will take on the role of the flux ϕ. For some given leaf density $\alpha(\cdot, t)$ let $L : \mathbb{R}^3 \times \mathbb{R}_+ \to \mathbb{R}$ be defined by

$$L(x, t) = \int_{S_+^2} \lambda(x, v) \cdot \exp\left(-\Lambda \cdot \int_{x+\mathbb{R}_+ \cdot v} \lambda(\xi, v) \cdot \alpha(\xi, t)\, d\xi\right) \cdot$$
$$\text{PAR}\,(v, t)\, dv \quad (8)$$

The function L measures the intercepted light in x per m^2 leaf area. The gradient $\nabla_x L$ points locally in the direction of the greatest rate of increase of intercepted light. In addition, similar to Beyer et al. (2014) we define the flux to correspond to the existing leaf density in x, so that finally we have

$$\phi(x, t) = k \cdot \alpha(x, t) \cdot \nabla_x L(x, t) \quad (9)$$

for a mobility constant k. This local gradient approach is motivated by "the observation that a tree is capable of acquiring also gradient information about its environment and that growth might be directed along these gradients (Schmidt and Wulff, 1993; Aphalo and Ballare, 1995)" (Sonntag, 1996).

The term $\nabla_x \cdot \phi$ describing a movement of leaf density toward the light contains spatial derivates of a function of integrals over α, which makes (7) a partial integro-differential equation.

2.3. SIMULATIONS

In this section we illustrate some structural properties of the model. For convenience we simplified radiation to be vertical only. Some details of the numerical implementation of the model are presented in the appendix.

Figures 1, 2 illustrate the evolution of leaf density in the course of time, as well as the vector field ϕ. The term is sensitive to any change in the local light conditions induced by shading; ϕ instantaneously adapts and points in the direction of the greatest light increase. Aside the general spatial expansion toward the light, we notably observe the predominant presence of foliage at the crown hull rather than its interior.

2.3.1. Population of Trees

Together with the adjustments in terms of biomass production addressed at the end of section 2.1, the approach generalizes to competition scenarios when $\alpha(\cdot, t)$ is replaced by $\sum_{i \geq 1} \alpha_i(\cdot, t)$ in (8), alongside the different initial states $\alpha_1(\cdot, 0), \alpha_2(\cdot, 0), \dots$. We illustrate the dynamic effects to which competition gives rise by means of a simplified scenario: Consider a sufficiently large stand, in which the trees' stem bases, as a point set in $\mathbb{R}^2 \times \{0\}$, generate a Voronoi-tesselation which is regular. If radiation is assumed to be radially symmetric (as done e.g., by Perttunen et al., 1998), the analysis of all competing trees reduces to that of a single one for which periodic boundary conditions for (7) are added on the boundary of the tree's 3D cell, i.e., the extension of the appropriate 2D Voronoi cell in the x_3-dimension.

FIGURE 1 | (x_1, x_3)-cross section of a leaf density-characterized crown in the course of time, subject to the present model dynamics, corresponding to t = 10 (A), 20 (B), 30 (C) and 40 (D) years with simulation parameters adopted from Letort et al. (2008). A darker color indicates a higher leaf density α. The arrows in **(D)** indicate the vector field ϕ.

FIGURE 2 | 3D view of Figure 1D.
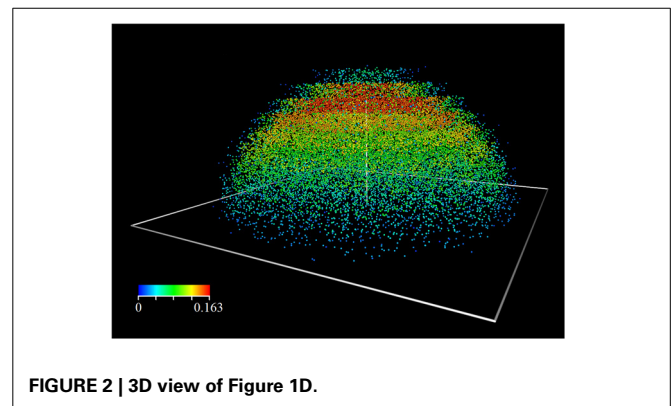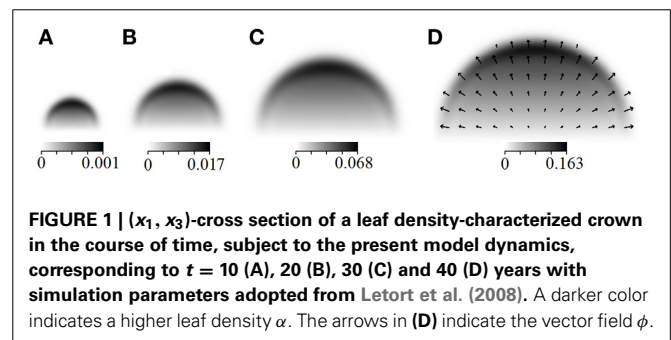
Periodic boundary conditions induce that the light conditions on the other side of the boundary are considered identical to those within, accounting for another tree growing in equal measure and shading its environment.

This implies that, when, for simplicity, further assuming the essential light incidence to be vertical, periodic boundary conditions reduce to no flux conditions on the boundary: There, due to the identical light conditions on the other side of the boundary, the light gradient $\nabla_x L$, governing the flux ϕ, changes from pointing further outwards to a zero flux.

Figure 3 shows the different stages of this scenario for an underlying square tesselation.

The overly sharp boundary between two crowns is a consequence of the unrestrained mobility of foliage in this simplified approach, and would fade when additional features corresponding to a branch structure are included, cf. section 3.

The conspicuous concentration of leaf density at the upper edges of the canopy in the competition case (cf. **Figure 3C**) results from the two factors of (i) the regular expansion of leaf density uninfluenced by the boundary condition and (ii) the immigration of leaf density from lower regions whose horizontal expansion had abruptly turned into a vertical one after reaching the Voronoi cell boundary. We are unable to provide evidence or counterevidence to determine whether this phenomenon corresponds to reality. In any case, as observable in **Figure 3D**, this is only an intermediate state, before in the long-term a homogeneously distributed high concentration of leaf density in the top canopy establishes itself.

Wheras an isolated tree grows radially symmetric, this symmetry is eventually broken for a non-circular Voronoi cell, such as the square used just now. **Figure 4** illustrates this.

3. DISCUSSION AND FUTURE PROSPECTS

The aim of this article was to show how local leaf area density, a concept opposing geometrically detailed individual leaf configurations, can be used to approach macroscopic tree crown dynamics. Its integration into the formal framework of partial differential equations allowed to rigorously formulate the growth toward light. In the simulations we observed the generation of self-organization and adaptiveness that come along with this modeling approach. The simplistic model framework was meant to draw attention to the key mechanisms and their dynamic effects.

Foliage dynamics are by nature coupled to the tree's branch structure, which has not been taken into account on a topological or geometric level in this article. Future work, with the aim of introducing more spatial heterogeneity to the approach, begins here. Taking merely the stem and the most vigorous primary branches into account while leaving the finer structures to the leaf area density concept may already suffice to tackle crown plasticity satisfactorily. While in the present simplified model the motion of local leaf area density is governed by light only and otherwise unrestrained, a simple branch architecture can add sort of directional inertia to that motion, channeling local leaf area density in several major directions, resulting in heterogeneous foliage clustering, representing individual branches. In particular, this includes the incorporation of genetically predetermined branching angle spectra. Introducing a branch structure, even if only a rough one, is moreover accompanied by a refinement of the pipe length term (1), governing the distribution of mass

FIGURE 4 | Cross-section of (A) a diagonal plane (B) the (x_1, x_3)-plane at $t = 15$ years. (C) 3D view.

FIGURE 3 | (x_1, x_3)-cross section and 3D view of the stages in a competition scenario at $t =$ 10 (A), 20 (B), 30 (C) and 40 (D) years with periodic bounday conditions at 3.5 m. Due to properties of self-symmetry, visible in **Figure 1**, these stages are in fact qualitatively similar no matter the cell size.
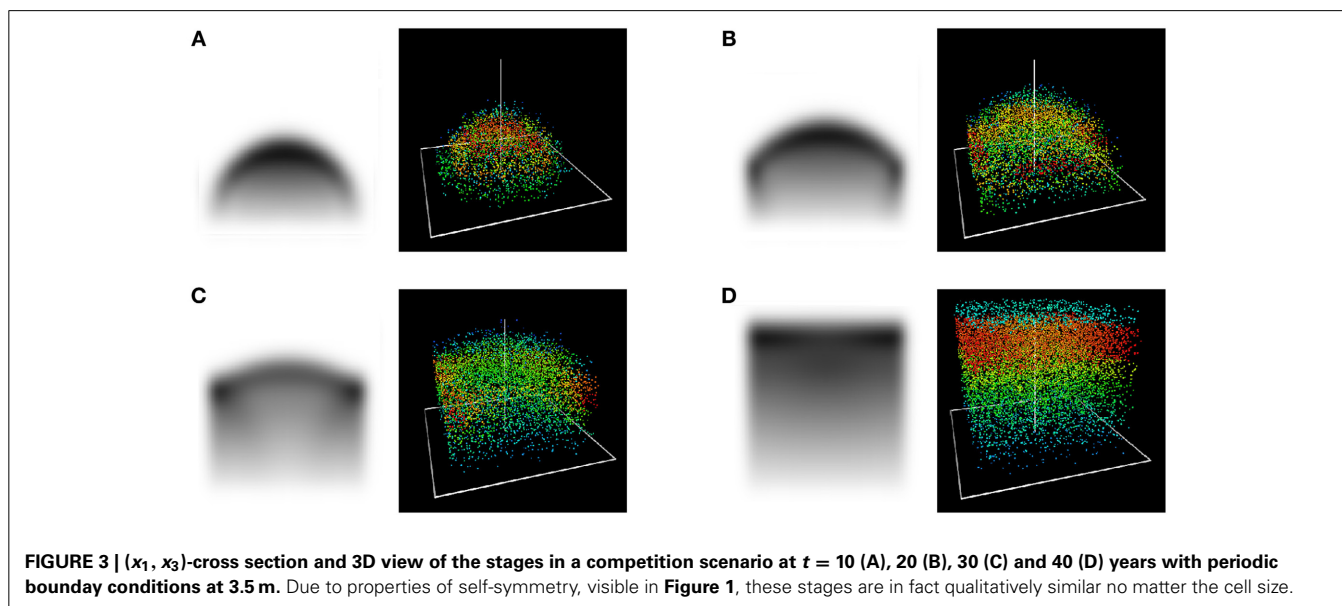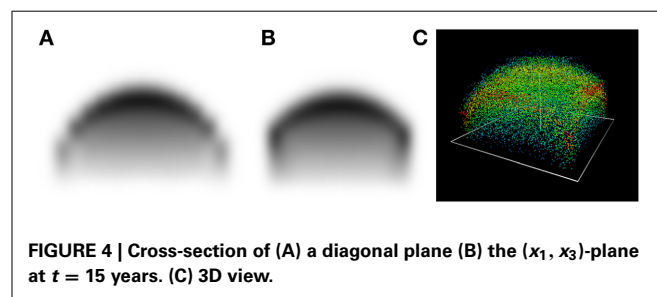
between foliage and wood according to the pipe model theory, thus determining secondary growth.

Taking into account the organization of growth units, i.e., as weakening our assumptions on neoformation and polycyclism in section 2.1.1, or considering immediate vs. delayed bud outbreak, would bring the model closer to actual tree architecture dynamics.

Alongside the phototropism considered in this article, more biomechanical constraints that have feedback influences on the growth, such as hydraulic aspects sensu (Ryan and Yoder, 1997; Tyree and Zimmermann, 2002), in particular in the context of growth limitation, the avoidance of interlocked growth due to mechanical stress of touching branches (Oliver and Larson, 1990) or gravitropism represent perspectives for model extensions.

The application and validation of a refined model based on the theoretical framework presented in this paper will benefit from empirical data on local leaf area density. Conceivable ways to obtain this include the following three, which are currently being practically explored: Firstly, from the direct recordings of local light intensities at various positions $\{x^{(1)}, \ldots, x^{(n)}\} \subset \mathbb{R}^3$ within a canopy, the map

$$\{x^{(1)}, \ldots, x^{(n)}\} \rightarrow \mathbb{R}_{\geq 0}$$
$$x \mapsto \alpha(x)$$

for a discrete, but arbitrary fine domain can be obtained by applying Beer-Lambert's law in the reverse way. Secondly, high-definition multi-directional 3D terrestrial laser scan data and appropriate skeletonization algorithms allow to relate to a leafless tree a set of cylinders representing branch segments (Raumonen et al., 2013). Automatically removing all scan points corresponding to cylinder diameters (i.e., branch thicknesses) above a certain threshold allows to spatially isolate recent shoots, for which then a relation to foliage can be assumed. Thirdly, scanning a tree at the beginning of spring during the process of bud opening, when—in contrast to the case of a fully developed canopy—laser rays still reasonably penetrate the crown, and deducting from this image the point cloud yielded by a scan of the completely leafless tree, may allow to obtain a local bud density, from which the the leaf density can be deduced. Thus, assessing the spatial foliage distribution in terms of local leaf area density in a functional-structural crown dynamics model can make good use of this data type for model calibration and validation.

The property of locally and spontaneously adapting to changing light conditions suggests that the present partial differential equation approach can be applied to competition scenarios both in pure as in mixed tree groups. Empirical findings, based on laser scans, about the plasticity Bayer et al. (2013) may thus be approached from a functional-structural modeling point of view. These perspectives are currently being explored.

ACKNOWLEDGMENTS

REFERENCES

Allen, M., Prusinkiewicz, P., and Dejong, T. (2005). Using L-Systems for Modeling the Architecture and Physiology of Growing Trees: The L-PEACH Model. *New Phytol.* 166, 869–880. doi: 10.1111/j.1469-8137.2005.01348.x

Aphalo, P., and Ballare, C. (1995). On the importance of information-acquiring systems in plant-plant interactions. *Funct. Ecol.* 9, 5–14. doi: 10.2307/2390084

Barthélémy, D., and Caraglio, Y. (2007). Plant architecture: a dynamic, multilevel and comprehensive approach to plant form, structure and ontogeny. *Ann. Bot.* 99, 375–407. doi: 10.1093/aob/mcl260

Bayer, D., Seifert, S., and Pretzsch, H. (2013). Structural crown properties of Norway spruce (Picea abies [L.] Karst.) and European beech (Fagus sylvatica [L.]) in mixed versus pure stands revealed by terrestrial laser scanning. *Trees* 27, 1035–1047. doi: 10.1007/s00468-013-0854-4

Beyer, R., Etard, O., Cournède, P.-H., and Laurent-Gengoux, P. (2014). Modeling spatial competition for light in plant populations with the porous medium equation. *J. Math. Biol.* doi: 10.1007/s00285-014-0763-1. [Epub ahead of print].

Bouchon, J., de Reffye, P., and Barthélémy, P. (1997). *Modélisation et Simulation de L'architecture des Végétaux.* Montpellier: INRA.

Chelle, M., and Andrieu, B. (2007). Modelling the light environment of virtual crop canopies. *Funct. Struct. Plant Model. Crop Product.* 22, 75–89. doi: 10.1007/1-4020-6034-3_7

Cournède, P.-H., Kang, M., Mathieu, A., Barczi, J.-F., Yan, H., Hu, B., et al. (2006). Structural factorization of plants to compute their functional and architectural growth. *Simulation* 82, 427–438. doi: 10.1177/0037549706069341

Cournède, P.-H., Mathieu, A., Houllier, F., Barthélémy, D., and de Reffye, P. (2008). Computing competition for light in the GREENLAB model of plant growth: a contribution to the study of the effects of density on resource acquisition and architectural development. *Ann. Bot.* 101, 1207–1219. doi: 10.1093/aob/mcm272

Deleuze, C., and Houllier, F. (2002). A flexible radial increment taper equation derived from a process-based carbon partitioning model. *Ann. Forest Sci.* 59, 141–154. doi: 10.1051/forest:2002001

Dupuy, L., Gregory, P., and Bengough, A. (2010). Root growth models: towards a new generation of continuous approaches. *J. Exp. Bot.* 61, 2131–2143. doi: 10.1093/jxb/erp389

Fu, P., and Rich, P. (1999). "Design and implementation of the Solar Analyst: an ArcView extension for modeling solar radiation at landscape scales," in *Proceedings of the 19th Annual ESRI User Conference*, (San Diego).

Grote, R., and Pretzsch, H. (2002). A model for individual tree development based on physiological processes. *Plant Biol.* 4, 167–180. doi: 10.1055/s-2002-25743

Hallé, F., Oldeman, R., and Tomlinson, P. (1978). *Tropical Trees and Forests.* Berlin: Springer-Verlag. doi: 10.1007/978-3-642-81190-6

Kurth, W., and Sloboda, B. (1999). Tree and stand architecture and growth described by formal grammars. II. Sensitive trees and competition. *J. Forest Sci.* 45, 53–63.

Letort, V., Cournède, P.-H., Mathieu, A., de Reffye, P., and Constant, T. (2008). Parametric identification of a functional-structural tree growth model and application to beech trees (Fagus sylvatica). *Funct. Plant Biol.* 35, 951–963. doi: 10.1071/FP08065

Monteith, J. (1969). "Light interception and radiative exchange in crop stands," in *Physiological Aspects of Crop Yield*, eds J. Eastin, F. Haskins, C. Sullivan, and C. van Bavel(Madison, WI: American Society of Agronomy and Crop Science Society of America), 89–111.

Monteith, J. (1977). Climate and the efficiency of crop production in britain. *Proc. R. Soc. Lond B* 281, 277–294. doi: 10.1098/rstb.1977.0140

Nouvellon, Y., Begue, A., Moran, M., Seen, D., Rambal, S., Luquet, D., et al. (2000). PAR extinction in shortgrass ecosystems: effects of clumping, sky conditions and soil albedo. *Agric. Forest Meteorol.* 105, 21–41. doi: 10.1016/S0168-1923(00)00194-5

Okubo, A., and Levin, S. (2002). *Diffusion and Ecological Problems, Modern Perspectives, 2nd Edn.* Berlin; Heidelberg; New York, NY: Springer.

Oliver, C., and Larson, B. (1990). *Forest stand dynamics.* New York, NY: F. McGraw-Hill.

Page, E., and Gerwitz, A. (1974). Mathematical models, based on diffusion equations, to describe root systems of isolated plants, row crops, and swards. *Plant Soil* 41, 243–254. doi: 10.1007/BF00017252

Perttunen, J., Sievänen, R., and Nikinmaa, E. (1998). LIGNUM: a model combining the structure and the functioning of trees. *Ecol. Modell.* 108, 189–198. doi: 10.1016/S0304-3800(98)00028-3

Perttunen, J., Sievänen, R., Nikinmaa, E., Salminen, H., Saarenmaa, H., and Vakeva, J. (1996). LIGNUM: a tree model based on simple structural units. *Ann. Bot.* 77, 87–98. doi: 10.1006/anbo.1996.0011

Pouderoux, S., Deleuze, C., and Dhôte, J. (2001). Analyse du rendement des houppiers dans un essai d'éclaircie de hètre grace à un modèle à base écophysiologique. *Ann. Forest. Sci.* 58, 261–275. doi: 10.1051/forest:2001125

Pretzsch, H. (1992). Modellierung der kronenkonkurrenz von fichte und buche in rein- und mischbeständen. *Allgemeine Forst- und Jagdzeitung* 163, 203–213.

Purves, D., Lichstein, J., and Pacala, S. (2007). Crown plasticity and competition for canopy space: a new spatially implicit model parameterized for 250 north american tree species. *PLoS ONE* 2:e870. doi: 10.1371/journal.pone.0000870

Raumonen, P., Kaasalainen, M., Akerblom, M., Kaasalainen, S., Kaartinen, H., Vastaranta, M., et al. (2013). Fast automatic precision tree models from terrestrial laser scanner data. *Remote Sens.* 5, 491–520. doi: 10.3390/rs5020491

Reddy, V., and Pachepsky, Y. (2001). Testing a convective-dispersive model of two-dimensional root growth and proliferation in a greenhouse experiment with maize plants. *Ann. Bot.* 87, 759–768. doi: 10.1006/anbo.2001.1409

Ryan, M., and Yoder, B. (1997). Hydraulic limits to tree height and tree growth. *Bioscience* 47, 235–242. doi: 10.2307/1313077

Schmidt, J., and Wulff, R. (1993). Light Spectral Quality, Phytochrome and Plant Competition. *Trends Ecol. Evol.* 8, 46–51.

Shinozaki, K., Yoda, K., Hozumi, K., and Kira, T. (1964). A quantitative analysis of plant form - the pipe model theory I. Basic Analysis. *Japan. J. Ecol.* 14, 97–105.

Sievänen, R., Perttunen, J., Nikinmaa, E., and Kaitaniemi, P. (2008). Toward extension of a single tree functional-structural model of scots pine to stand level: effect of the canopy of randomly distributed, identical trees on development of tree structure. *Funct. Plant Biol.* 35, 964–975. doi: 10.1071/FP08077

Sinoquet, H., Sonohat, G., Phattaralerphong, J., and Godin, C. (2005). Foliage randomness and light interception in 3-D digitized trees: an analysis from multiscale discretization of the canopy. *Plant Cell Environ.* 28, 1158–1170. doi: 10.1111/j.1365-3040.2005.01353.x

Sonntag, M. (1996). Effect of morphological plasticity on leaf area distribution, single tree, and forest stand dynamics. *Bayreuther Forum Ökologie* 52, 205–222.

Sorrensen-Cothern, K., Ford, E., and Sprugel, D. (1993). A model of competition incorporating plasticity through modular foliage and crown development. *Ecol. Monogr.* 63, 277–304. doi: 10.2307/2937102

Sterck, F., Schieving, F., Lemmens, A., and Pons, T. (2005). Performance of trees in forest canopies: explorations with a bottom-up functional-structural plant growth model. *New Phytol.* 166, 827–843. doi: 10.1111/j.1469-8137.2005.01342.x

Takenaka, A. (1994). A simulation model of tree architecture development based on growth response to local light environment. *J. Plant Res.* 107, 321–330. doi: 10.1007/BF02344260

Toro, E. (2009). *Riemann Solvers and Numerical Methods for Fluid Dynamics*. Berlin; Heidelberg; New York, NY: Springer. doi: 10.1007/b79761

Tyree, M. (1988). A dynamic model for water flow in a single tree: evidence that models must account for hydraulic architecture. *Tree Physiol.* 4, 195–217. doi: 10.1093/treephys/4.3.195

Tyree, M., and Zimmermann, M. (2002). *Xylem Structure and the Ascent of Sap, 2nd Edn.* Berlin; Heidelberg; New York, NY: Springer. doi: 10.1007/978-3-662-04931-0

Wang, W., Li, Z., and Su, H. (2007). Comparison of leaf angle distribution functions: effects on extinction coefficient and fraction of sunlit foliage. *Agric. Forest Meteorol.* 143, 106–122. doi: 10.1016/j.agrformet.2006.12.003

Yan, H., Kang, M., de Reffye, P., and Dingkuhn, M. (2004). A dynamic, architectural plant model simulating resource-dependent growth. *Ann. Bot.* 93, 591–602. doi: 10.1093/aob/mch078

Conflict of Interest Statement: The authors declare that the research was conducted in the absence of any commercial or financial relationships that could be construed as a potential conflict of interest.

4. APPENDIX

NUMERICAL IMPLEMENTATION

A finite volume scheme Toro (2009) is used, in which we consider $\overline{\alpha}_{ijk} := \frac{1}{\Delta^2} \int_{\Sigma_{ijk}} \alpha(x,t)dx$ (with a similar notation for the other variables) on a regular mesh with cells $\Sigma_{ijk} = [i\Delta x, (i+1)\Delta x[\times [j\Delta x, (j+1)\Delta x[\times [k\Delta x, (k+1)\Delta x]$ for $i,j,k \in \mathbb{Z}$ and $\Delta x \ll 1$.

The local light incidence (8) (and similarly the local biomass production (4)) for vertical radiation, $v = e_3$, is computed as

$$\overline{L}_{ijk}(t) = \overline{\lambda}_{ijk}(e_3) \cdot \exp\left(-\Lambda \cdot \Delta x \cdot \sum_{\kappa \geq k} \overline{\lambda}_{ijk}(e_3) \cdot \overline{\alpha}_{ijk}(t) \cdot \right.$$
$$\left. \text{PAR}(e_3, t)\, dv \right)$$

The general case for $v \in S_+^2$ is conceptually similar, yet technically more extensive: For a given v, the above sum reaches over all cells $\Sigma_{i'j'k'}$ whose intersection with the line through the center of the cell $\Sigma_{i'j'k'}$ and pointing in the direction v is non-empty, taking

into accout the individual length $\ell_{i'j'k'}(v) \leq \Delta x$ of this intersection by means of the additional coefficient $\frac{\ell_{i'j'k'}(v)}{\Delta x}$ in the sum term.

As for the PDE, let

$$\overline{\phi}_{1,ijk}(t) = k \cdot \frac{\overline{\alpha}_{i+1jk}(t) + \overline{\alpha}_{ijk}(t)}{2} \cdot \frac{\overline{L}_{i+1jk}(t) - \overline{L}_{ijk}(t)}{\Delta x}$$

and $\overline{\phi}_{2,ijk}$, $\overline{\phi}_{3,ijk}$ be defined accordingly for the other spatial entries. The standard discretization of the divergence is given by

$$\overline{\text{div}}_{ijk}(t) = \frac{\overline{\phi}_{1,ijk}(t) - \overline{\phi}_{1,i-1jk}(t)}{\Delta x} + \frac{\overline{\phi}_{2,ijk}(t)) - \overline{\phi}_{2,ij-1k}(t)}{\Delta x}$$
$$+ \frac{\overline{\phi}_{3,ijk}(t)) - \overline{\phi}_{3,ijk-1}(t))}{\Delta x}$$

and finally, using the Euler method for $\Delta t \ll 1$, we obtain

$$\overline{\alpha}_{ijk}(t + \Delta t) = \overline{\alpha}_{ijk}(t) + \Delta t \cdot \overline{\text{div}}_{ijk}(t).$$

Using cellzilla for plant growth simulations at the cellular level

Bruce E. Shapiro[1,2]*, Elliot M. Meyerowitz[3] and Eric Mjolsness[4]

[1] Department of Mathematics, California State University, Northridge, CA, USA
[2] Biological Network Modeling Center, Caltech, Pasadena, CA, USA
[3] Division of Biology, Howard Hughes Medical Institute, Caltech, Pasadena, CA, USA
[4] Department of Computer Science, University of California, Irvine, CA, USA

Cellzilla is a two-dimensional tissue simulation platform for plant modeling utilizing Cellerator arrows. Cellerator describes biochemical interactions with a simplified arrow-based notation; all interactions are input as reactions and are automatically translated to the appropriate differential equations using a computer algebra system. Cells are represented by a polygonal mesh of well-mixed compartments. Cell constituents can interact intercellularly via Cellerator reactions utilizing diffusion, transport, and action at a distance, as well as amongst themselves within a cell. The mesh data structure consists of vertices, edges (vertex pairs), and cells (and optional intercellular wall compartments) as ordered collections of edges. Simulations may be either static, in which cell constituents change with time but cell size and shape remain fixed; or dynamic, where cells can also grow. Growth is controlled by Hookean springs associated with each mesh edge and an outward pointing pressure force. Spring rest length grows at a rate proportional to the extension beyond equilibrium. Cell division occurs when a specified constituent (or cell mass) passes a (random, normally distributed) threshold. The orientation of new cell walls is determined either by Errera's rule, or by a potential model that weighs contributions due to equalizing daughter areas, minimizing wall length, alignment perpendicular to cell extension, and alignment perpendicular to actual growth direction.

Keywords: mathematical model, computational model, software, meristem, cellerator, cellzilla, wuschel, clavata

INTRODUCTION

In recent years, there has been much interest in accurate multi-scale models of morphogenesis. Due to the various levels of complexity and the wide variety of tissue, there has necessarily been a trade-off between generality and specificity; an excellent review is given by Koumoutsakos et al. (2011). Of the most interest to plant biologists, perhaps, are platforms that describe the high-level structure of complete organisms, systems, or organs such as a meristem or sepal. Very few general purpose tools exist at all, and even fewer are specific to plants. L-System based tools, the best known being L-Studio (Karwowski and Prusinkiewicz, 2004), were among the first; they are ideally suited to branching structures because they are based on formal language theory (a grammar based on axioms, a short alphabet, strings derived from that alphabet based on specific production rules that are tuned to branching). L-system rules have been embedded in higher level languages such as C [specifically, *cpfg*, (Prusinkiewicz and Lindenmayer, 1990)] to allow the encoding of models and the description of geometrical and topological relationships. The Virtual Plant's OpenAlea Platform (Pradal et al., 2008) provides a general-purpose collection of simulation modules that use Python as the primary scripting language and allows L-systems to be incorporated (Boudon et al., 2012).

Outside of plant biology, much of the interest has focused on grid-based models such as the Cellular Potts Model (CPM)

(Graner and Glazier, 1992), which discretize to the desired sub-cellular level of detail as collections of entities driven by particle-particle interactions; and finite element models (FEM) which instead discretize to a sufficiently fine web-work of straight lines under the influence of mechanical forces. Because of the molecular level of detail of these methods they are often primarily stochastic in nature (Gilllespie, 1976). There has been some effort to provide general purpose platforms; examples include MCell (Stiles and Bartol, 2001), designed originally to simulate the synaptic junction; Smoldyn (Andrews, 2012), primarily emphasizing nano-scale specificity; ChemCell (Plimpton and Slepoy, 2005), which models protein networks within cells; and CompuCell3D (Cickovski et al., 2007) which focuses on cellular function.

Of particular interest is the use of rule-based models, e.g., BioNetGen (Faeder et al., 2005, 2009) and NFSIM (Sneddon et al., 2011). In a rule-based model, molecules are considered structured objects and their interactions are described by rules for transforming these objects. Rule based models are interesting because every process that occurs within a biosystem, such as chemical and physical interactions and growth, development, and cell division and death, can be described by rules. Similarly, Dynamical Grammars (Mjolsness and Yosiphon, 2006; Yosiphon, 2009; Mjolsness, 2013) define models in terms of operator algebras of stochastic processes, with simulation algorithms

derived from the composition and expansion of time-evolution operators.

At an intermediate level of complexity there are tools that describe tissue at the multicellular level, treating each cell as a well-mixed compartment. Cells can be described either as simple point (or spherical) objects connected by breakable springs (Jönsson et al., 2004, 2005a,b; Mjolsness, 2006), or at some level of geometric complexity with springs between polygonal vertices (Rudge and Haseloff, 2005; Sahlin and Johnsson, 2010), as is currently done by Cellzilla. The VirtualLeaf (Merks et al., 2011) provides an interesting hybrid that uses the CPM in combination with mechanical springs with a Markovian relaxation algorithm to describe tissue growth. Cellzilla has the distinction among these software implementations of extending the collection of Cellerator Arrows to include multicellular interactions (Shapiro et al., 2003).

MATERIALS AND METHODS

CELLERATOR REACTIONS

Interactions are described in terms of Cellerator arrows (Shapiro et al., 2003); the basic canonical form is $\{X \rightarrow Y, k\}$. When several species are interacting the arrow expression is written as

$$e_1 X_1 + e_2 X_2 + \cdots \rightarrow f_1 Y_1 + f_2 Y_2 + \cdots \qquad (1)$$
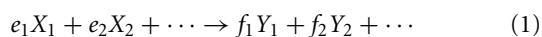
where the e_i and f_j are stoichiometries. Each reactant is converted to a single term in a differential equation according to mass action kinetics:

$$\frac{dU_j}{dt} = (f_j - e_j) k X_1^{n_1} X_1^{e_1} X_2^{e_2} \cdots \qquad (2)$$

where e_j and f_j are the stoichiometries of species U_j in the reaction on the left and right hand side of the reaction, respectively, and k is the rate constant of the reaction. More complex expressions can be built from this canonical form to represent exact mass action descriptions of multi-species complex enzymatic reactions, as summarized in **Table 1**, and numerous regulatory approximations such as Michaelis-Menten, Hill functions, and MWC equations, as summarized in **Table 2**. Furthermore, a large number of exact enzymatic expansions have been implemented using the basic canonical form via the KMech toolbox, including BiBi, BiTer, BiUni, MulS, OrderedBiBi, OrderedBiUni, PingPong, PingPongTerTerF, PingPongTerTerR, RandomBiBi, TerBi, TerTer, UniBi, and UniUni reactions (Yang et al., 2005).

Cellzilla is implemented in Mathematica and is invoked using the standard notebook interface. The details of numerical integration are normally hidden from the user, e.g., models (such as (30)–(32)) are submitted to the kernel by the Cellzilla `Grow` command and Cellerator `run` along with a list of simulation control parameters and initial conditions. These front-end commands directly invoke Mathematica's NDSolve. Normally, the default solver in NDSolve is chosen, unless the user selects otherwise; any control option for NDSolve may be passed along by `Grow` command. For ordinary differential equations, NDSolve switches between a non-stiff Adams method and a stiff Gear Backward Differentiation formula. However, users may optionally change the parameters or choose another solver.

TISSUE DESCRIPTION

Tissues are described by a polygonal lattice, with each lattice cell representing one biological cell. The `Tissue` data structure consists of: (1) a vertex list **V**, where each vertex $\mathbf{V}_i$ is an (x, y) pair; (2) an edge list **E**, where each edge $\mathbf{E}_k = (i_k, j_k)$ is a pair of integers giving indices of vertices at the endpoints of the edge; and (3) a list of cells **C**, where each cell $\mathbf{C}_k = \{k_1, k_2, k_3, \ldots\}$ is an ordered list of edge indices. Externally the tissues may be saved (either read or written) as CSV files, either as lists of vertices, edges, and cells, or in a flattened versions with the edges omitted and the cells represented as ordered sequences of vertices. Internally the edges are always reconstructed since it is more efficient computationally to always have the edge information available, but it is user taste which I/O format is used. It was decided to use the CSV format for these files because of the wide availability of parsing tools and the ease of human readability should that be necessary.

Species in different cells are referenced by an index; e.g., the reaction $X[17] \rightarrow Y[17]$ takes place in cell 17. When a reaction network is expanded in every cell in the system it is not necessary to repeat this manually, as this is done automatically. Constituents in different cells can interact in the following ways: (a) diffusion; (b) action at a distance; (c) transport across the cell wall. Each of these may be specified in the model by one of the additional Cellzilla Arrow forms listed in **Table 3**. Such interactions are allowed to depend on a function $f(i, j, k)$ that depends on the properties of the constituents of the cells (i = present cell number, j = connecting cell numbers) and cell wall (k) between cells i and j. The basic single cell models may be input and output as SBML files using the Cellerator/MathSBML extensions for SBML (Hucka et al., 2003; Shapiro et al., 2004).

Table 1 | Examples of Cellerator mass action arrow form expansion, from the base from $A \rightarrow B$.

Arrow form*	Expansion
$e_1 X_1 + e_2 X_2 + \cdots \rightleftarrows$ $f_1 Y_1 + f_2 Y_2 + \cdots$	$e_1 X_1 + e_2 X_2 + \cdots \rightarrow f_1 Y_1 + f_2 Y_2 + \cdots$ $f_1 Y_1 + f_2 Y_2 + \cdots \rightarrow e_1 X_1 + e_2 X_2 + \cdots$
$X \underset{}{\overset{\mathcal{E}}{\rightleftarrows}} Y$	$X + \mathcal{E} \rightleftarrows X\_\mathcal{E}$ $X\_\mathcal{E} \rightleftarrows Y + \mathcal{E}$
$X \underset{\mathcal{F}}{\overset{\mathcal{E}}{\rightleftarrows}} Y$	$X \overset{\mathcal{E}}{\rightleftarrows} Y$ and $Y \overset{\mathcal{F}}{\rightleftarrows} X$
$X \underset{}{\overset{\mathcal{E}}{\rightleftharpoons}} Y$	$X + \mathcal{E} \rightleftarrows X\_\mathcal{E}$ $X\_\mathcal{E} \rightleftarrows Y\_\mathcal{E}$ $Y\_\mathcal{E} \rightleftarrows Y + \mathcal{E}$
$X \rightleftarrows Y \overset{\mathcal{E}}{\rightleftarrows} Z \rightleftarrows \cdots$	$X \overset{\mathcal{E}}{\rightleftarrows} Y, Y \overset{\mathcal{E}}{\rightleftarrows} Z, \ldots$
$X \rightleftarrows Y \underset{\mathcal{F}}{\overset{\mathcal{E}}{\rightleftarrows}} Z \cdots$	$X \overset{\mathcal{E}}{\underset{\mathcal{F}}{\rightleftarrows}} Y, Y \overset{\mathcal{E}}{\underset{\mathcal{F}}{\rightleftarrows}} Z, \ldots$

*The complete syntax of an arrow form is {arrowform, $k_1, \ldots$} where $k_1, \ldots$ is a sequence of numeric or symbolic rate constants. The subscripts e_i and f_j are stoichiometries.

Table 2 | Cellerator user defined, regulatory, and enzymatic arrow forms.

Arrow form[a,b]	Typical ODE Term[c]
$\{e \cdot X \Rightarrow f \cdot Y,\ g(X)\}$	$[X_i]' = -e_i g(X),\ \ [Y_i]' = f_i g(X)$
$\left\{ X \xrightarrow{\mathcal{E}} Y,\ \texttt{Hill}[v, n, K, a, \mathbf{T}] \right\}$	$[Y]' = \dfrac{v[\mathcal{E}]\,(a + \mathbf{T} \cdot [X])^n}{K^n + (a + \mathbf{T} \cdot [X])^n}$
$\left\{ X \xrightarrow{\mathcal{E}} Y,\ \texttt{GRN}[v, \mathbf{T}, n, h] \right\}$	$[Y]' = \dfrac{v[\mathcal{E}]}{1 + \exp(-h - \mathbf{T} \cdot [X]^n)}$
$\left\{ X \xrightarrow{\mathcal{E}} Y,\ \texttt{SSystem}[\tau, C_+, C_-, \mathbf{n}^+, \mathbf{n}^-] \right\}$	$[Y]' = \dfrac{[\mathcal{E}]}{\tau}\left\{ C_+ \prod_i X_i^{n_i^+} - C_- \prod_i X_i^{n_i^-} \right\}$
$\left\{ X \xrightarrow{\mathcal{E}} Y,\ \texttt{NHCA}[v, \{\mathbf{T}^+, \mathbf{T}^-\}, \mathbf{n}, m, k] \right\}$	$[Y]' = \dfrac{v[\mathcal{E}] \prod_i \left(1 + T_i^+ [X]_i^{n_i}\right)^m}{k \prod_i \left(1 + T_i^- [X]_i^{n_i}\right)^m + \prod_i \left(1 + T_i^+ [X]_i^{n_i}\right)^m}$
$\{\{X, Y\} \implies \texttt{rational}[\mathbf{a}, \mathbf{d}, \mathbf{m}, \mathbf{n}]\}$	$[Y]'^d = \dfrac{a_0 + \texttt{rest}(\mathbf{a}) \cdot [X]^{\mathbf{n}}}{d_0 + \texttt{rest}(\mathbf{d}) \cdot [X]^{\mathbf{n}}}$
$\{X \mapsto Y,\ \texttt{USER}[v, \mathbf{T}, \mathbf{n}, h, f]\}$	$[Y]' = vf(h - \mathbf{T} \cdot [X]^{\mathbf{n}})$
$\left\{ X \xRightarrow{\mathcal{E}} Y,\ \texttt{MM}[K, v] \right\}$	$[Y]' = -[X]' = \dfrac{v[\mathcal{E}][X]}{K + [X]}$
$\left\{ X \xRightarrow{\mathcal{E}} Y,\ \texttt{MWC}[k, n, c, L, K] \right\}$	$[Y]'^e = -[X]' = k[\mathcal{E}] \dfrac{\alpha(1+\alpha)^{n-1} + L\alpha c(1+\alpha c)^{n-1}}{(1+\alpha)^n + L(1+\alpha c)^{n-1}}$

[a] The catalyst species $\mathcal{E}$ is optional and may be omitted.

[b] Boldface quantities may be either scalars or vectors. Vectors enclosed by curly brackets. The notation $\mathbf{v} = \mathbf{p}^{\mathbf{q}}$ means a vector $\mathbf{v}$ with components $v_i = p_i^{q_i}$.

[c] If the catalyst is omitted replace $[\mathcal{E}]$ with 1.

[d] In $\texttt{rational}$, $\texttt{rest}(\mathbf{x})$ is the vector $\mathbf{x}$ with its first element removed.

[e] In MWC, $\alpha = [X]/K$.

Table 3 | Additional Cellzilla arrow forms not recognized by Cellerator.

Arrow form*	Description
$\{X \longrightarrow X,\ \texttt{Diffusion}[P_I, P_0]\}$	Diffusion of X through the tissue. P_I is the permeability of internal cell walls; the optional P_0 is the permeability of tissue boundary cell walls. Each may be specified as $f[i, j, k]$ where i, j, k are cell and wall indices.
$\{X \longrightarrow X,\ \texttt{Transport}[fout, fin]\}$	Controlled transport of X across the cell wall.
$\{X \mapsto Y,\ \texttt{IGRN}[v, \mathbf{T}, \mathbf{n}, h]\}$	$[Y[j]]' = \dfrac{v}{1 + \exp(-h - \mathbf{T} \cdot [X[i]]^n)}$
$\{\texttt{cell} \longrightarrow \texttt{cell},\ \texttt{Grow}[\cdots]\}$	Specification of cell growth parameters: Pressure, growth rate, spring constant.
$\{\texttt{cell} \longrightarrow \texttt{cell} + \texttt{cell},\ model[\cdots]\}$	Specification of cell division model and parameters.

*Except for the $\texttt{IGRN}$ the arrows here are longer versions of the right-pointing arrows used by the canonical Cellerator mass-action expansion.

Diffusion across cell boundaries is implemented according to Fick's law, so that the flux J through any membrane (e.g., in molecules/(cm^2-s)) with diffusion constant D (e.g., in cm^2/s) is

$$J = -D \frac{\partial X}{\partial x} \qquad (3)$$

Defining the membrane permeability as $\beta = D/\delta$ (e.g., in cm/s), where δ the membrane (or wall) thickness gives

$$J = -\beta\delta \times \frac{\Delta X}{\delta} = -\beta \Delta X \qquad (4)$$

where ΔX is the concentration difference across the membrane. Let cell i have area A_i and depth d (orthogonal to the simulation);

the the volume of cell j is $V_j = A_j d$, and the area of the cell wall between cell i and cell j is $\ell_k d$ where ℓ_k is the length of the wall between the cells. The flux across wall k into cell i is (for constant area):

$$J = \left(\frac{d[X_i]}{dt} \times A_i d \right) \times \left(\frac{1}{\ell_k d} \right) = \frac{A_i}{\ell_k} \frac{d[X_i]}{dt} \qquad (5)$$

Therefore

$$\frac{d[X_i]}{dt} = \frac{\beta \ell_k}{A_i} \left([X_j] - [X_i] \right) \qquad (6)$$

Rather than implementing this equation directly, it is implemented as equivalent Cellerator reactions

$$\left\{ \texttt{X[i]} \rightleftarrows \emptyset, \frac{\ell_k}{A_i}\texttt{f(i, j, k)}, \frac{\ell_k}{A_i}\texttt{f(i, j, k)X[j]} \right\} \qquad (7)$$

where f is the input concentration-dependent permeability. Diffusion is specified to Cellzilla by incorporating arrows of the following form into the model:

$$\{\texttt{X} \longrightarrow \texttt{X}, \texttt{Diffusion[f[i, j, k]]}\} \qquad (8)$$

where f is either a Mathematica pure function or a function that has been defined previously in the simulation.

Action at a distance is technique for describing the way constituents in cell i can affect constituents in another cell j without specifying any of the intermediate reactions. We restrict action at a distance to adjacent cells with Cellerator GRN-like reactions written as $\{\texttt{X} \mapsto \texttt{Y}, \texttt{IGRN}[\nu, \beta, n, h]\}$ which means that constituent X_i affects constituent Y_j in neighboring cell j according to (Mjolsness et al., 1991)

$$\frac{d[\texttt{Y}_j]}{dt} = \frac{\nu}{1 + e^{-h - \beta[\texttt{X}_i]}} \qquad (9)$$

Facilitated membrane transport from cell j to cell i is described by the equations

$$\frac{d[X_i]}{dt} = \frac{\ell_k}{A_i}\big(f_{in}(i, j, k) - f_{out}(i, j, k) - f_{in}(j, i, k) + f_{out}(j, i, k)\big) \quad (10)$$

where $f_{out}(i, j, k)$ is the positive outward molecular flux from i through edge k, to j, and $f_{in}(i, j, k)$ is the positive inward molecular flux to cell i through edge k, originating from cell j. In most cases one will only want to specify one of f_{out} or f_{in}. These are implemented internally via the Cellerator reactions

$$\{\texttt{X[i]} \Rightarrow \emptyset, (\ell_k/A_i)(\texttt{f}_{out}\texttt{[i, j, k]} + \texttt{f}_{in}\texttt{[j, i, k]})\} \qquad (11)$$

$$\{\emptyset \Rightarrow \texttt{X[i]}, (\ell_k/A_i)(\texttt{f}_{in}\texttt{[i, j, k]} + \texttt{f}_{out}\texttt{[j, i, k]})\} \qquad (12)$$

Transport reactions of this sort are specified to Cellzilla by including arrows of the form

$$\{\texttt{X} \longrightarrow \texttt{X}, \texttt{Transport[fout, fin]}\} \qquad (13)$$

where the function fout should be set to zero if only f_in is utilized.

GROWTH MODEL
Cellzilla implements two types of time-dependent simulations: static, and growing. In static simulations the shape of the tissue and its component parts do not change but its constituents are allowed to vary as described previously. In a growing tissue, the shape of the cells are also allowed to evolve with time. Cell growth

is described by associating a Hooke's law spring potential of the form

$$V_{ij} = \frac{1}{2}\sum k_{ij}\left(\delta_{ij} - \ell_{ij}\right)^2 \qquad (14)$$

with the edge connecting vertices $\mathbf{x}_i$ and $\mathbf{x}_j$. Here δ_{ij} is an equilibrium length assigned to the edge, ℓ_{ij} is the actual length, and k_{ij} is a constant. When the wall is under compression (so that $\delta_{ij} > \ell_{ij}$) there will be a force, acting along the length of the edge, pushing the two vertices apart; when the wall is extended ($\delta_{ij} < \ell_{ij}$), the force will tend to pull the vertices toward one-another. The magnitude of this force is equal to the negative gradient of V_{ij}. In addition, a pressure P_a associated with each cell a is, is applied outward at each vertex. The net force on each vertex is proportional to each wall incident on that vertex and, and is split evenly between the vertices. Then equation of motion for vertex $\mathbf{x}_i$ is then

$$\frac{d\mathbf{x}_i}{dt} = -\sum_j k_{ij}\hat{\mathbf{x}}_{ij}(\ell_{ij} - \delta_{ij}) + \frac{1}{2}\sum_{j,a}P_a\mathbf{n}_{ij,a}\ell_{ij} \qquad (15)$$

where $\hat{\mathbf{x}}_{ij}$ is a unit vector pointing from $\mathbf{x}_i$ to $\mathbf{x}_j$. The sum in the first term is over all the neighbors j of vertex i. In the second term, $\mathbf{n}_{ij,a}$ is an outward pointing unit-normal vector from cell a, normal to edge ℓ_{ij}, and the sum is over all neighbors j of i and and over all cells a in incident at vertex i. The pressure force will cause the springs to extend, simulating cell growth. The resting length is allowed to increase linearly at a rate proportional to the extension beyond resting length,

$$\frac{d\delta_{ij}}{dt} = \mu_{ij}\Theta(\ell_{ij} - \delta_{ij}) \qquad (16)$$

where

$$\Theta(x) = \frac{1}{2}(x + |x|) = \begin{cases} x & \text{if } x \geq 0 \\ 0 & \text{otherwise} \end{cases} \qquad (17)$$

If the spring is not extended, then growth does not occur. Equations (15) and (16) capture the phenomenological behavior observed in nature by both plant and animal cells. Pressure drives cell expansion; as pressure increases, cells expand more quickly. The growth rate is limited by the spring force. The dynamics of (15) can be solved exactly for a square cell to give

$$\frac{1}{L}\frac{dL}{dt} = k\left(\frac{P}{k} - \frac{2\Delta}{L}\right) \qquad (18)$$

where L is the cell perimeter and $\Delta = \sum_i \delta_i$ is the sum of the resting lengths. Consequently, when $\mu_{ij} = 0$ in (16), the sigmoidal growth pattern of plant cells is observed [e.g., when extensibility decreases linearly over time and osmotic pressure is held constant, as in Figure 1 of Lockhart (1965)]. Comparing (18) to the Lockhart equation $\ell'/\ell = \Phi(P - P_E)$ we see that the k and δ are parameters that can tuned to fit effective extensibility Φ and yield pressure P_E; for constant P and k sigmoidal behavior can be tuned for $P < 2k$ in square cells. Additionally, allowing $\mu > 0$, along

with the spring force produces a more general growth model that is more generally applicable, not just in plant tissue, as the springs can be cut beyond a specified threshold, thereby removing cell–cell interactions (Shapiro and Mjolsness, 2001).

Let r be the index of the edge connecting vertices i and j, so that δ_r and ℓ_r are short notations δ_{ij} and ℓ_{ij}. The spring dynamics of (16) are implemented internally as

$$\left\{ \emptyset \to \mathbf{x}[i,p], \sum_{\text{Neighbors}(i)} \mathtt{k}[r](\mathbf{x}[j,p] - \mathbf{x}[i,p])(1 - \delta_r/\ell_r) \right\} \tag{19}$$

where $\mathbf{x}[i,p]$ is the pth Cartesian component ($p = 1, 2$ for x or y) of vertex $\mathbf{x}_i$, and $\mathtt{k}[r]$ is a spring constant whose value may depend on the properties (e.g., constituents of) the cells abutting edge r. Similarly, the growth of edge δ_r described by (16) is implemented internally as the Cellerator reactions

$$\{\emptyset \to \delta_r, \mu[p,q,r](\ell_r - \delta_r)\} \tag{20}$$

where $\mathtt{p}$ and $\mathtt{q}$ are the indices of the cells that about edge r. The pressure force in (15) on vertex x_i due to cell a on the edge connecting vertices $\mathbf{x}_i$ and $\mathbf{x}_j$ is implemented internally as

$$\left\{ \emptyset \to \mathbf{x}[i,k], \frac{1}{2}\mathtt{P}[a]\mathtt{n}[a,i,j,k] \right\} \tag{21}$$

where $\mathtt{k} = 1, 2$ (to indicate x or y Cartesian component); $\mathtt{P}[a]$ is the pressure in cell a; and $\mathtt{n}[a,i,j,k]$ is the $\mathtt{k}^{th}$ component of a unit normal vector to edge ℓ_{ij} pointing outwards from cell a.

Cell growth is specified in a Cellzilla model by a reaction of the form

$$\{\mathtt{cell} \longrightarrow \mathtt{cell}, \mathtt{Grow}[\cdots]\} \tag{22}$$

where the arguments to $\mathtt{Grow}$ specify growth parameters such as the dependence of $\mathtt{k}$, $\mathtt{P}$, and μ on cell constituents (see **Table 3**). Chemical concentrations change during growth in each cell occur even in the absence of reactions. If there are n molecules of X in volume V then $[X]' = (n/V)' = (Vn' - nV')/V^2 = n'/V - [X]V'/V$. The second term gives the correction in $[X]'$ due to volume changes.

CELL DIVISION
Division occurs when a cell's area passes a threshold. Upon birth, each cell is assigned a threshold that is distributed normally (with the mean μ and standard deviation σ as optional control parameters). Chemical concentrations are distributed equally between the child cells (so that the chemical amounts are proportional to cell area). A single (linear) near cell wall is placed according to one of two user-selectable model: the standard modern interpretation of (Errera, 1888) and a potential model. In the modern interpretation of Errera's rule, the shortest wall that divides the two cells in half (by area) is chosen. [Technically, this is not Errera's rule, which only defines the shape of the cell wall, once the endpoints are already know; however, the area-equalization constraint is typically added to provide this boundary condition. (Smith, 2001; Besson and Dumais, 2011; Prusinkiewicz and

Runions, 2012)] In the potential model (Shapiro et al., 2010) a function

$$V(\theta_1, \theta_2) = \sum_i w_i V_i(\theta_1, \theta_2) \tag{23}$$

is minimized over the central angles θ_1 and θ_2. These give the central angles of the end points of the new wall measured from the cell centroid. Here $\mathbf{w}$ is a weight vector, and V_i represents each contributor to cell division, where $i \in \{A, L, e, g\}$, as described in the below.

The area potential V_A is minimized when the cell divides in half; if the daughter cells have areas A_1 and A_2, respectively, then we define

$$V_A = \left(\frac{A_1 - A_2}{A}\right)^2 \tag{24}$$

The function is squared to improve computational stability near the minimum (which would otherwise have a non-differentiable corner there). The disadvantage of this potential is that it does not have a unique global minimum, i.e., any line of cell division will that divides the area in half will give a value of zero. Thus, the area potential must be tempered by either an additional potential function (such as the perpendicularity and/or length potential) or an additional heuristic to select the desired minimum value that does not require a unique minimum (e.g., randomly select division direction from amongst all equivalent minima).

The length potential V_L will be minimized when the new cell wall is most closely aligned with the shortest possible diameter d_{min} that this, the shortest line segment dividing the cell passing through the cell center. If d is the length of the new cell wall, then V_L is given by

$$V_L = \frac{(d - d_{min})^2 + \epsilon_L \Delta^2}{(d + d_{min})^2} \tag{25}$$

where Δ is the shortest distance between the new wall and the cell center, and ϵ_L is a tunable parameter.

For V_e and V_g we define a perpendicularity potential $V_\perp(\mathbf{v})$ that is minimized when the new wall is perpendicular to particular unit vector $\mathbf{v}$. Let $\mathbf{W}$ be a unit vector parallel to the new wall. Then

$$V_\perp(\mathbf{v}) = \mathbf{v} \cdot \mathbf{W} + \frac{\epsilon_\perp \Delta}{d} \tag{26}$$

where $\epsilon_\perp$ is a parameter. Letting $\mathbf{e}$ be the direction of maximal cell extension and $\mathbf{g}$ be the direction of maximal cell growth, we then define

$$V_e = V_\perp(\mathbf{e}) \tag{27}$$

$$V_g = V_\perp(\mathbf{g}) \tag{28}$$

so that V_e and V_g are minimized when $\mathbf{W}$ is most nearly perpendicular to the directions of maximal extension and maximal cell growth, respectively. The direction of maximal extension is taken

as the unit eigenvector corresponding to the larger eigenvalue of the covariance matrix $\mathbf{M} = (\mathbf{X}^T\mathbf{X})/(n-1)$ where n is the number of cell vertices; and $\mathbf{X} = [\,\mathbf{x} - \mathbf{x}_c\,|\,\mathbf{y} - \mathbf{y}_c\,]$, where $\mathbf{x}$ and $\mathbf{y}$ are column vectors of cell vertex coordinates $\{(x_1, y_1), \ldots, (x_n, y_n)\}$ and $\mathbf{x}_c$ and $\mathbf{y}_c$ is their mean. The direction of instantaneous maximal growth is found in the same manner, using the velocities of the vertices. The covariance matrix $\mathbf{M}$ is calculated using the Mathematica function Covariance.

Cell division is specified in a Cellzilla model with the arrow

$$\{\texttt{cell} \longrightarrow \texttt{cell} + \texttt{cell}, \texttt{model}[\cdots]\} \tag{29}$$
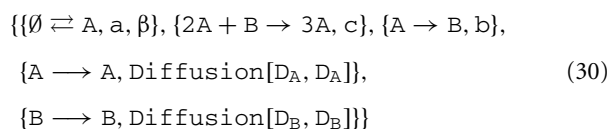
where `model` is either `ErreraModel` or `Potential`, and the arguments specify the threshold variable, mean, standard deviation, and weight vector (for the potential model). A more generalized version of this notation has been introduced by Yosiphon (2009).
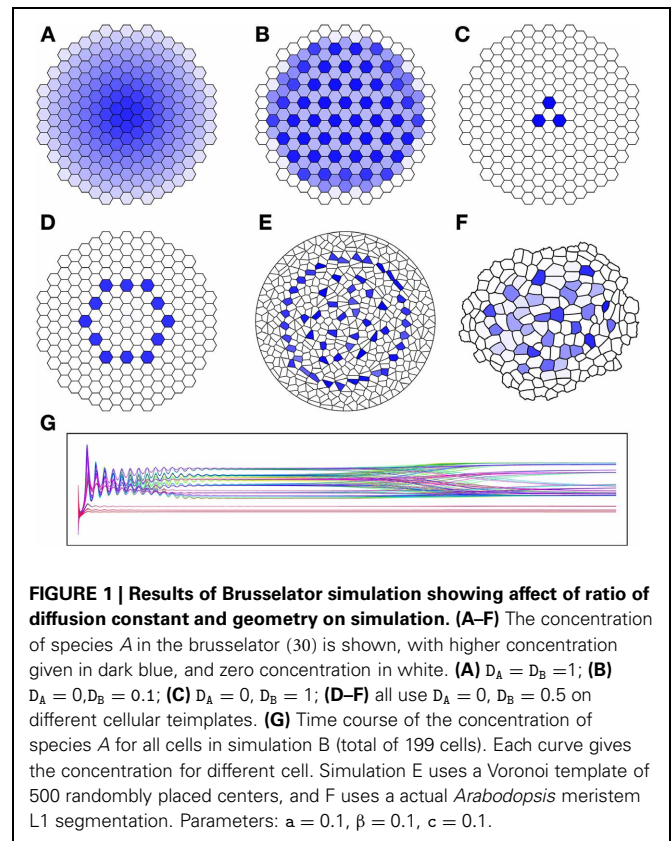
RESULTS

TEMPLATES AND THE BRUSSELATOR

Cellzilla has variety of shapes that can be used for basic simulations such as rectangular and hexagonal arrays, as well as circular, semicircular and parabolic templates that can be populated with randomly placed Voronoi centers. Alternatively the user can supply a template of his or her own consisting either of cell enters (in which case the walls will be interpolated with a Voronoi algorithm) or cell walls as described previously. Here we present the use of several of these templates (hexagonal, Voronoi, and user-supplied) to implement a common reaction-diffusion system.

The Brusselator (Prigogine and Lefever, 1968) is frequently cited in mathematical modeling because it consists of a system of chemical reactions that in the appropriate parameter regime will maintain sustained oscillations. When combined with diffusion such a system can also be used to establish a wide variety of interesting patterns such as stripes, spirals, and central maxima. The establishment of these different patterns depends on the choice of system geometry, boundary conditions, and parameter values. A diffusible Brusselator is easily implemented in Cellzilla with
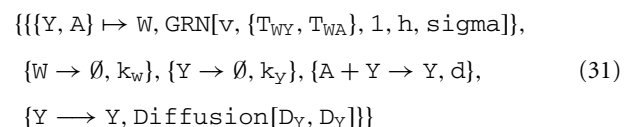
$$\{\{\emptyset \rightleftarrows \texttt{A}, \texttt{a}, \beta\}, \{2\texttt{A} + \texttt{B} \rightarrow 3\texttt{A}, \texttt{c}\}, \{\texttt{A} \rightarrow \texttt{B}, \texttt{b}\},$$
$$\{\texttt{A} \longrightarrow \texttt{A}, \texttt{Diffusion}[\texttt{D}_\texttt{A}, \texttt{D}_\texttt{A}]\}, \tag{30}$$
$$\{\texttt{B} \longrightarrow \texttt{B}, \texttt{Diffusion}[\texttt{D}_\texttt{B}, \texttt{D}_\texttt{B}]\}\}$$

where a, β, b, c, D_A and D_B are tunable parameters. As illustrated in **Figure 1**, the ratio of the diffusion constants will change the number of maxima achieved. In the second row of the figure we see that the geometry is also significant. While the qualitative features of each of the results D-F are identical, their symmetry becomes more and more broken as the symmetry of the template becomes lost. With the exception of the diffusion constants, all other parameters were identical through each of these simulations. We are particularly interested in the parameter set shown in **Figure 1A**, because it can be used as described in the following section to establish an organizing center for simulation of the WUS/CLV network.

FIGURE 1 | Results of Brusselator simulation showing affect of ratio of diffusion constant and geometry on simulation. (A–F) The concentration of species *A* in the brusselator (30) is shown, with higher concentration given in dark blue, and zero concentration in white. **(A)** $D_A = D_B = 1$; **(B)** $D_A = 0, D_B = 0.1$; **(C)** $D_A = 0, D_B = 1$; **(D–F)** all use $D_A = 0$, $D_B = 0.5$ on different cellular teimplates. **(G)** Time course of the concentration of species *A* for all cells in simulation B (total of 199 cells). Each curve gives the concentration for different cell. Simulation E uses a Voronoi template of 500 randombly placed centers, and F uses a actual *Arabodopsis* meristem L1 segmentation. Parameters: a = 0.1, β = 0.1, c = 0.1.

ESTABLISHMENT OF STEM CELL NICHE

In Jönsson et al. (2005a,b) we presented a predictive model of feedback interaction between the Wuschel (WUS) and Clavata3 (CLV) signals in the shoot apical meristem. This simplified model was able both to organize the WUS expression domain and to predict the reorganization due to the removal of the CLV signal from the WUS domain as seen in experiments when cells are ablated. This model uses a reaction-diffusion mechanism to induce WUS; the pattern is induced by a Brusselator. The original model relies on a diffusible parameter *Y* that is produced only in the *L*1 layer of a slice. We present an implementation in which our slice has the L1 layer omitted, and replace this with a boundary condition in which *Y* is held fixed, and allowed to diffuse inward. Assuming the Brusselator is implemented by (30), the Cellzilla network for the WUS activator is given by

$$\{\{\{\texttt{Y}, \texttt{A}\} \mapsto \texttt{W}, \texttt{GRN}[\texttt{v}, \{\texttt{T}_\texttt{WY}, \texttt{T}_\texttt{WA}\}, 1, \texttt{h}, \texttt{sigma}]\},$$
$$\{\texttt{W} \rightarrow \emptyset, \texttt{k}_\texttt{w}\}, \{\texttt{Y} \rightarrow \emptyset, \texttt{k}_\texttt{y}\}, \{\texttt{A} + \texttt{Y} \rightarrow \texttt{Y}, \texttt{d}\}, \tag{31}$$
$$\{\texttt{Y} \longrightarrow \texttt{Y}, \texttt{Diffusion}[\texttt{D}_\texttt{Y}, \texttt{D}_\texttt{Y}]\}\}$$

where v, T_{WY}, T_{WA}, h, k_w, k_y and D_y are tunable parameters, and the control word `sigma` tells Cellerator to replace the usual logistic control function $f(x) = 1/(1 + e^{-x})$ with $f(x) = (1 + 1/\sqrt{1 + x^2})/2$ (in fact, any monotonic increasing saturating function would work). The results illustrated in **Figure 2** show that both the original central maximum (in wild type) and dual, smaller maxima result (in the ablation experiment) as modeled

previously. In addition, we show the steady state distribution of the constituent Y in **Figure 2C**, illustrating how it forms a ring in the outer cells abutting L1 and decreasing inward, as desired.

GROWTH INDUCED BY ORGANIZING CENTER

The Brusselator is a useful mathematical/computational artifice for establishing patterns that can be otherwise studied but its biological meaning becomes lost if the variables in the equations do not have biological analogues that are present in the actual tissue. It is more meaningful if the organizing tissue can be established based on specific networks whose constituents have been observed and whose interactions are believed to be present, although this may at times be more computationally intensive. For example, Nikolaev (Nikolaev et al., 2007, 2013) has shown that a combination of reaction-diffusion and feedback in the WUS/CLV network is sufficient to establish a stem cell niche. In a one dimensional dynamic model including cell division, Chickarmane et al. (2012) has shown that negative feedback between WUS and cytokinin synthesis may be sufficient for maintenance of this niche as the tissue grows. Here we present for illustrative purposes of Cellzilla capability a simplified version of a Chickarmane-inspired model, in which two diffusible species are used to establish the pattern: U (e.g., that may be part of the cytokinin network), which is produced only in the cells at the tip of the meristem; and a second species V that is produced in the L1 layer (e.g., that may produced as part of the CLV network). The species that represents the organizing center is called W; U and V then activate and repress W, respectively, while W is self-activating, perhaps through an intermediate. Positive feedback of W onto V is provided by a third diffusible species X; and the epidermis is impermeable to U, V and W. Finally, the constitutive degradation of W is slightly enhanced in the L2 layer, but occurs everywhere. The network is
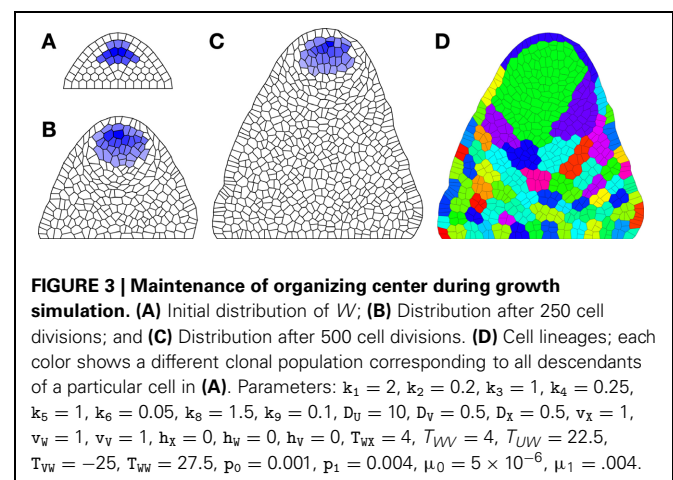
$$\{\{\emptyset \rightarrow \texttt{U}, \texttt{k}_1 \texttt{TIP[t]}\}, \{\texttt{U} \rightarrow \emptyset, \texttt{k}_2\}, \{\texttt{U} \longrightarrow \texttt{U}, \texttt{Diffusion[D}_\texttt{U}]\},$$

$$\{\emptyset \rightarrow \texttt{V}, \texttt{k}_3 \texttt{L1[t]}\}, \{\texttt{V} \rightarrow \emptyset, \texttt{k}_4\}, \{\texttt{V} \longrightarrow \texttt{V}, \texttt{Diffusion[D}_\texttt{V}]\},$$

$$\{\emptyset \rightleftarrows \texttt{Z}, \texttt{k}_7, \texttt{k}_8\texttt{U[t]}\}, \{\texttt{X} \mapsto \texttt{V}, \texttt{GRN[v}_\texttt{V}, \texttt{T}_\texttt{WV}, 1, \texttt{h}_\texttt{V}]\},$$

$$\{\{\texttt{U}, \texttt{V}, \texttt{W}\} \mapsto \texttt{W}, \texttt{GRN[v}_\texttt{W}, \{\texttt{T}_\texttt{UW}, \texttt{T}_\texttt{VW}, \texttt{T}_\texttt{WW}\}, 1, \texttt{h}_\texttt{W}]\},$$

$$\{\texttt{W} \rightarrow \emptyset, \texttt{k}_6\texttt{Z[t]} + \texttt{k}_9\texttt{L2[t]}\},$$

$$\{\texttt{W} \mapsto \texttt{X}, \texttt{GRN[v}_\texttt{X}, \texttt{T}_\texttt{WX}, 1, \texttt{h}_\texttt{X}]\}, \{\texttt{X} \rightarrow \emptyset, \texttt{k}_5\},$$

$$\{\texttt{X} \longrightarrow \texttt{X}, \texttt{Diffusion[D}_\texttt{X}]\},$$

$$\{\texttt{cell} \longrightarrow \texttt{cell}, \texttt{Grow[GrowthRate[}\mu, \texttt{f}_\mu],$$

$$\texttt{Pressure[P}, \texttt{f}_\texttt{P}], \texttt{Spring[k}, \texttt{f}_\texttt{k}]\},$$

$$\{\texttt{cell} \longrightarrow \texttt{cell} + \texttt{cell}, \texttt{Errera[cell}, \mu, \sigma]\}\} \tag{32}$$
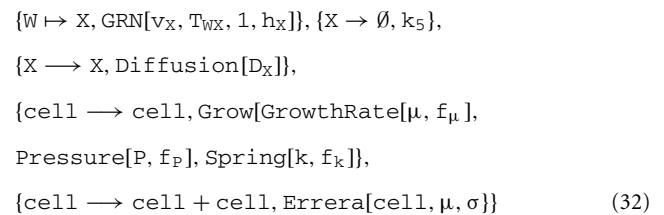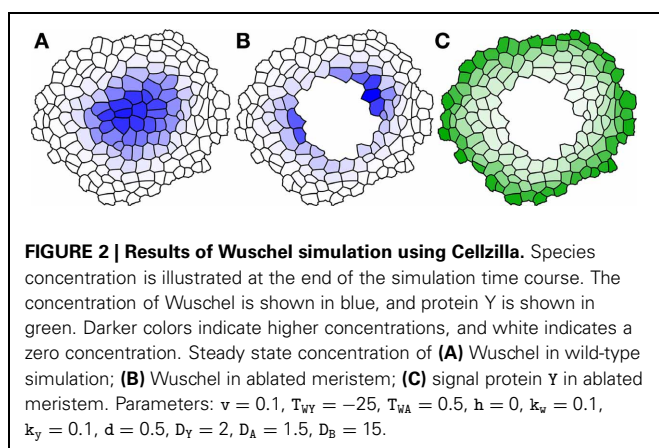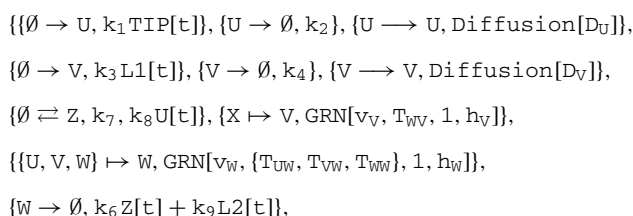
where $\texttt{k}_1$, $\texttt{k}_2$, $\texttt{k}_3$, $\texttt{k}_4$, $\texttt{k}_5$, $\texttt{k}_6$, $\texttt{k}_7$, $\texttt{k}_8$, $\texttt{k}_9$, $\texttt{h}_\texttt{V}$, $\texttt{h}_\texttt{W}$, $\texttt{v}_\texttt{V}$, $\texttt{v}_\texttt{W}$, $\texttt{T}_\texttt{WX}$, $\texttt{T}_\texttt{UW}$, $\texttt{T}_\texttt{VW}$, $\texttt{T}_\texttt{WW}$, $\texttt{T}_\texttt{WV}$, $\texttt{D}_\texttt{U}$, $\texttt{D}_\texttt{V}$, and $\texttt{D}_\texttt{X}$ are tunable parameters; $\texttt{L1[t]}$, $\texttt{L2[t]}$, and $\texttt{Tip[t]}$ are built in indicator functions for these cell locations; and the functions $\texttt{f}_\texttt{P}$ and $\texttt{f}_\mu$ describe pressure and growth feedback; e.g., $P[i] = p_0 + p_1 W[i]$ and $\mu[j] = \mu_0 + \mu_1(W[i] + W[j])$ (where p_0, p_1, and μ_0 are tunable control parameters). The user would type these function definitions either in the lines before the model or in line as lambda functions in place of the function references in the model. Simulation results are shown in **Figure 3**. As seen in **Figures 3A–C**, the stem cell niche is maintained through at least 500 cell divisions.

DISCUSSION

We have illustrated that meaningful quantitative results for plant morphodynamics can be obtained using a simple polygonal tissue model coupled with a spring growth equations. In particular, our implementation utilizes and extends an existing arrow-based computational framework that is easy and intuitive to use. This framework is built within a standardized computer algebra system (Mathematica) that is widely available and provides access to a wide selection of analytical tools. In addition we believe that our framework is generalizable and extensible to the wider world or rule-based systems. While more detailed particle-based or molecular dynamics frameworks will certainly produce more accurate frameworks their ultimate extensibility is limited by CPU availability and time constraints. Our implementation provides a useful platform for rapid model development and testing that can easily by transformed to one of the more detailed frameworks, if desired, once suitable results are obtained.

Cellzilla can be used for 2D simulations of plant tissues at the multicellular level. Because models can be rapidly built and

FIGURE 2 | Results of Wuschel simulation using Cellzilla. Species concentration is illustrated at the end of the simulation time course. The concentration of Wuschel is shown in blue, and protein Y is shown in green. Darker colors indicate higher concentrations, and white indicates a zero concentration. Steady state concentration of **(A)** Wuschel in wild-type simulation; **(B)** Wuschel in ablated meristem; **(C)** signal protein Y in ablated meristem. Parameters: $v = 0.1$, $T_{WY} = -25$, $T_{WA} = 0.5$, $h = 0$, $k_w = 0.1$, $k_y = 0.1$, $d = 0.5$, $D_Y = 2$, $D_A = 1.5$, $D_B = 15$.

FIGURE 3 | Maintenance of organizing center during growth simulation. (A) Initial distribution of W; **(B)** Distribution after 250 cell divisions; and **(C)** Distribution after 500 cell divisions. **(D)** Cell lineages; each color shows a different clonal population corresponding to all descendants of a particular cell in **(A)**. Parameters: $k_1 = 2$, $k_2 = 0.2$, $k_3 = 1$, $k_4 = 0.25$, $k_5 = 1$, $k_6 = 0.05$, $k_8 = 1.5$, $k_9 = 0.1$, $D_U = 10$, $D_V = 0.5$, $D_X = 0.5$, $v_X = 1$, $v_W = 1$, $v_V = 1$, $h_X = 0$, $h_W = 0$, $h_V = 0$, $T_{WX} = 4$, $T_{WW} = 4$, $T_{UW} = 22.5$, $T_{VW} = -25$, $T_{WW} = 27.5$, $p_0 = 0.001$, $p_1 = 0.004$, $\mu_0 = 5 \times 10^{-6}$, $\mu_1 = .004$.

tested it allows one to quickly test developmental models both in steady-state and during growth. However, several improvements are planned for future versions. In the current version, only simple transport and diffusion are considered; however, in many cell types, not just plant cells, osmotic and electrical gradients are significant. We plan to implement rules to incorporate both features in future releases. Furthermore, with the addition of osmotic models and pressure gradients we plan to add additional plant-specific growth models (Lockhart, 1965; Ortega, 1985; Geitmann and Ortega, 2009). These can be optionally used in place of the phenomenologically-based spring-based growth model. Additions to the cell division model will be included. For example, the constraints used in the Errera implementation of linear walls and equal areas can be relaxed to quadratic and circular arcs, and the areas can be randomized in a cloud about equality.

A three-dimensional model is also planned, although we expect that this will have significantly greater computational demands. To avoid mathematically unstable solutions in three dimensions the spring model will need to be modified or replaced, most likely with an elastic dynamics model incorporating pressure and stress tensors. An alternative is the use of triangular springs (Delingette, 2008).

DATA SHARING

All of the software described here is open source Mathematica (GPL license) and freely downloadable from launchpad at https://launchpad.net/cellerator. The software is fully documented and all examples are available at the project website https://www.cellzilla.info.

REFERENCES

Andrews, S. (2012). "Spatial and stochastic cellular modeling with the smoldyn simulator," in *Bacterial Molecular Networks: Methods and Protocols: Methods in Molecular Biology*, eds J. van Helden, A. Toussaint, and D. Thieffry (New York, NY: Springer), 519–540.

Besson, S., and Dumais, J. (2011). Universal rule for the symmetric division of plant cells. *Proc. Natl. Acad. Sci. U.S.A.* 108, 6294–6299. doi: 10.1073/pnas.1011866108

Boudin, F., Pradal, C., Cokelaer, T., Prusinkiewicz, P., and Godin, C. (2012). L-Py: an L-system simulation framework for modeling plant architecture development based on a dynamic language. *Front. Plant Sci.* 3:76. doi: 10.3389/fpls.2012.00076

Chickarmane, V. S., Gordon, V., Tarr, S. P., Heisler, M. G., and Meyerowitz, E. M. (2012). Cytokinin signaling as a positional cue for patterning the apicalbasal axis of the growing arabidopsis shoot meristem. *Proc. Natl. Acad. Sci. U.S.A.* 109, 4002–4007. doi: 10.1073/pnas.1200636109

Cickovski, T., Aras, K., Swat, M., Merks, R., Glimm, T., George, H., et al. (2007). From genes to organisms via the cell: a problem-solving environment for multicellular development. *Comput. Sci. Eng.* 9, 50–60. doi: 10.1109/MCSE.2007.74

Delingette, H. (2008). Triangular springs for modeling nonlinear membranes. *IEEE Trans. Vis. Comput. Graph.* 14, 239–241. doi: 10.1109/TVCG.2007.70431

Errera, L. (1888). Ber zellformen und seifenblasen *Bot. Centralbl.* 34, 395–398. doi: 10.1002/cplx.20074

Faeder, J. R., Blinov, M. L., Goldstein, B., and Hlavacek, W. S. (2005). Rule-based modeling of biochemical networks. *Complexity* 10, 22–39. doi: 10.1002/cplx.20074

Faeder, J. R., Blinov, M. L., and Hlavacek W. S. (2009). "Rule based modeling of biochemical systems with BioNetGen," in *Systems Biology*, ed I. V. Maly (New York, NY: Springer), 113–167.

Geitmann, A., and Ortega, J. K. E. (2009). Mechanics and modeling of plant cell growth. *Trends Plant Sci.* 14, 1360–1385. doi: 10.1016/j.tplants.2009.07.006

Gilllespie, D. T. (1976). A general method for numerically simulating the stochastic time evlolution of coupled chemical reactions. *J. Comput. Phys.* 22, 403–434. doi: 10.1016/0021-9991(76)90041-3

Graner, F., and Glazier J. A. (1992). Simulation of biological cell sorting using a two-dimensional extended potts model. *Phys. Rev. Lett.* 69, 2013–2016. doi: 10.1103/PhysRevLett.69.2013

Hucka, M., Finney, A., Sauro, H. M., Bolouri, H., Doyle, J. C., Kitano, H., et al. (2003). The systems biology markup language (SBML): a medium for representation and exchange of biochemical network models. *Bioinformatics* 19, 513–523. doi: 10.1093/bioinformatics/btg015

Jönsson, H., Heisler, M., Reddy, G. V., Agrawal, V., Gor, V., Shapiro, B. E., et al. (2005a). Modeling the organization of the wuschel expression domain in the shoot apical meristem. *Bioinformatics* 21, i232–i240. doi: 10.1093/bioinformatics/bti1036

Jönsson, H., Heisler, M., Shapiro, B. E., Meyerowitz, E. M., and Mjolsness, E. (2005b). An auxin-drive polarized transport model for phyllotaxis. *Proc. Natl. Acad. Sci. U.S.A.* 103, 1633–1638. doi: 10.1073/pnas.0509839103

Jönsson, H., Shapiro, B. E., Meyerowitz, E. M., and Mjolsness, E. (2004). "Modeling plant development with gene regulation networks including signaling and cell division," in *Bioinformatics of Genome Regulation and Structure*, eds R. Hofestaedt and N. Kolchanov (New York, NY: Kluwer Publications), 311–318.

Karowowski, R., and Prusinkiewicz, P. (2004). "The L-System-based plant-modeling environment L-Studio 4.0," in *Presented at 4th International Workshop on Functional and Structural Plant Models* (Montpelier).

Koumoutsakos, P., Bayati, B., Milde, F., and Tauriello, G. (2011). Particle simulations of morphogenesis. *Math. Models Methods Appl. Sci.* 21(Suppl.), 995–1006. doi: 10.1142/S021820251100543X

Lockhart, J. (1965). An analysis of irreversible plant cell elongation. *J. Theor. Biol.* 8, 264–275. doi: 10.1016/0022-5193(65)90077-9

Merks, R. M. H., Guravage, M., Inze, D., and Beemster, G. T. S. (2011). Virtualleaf: an open-source framework for cell-based modeling of plant tissue growth and development. *Plant Physiol.* 155, 656–666. doi: 10.1104/pp.110.167619

Mjolsness, E. (2006). The growth and development of some recent plant models: a viewpoint. *J. Plant Growth Regul.* 25, 270–277. doi: 10.1007/s00344-006-0069-7

Mjolsness, E. D. (2013). Time-ordered product expansions for computational stochastic systems biology. *Phys. Biol.* 10:035009. doi: 10.1088/1478-3975/10/3/035009

Mjolsness, E. D., Sharp, D. H., and Reinitz, J. (1991). A connectionist model of development. *J. Theor. Biol.* 152, 429–453. doi: 10.1016/S0022-5193(05)80391-1

Mjolsness, E. D., and Yosiphon, G. (2006). Stochastic process semantics for dynamical grammars. *Ann. Math. Artif. Intell.* 47, 329–395. doi: 10.1007/s10472-006-9034-1

Nikolaev, S. V., Penenko, A. V., Lavreha, V. V., Mjolsness, E. D., and Kolchanov, N. A. (2007). A model study of the role of proteins CLV1, CLV2, CLV3, and WUS in regulation of the structure of the shoot apical meristem. *Russ. J. Dev. Biol.* 38, 383–388. doi: 10.1134/S1062360407060069

Nikolaev, S. V., Zubairova, U. S., Penenko, A. V., Mjolsness, E. D., Shapiro, B. E., and Kolchanov, N. A. (2013). Model of structure regulation of stem cell niche in shoot apical meristem of *Arabidopsis thaliana* (in Russian). *Doklady Akademii Nauk* 453, 336–338.

Ortega, J. K. E. (1985). Augmented growth equation for cell wall

expansion. *Plant Physiol.* 79, 318–320. doi: 10.1104/pp.79.1.318

Plimpton, S. J., and Slepoy, A. (2005). Microbial cell modeling via reacting diffusing particles. *J. Phys.* 16, 305–309. doi: 10.1088/1742-6596/16/1/042

Pradal, C., Dufour-Kowalski, S., Boudon, F., Fournier, C., and Godin, C. (2008). Openalea: a visual programming and component-based software platform for plant modeling. *Funct. Plant Biol.* 35, 751–760. doi: 10.1071/FP08084

Prigogine, L., and Lefever, R. (1968). Symmetry breaking instabilities in dissipative systems. II. *J. Chem. Phys.* 48, 1695–1700 doi: 10.1063/1.1668896

Prusinkiewicz, P., and Lindenmayer, A. (1990). *Algorithmic Beauty of Plants.* New York, NY: Springer Verlag.

Prusinkiewicz, P., and Runions, A. (2012). Computational models of plant development and form. *New Phytol.* 193, 549–569. doi: 10.1111/j.1469-8137.2011.04009.x

Rudge, T., and Haseloff, J. (2005). A computational model of morphogenesis in plants. *Adv. Artif. Life* 3630, 78–87,

Sahlin, P., and Jönsson, H. (2010). A modeling study of how cell division affects properties of epithelial tissues under isotropic growth. *PLoS ONE* 5:e11750. doi: 10.1371/journal.pone.0011750

Shapiro, B. E., Heisler, M., Tobin, C., Cunha, A., Davis, A., Mjolsness, E. D., et al. (2010). "Using geometric markers to predict the cell division plane in meristem cells," in *Proceedings of the 6th International Workshop on Functional-Structural Plant Models*, eds T. DeJong and D. Da Silva (Davis, CA: University of California), 144–146.

Shapiro, B. E., Hucka, M., Finney, A., Doyle, J. (2004). MathSBML: a package for manipulating SBML based biological models. *Bioinformatics* 20, 2829–2831. doi: 10.1093/bioinformatics/bth271

Shapiro, B. E., Levchenko, A., Meyerowitz, E. M., Wold, B. J., and Mjolsness, E. D. (2003). Cellerator: extending a computer algebra system to include biochemical arrows for signal transduction simulations. *Bioinformatics* 19, 677–678. doi: 10.1093/bioinformatics/btg042

Shapiro, B. E., and Mjolsness, E. D. (2001). "Developmental simulations with cellerator," in *International Conference on Systems Biology* (Pasadena, LA).

Smith, L. G. (2001). Plant Cell Division: Building Walls in the Right Places. *Nat. Rev.* 2, 33–39. doi: 10.1038/35048050

Sneddon, M. W., Faeder, J. R., Emonet, T. (2011). Efficient modeling, simulation an dcoarse graining of biological complexity with nfsim. *Nat. Methods* 8 177–183. doi: 10.1038/nmeth.1546

Stiles, J. R., and Bartol, T. M. (2001). "Monte carlo methods for simulating realistic synaptic microphysiology using MCell," in *Computational Neuroscience: Realistic Modeling for experimentalists*, ed E. De Schutter (Boca Raton, FL: CRC Press), 87–127.

Yang, C.-R., Shapiro, B. E., Mjolsness, E. D., and Hatfield, G. W. (2005). An enzyme mechanism language for the mathematical modeling of metabolic pathways. *Bioinformatics* 21, 774–780. doi: 10.1093/bioinformatics/bti068

Yosiphon, G. (2009). *Stochastic Parameterized Grammars: Formalization, Inference, and Modeling Applications.* PhD Thesis, UC Irvine.

Constructing a framework for risk analyses of climate change effects on the water budget of differently sloped vineyards with a numeric simulation using the Monte Carlo method coupled to a water balance model

*Marco Hofmann , Robert Lux and Hans R. Schultz **

Institut für Allgemeinen und ökologischen Weinbau, Hochschule Geisenheim University, Geisenheim, Germany

Grapes for wine production are a highly climate sensitive crop and vineyard water budget is a decisive factor in quality formation. In order to conduct risk assessments for climate change effects in viticulture models are needed which can be applied to complete growing regions. We first modified an existing simplified geometric vineyard model of radiation interception and resulting water use to incorporate numerical Monte Carlo simulations and the physical aspects of radiation interactions between canopy and vineyard slope and azimuth. We then used four regional climate models to assess for possible effects on the water budget of selected vineyard sites up 2100. The model was developed to describe the partitioning of short-wave radiation between grapevine canopy and soil surface, respectively, green cover, necessary to calculate vineyard evapotranspiration. Soil water storage was allocated to two sub reservoirs. The model was adopted for steep slope vineyards based on coordinate transformation and validated against measurements of grapevine sap flow and soil water content determined down to 1.6 m depth at three different sites over 2 years. The results showed good agreement of modeled and observed soil water dynamics of vineyards with large variations in site specific soil water holding capacity (SWC) and viticultural management. Simulated sap flow was in overall good agreement with measured sap flow but site-specific responses of sap flow to potential evapotranspiration were observed. The analyses of climate change impacts on vineyard water budget demonstrated the importance of site-specific assessment due to natural variations in SWC. The improved model was capable of describing seasonal and site-specific dynamics in soil water content and could be used in an amended version to estimate changes in the water budget of entire grape growing areas due to evolving climatic changes.

Keywords: climate change, grapevine, model, radiation interception, sap flow, soil water budget, steep slope, vine transpiration

INTRODUCTION

Grapevines are cultivated on 6 out of 7 continents, between latitudes 4° and 51° in the Northern Hemisphere (NH) and between 6° and 45° in the Southern Hemisphere (SH) across a large diversity of climates (Tonietto and Carbonneau, 2004). Accordingly, the range and magnitude of environmental factors and the principal environmental constraints differ considerably from region to region. Wine grapes are traditionally grown in geographical regions where the growing season (April–October for the NH) mean temperature is within the range of 12–22°C (Jones, 2006). Warming during the growing season has been observed in all studied wine regions over the past 50–60 years (i.e., Schultz, 2000; Jones et al., 2005a; Webb et al., 2007, 2011; Santos et al., 2012). Observed and predicted changes in temperature have a pronounced effect on the geographical distribution of where grapevines can be grown (Kenny and Harrison, 1992; Jones et al., 2005b; Schultz and Jones, 2010; Santos et al., 2012). Observed

advancement in phenological events and specifically maturity have recently also been correlated to a continuous reduction in soil water content as a co-factor to temperature (Webb et al., 2012). Within the existing production areas, water shortage is probably the most dominant environmental constraint (Williams and Matthews, 1990) and even in moderate temperate climates, grapevines often face some degree of drought stress during the growing season (Morlat et al., 1992; van Leeuwen and Seguin, 1994; Gaudillère et al., 2002; Gruber and Schultz, 2005).

Recent projections for the major world grape growing areas using various model approaches driven by 17 global climate models (GCMs) projected substantial reductions in suitable area for Viticulture largely due to changes in water availability related to shifts in precipitation rate and/or distribution, increases in evaporative demand and in many cases reduced access to water for irrigation (Hannah et al., 2013). Most European grape growing areas are non-irrigated and there is a rising concern if this is

sustainable in the future. Additionally, many of the most valuable areas in terms of quality and reputation are located on steep slopes which may exacerbate the impact of climate change due to a reduced potential for adaptation (high labor costs, technical challenges, access to water a.s.o). Southern Germany has many examples for these landscapes since wine-growing regions are mainly located in river valleys where Viticulture has been practized on steep slopes for hundreds sometimes several thousand years (Weeber, 1993). Mean annual precipitation (530–750 mm) is generally low in these regions and soil water holding capacity (SWC) is very heterogeneous, with the percentage of vineyards with low SWC being relatively high (example Rheingau region; SWC < 125 mm for nearly 50% of steep slope areas, Löhnertz et al., 2004). Therefore, risk assessment of possible consequences of climate change on soil and plant water budget needs to be on a finer scale and requires a functional plant or vineyard model, respectively, which can be scaled up from vineyard plots to entire regions.

There are several approaches which have been taken previously to model the water budget of vineyards and the use of crop coefficients is the most widely spread (Allen et al., 1998). However, grapevine canopies represent a large array of possible structures (shape, leaf/fruit/stem distribution, density) imbedded in an equally large spectrum of possible vineyard geometries (distances between and within rows) which in conjunction with a variety of management practices and soil properties affect vineyard transpiration and render the use of standard crop coefficients (K_c) difficult (Williams and Ayars, 2005; Fandiño et al., 2012). These difficulties are also reflected in other approaches based on the Shuttleworth and Wallace (1985) model which could separate between vine transpiration and soil evaporation, by applying individual evapotranspiration controlling resistances to plants or the soil and combining one dimensional models of crop transpiration and soil evaporation. This model proved to be very sensitive to the parameterization of the leaf area index (LAI, used to model net energy separation) and canopy resistance, and might be combined with a more detailed model to separate net radiation on plants or soil in order to apply the model to complete growing regions (Ortega-Farias et al., 2007, 2010; Poblete-Echeverría and Ortega-Farias, 2009).

There has been substantial progress in the description of grape canopy structure and its effect on light interception using two-dimensional modeling (Schultz, 1995) and later three-dimensional digitizing technology (Mabrouk et al., 1997; Sinoquet et al., 1998; Louarn et al., 2007) which consequently lead to the development of complex three-dimensional models of plant architecture on an organ scale (Louarn et al., 2008a; López-Lozano et al., 2009; Iandolino et al., 2013). Beside of many applications of functional-structural models of this detail in assessing plant architecture effects on radiative transfer and whole plant gas exchange (Louarn et al., 2008b; López-Lozano et al., 2011; Prieto et al., 2012) they remain difficult to parameterize and have not yet been scaled up to asses for vineyard water use. Lebon et al. (2003) have used a somewhat intermediate approach between simplistic and highly complex to describe the light interception inside of a vineyard in order to separate the evapotranspiration fluxes of grapevines or bare soil and validated the model for different

vineyard sites. Celette et al. (2010) extended the model to account for changes in water use by the presence of cover crops. In principle, the model goes back to a geometrical vineyard model of radiation interception and distribution proposed by Riou et al. (1989) with the basic assumption that these are the key drivers of transpiration and evaporation. The model was then extended to include soil water reservoirs (Riou et al., 1994), to account for the feedback of water stress on transpiration (Lebon et al., 2003), to simulate meaningful physiological plant parameters describing the level of water deficit such as predawn water potential (Schultz and Lebon, 2005) and to characterize the radiative balance within important parts of a vineyard canopy such as the fruiting zone (Pieri, 2010a,b). However, the model has never been used to describe radiation interception, and consequently, the water budget in sloped vineyards, where slope and azimuth in conjunction with the degree of latitude have substantial impact on the received solar radiation (Geiger, 1980) and their partitioning on vines or soil, nor has it been coupled to regionalized climate models in order to project changes in vineyard water balance possibly brought about by climate change under these situations.

We therefore had several key objectives:

(1) to improve the canopy-structure module;
(2) to adapt the model environment so that different degrees of slope and azimuth can be accounted for;
(3) to validate the model on different sites against sap flow and soil moisture data and;
(4) to use the model in conjunction with several regionalized climate models to project changes in soil and plant water budget for different vineyard sites for the period of the current century.

MATERIALS AND METHODS
VINEYARD SITE DESCRIPTION
Three commercial vineyards located near Rüdesheim (49°58′N, 7°55′E) with different soil water holding capacities, management practices, canopy geometries and differences in the degree of slope and azimuth were chosen as validation sites for the model (**Figure 1**). The plots were named Ehrenfels (EF), Burgweg (BU), and Wilgert (WI), planted with *Vitis Vinifera* cv. "Riesling" and trained to a cane or spur pruned VSP Trellis system. The geometry of the canopy (**Table 1**) was conserved after bloom (mid-June) by hedging two or three times during the summer.

BU and WI were planted in 1983 and grafted onto the rootstock 5C and EF was planted in 1996 and grafted onto Börner. Vineyards EF and BU were on steep slopes (**Table 1**) with shallow stony soils (<1.5 m depth), poor in loess-loam on largely carbonate-free bedrock (class I, Löhnertz et al., 2004), whereas the soil of WI was medium deep (>1.5 m) with a high proportion of loam and hence a higher water holding capacity than EF and BU (class II, Löhnertz et al., 2004).

All soils were partly covered by a natural population of cover crops and weeds (mainly grasses) whereby the surface area fractions occupied by these plants (f_{cc}) differed between sites (**Table 1**). A strip of approximately 0.4 m width beneath the vines was kept bare in all plots through the use of herbicides. In EF and WI the soil of each row was covered by cover crops whereas in BU

alternating rows were kept free of vegetation by frequent tillage. Inter-row vegetation was kept short through frequent mowing in all vineyards. These types of soil management are representative for many German steep slope wine regions.

RADIATION PARTITIONING MODEL

The original model of Lebon et al. (2003) calculated the amount of radiation absorbed by the vineyard and partitioned this to soil and canopy. The geometry of the canopy was described by the distance between the rows, *D*, and the width, *L*, and the height, *H*, of the grapevine foliage (see **Table 2** for a list of symbols). Height and width of the canopy composed a cuboid, whose third edge length corresponded to the length of the grapevine row and was considered infinite. Further input variables were the perpendicular porosity of the vertical foliage walls, the soil

FIGURE 1 | Upper part: Graphical outline of three experimental vineyards true to scale in row distance, canopy height and width, slope and aspect ratios. Green cuboids illustrate grapevine rows, soil is gray. **Bottom part:** The experimental vineyard EF with the castle ruin Ehrenfels in the background.

surface and leaf albedos, the incoming direct and diffuse solar radiation and the direction of the direct solar radiation. The horizontal faces bordering the top and the bottom of the foliage were considered opaque.

Based on the allocation of radiation to the vine and soil components, Lebon et al. (2003) formulated equations for potential vine transpiration $T_{0,v}$ and potential soil evaporation E_0:

$$T_{0,v} = \frac{R_v}{R_{vy}} ET_0, \tag{1}$$

$$E_0 = \frac{R_s}{R_{vy}} ET_0, \tag{2}$$

where R_v, R_s, R_{vy} represent the radiation absorbed by the vines, the soil or the vineyard, respectively, ($R_{vy} = R_v + R_s$) and ET_0 is the potential evapotranspiration.

We replaced this simple radiation partitioning module (Riou et al., 1989; Lebon et al., 2003) by a numerical simulation approach for three reasons: (1) under conditions of high gap frequency (high porosity) we found that calculated vine transpiration could be substantially higher than measured transpiration; (2) considering the horizontal faces as opaque might overestimate the radiation absorbed by the vines, if the proportion of canopy width to row distance and the porosity are high; and (3) for the use of the model in climate impact studies for entire steep slope grape growing regions, situations described in (1) and (2) are very frequent due to the age of the vineyards (small row distances) and the low SWC (high porosity).

We therefore used a numerical simulation approach based on the Monte Carlo method which is widely used in physics to describe radiative transfer (Modest, 2003). We maintained the same geometrical framework in order to keep the input variables unchanged. For a better account for radiation scattered back from soil to the bottom of the foliage we introduced the parameter stem height *S*, representing the distance between foliage and soil surface (**Figure 2**). The bottom and top side of the canopy were not treated as opaque and the porosity of the canopy was not set to a fixed value as in previous versions (Lebon et al., 2003). Radiative transfer depended on the possible travel distance of radiation inside the cuboid. Radiation extinction in plant canopies is normally modeled by applying the Beer–Lambert law, where the extinction is the product of the extinction coefficient and the cumulated LAI in the pathway (Hirose, 2005). If the leaf area dispersion is assumed to be homogenous, the cumulated LAI can be replaced by the travel distance of radiation
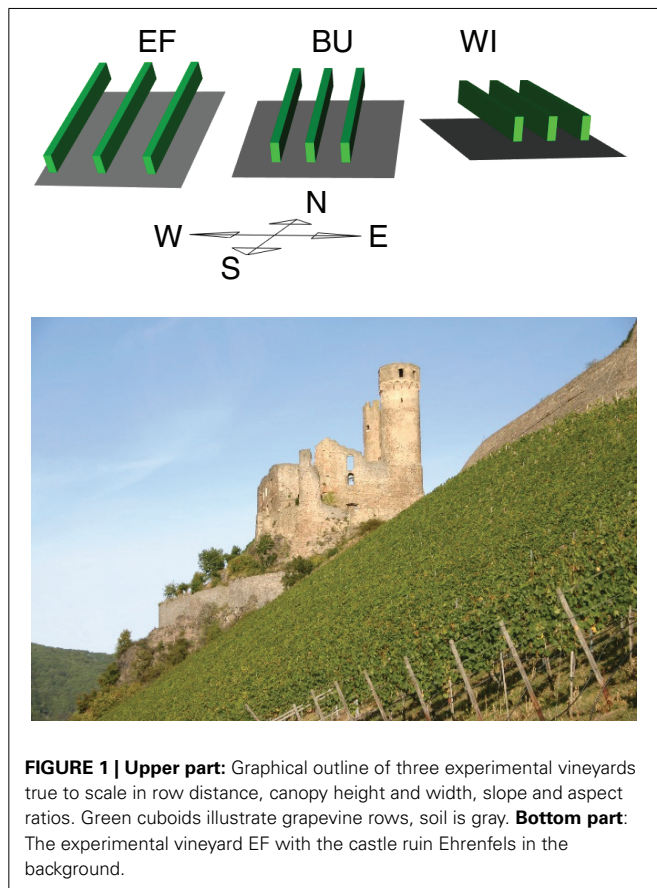
Table 1 | Main characteristics of the three commercial vineyards used in the study (azimuth angles east of south are negative and west of south positive).

Site	Planting density (vines/ha)	Total transpirable soil water (mm), max. depth 1.60 m	Canopy height (m)	Canopy width (m)	Row distance (m)	Porosity (min.)	Slope/azimuth	Fraction of soil covered by vegetation
EF	4400	85	1.00	0.40	2.50	0.40	35°/8°	0.84
BU	6875	115	1.10	0.40	1.60	0.25	27°/4°	0.40
WI	6875	160	1.35	0.40	1.60	0.25	15°/−21°	0.75

Table 2 | List of symbols and abbreviations used.

$a_{dif,v}$	Intercepted fraction of diffuse solar radiation by the vines
a_v, a_s	Intercepted fraction of direct solar radiation by the vines or the soil, respectively
E	Evaporation ($lm^{-2}day^{-1}$)
E_s	Evaporation of the vineyard ($lm^{-2}day^{-1}$)
E_0	Potential soil evaporation ($lm^{-2}day^{-1}$)
ET_a	Actual evapotranspiration of the vineyard ($lm^{-2}day^{-1}$)
$ET_{a,cc}$	Evapotranspiration of the cover crops ($lm^{-2}day^{-1}$)
ET_0	Potential evapotranspiration (horizontal equivalent) ($lm^{-2}day^{-1}$)
ET_{0s}	Potential evapotranspiration of the soil surface ($lm^{-2}day^{-1}$)
$FTSW$	Fraction of transpirable soil water
$FTSWcc$	Fraction of transpirable soil water accessible by cover crops
f_{cc}	Surface area fraction covered by cover crops or weeds (constant parameter depending on management practices)
f_g	Ground cover coefficient
$f_{R,v}$ $f_{R,s}$	Relative fractions of absorbed radiation by grapevines or soil
D	Distance between vine rows (m)
H	Height of the grapevine foliage (without stem height) (m)
I	Radiant flux density (Wm^{-2})
$k_{c,v}$	Grapevine transpiration coefficient
K_e	Soil evaporation coefficient
K_r	Soil evaporation reduction coefficient
k_s	Water stress coefficient
$k_{s,cc}$	Cover crop water coefficient
$k_{s,v,cc}$	Water extraction coefficient (considers the water extraction of grapevines from the cover crops reservoir)
L	Width of the grapevine foliage (m)
LAI	Leaf area index
L_e	Radiance ($Wm^{-2}sr^{-1}$)
N	Number of emitted or absorbed photons in a numerical Monte Carlo simulation
p	Porosity of the foliage (probability for no interception of a photon)
P	Precipitation (lm^{-2})
p_{FTSW}	Threshold value for $FTSW$
R_0	Extraterrestrial radiation (Wm^{-2})
R_{dif}	Diffuse solar radiation (Wm^{-2})
R_{dir}	Direct solar radiation (Wm^{-2})
$R_{dif,v}$	Diffuse solar radiation absorbed by the grapevine canopy (Wm^{-2})
R_{glob}	Global solar radiation (Wm^{-2})
R_s	Radiation absorbed by the soil (Wm^{-2})
R_v	Radiation absorbed by the grapevines (Wm^{-2})
R_{vy}	Radiation absorbed by the vineyard (Wm^{-2})
REW	Readily evaporable water (lm^{-2})
S	Height of the foliage above ground (stem height)
SWC	Soil water holding capacity (lm^{-2} and rooting depth)
$T_{0,v}$	Potential grapevine transpiration ($lm^{-2}day^{-1}$)
$T_{a,v}$	Actual grapevine transpiration ($lm^{-2}day^{-1}$)
TEW	Total evaporable water (lm^{-2})
TSW	Transpirable soil water (lm^{-2})
TSW_{cc}	Transpirable soil water (accessible by cover crops) (lm^{-2})
TSW_r	Transpirable water of the remaining (non-cover crop) reservoir (lm^{-2})

(Continued)

Table 2 | Continued

$TTSW$	Total transpirable soil water (lm^{-2})
$TTSW_{cc}$	Total transpirable soil water (accessible by cover crops) (lm^{-2})
$TTSW_r$	Total transpirable soil water of the remaining (non-cover crop) reservoir (lm^{-2})
VPD	Vapor pressure deficit
α_v, α_s	Absorptance of the grapevine foliage or the soil (for single photons)
β	Slope angle of the vineyard
γ	Vineyard azimuth angle (the aspect of the vineyard)
γ_s	Solar azimuth angle
γ_v	Vineyard solar azimuth angle
θ	Angle of incidence (angle between direct radiation beam and the normal to the surface of the vineyard)
θ_z	Zenith angle of the sun
ρ_s, ρ_l	Shortwave reflectivity (albedo) of soil or leaves, respectively
ρ_{vy}	Albedo of the vineyard (simulated)
τ	Transmittance of the grapevine foliage (for single photons)
ψ_{pd}	Predawn leaf water potential (MPa)
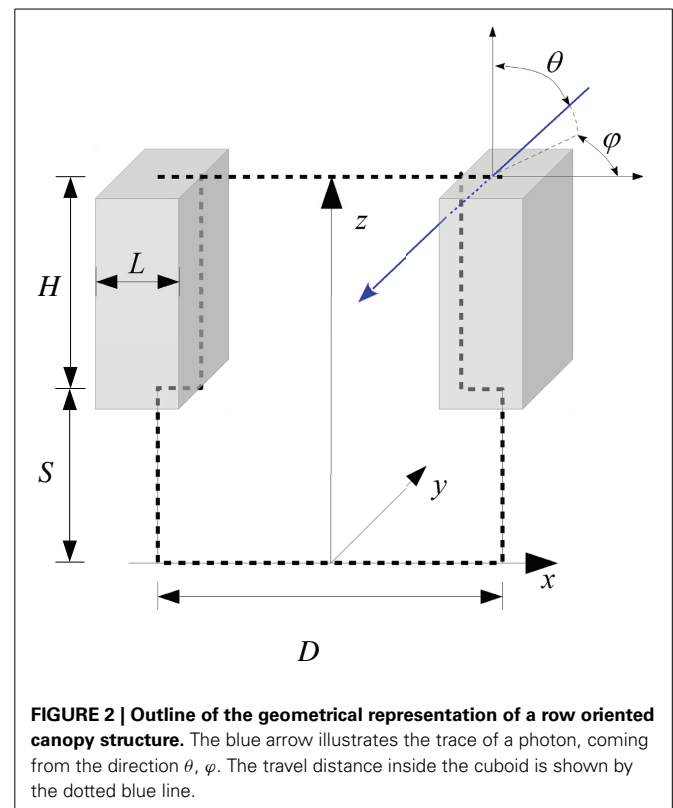
FIGURE 2 | Outline of the geometrical representation of a row oriented canopy structure. The blue arrow illustrates the trace of a photon, coming from the direction θ, φ. The travel distance inside the cuboid is shown by the dotted blue line.

inside the cuboid and the extinction coefficient by an expression depending on the porosity of a vertical foliage wall and the corresponding width of the foliage, which were both easy measurable parameters. The model is outlined in more detail in Appendix A.

The model allows us to determine interception fractions for direct and diffuse radiation of the vines and the soil and

subsequently to calculate R_v, R_s, and R_{vy} in 30 min time steps. This allows a higher frequency of calculations of soil evaporation and vine transpiration as in the original model. Nevertheless, throughout the paper, data are presented for daily time steps based on the sums of each half hour estimation. The corresponding relative fractions of absorbed radiation by grapevines or soil ($f_{R,v}$, $f_{R,s}$) are expressed by:

$$f_{R,v} = R_v / R_{vy}, \qquad (3a)$$

$$f_{R,s} = R_s / R_{vy}. \qquad (3b)$$

Daily values of $f_{R,v}$ and $f_{R,s}$ were calculated by summarizing R_v, R_s, and R_{vy} from radiation data of 30 min temporal resolution.

The interception fractions for direct radiation (grapevines and soil) depend on the direction of the radiation beam relative to the grapevine rows, vineyard slope and aspect and the position of the sun. This adaptation of the model to slopes is described in detail in Appendix B.

The development of height, width, and porosity of the vine canopy are calculated by linear functions depending on thermal time and thresholds for bud burst, hedging, onset and end of leaf abscission as described in detail in Lebon et al. (2003).

THE SOIL WATER BALANCE MODEL

Two options exist to adapt a soil water balance model to sloped surfaces. One is to calculate the water fluxes at the normal of the slope surface and the other is to use horizontal equivalents. Since precipitation and soil water content (with vertically installed access tubes) are measured in horizontal equivalents, evapotranspiration is also expressed in l/m² referring to a horizontal surface. All water fluxes or quantities are expressed in l/m² or the equivalent mm.

The soil water balance model is based on the model of Lebon et al. (2003) with some extensions introduced by Celette et al. (2010). The soil water is represented by a reservoir characterized by its total transpirable soil water ($TTSW$), representing the difference between maximum and minimum (extractable) water content, the transpirable soil water (TSW) and the fraction of transpirable soil water ($FTSW = TSW/TTSW$) remaining at any time during the season (Sinclair and Ludlow, 1986). The reservoir incorporates two sub reservoirs, one for cover crops and one for bare soil. The sub reservoirs are used to calculate individual water balance routines for cover crops and bare soil in order to separate the actual evapotranspiration fluxes between cover crops, bare soil, and grapevines (Celette et al., 2010). Cover Crops can only extract water from the cover crop reservoir, which is therefore characterized by its own $TTSW_{cc}$. Grapevine roots are present in the complete reservoir and extract water from all sub reservoirs (Celette et al., 2008). Model calculations and data analysis were implemented in the R programming language (R development core team, 2012).

Evaporation of bare soil

In the previous model versions (Lebon et al., 2003; Celette et al., 2010) the evaporation of the bare soil was calculated according to Ritchie (1972) and Brisson and Perrier (1991). This part was replaced by the approach of Allen et al. (1998) in the FAO guidelines for computing crop water requirements which has recently been modified to account for small precipitation events and its effects on soil surface evaporation (Allen, 2011). The parameterization of that model seemed more suitable for our application and it has been demonstrated to be robust and apply to different soil types (Allen et al., 1998). Both models (the original one used and the new approach) divide the evaporation process in two stages, where in the first stage evaporation is only limited by the energy available at the soil surface. In the second stage the evaporation rate is lower, because the transport of sub-surface water to the evaporating surface is reduced by the dry topsoil layer. That is described by a function depending on the square root of time in Ritchie (1972) and Brisson and Perrier (1991) and by a function depending on the relative content of evaporable water remaining in the evaporation layer in Allen et al. (1998). Allen et al. (1998) assumed that the upper 0.10–0.15 m of the soil layer can be dried by evaporation. This layer is characterized by the total amount of evaporable water (TEW) which is the maximum amount of water that can be evaporated during a drying cycle. The amount of water which can evaporate in the first stage is termed readily evaporable water (REW) and can be derived from TEW. The feedback of the dry topsoil on the evaporation rate in the second stage is described by a soil evaporation reduction coefficient K_r ([0–1], dimensionless) which equals the quotient of the amount of evaporable water actual remaining in the complete evaporation layer to the difference TEW–REW. To account for small precipitation events, Allen (2011) introduced an additional skin layer to the model, which is located at the topsoil (as a part of the evaporation layer) and its amount of evaporable water is equivalent to REW. The skin layer is recharged first by precipitation. In general, water evaporates during the first stage ($K_r = 1$) if water is available in the skin layer and the reduction of the evaporation rate described by K_r is only effective if the skin layer is dry. Therefore, small amounts of rain falling on a dry soil evaporate more quickly (first stage) as in the previous approach of Allen et al. (1998). The evaporation model of Allen (2011) calculates a daily water balance routine, where ET_0 is one of the input variables. To apply this model to our approach, the water balance routine was calculated for a completely bare soil as described in the dual crop coefficient approach of Allen (2011) (as briefly described above), but instead of the daily ET_0 values the product $f_{R,s}ET_0$ (Equation 3b) is used to account for the potential evapotranspiration effective at the soil surface, which is reduced due to the shading effects of the grapevine canopy. The daily water balance routine calculates a soil evaporation coefficient K_e (depending on K_r) with which the evaporation of bare soil of the vineyard E_s can be described by:

$$E = K_e f_{R,s} ET_0, \qquad (4)$$

$$E_s = E(1 - f_{cc}), \qquad (5)$$

where E is the evaporation of a completely bare soil. The factor f_{cc} is the area fraction of the soil, which is covered by cover crops and depends on management practices.

The amount of transpiration of grapevines or cover crops from the evaporation layer is neglected in the daily water balance routine as recommended by Allen et al. (1998). TEW was estimated

from the *TTSW* for the upper 0.15 m soil depth from soil water data of the access tubes and is in line with tabled values of Allen et al. (1998) (**Table 3**).

Transpiration of grapevines

The approach to calculate the transpiration of grapevines is similar to the model of Lebon et al. (2003). Following Equation (3a), describing the fraction of radiation absorbed by the grapevine canopy, Equation (1) can be rewritten as:

$$T_{0,v} = f_{R,v} ET_0, \qquad (6)$$

where $T_{0,v}$ is an expression for the potential vine transpiration in the absence of a water deficit. To calculate actual transpiration of grapevines ($T_{a,v}$), $T_{0,v}$ is multiplied with two coefficients:

$$T_{a,v} = k_{c,v} k_s T_{0,v}, \qquad (7)$$

where k_s is a water stress coefficient [0–1] accounting for the influence of soil water shortage on $T_{a,v}$. The k_s coefficient was introduced by Lebon et al. (2003) to describe the stomatal response to water deficit (Trambouze and Voltz, 2001). This response is described with a bilinear function where during the first stage of water depletion the relative vine transpiration rate, $T_{a,v}/T_{0,v}$ is not limited by available soil water and transpiration is maximal. When *FTSW* falls below a threshold value p_{FTSW}, $T_{a,v}/T_{0,v}$ declines linearly with *FTSW* to zero (Lebon et al., 2003), thus k_s depends on *FTSW* as follows:

$$k_s = \begin{cases} FTSW/p_{FTSW} & (0 \leq FTSW \leq p_{FTSW}) \\ 1 & (p_{FTSW} < FTSW \leq 1) \end{cases}, \qquad (8)$$

which is an analogous concept to the framework of *REW* and *TEW* used by Allen et al. (1998) to account for the influence of soil water content on crop transpiration. Since grapevine roots are present in the complete soil water reservoir (Celette et al., 2008), *FTSW* is calculated depending on the total amount of available water over the soil profile, $FTSW = TSW/TTSW$. The threshold value p_{FTSW} was set at 0.4 in the previous model based on measurements of stomatal conductance (Lebon et al., 2003). We estimated the threshold value independently using measurements of sap flow and soil water content in this study and found the same value (see Results Sections on sap flow and soil water measurements).

The second factor $k_{c,v}$ is a grapevine specific transpiration coefficient resulting from the sap flow measurements. This factor was necessary to describe the ratio of measured grapevine

transpiration (via sap flow) to calculated potential grapevine transpiration ($T_{a,v}/T_{0,v}$) in situations without soil water shortage ($k_s = 1$). The coefficient $k_{c,v}$ was set to 0.56 as explained in the Results Section. The remaining $TSW(i + 1)$ of the complete reservoir on any day derives from:

$$TSW(i + 1) = TSW(i) + P(i) - ET_a, \qquad (9)$$

where *TSW* is limited to the range $0 \leq TSW \leq TTSW$, $i \in \{1, 2, 3, \ldots, n\}$ refers to the day, $P(i)$ is the precipitation rate and:

$$ET_a = T_{a,v} + ET_{a,cc} + E_s \qquad (10)$$

is the evapotranspiration of the vineyard, where $ET_{a,cc}$ is the evapotranspiration of the cover crops.

Transpiration of cover crops

The transpiration rates of the cover crops highly depend on the total transpirable soil water of the cover crop reservoir, $TTSW_{cc}$, which itself depends on soil characteristics and the soil volume from which the cover crops can extract water. Measurements of extraction profiles of soil water before grapevine transpiration commences in spring showed that soil water was not depleted substantially beyond a depth of 1 m (**Figure 3**, difference between black line and 0% depletetion), which was therefore used as a good estimate of the root zone of cover crops for all vineyards in this study. This is in line with Celette et al. (2005) who found the same rooting depth for a vine-tall fescue intercropping system in southern France and roughly comparable to values of Allen et al. (1998) for maximum root depth of cool season grass varieties (bluegrass, ryegrass, fescue) of 0.5–1 m. This has also been confirmed by direct measurements on different species in the region of the present study (Uliarte et al., 2013). However, Celette et al. (2008) observed a maximum depth of soil water use by cover crops of 1.5 m under very dry conditions in the south of France. Based on our measurements and the assumption that a relatively higher frequency of summer rainfall at the study sites may prevent
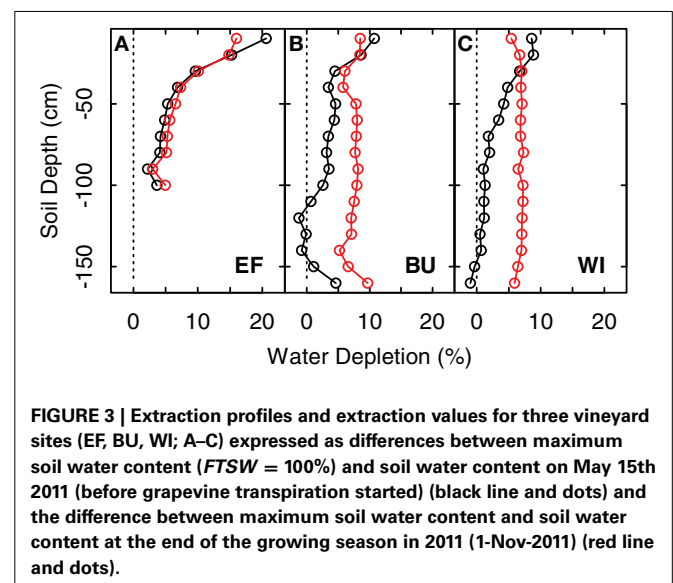

FIGURE 3 | Extraction profiles and extraction values for three vineyard sites (EF, BU, WI; A–C) expressed as differences between maximum soil water content (*FTSW* = 100%) and soil water content on May 15th 2011 (before grapevine transpiration started) (black line and dots) and the difference between maximum soil water content and soil water content at the end of the growing season in 2011 (1-Nov-2011) (red line and dots).

Table 3 | Total evaporable soil water (*TEW*) and readily evaporable soil water (*REW*) for three experimental vineyards over a soil depth of 0.15 m.

Site	TEW (mm)	REW (mm)
EF	26.9	11.0
BU	21.5	9.2
WI	21.4	9.1

the necessity of cover crop plants to exploit soil depths beyond 1 m, we calculated the $TTSW_{cc}$ of the cover crop reservoir as:

$$TTSW_{cc} = TTSW(1\,m)f_{cc},\qquad(11)$$

where $TTSW(1\,m)$ refers to the $TTSW$ of the upper 1 m soil layer and f_{cc} represents the area fraction covered by cover crop plants (Equation 5).

The daily remaining water in the cover crop reservoir is therefore computed by:

$$TSW_{cc}(i+1) = TSW_{cc}(i) + P(i)f_{cc} - ET_{a,cc}(i)$$
$$-k_{s,v,cc}\,k_{c,v}T_0,\qquad(12)$$

where $TSW_{cc}(i+1)$ is the remaining transpirable soil water kept within the range of $0 \leq TSW_{cc} \leq TTSW_{cc}$ and P is the precipitation. The last term in Equation (12) is the amount of water extracted by the grapevines from the cover crop reservoir. Based on the condition that the sum of extracted water from the sub reservoirs must equal the actual grapevine transpiration:

$$T_{a,v} = k_s k_{c,v} T_{0,v} = \left(k_{s,v,cc} + k_{s,v,r}\right)k_{c,v}T_{0,v},\qquad(13)$$

where $k_{s,v,cc}$ and $k_{s,v,r}$ are coefficients integrating the partitioning of transpiration and the feedback of water stress appearing in the cover crop ($k_{s,v,cc}$) or the remaining (non-cover crop, $k_{s,v,r}$) reservoir onto grapevine transpiration. A case differentiation considering the feedback of water stress from the complete or the individual sub reservoirs results in:

$$k_{s,v,cc} =$$
$$\begin{cases}
\frac{TSW_{cc}}{p_{FTSW}TTSW} & (k_s < 1) \\
\frac{TSW_{cc}}{TTSW} & \left(k_s = 1 \wedge \frac{TSW_{cc}}{TTSW_{cc}} \geq p_{FTSW} \wedge \frac{TSW_r}{TTSW_r} \geq p_{FTSW}\right) \\
\frac{TSW_{cc}}{p_{FTSW}TTSW} & \left(k_s = 1 \wedge \frac{TSW_{cc}}{TTSW_{cc}} < p_{FTSW} \wedge \frac{TSW_r}{TTSW_r} \geq p_{FTSW}\right) \\
1 - \frac{TSW_v}{p_{FTSW}TTSW} & \left(k_s = 1 \wedge \frac{TSW_{cc}}{TTSW_{cc}} \geq p_{FTSW} \wedge \frac{TSW_r}{TTSW_r} < p_{FTSW}\right)
\end{cases},$$
$$(14)$$

where TSW_r and $TTSW_r$ are the transpirable or the total transpirable soil water of the remaining reservoir ($TSW_r = TSW - TSW_{cc}$, $TTSW_r = TTSW - TTSW_{cc}$), respectively.

In order to estimate the contribution of cover crops to water use throughout the annual cycle we followed the system devised by Allen et al. (1998). They divided the growing season into four growth stages, an initial stage, a development stage, a mid-season stage, and a late-season stage. The start of the cover crop growing season was set at 7 days before the last occurrence of $-4°C$ (air temperature) in spring (usually beginning of March but can be substantially earlier) and the end at 7 days after the first $-4°C$ in fall/winter (usually end of November – beginning of December) (Allen et al., 1998). The start denotes the onset of the initial stage and the end date denotes the start of the late season stage. To avoid that a late spring frost occurring in April or May would artificially retard cover crop development (because of the 7 day before $-4°C$ rule), events such as these are ignored in the current

model. As evapotranspiration coefficients were not available for the native vegetation at the experimental sites, it was assumed that the cover crops are not active during the late and initial stages and that evapotranspiration only occurs as evaporation (Allen et al., 1998). This has recently been confirmed by direct measurements (Uliarte et al., 2013). During the development period cover crops grow and reach full ground cover at the end of this stage so that evapotranspiration during the mid-season follows actual evapotranspiration of the crops. The transition from evaporation to evapotranspiration was described by a ground cover coefficient f_g, which equals 0 during the late and initial stage, increases linearly from 0 to 1 during the developmental stage and equals 1 during the mid-season stage. The duration of the initial and development stage was set to 30 and 50 days, respectively, which provided good results in spring and is in agreement with local observations (Uliarte et al., 2013). This process could clearly be refined if a degree day system would be used or other plant growth models.

The evapotranspiration of cover crops ($ET_{a,cc}$) is then calculated as:

$$ET_{a,cc} = f_{cc}\left(f_g k_{s,cc}f_{R,s}ET_0 + \left(1 - f_g\right)E\right),\qquad(15)$$

where $k_{s,cc}$ is the cover crop water stress coefficient $[0–1]$, calculated in analogy to Equation (8) for $FTSW_{cc} = TSW_{cc}/TTSW_{cc}$ and a threshold value for $p_{FTSW} = 0.4$ as reported for rye grass in Allen et al. (1998).

WEATHER DATA, SURFACE RUNOFF AND EVAPOTRANSPIRATION

Weather data were provided by weather stations of the Geisenheim branch office of the Deutscher Wetterdienst (Germany's National Meteorological Service, DWD). The climate in Geisenheim can be categorized as humid temperate. Annual precipitation is 544 mm (1981–2010) (DWD) and is approximately equally distributed throughout the year (maximum in July with 60 mm, minimum in April with 35 mm). Light precipitation events (<10 mm/day) dominate and contribute 65% of total precipitation, whereas daily precipitation events larger than 20 mm contribute only 9%, respectively. Severe precipitation events are rare, the three highest amounts of daily rainfall ever recorded (1981–2010) were 75 mm (6-Jul-1999), 52 mm (13-Aug-1995), and 37 mm (9-Aug-1981). Emde (1992) showed that under these circumstances no surface runoff occurs if cover crops are used. He also demonstrated that surface runoff depended on precipitation intensities on very short time scales (minutes) and that clean cultivated vineyards soils were most vulnerable. We therefore assumed that the total amount of surface runoff was generally negligible and only rainfall amounts exceeding soil storage capacity were treated as lost, whereby no distinction was made between losses as surface runoff or deep percolation. Mean ET_0 between April 1 and September 30 is 605 mm.

For EF and BU, weather data of a station located directly in the EF plot were used which provided temperature, wind speed, precipitation, relative humidity and global solar radiation. For WI the same data with the exception of solar radiation was available from a nearby weather station (<200 m distance). For this site, radiation data from the main station at Geisenheim (3 km

distance to WI) were used which also provided the direct and diffuse fractions of global radiation.

In order to estimate these components for EF and BU, a correlation between the diffuse fraction of global radiation and a clearness index as described in Duffie and Beckman (2006) was derived from the Geisenheim data and assumed to be valid for the EF and BU sites. The correlation is outlined in Appendix C. The extraterrestrial radiation of the steep slope sites (needed to calculate the clearness index) was calculated as described by Allen et al. (2006).

Potential evapotranspiration was calculated according to Allen et al. (2005) taking into consideration that net radiation at the slope surface is altered. We therefore projected the solar radiation from the horizontal to the slopes by using the HDKR model (Reindl et al., 1990; Duffie and Beckman, 2006) with radiation partitioning (diffuse-direct) calculated by Equations (C1, C2). Longwave radiation emitted or reflected from the surrounding topography was neglected because a simple estimation based on the assumption that the slope emits as much longwave radiation to the surrounding terrain (assumed to be horizontal) as it receives, so that only the net longwave radiation part related to the view factor of the slope to the sky is considered, increased the potential evapotranspiration for EF (35° slope) by only 1%. The resulting potential evapotranspiration refers to the surface of the slope (ET_{0s}) and was re-projected to the horizontal to calculate the horizontal equivalent of evapotranspiration (to be congruent with precipitation data in the water balance calculation, Allen et al., 2006) by:

$$ET_0 = ET_{0s} / \cos \beta \qquad (16)$$

where β is the slope angle.

CLIMATE CHANGE RISK ANALYSIS

Projections of possible future water budget changes for the three vineyard sites were calculated by feeding the described water budget model with the data of a small ensemble of four Regional Climate Models (RCMs). The used RCMs were different in their downscaling approaches (statistic or dynamic) and/or in the GCM [ECHAM5/OM, Max-Planck-Institute of Meteorology (MPI-M) in Hamburg, Germany or HadCM3, Met Office Hadley Center in Exeter, UK] driving them. All projections were for the A1B emission scenario of the IPCC (Nakicenovic et al., 2000). The climate projections used were: (1) A projection for the Geisenheim weather station of the statistical model WETTREG2010 (Kreienkamp et al., 2010) driven by ECHAM5/OM, (2) two projections of the dynamic RCM CLM model (Rockel et al., 2008), one driven by ECHAM5/OM (Lautenschlager et al., 2009) and one driven by HadCM3 (Schär and Christensen, 2013), and (3) one projection of the dynamic RCM REMO/ECHAM5 (Jacob, 2005). Additionally, original daily weather data from 1955 to 2012 of the weather station in Geisenheim were available.

The grid box data of the dynamic RCMs are areal average values and cannot reproduce the variability of small scale precipitation, which is high around Geisenheim because of the local orography. In general, modelers recommend to aggregate over several grid boxes and to finally perform a spatial averaging of the results of the impact model (Kreienkamp et al., 2012). The impact model in this study needs site-specific data, a spatial averaging of the results is therefore not reasonable. To overcome this discrepancy between the spatial scale of the RCM data and the site-specific character of the study (Maraun et al., 2010), the time series of 9 grid boxes covering the area of the experimental site (one enclosing the plots and eight around) were evaluated. The comparison of the 9 time series per model revealed that they differed in the calculated absolute numbers of drought stress days (mainly caused by the different bias of mean annual precipitation compared to the observed data), but showed very similar temporal courses and change signals. Therefore, only the results of the grid box are shown which revealed the smallest difference between original and calculated number of drought stress days for the period from 1971 to 2000.

The results were meant to form the basis for a site-specific evaluation with respect to possibly increasing risks of developing a higher frequency of drought events. The evaluation of drought stress occurrence and severity is based on a relationship between $FTSW$ and vine predawn leaf water potential (ψ_{pd}) reported by several authors (Lebon et al., 2003; Pellegrino et al., 2004; Gruber and Schultz, 2005; Schultz and Lebon, 2005). Since ψ_{pd} is a widely used physiological parameter to quantify plant water deficit and since it has been related to many physiological responses in the vegetative and reproductive development of plants (Williams and Matthews, 1990) it provides the opportunity to couple soil and plant water status for the estimation of future developments. The relationship $FTSW$ to ψ_{pd} has proven to be valid over a large scale of different soil water holding capacities and for different vineyard sites (Gruber and Schultz, 2005). From the published data of these authors follows, that the common threshold value for severe stress of $\psi_{pd} = -0.6$ MPa corresponds with $FTSW$ values in the range of $0 \leq FTSW \leq 0.2$. Since it is uncertain if the water balance model can account correctly for small changes in that extreme dry range and because of the limited amount of data available from field experiments, the threshold for severe water stress was set to $FTSW \leq 0.15$. With this threshold it was possible to classify the water availability of each day with respect to its physiological consequences and to sum up the number of days in the range of severe water stress over the growing season (1 May–30 September).

MEASUREMENTS TO VALIDATE THE WATER BALANCE MODEL
Soil and plant water status measurements

Soil water status measurements were performed with a portable capacitance sensor system (Diviner 2000, Sentek, Australia) based on the frequency domain reflectometry technique. Because of differences of soil texture between sites or soil depth, the default calibration equation of the manufacturer was used to estimate soil water content. Following the $FTSW$ concept (Section The Soil Water Balance Model), soil water content was therefore expressed as differences ($TTSW$, TSW) or relative changes ($FTSW$). In each vineyard we installed at least six soil water access tubes up to a depth of maximal 1.60 m. The tubes were positioned vertically (not in the normal of the sloped surface) and thus measured horizontal equivalents of soil water content. In EF and BU not all tubes reached this depth because of thin soil layers above the

bedrock at these sites. The *TTSW* of EF and BU was estimated from the difference between maximum and minimum water content over several seasons and the entire soil/root profile (Sinclair and Ludlow, 1986). For WI, the *TTSW* was estimated from measurements of vine predawn leaf water potential (ψ_{pd}) and the established relationship between *FTSW* and ψ_{pd} previously reported (Lebon et al., 2003; Gruber and Schultz, 2005), because a minimum water content was not reached during the study period. There are also some doubts with respect to covering the entire rooting depth with a measurement technique which is limited to a depth of 1.60 m. However, this certainly covers the main water extraction reservoir of vineyard soils.

Water potential at WI was determined with a pressure chamber predawn (Soilmoisture Corp. Santa Barbara USA) on six fully expanded leaves per treatment and date.

Soil water measurements were performed in weekly time steps except during the winter months where 2–4 week intervals were chosen to monitor the refilling of the soil and to find the maximum point of replenishment. Two access tubes, equipped with a permanent measuring technique (Enviroscan, Sentek, Australia) additionally monitored the soil water content at five measuring depths in EF to have more information with a higher temporal resolution.

Sap flow measurements

Sap flow was measured from June until the end of the growing season on six grapevines in each vineyard with custom made Granier-type sap flow sensors. This measurement technique has been adopted to grapevines and validated by Braun and Schmid (1999b). Trunk cross sections were roughly elliptical shaped, the length of the mean minor and major axis were 22/27 mm (EF), 33/41 mm (BU), and 33/39 mm (WI). We used probes with a length of 18 mm for BU and WI, and 14 mm for EF. The probes were inserted into the trunk between 10 cm above the graft union and 10 cm below the pruning zone with a distance between the probes of approximately 15 cm on trunk segments which were free of wounds. The segments were insulated with foam material and aluminum foil in the area of the installed probes. The constant heating power was adjusted to 0.20 W for BU and WI and to 0.16 W for EF, to ensure a constant heat output per unit probe length in the range of previously reported applications (Lu et al., 2004). The original calibration equation of Granier (1985) was used as Braun and Schmid (1999b) found this equation to be valid for grapevines over a wide range of sap flux densities. Nocturnal sap flow was not considered, because an analysis of potential evapotranspiration on 30-min temporal resolution showed that the occurrence of a substantial evaporative demand of the atmosphere during nights were rare events for the climate conditions of the study area.

Porosity measurements

The porosity of the canopy is an important parameter for the estimation of the distribution of radiation within the canopy and consequently for the estimation of canopy water use. We therefore estimated canopy porosity of the experimental sites every year a few weeks before harvest by taking digital *RGB* pictures of the vine stocks with fully developed foliage (width 40–45 cm,

perpendicular to the vertical foliage walls) which were used for sap flow measurements.

RGB pictures were also used to validate Equation (A4), which describes the relationship between the porosity and the travel distance of the radiation in the foliage. Therefore, pictures of a square of 70 cm (serving as an image detail of a vertical foliage wall) were taken from a distance of 5 m at different viewing angles along a horizontal semicircle resulting in different distances the light had to travel across the foliage.

A white sheet was always used to provide a background behind the vine row. We classified each pixel of the pictures by using chromatic coordinates (Sonnentag et al., 2012) and appropriate thresholds assessed by kernel density estimation and were able to calculate the porosity values. The R package biOps (Bordese and Alini, 2012) was used for image processing.

RESULTS

RADIATION PARTITIONING

A comparison between the original radiation model of Riou et al. (1989) and the new Monte Carlo approach showed very similar results for the amount of radiation received by the grapevine canopy for a porosity level of 0.25 which would be indicative of average to vigorous growing conditions (**Figures 4A,C**). For situations with lower vigor (porosity = 0.5) the simulated R_v of the Riou et al. (1989) model is higher than the Monte Carlo simulation (**Figures 4B,D**). That is likely due to the fact that the Riou et al. (1989) model treats the horizontal faces as opaque which artificially increases radiation absorption specifically at small ratios of row distance to canopy width.
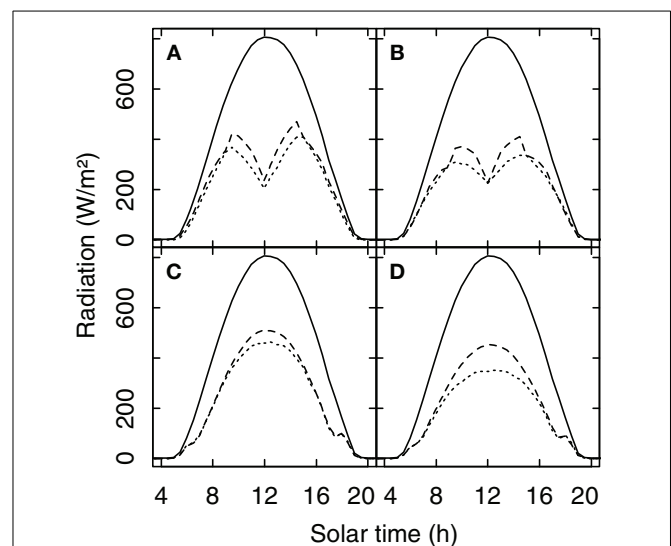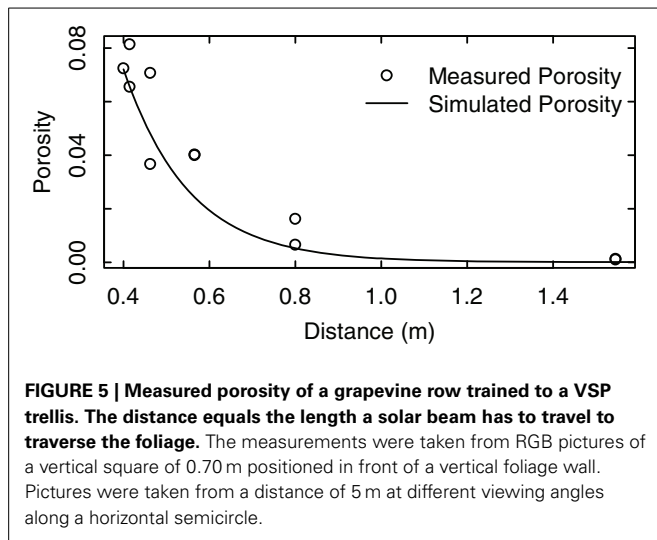

FIGURE 4 | Global radiation and the simulated amount of radiation received by a row oriented grapevine canopy (R_v) (row distance 1.60 m, width = 0.40 m, height 1.10 m, 0.80 m above ground). For North-South **(A,B)** and for South-East **(C,D)** row orientation and for porosity levels of the foliage of 0.25 **(A,C)** and 0.5 **(B,D)**. Solid lines show global radiation for a clear sky day in Geisenheim, Germany (20-Aug-2011), the dashed lines show R_v simulated with the model of Riou et al. (1989), and the dotted line R_v calculated with a Monte Carlo simulation.

FIGURE 5 | Measured porosity of a grapevine row trained to a VSP trellis. The distance equals the length a solar beam has to travel to traverse the foliage. The measurements were taken from RGB pictures of a vertical square of 0.70 m positioned in front of a vertical foliage wall. Pictures were taken from a distance of 5 m at different viewing angles along a horizontal semicircle.

MEASUREMENT OF POROSITY FOR DIFFERENT LIGHT TRAVEL DISTANCES INSIDE THE FOLIAGE

We compared the measured porosity values with the calculated values in their dependence on light travel distances within the canopy (Equation A4, **Figure 5**). The results showed that the decrease of porosity with the increase of light travel distance could be well approximated by Equation (A4). Refinements of this approach may have to take into account measured leaf area distributions or inhomogeneous leaf angle dispersion inside the canopy due to different canopy forms and shoot orientation.

SITE CHARACTERISTICS

Differences in $TTSW$ of the plots caused differences in grapevine transpiration rates as measured by sap flow. These differences (expressed as relative transpiration, $T_{a,v}/T_{0,v}$) were more pronounced in 2012 than in 2011 (**Figure 6**). In 2011 the ratio of $T_{a,v}/T_{0,v}$ of EF (smallest $TTSW$) was significantly lower (tested with a pair-wise comparison ($p < 0.1$) of an analysis of variance of the relative transpiration rates of 6 vines per vineyard for each day) in the first half of July compared to BU and WI, which can be explained by a short period with low rainfall at the end of June and a decrease in soil water content (see **Figures 9A,D**). High rainfall amounts during August and September 2011 resulted in an increase of soil water content in all vineyards (see **Figure 9**) and in an increase of relative transpiration rates for EF and BU (**Figure 6A**). During that period the mean values of $T_{a,v}/T_{0,v}$ for WI were lower compared to EF and BU, but significant differences appeared only on a few days. In 2012 the ratio of $T_{a,v}/T_{0,v}$ was highest for BU during the first half of July (significant, **Figure 6B**). Thereafter, $T_{a,v}/T_{0,v}$ declined first in EF (smallest $TTSW$), followed by BU, probably caused by a decrease in soil water content (cf. **Figure 9**). In WI (high $TTSW$) the ratio remained almost constant during both growing seasons and was significantly higher than EF and BU during August and September 2012, except for brief recoveries of transpiration rates in EF and BU caused by intermittent precipitation events (**Figure 6B**).
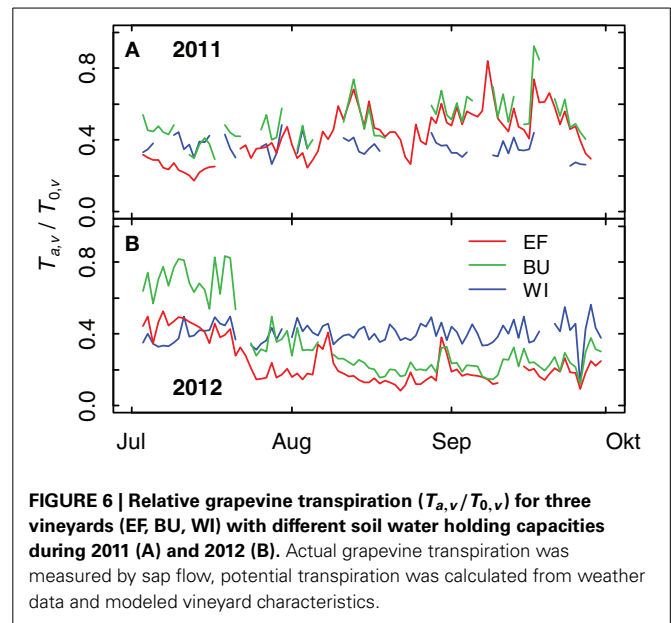

FIGURE 6 | Relative grapevine transpiration ($T_{a,v}/T_{0,v}$) for three vineyards (EF, BU, WI) with different soil water holding capacities during 2011 (A) and 2012 (B). Actual grapevine transpiration was measured by sap flow, potential transpiration was calculated from weather data and modeled vineyard characteristics.

Table 4 | Ratios of actual to potential transpiration of grapevines for three different vineyards during periods well supplied with water.

Vineyard	$k_{c,v}$
EF	0.57 ± 0.14
BU	0.68 ± 0.32
WI	0.42 ± 0.22
Mean	0.56 ± 0.32

Error values represent means of the confidence intervals ($p < 0.05$) of daily sap flow data of six vines per vineyard.
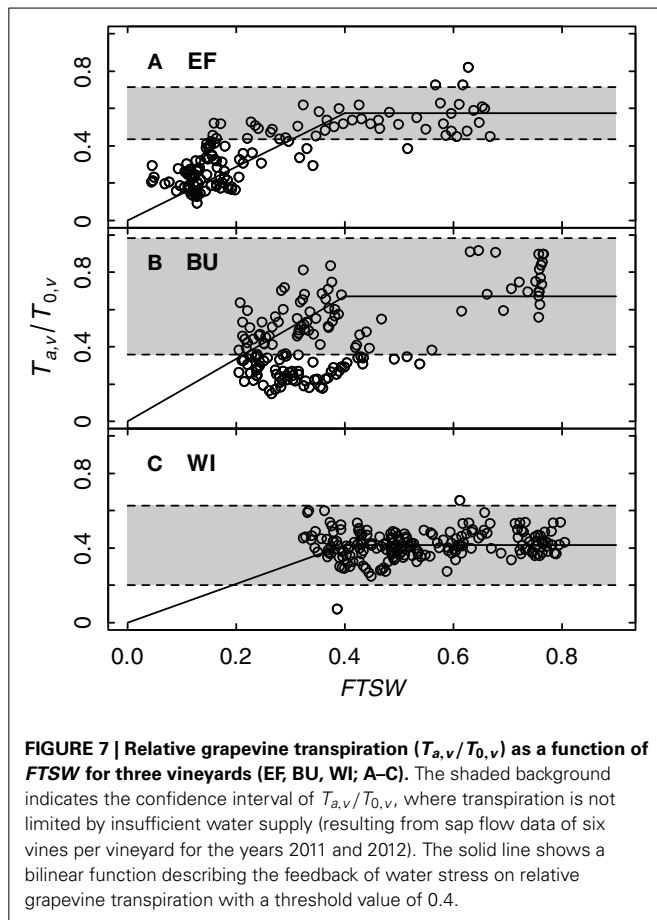
EVALUATION OF MODEL PARAMETERS

Grapevine transpiration coefficient $k_{c,v}$

The transpiration coefficient $k_{c,v}$ in Equation (7) represents the ratio of $T_{a,v}/T_{0,v}$ under conditions where soil water content does not limit transpiration (i.e., $k_s = 1$). It had to be introduced because measured transpiration rates (sap flow) never matched calculated potential transpiration rates despite the fact that previous versions of the model adequately described soil water content dynamics (Lebon et al., 2003; Pellegrino et al., 2004), yet individual components [vine transpiration and soil (+cover crop)] had never been individually validated. We therefore determined the $k_{c,v}$ value for each of the three vineyards by calculating the mean of the daily ratios of measured sap flow ($T_{a,v}$) to calculated potential grapevine transpiration ($T_{0,v}$) for periods where drought stress was absent ($FTSW > 0.4$). The $k_{c,v}$ value then used in the model represented the mean of the individual $k_{c,v}$ values (**Table 4**).

Influence of soil water availability on grapevine transpiration

Sap flow and soil water content data were used to validate if the bilinear function of Equation (8) is capable to describe the dependence of transpiration, as $T_{a,v}/T_{0,v}$, on soil water availability ($FTSW$) and to assess if the selected threshold value $p_{FTSW} =$

FIGURE 7 | Relative grapevine transpiration ($T_{a,v}/T_{0,v}$) as a function of FTSW for three vineyards (EF, BU, WI; A–C). The shaded background indicates the confidence interval of $T_{a,v}/T_{0,v}$, where transpiration is not limited by insufficient water supply (resulting from sap flow data of six vines per vineyard for the years 2011 and 2012). The solid line shows a bilinear function describing the feedback of water stress on relative grapevine transpiration with a threshold value of 0.4.

FIGURE 8 | Relative grapevine transpiration ($T_{a,v}/T_{0,v}$) for three vineyards (EF, BU, WI; A–C) as a function of potential evapotranspiration at the vineyard surface (ET_{0s}, including the slope) for situations without water stress. $T_{a,v}$ was based on sap flow data of six vines per vineyard from the years 2011 and 2012.

0.4 (Lebon et al., 2003), which differentiates non-water limiting and water limiting stages accurately reflects the situations at our experimental sites.

To get more data points on FTSW, which was determined weekly, data for each day were estimated by linear approximation between successive measurements. **Figure 7** shows the ratio of $T_{a,v}/T_{0,v}$ as a function of FTSW for the three experimental vineyards. Following Equation (7) the ratio of $T_{a,v}/T_{0,v}$ equals the product of the transpiration coefficient $k_{c,v}$ and the water stress coefficient k_s. Since the transpiration coefficient is constant (**Table 4**), a deviation from this value indicates the onset of water deficit caused by a decrease of k_s to values < 1. The FTSW value at which this happens denotes the threshold p_{FTSW}. This value was estimated in our case from FTSW values where $T_{a,v}/T_{0,v}$ data decreased below the lower limit of the confidence interval of $k_{c,v}$ (**Table 4**) suggesting the onset of water deficit. **Figure 7** shows, that for all three vineyard sites a value of $p_{FTSW} = 0.4$ described reasonably well the point at which this deviation occurred confirming the Lebon et al. (2003) approach (determined by measurements of stomatal conductance) with sap flow data.

Influence of environmental conditions on grapevine transpiration

Stomatal conductance of grapevines can be sensitive to vapor pressure deficit (VPD). Since $T_{a,v}/T_{0,v}$ can also be taken as
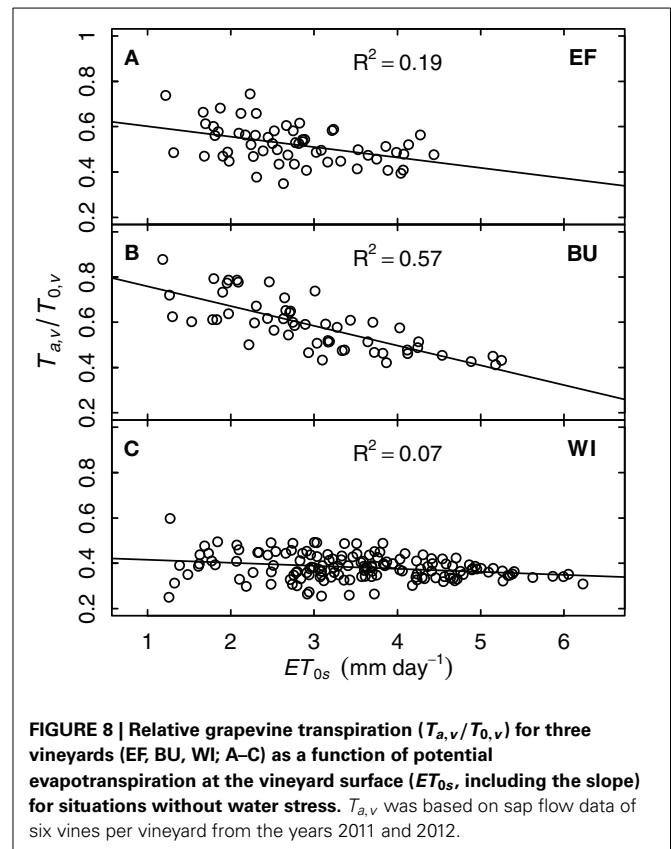
an indicator of whole-plant conductivity for water, one could expect a decrease of $T_{a,v}/T_{0,v}$ with increasing VPD. Since VPD effects have a diurnal pattern and model and measurements were on daily time-steps, we investigated the relationship between $T_{a,v}/T_{0,v}$ and ET_0, whereby ET_0 integrates more environmental variables to express the evaporative demand the plants are exposed to. To exclude the influence of soil water shortage, only data during periods without drought stress (FTSW > 0.4, $k_s = 1$) were examined. The strongest correlation was found between $T_{a,v}/T_{0,v}$ and ET_{0s} [i.e., for BU: $R^2 = 0.57$, $T_{a,v}/T_{0,v} = f(ET_{0s})$] but this was not consistent for all plots (**Figure 8**). Only the steep slope sites EF and BU showed a decrease in relative transpiration rate with increasing evaporative demand, whereas WI exhibited only a small response.

VALIDATION OF THE WATER BALANCE MODEL
Simulations of the soil water budget
Simulations with the water budget model over two years showed that the model traced measured FTSW values of the three vineyards well and was able to mimic the dynamics in soil water content during different seasons including soil recharge in winter and the transition from evaporation to evapotranspiration due to cover crop development in spring (**Figures 9A–C**). Changes in FTSW in EF in summer resulted mainly from changes in the upper soil layer (0–30 cm, data not shown). Precipitation caused more rapid responses of FTSW in EF compared to BU and WI because of the lower TTSW. This can also be seen from the

FIGURE 9 | Simulated and measured seasonal time courses for precipitation (D) and the fraction of transpirable soil water (FTSW) over the rooting profile for three vineyards (EF, BU, WI) and the years 2011 and 2012 (A–C). Solid lines represent simulated FTSW, symbols represent measured FTSW (means of at least 5 access tubes per vineyard, error bars refer to confidence intervals, $p < 0.05$). The dotted line in **(A)** represents one continuously measuring access tube in EF.

course of daily data of one continuous measuring tube in EF (**Figure 9A**). FTSW in WI was slightly underestimated in both years in spring. In general the model was able to operate on small time scales and was capable to cover the effects of canopy development and different management practices on whole vineyard water consumption.

Simulation of grapevine transpiration

Figure 10 shows simulated grapevine transpiration rates using a uniform transpiration coefficient ($k_{c,v} = 0.56$, **Table 4**). A comparison between measured and simulated sap flow showed that the model could reproduce sap flow within the measured confidence intervals for most parts of the seasons, sites and years. A distinct overestimation was calculated for BU in 2012 (**Figure 10D**). This overestimation between mid July and the end of August was 18 mm as compared to the measured mean values, yet it was not reflected in the soil water budget (**Figure 9B**). The nearly consistent and small overestimation of transpiration for WI (**Figures 10E,F**) was related to the used uniform grapevine transpiration coefficient in the simulations, which was slightly higher than the site specific one. In contrast to EF and BU no impact of soil water shortage on grapevine transpiration was detectable for WI (**Figures 10E,F**) over both growing seasons.

Sensitivity analysis

Sensitivity analyses of previous versions of the model or parts thereof were already conducted for several parameters (Trambouze and Voltz, 2001; Lebon et al., 2003; Celette et al., 2010). Two new model aspects were analyzed here. First, the adaptation to steep slopes was evaluated to quantify the impact of the degree of slope and slope orientation on potential evapotranspiration and, second, the introduction of the grapevine transpiration coefficient $k_{c,v}$ was assessed for its impact on water use.

Annual ET_0 increased by about 25% between an inclination angle of 0°–30° with a south orientation (**Table 5**) indicating that sloped areas face a substantially higher risk of developing water deficit independent of soil type and depth. This effect has two reasons, one is that the surface receives more solar energy to evaporate water and the second is that the evaporating surface per horizontal equivalent increases.

The introduced grapevine transpiration coefficient, $k_{c,v}$, was set to 0.56 as a result of experimental data from the three vineyard sites. Consequently the model calculated only about half of the grapevine transpiration rates compared to the approaches of Lebon et al. (2003) and Celette et al. (2010) who did not use a coefficient and did not try to validate grapevine transpiration against an independent measurement method such as sap flow.
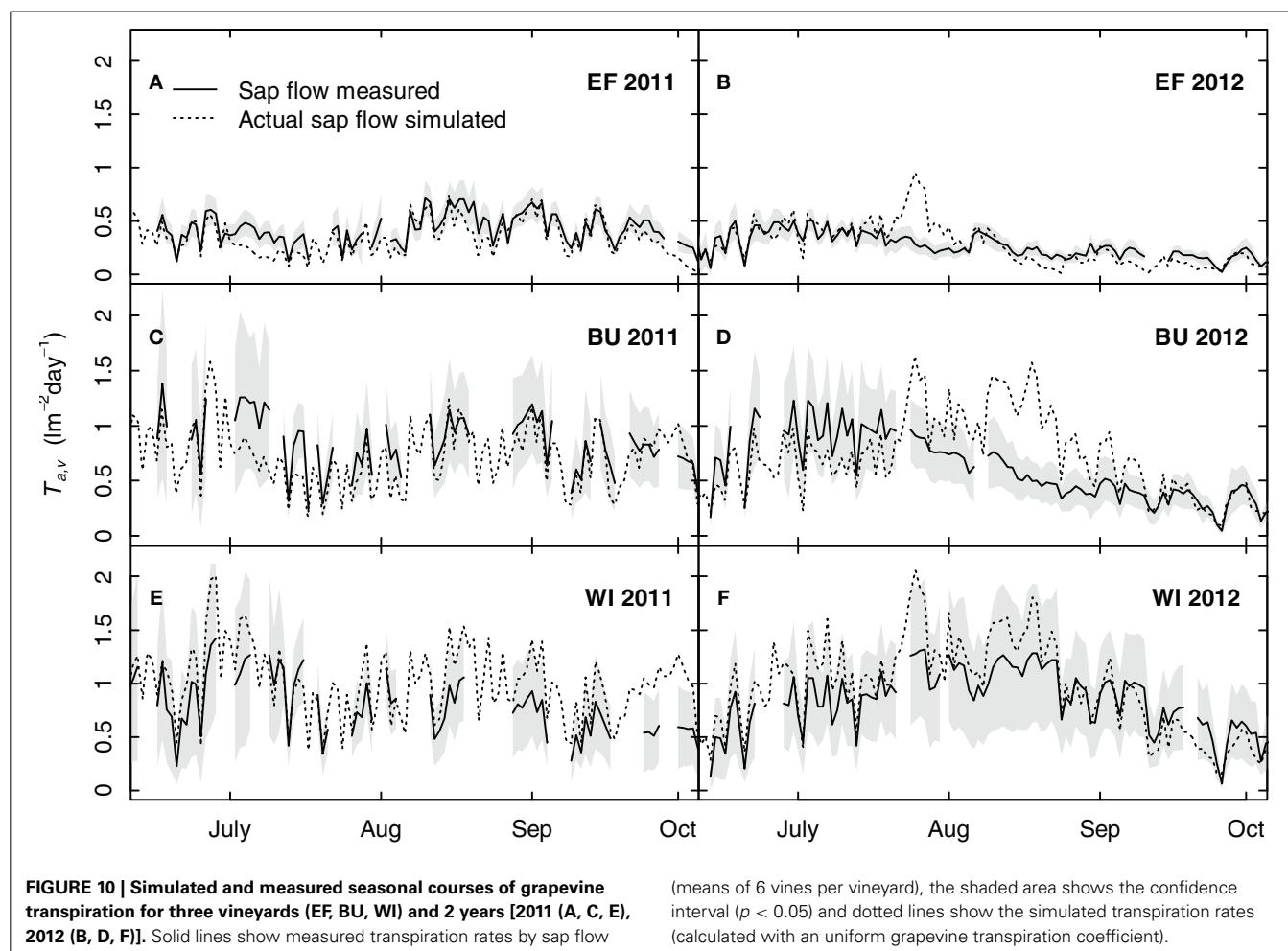
FIGURE 10 | Simulated and measured seasonal courses of grapevine transpiration for three vineyards (EF, BU, WI) and 2 years [2011 (A, C, E), 2012 (B, D, F)]. Solid lines show measured transpiration rates by sap flow (means of 6 vines per vineyard), the shaded area shows the confidence interval ($p < 0.05$) and dotted lines show the simulated transpiration rates (calculated with an uniform grapevine transpiration coefficient).

Table 5 | Calculation of annual sums of the horizontal equivalent of potential evapotranspiration, ET_0, for a slope (50° latitude North, Geisenheim) with different inclination angles (in ° and % slope) and aspects using weather data of 2012 (Geisenheim weather station, DWD).

Aspect Inclination	ET_0 (mm/year)				
	S	SW/SE	W/E	NW/NE	N
0° (0%)	800	800	800	800	800
5° (9%)	823	818	802	786	779
10° (17%)	850	840	811	777	762
15° (25%)	882	868	825	771	748
20° (33%)	919	902	846	771	737
25° (41%)	961	942	874	776	731
30° (48%)	1012	991	910	789	729

Running the model with a $k_{c,v}$ value of 1 led to an underestimation of soil water content. The simulated mean $FTSW$ (May–September) was reduced by 22 and 20% for EF, 32 and 28% for BU, and by 29% for WI for the years 2011 and 2012, respectively. Thus, the underestimation increased with increasing ratio of

grapevine transpiration to actual evapotranspiration. This ratio is low in EF because of wide row spacing and reduced grapevine transpiration rates as a consequence of frequent water shortage, but high in WI, where grapevines did not suffer water shortage. Compared to the large differences caused by different $k_{c,v}$ values, the effect of deviations of calculated to measured grapevine transpiration rates (**Figure 10**) on vineyard soil water content was low (see **Figure 9**). This is probably related to the interactions between vine and cover crop water use, respectively, soil evaporation which had compensatory effects on the development of $FTSW$.

COMPARISON OF DIFFERENT SIMULATED EVAPOTRANSPIRATION FLUXES

A comparison of the different simulated water fluxes of the vineyards for the year 2012 showed the effects of different row distances (**Table 1**) and soil management practices (inter-rows with cover crops in EF and WI, alternating bare soil and cover crop in BU, **Table 1**) on soil water budget (**Figure 11**). The fraction of grapevine water consumption of the vineyards actual evapotranspiration was 18% for EF (2.50 m row distance) and 38% and 45% for BU und WI (1.60 m row distance), respectively, during the period with fully developed canopy. Relative

FIGURE 11 | Simulation examples for the transpiration of grapevines, the evapotranspiration of cover crops and the evaporation of bare soil for three vineyards for 2012 (A–C). The cover crop development is divided into growing stages. It is assumed that the cover crops are destroyed by severe frost and recover during spring. **(D)** Potential evapotranspiration for site EF and WI. **(E)** Simulated relative evapotranspiration of the vineyards.

evapotranspiration (expressed as ET_a/ET_0) was maximum during the winter months (**Figure 11E**) due to wet soil and humid weather, but declined rapidly in late winter/early spring in all plots (**Figures 11A–C,E**), during the transition of mainly cover crop to mainly bare soil and back. Absolute values for the evapotranspiration of cover crops in WI were in the range of 1–4 mm/day after recovery in spring and between 1 and 2 mm/day from June to the end of August associated with a developed grapevine canopy and high ET_0 values. Values for EF were slightly higher during that period (0.5–3 mm/day), because of the wider row spacing. Evaporation from bare soil was over the year the most dominant water loss process for BU. Only when grapevines had developed a full canopy, transpiration did exceed soil evaporation.

ASSESSMENT OF CLIMATE CHANGE IMPACT ON FUTURE VINEYARD WATER BUDGET

Model runs with original (1955–2012) and climate projection data incorporating specific site characteristics were performed for EF, BU, and WI. The analyses revealed that the number of

days with drought stress ($FTSW < 0.15$; closely equivalent to $\psi_{pd} = -0.6$ MPa) between 1 May and 30 Sep. (152 days) has already increased significantly ($p < 0.05$; Mann–Kendall trend test; McLeod, 2011) in the past for the sites EF and BU but not for WI (**Figure 12**). For WI 64% of the years had almost no days with drought stress and a substantial number of stress days (>20 days) occurred during 26% of the years (**Figure 12C**).

Climate models differed substantially in their projections of absolute numbers of drought occurrence both for the past and for the future. As a result of model specific biases compared to the Geisenheim weather station, ECHAM5-REMO, ECHAM5-CLM, and HADCM3-CLM underestimated and WETTREG2010 overestimated the frequency of drought days for the past (**Figures 12A–C**). The strongest increase in the number of drought stress days was projected by WETTREG2010, the statistical model. This model provides ten individual runs per climate scenario analysis which are all plotted in **Figure 12** and which show a large variability. Contrary to the other models, WETTREG2010 already overestimated the developments in the past and this overestimation of drought days was more pronounced for the dry sites (**Figures 12A–C**). In general all models proposed a significant increase in the frequency of the occurrence of drought stress days as compared to simulated mid-last century numbers. The range of this increase was comparable between the dynamic models (REMO, CLM) and all three sites. Irrespective of the type of model used, the increase in the number of days with drought stress was projected to be strongest around the middle of the century and to become less intense at the end of the century. To further understand risks associated with these projections a more in-depth analysis of the year to year variability would be necessary.

DISCUSSION

The revised and amended model to simulate vineyard water balance is an example for a "sandwich" approach to couple a canopy-based plant water relations model to soil characteristics and climate projections in order to provide a risk assessment for different vineyard sites. The adaptation of the radiation module using a Monte Carlo numerical simulation overcame one of the shortcomings of the original approach of Riou et al. (1989) to treat all horizontal faces of the canopy as opaque which overestimated radiation interception and thus water consumption especially in closely spaced vineyards (Lebon et al., 2003; **Figure 4**). With this adaptation a new and improved estimation of canopy porosity, $p(x)$, was introduced and experimentally verified which made porosity dependent on the distance a solar beam travels inside of the canopy. This however, will still need adaptation to different canopy forms where leaf area density may be lower than in the VSP systems used in the vineyards of this study, and where thus beam attenuation may follow a different pattern (Poni et al., 1996). Additionally, under prolonged and severe water deficit, leaf drop will increase $p(x)$, and thus reduce transpiration. Nevertheless, sensitivity analyses of previous model versions showed, that a 10% change in $p(x)$ only decreased water loss by 1.6% (Trambouze and Voltz, 2001).

At the current state the model does not include stomatal responses to elevated CO_2 concentrations, which would be

FIGURE 12 | Smoothed 30-year running means of the yearly sum of days with drought stress for three different vineyards (EF, BU, WI; A–C), calculated using a soil water balance model, original weather data (from Geisenheim) and projections of regional climate models. Drought days were defined as days when predawn water potential decreased to −0.6 MPa.
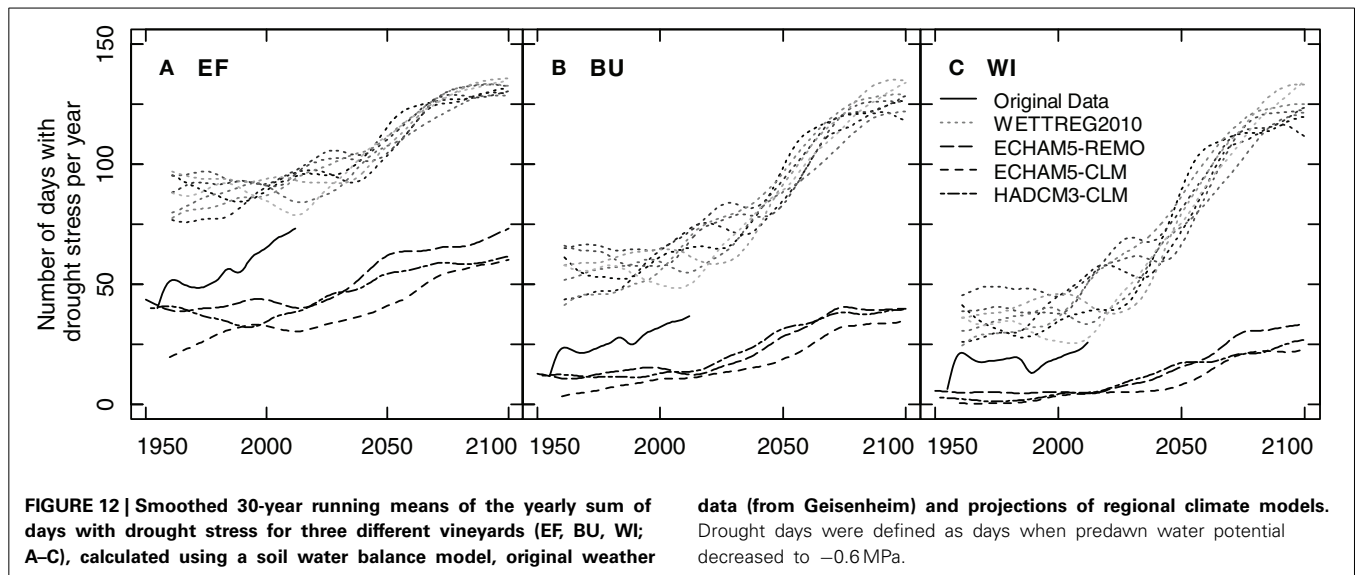
important for a more precise impact estimation of future climates on vineyard water relations (Yin, 2013). A general survey of the response of stomatal aperture to an increase to 560 μmol mol^{-1} in CO_2-concentration (from 380 μmol mol^{-1}, Ainsworth and Rogers, 2007) across a variety of plant species showed an approximate reduction of about 20%. Experiments on grapevines have confirmed this value (Schultz and Stoll, 2010) but a reduction in stomatal conductance and possibly the threshold value of FTSW to water deficit do not consider possible changes in VPD due to climate change. Recent results from models including the physiological impact of CO_2 on plants (i.e., reduced stomatal conductance) suggest that rising CO_2 will increase the temperature driven water evaporation from oceans resulting in increased absolute water vapor content of the air. However, the decrease in evapotranspiration over land (because stomatal conductance is decreasing) would still lead to an overall decrease in relative humidity and an increased evaporative demand (Boucher et al., 2009).

Since many vineyard areas in Europe are on slopes with shallow soils more prone to water deficit, the model was adapted to account for the changed radiation budget of sloped vineyards with its consequences on vineyard water relations. A recent study on possible effects of climate change on regional vineyard water budgets did not include inclined surfaces and assumed bare soils (Pieri and Lebon, 2014) which is sufficient for a rough estimate but does not account for large intra-regional variations.

One of the further goals is a scale-up approach to estimate the water budget of entire wine regions based on existing maps of soil water content (i.e., Löhnertz et al., 2004). So far mostly meteorological approaches have been used in studies of climate change effects on Viticulture, where changes in regional water budgets have been either predicted based on extremely rough soil water data with very low spatial resolution (i.e., Malheiro et al., 2010 based on Tonietto and Carbonneau, 2004), used fixed SWC values (Pieri, 2012; Pieri and Lebon, 2014) for all regions, or based their estimations on sub models creating water stress indices which have never been proved to be applicable to vineyard situations

(Hannah et al., 2013 based on Alcamo et al., 2003 and Pfister et al., 2009).

We tried to validate the calculated water fluxes through vine canopies by direct measurements of sap flow. However, the model only correlated with sap flow data when a grapevine transpiration coefficient $k_{c,v}$ of 0.56 was introduced. Only then was the seasonal dynamic of FTSW accurately simulated. In all previous cases where the original (Lebon et al., 2003) and adapted versions of the model (i.e., Pellegrino et al., 2005; Celette et al., 2010) were compared to measured soil water content (not sap flow), the correlations were excellent without a transpiration coefficient, whether the soil was bare (Lebon et al., 2003; Pellegrino et al., 2005) or had different degrees and/or different types of cover crops (Celette et al., 2010). Explanations for these differences might be that Lebon et al. (2003) used a very low value for the REW in their bare soil sub model, possibly indicating an underestimation of bare soil evaporation compensated by an overestimation of grapevine transpiration and Pellegrino et al. (2005) as well as Celette et al. (2010) did their field trials in vineyards with wide row spacings (>2.30 m), where the overall fraction of grapevine transpiration on total evapotranspiration is comparably small (**Figure 6**). Additionally, as compared to Mediterranean type climates (Pellegrino et al., 2005; Celette et al., 2010) vineyard cover crops in temperate, summer rainfall areas have a larger contribution to whole vineyard evapotranspiration due to less frequent water deficits (Uliarte et al., 2013).

Partitioning of water fluxes between soil, cover crop and grapevines showed that different components dominated during different parts of the season and that soil management had a large impact on flux partitioning. Simulated evaporation levels from soil and transpiration from cover crops were in agreement with direct measurements conducted in the same area (Uliarte et al., 2013) and agreed with those by Celette et al. (2010) for a vineyard with a permanent intercrop and the same row distance when water was not limiting. The rapid decline of bare soil evaporation within a few days after precipitation events simulated by the

model was also observed by Uliarte et al. (2013) under similar weather conditions.

The low values in sap flow were surprising but are roughly in line with previous measurements on the same variety (Schmid, 1997). The technique used to measure sap flow was first adopted for grapevines by Braun and Schmid (1999b) and was validated by independent methods at the time (i.e., weighing of large pots). One important restriction of that method, as with any sap flow estimation, is that severe pruning wounds at the trunk can cause large inhomogeneities of the water flux density over the cross sectional area of the trunk (Braun and Schmid, 1999a). This could lead to an overestimation of sap flow if the heating probe is within areas of high flux densities and to an underestimation if the heating probe is located near or in necrotic areas (Schmid, 1997). Since the likelihood of uneven flux density increases with vine age, this may have been part of the reason for the larger confidence intervals of sap flow data for BU and WI, the two older vineyards.

One of the advantages of the formulation of potential grapevine transpiration $T_{0,v}$ in form of Equation (1) is, that different radiation distributions caused by differences in vineyard geometries and vine training systems are considered and, therefore, ratios for $T_{a,v}/T_{0,v}$ can be directly compared to values from the literature where sap flow has also been estimated. Riou et al. (1994) and Trambouze and Voltz (2001) found ratios which would have been equivalent to $k_{c,v}$ values of 1.25 and 1.12 for a typical vineyard in Bordeaux and 18-year old Shiraz vines in Southern France, respectively. In both cases, the stem heat balance method was used to measure $T_{a,v}$ as described by Valancogne and Nasr (1993). However, Braun and Schmid (1999a) reported that the heat balance system might overestimate actual sap flow by 50–100% at high flow rates in older grapevines. Using heat pulse sensors, Yunusa et al. (2004) found a ratio of T_a/ET_0 of 0.17 for non-stressed drip irrigated Sultana vines in Australia. Considering the fractions of shortwave radiation intercepted by the vine canopy for two periods during the growing season in their study resulted in $k_{c,v}$ values of 0.38 and 0.46 which are in the range of our findings. Nevertheless, with the same technique Intrigliolo et al. (2009) found a ratio of T_a/ET_0 of 0.49 and a $k_{c,v}$ of 1.6 for 2-year old Riesling vines when sap flow readings were recalibrated with canopy gas exchange measurements (which roughly doubled the calculated transpiration rates). Since sap flow values were similar for all experimental sites under conditions without water deficit in our study and clearly responded to deficit situations, they reflected actual vine responses despite uncertainties with respect to their absolute quantitative accuracy.

One additional aspect of these discrepancies is the large spectrum of stomatal sensitivity to alterations of environmental variables between cultivars and cultivar/rootstock combinations for grapevines (Schultz, 2003; Soar et al., 2006; Williams and Baeza, 2007; Poni et al., 2009; Collins et al., 2010). It is therefore unlikely that a universally valid $k_{c,v}$ exists. Even though $k_{c,v}$ values were similar for the three sites in this study, there were notable differences in the response of $T_{a,v}/T_{0,v}$ to increasing evaporative demand (**Figure 8**). Although only periods were considered where *a priori* soil water was not limiting (*FTSW* > 0.4), the reduction in $T_{a,v}/T_{0,v}$ with increasing ET_0 for the

two drier vineyard sites might have been a response to vapor pressure deficit, *VPD*. High *VPD* in the atmosphere can cause a decline in stomatal conductance in grapevines to control water loss (Soar et al., 2006; Poni et al., 2009; Rogiers et al., 2011) and soil water deficit can exacerbate this response (Soar et al., 2006; Pou et al., 2008; Rogiers et al., 2011; Zhang et al., 2012). Whether this reaction is driven by some factors residing close to the stomatal pores (Peak and Mott, 2011) or depends on hormonal (Soar et al., 2006; Rogiers et al., 2011) or hydraulic long distance signaling (Christmann et al., 2013) inducing stomatal closure is unknown. However, since the driest sites experienced the strongest reduction in the transpiration to evapotranspiration ratio with increasing evaporative demand, it is likely that some form of root-to-shoot signaling was involved. This may have been related to parts of the grapevine root system being located in dry soil, due to inhomogeneous distribution of soil water which has been shown to induce stomatal closure and modulate the response to *VPD* (Poni et al., 2009). Both hormonal and hydraulic limitations have been incorporated into a conceptual water consumption model responsive to *VPD* (Tardieu and Simonneau, 1998) but it seems difficult to fit this into the current framework of the grapevine model although approaches relating the *VPD* response to soil water content parameters similar to the *FTSW* concept may make this possible (Oren et al., 1999; Rogiers et al., 2011). Since ET_0 increases substantially with the degree of slope (**Table 5**), it is necessary to incorporate these aspects into a more widely applicable model in the future in order to evaluate the propensity of drought risk on a regional scale.

Lebon et al. (2003) also discussed the roles of interception water and surface run-off as possible sources for errors. Run-off is usually negligible for soils with cover crops and small individual precipitation rates, which are dominant in the experimental area (Emde, 1992). To account for the direct interception of water the approach to introduce a skin layer in the bare soil model of Allen (2011) from which water evaporates after precipitation events was applied but that generated only small reductions in soil water content, could not be resolved by the accuracy of the soil water data and was limited to situations where rain fell on dry soils.

As a further adaptation to our climatic conditions, growing stages were introduced to describe the development of the cover crops during the year (Allen et al., 1998). The approach of Celette et al. (2010) to model cover crop development by changes in LAI, was not suitable for our conditions, because the model approach they used (Cros et al., 2003; Duru et al., 2009) did not take into account the destroying impact of frost in cold winters. Calculations assuming that the cover crops are active throughout the year, led to substantial overestimations of vineyard transpiration rates in spring (data not shown).

Additional errors might be introduced by subsurface lateral water flows, because the model does consider vertical flows only. By the occurrence of relief precipitation the variability of rainfall distribution is generally high in regions with slopes. For instance, only a few kilometers north of the Rheingau grape growing region toward the Taunus mountain range the mean annual rainfall is about 250 mm higher. Some but not all soil water access tubes showed an increase of soil water content at certain times in particular layers, which might have been the result of water

moving laterally downslope. However, this only occurred during the replenishment stage in winter or spring but not during summer and it cannot be distinguished between vertical or lateral water movements. Also, the increase was restricted to distinct layers and after saturation of the layer the lateral water flow is likely to be through flow. Therefore, the overall error is assumed to be small, but might be an explanation of the underestimation of soil water content by the model for WI in spring.

FTSW is strongly correlated with ψ_{pd} (Lebon et al., 2003; Pellegrino et al., 2004; Schultz and Lebon, 2005) which could also be confirmed in the present study (data not shown). This correlation allows the calculation of a water deficit indicator under any environmental situation for scenarios of future climate projections. The approach is appealing since it can serve in several ways to use the model as a tool in climate change research. First, ψ_{pd} can not only be related to physiological processes such as photosynthesis and stomatal conductance but also to the synthesis of grape compositional factors such as anthocyanins and tannins (i.e., Ojeda et al., 2001, 2002). Second, with databases of soil properties, water storage capacities, and rooting depths, available for certain wine regions (Löhnertz et al., 2004), it would be possible to estimate vineyard soil water balance on a regional scale for the next decades. Third, such a model could then be used to identify adaptation possibilities, such as changes in canopy or vineyard characteristics (van Leeuwen et al., 2010), varieties (Schultz and Stoll, 2010) or to recommend/not recommend the installation of irrigation systems (Gaudin and Gary, 2012).

Whereas the dynamic climate models proposed a moderate increase in the number of drought days for all vineyard sites (**Figure 12**), the statistical model WETTREG2010 projected a much larger effect. This is probably due to the fact, that WETTREG2010 not only projects an increase in temperature and a decrease in precipitation rate, but also a strong increase in global radiation (Kreienkamp, CEC-Potsdam, personal communication) leading to more frequent hot and dry weather conditions during the second half of the century. Nevertheless, the dynamic models CLM and REMO have been shown to be sensitive to the "windward- lee effect," i.e., an under– or overestimation of precipitation at mountain ranges demonstrated for the South of Germany, thus may have actually underestimated the number of drought days for the Rheingau region (Warrach-Sagi et al., 2013). We have observed such a bias in the precipitation grid data both for runs with the ECHAM5/OM and HadCM3 GCMs.

A risk analysis of probable water shortage in the future can only be as good as the regionalized model predictions of individual meteorological parameters driving the "sandwich" or crop models. Specifically with relation to the future development in summer precipitation and its variability, there is considerable disagreement between individual GCM's (Maraun et al., 2010). Recent analyses of the propensity for drought events in different parts of Europe showed, that the historic patterns observed across Europe were related to shifts in the North Atlantic summer storm tracks which so far are largely unpredictable (Dong et al., 2013).

Despite uncertainties in the projected regionalised precipitation rates, the model will contribute to enlarge the value of more statistical attempts to estimate changes in plant phenology and, thus, the dynamics of grapevine development which is important for water use (Bock et al., 2011; Urhausen et al., 2011).

CONCLUSION

We have coupled a soil water balance model with a numerical simulation approach to simulate the distribution of absorbed radiation in vineyards, also accounting for sparse canopies. Sub models, describing the influence of steep slopes, the use of cover crops, and bare soil cultivation on vineyard evapotranspiration were added or replaced to improve the model and simplify its parameterization with the aim to make the model applicable to complete growing regions. The model was validated against soil water and sap flow measurements over two years in three vineyards. Compared to former model approaches, a grapevine transpiration coefficient had to be introduced to accurately simulate measured grapevine transpiration rates. Soil water dynamics in the rooting profile could be adequately described throughout different seasons with different proportions of water loss through bare soil, cover crops or vines. Model runs with data of different RCMs projected an increase of future drought stress occurrence for all sites but varied largely with respect to the absolute number of expected drought days. Similar analyses are needed on a regional scale to develop adaptation scenarios.

REFERENCES

Ainsworth, E. A., and Rogers, A. (2007). The response of photosynthesis and stomatal conductance to rising [CO2]: mechanisms and environmental interactions. *Plant Cell Environ.* 30, 258–270. doi: 10.1111/j.1365-3040.2007.01641.x

Alcamo, J., Döll, P., Henrichs, T., Kaspar, F., Lehner, B., Rösch, T., et al. (2003). Development and testing of the WaterGAP 2 global model of water use and availability. *Hydrol. Sci. J.* 48, 317–337. doi: 10.1623/hysj.48.3.317.45290

Allen, R. G. (2011). Skin layer evaporation to account for small precipitation events—An enhancement to the FAO-56 evaporation model. *Agric. Water Manag.* 99, 8–18. doi: 10.1016/j.agwat.2011.08.008

Allen, R. G., Pereira, L. S., Raes, D., and Smith, M. (1998). *Crop Evapotranspiration-Guidelines for Computing Crop Water Requirements - FAO Irrigation and drainage paper 56*. Rome: FAO - Food and Agriculture Organization of the United Nations.

Allen, R. G., Trezza, R., and Tasumi, M. (2006). Analytical integrated functions for daily solar radiation on slopes. *Agric. Forest Meteorol.* 139, 55–73. doi: 10.1016/j.agrformet.2006.05.012

Allen, R. G., Walter, I. A., Elliot, R., Howell, T., Itenfisu, D., and Jensen, M. (2005). *The ASCE Standardized Reference Evapotranspiration Equation*. ASCE-EWRI Task Committee Report, Reston, VA.

Bock, A., Sparks, T., Estrella, N., and Menzel, A. (2011). Changes in the phenology and composition of wine from Franconia, Germany. *Clim. Res.* 50, 69–81. doi: 10.3354/cr01048

Bordese, M., and Alini, W. (2012). *biOps: Image processing and analysis*. Available online at: http://cran.r-project.org/package=biOps

Boucher, O., Jones, A., and Betts, R. A. (2009). Climate response to the physiological impact of carbon dioxide on plants in the met office unified model HadCM3. *Clim. Dyn.* 32, 237–249. doi: 10.1007/s00382-008-0459-6

Braun, P., and Schmid, J. (1999a). Sap flow measurements in grapevines (*Vitis vinifera* L.) 1. Stem morphology and use of the heat balance method. *Plant Soil* 215, 39–45. doi: 10.1023/A:1004756002983

Braun, P., and Schmid, J. (1999b). Sap flow measurements in grapevines (*Vitis vinifera* L.) 2. Granier measurements. *Plant Soil* 215, 47–55. doi: 10.1023/A:1004708119821

Brisson, N., and Perrier, A. (1991). A Semiempirical Model of Bare Soil Evaporation for Crop Simulation Models. *Water Resour. Res.* 27, 719–727. doi: 10.1029/91WR00075

Bronstein, I. N., Semendjajew, K. A. G., and Hühlig, H. (1999). *Taschenbuch der Mathematik*. Thun und Frankfurt am Main: Harri Deutsch.

Celette, F., Gaudin, R., and Gary, C. (2008). Spatial and temporal changes to the water regime of a Mediterranean vineyard due to the adoption of cover cropping. *Eur. J. Agron.* 29, 153–162. doi: 10.1016/j.eja.2008.04.007

Celette, F., Ripoche, A., and Gary, C. (2010). WaLIS–A simple model to simulate water partitioning in a crop association: the example of an intercropped vineyard. *Agric. Water Manag.* 97, 1749–1759. doi: 10.1016/j.agwat.2010.06.008

Celette, F., Wery, J., Chantelot, E., Celette, J., and Gary, C. (2005). Belowground Interactions in a Vine (*Vitis vinifera* L.)-tall Fescue (*Festuca arundinacea* Shreb.) intercropping system: water relations and growth. *Plant Soil* 276, 205–217. doi: 10.1007/s11104-005-4415-5

Christmann, A., Grill, E., and Huang, J. (2013). Hydraulic signals in long-distance signaling. *Curr. Opin. Plant Biol.* 16, 293–300. doi: 10.1016/j.pbi.2013.02.011

Collins, M. J., Fuentes, S., and Barlow, E. W. R. (2010). Partial rootzone drying and deficit irrigation increase stomatal sensitivity to vapour pressure deficit in anisohydric grapevines. *Funct. Plant Biol.* 37, 128–138. doi: 10.1071/FP09175

Cros, M.-J., Duru, M., Garcia, F., and Martin-Clouaire, R. (2003). A biophysical dairy farm model to evaluate rotational grazing management strategies. *Agronomie* 23, 105–122. doi: 10.1051/agro:2002071

Dong, B., Sutton, R. T., Woollings, T., and Hodges, K. (2013). Variability of the North Atlantic summer storm track: mechanisms and impacts on European climate. *Environ. Res. Lett.* 8:034037. doi: 10.1088/1748-9326/8/3/034037

Duffie, J. A., and Beckman, W. A. (2006). *Solar Engineering of Thermal Processes*. Hoboken: John Wiley & Sons.

Duru, M., Adam, M., Cruz, P., Martin, G., Ansquer, P., Ducourtieux, C., et al. (2009). Modelling above-ground herbage mass for a wide range of grassland community types. *Ecol. Model.* 220, 209–225. doi: 10.1016/j.ecolmodel.2008.09.015

Emde, K. (1992). "Experimentelle Untersuchungen zu Oberflächenabfluß und Bodenaustrag in Verbindung mit Starkregen bei verschiedenen Bewirtschaftungssystemen in Weinbergsarealen des oberen Rheingaus," in *Geisenheimer Berichte* (Geisenheim: Gesellschaft zur Förderung der Forschungsanstalt Geisenheim).

Fandiño, M., Cancela, J. J., Rey, B. J., Martínez, E. M., Rosa, R. G., and Pereira, L. S. (2012). Using the dual-Kc approach to model evapotranspiration of Albariño vineyards (*Vitis vinifera* L. cv. Albariño) with consideration of active ground cover. *Agric. Water Manag.* 112, 75–87. doi: 10.1016/j.agwat.2012.06.008

Gates, D. M. (1980). *Biophysical Ecology*. New York, NY: Springer-Verlag.

Gaudillère, J. P., Van Leeuwen, C., and Ollat, N. (2002). Carbon isotope composition of sugars in grapevine, an integrated indicator of vineyard water status. *J. Exp. Bot.* 53, 757–763. doi: 10.1093/jexbot/53.369.757

Gaudin, R., and Gary, C. (2012). Model-based evaluation of irrigation needs in Mediterranean vineyards. *Irrig. Sci.* 30, 1–11. doi: 10.1007/s00271-012-0349-x

Geiger, R. (1980). *The Climate Near the Ground*. Cambridge, MA: Harvard University Press.

Granier, A. (1985). Une nouvelle méthode pour la mesure du flux de sève brute dans le tronc des arbres. *Ann. Sci. For.* 42, 193–200. doi: 10.1051/forest:19850204

Gruber, B. R., and Schultz, H. R. (2005). Coupling of plant to soil water status at different vineyard sites. *Acta Hort. (ISHS)* 689, 381–390.

Hannah, L., Roehrdanz, P. R., Ikegami, M., Shepard, A. V., Shaw, M. R., Tabor, G., et al. (2013). Climate change, wine, and conservation. *Proc. Natl. Acad. Sci. U.S.A.* 110, 6907–6912. doi: 10.1073/pnas.1210127110

Hirose, T. (2005). Development of the Monsi-Saeki theory on canopy structure and function. *Ann. Bot.* 95, 483–494. doi: 10.1093/aob/mci047

Iandolino, A. B., Pearcy, R. W., and Williams, L. E. (2013). Simulating three-dimensional grapevine canopies and modelling their light interception characteristics. *Aust. J. Grape Wine Res.* 19, 388–400. doi: 10.1111/ajgw.12036

Intrigliolo, D., Lakso, A., and Piccioni, R. (2009). Grapevine cv. "Riesling" water use in the northeastern United States. *Irrig. Sci.* 27, 253–262. doi: 10.1007/s00271-008-0140-1

Jacob, D. (2005). REMO A1B SCENARIO RUN, UBA PROJECT, 0.088 DEGREE RESOLUTION, RUN NO. 006211, 1H DATA. World Data Center for Climate. CERA-DB "REMO_UBA_A1B_1_R006211_1H" Available online at: http://cera-www.dkrz.de/WDCC/ui/Compact.jsp?acronym=REMO_UBA_A1B_1_R006211_1H

Jones, G. (2006). Climate change and wine: observations, impacts and future implications. *Wine Ind. J.* 21, 21–26.

Jones, G., White, M., Cooper, O., and Storchmann, K. (2005b). Climate change and global wine quality. *Clim. Change* 73, 319–343. doi: 10.1007/s10584-005-4704-2

Jones, G. V., Duchêne, E., Tomasi, D., Yuste, J., Bratislavska, O., Schultz, H. R., et al. (2005a). "Changes in European Winegrape Phenology and Relationships with Climate," in *XIV International GESCO-Viticulture-Congress*, ed H. R. Schultz (Geisenheim: Gesellschaft zur Förderung der Forschungsanstalt Geisenheim), 55–61.

Kenny, G. J., and Harrison, H. A. (1992). The effects of climate variability and change on grape suitability in Europe. *J. Wine Res.* 3, 163–183. doi: 10.1080/09571269208717931

Kreienkamp, F., Enke, W., and Spekat, A. (2010). WR2010_EH5_1_A1B: UBA-WETTREG ECHAM5/OM 20C + A1B Lauf 1 realization run 1961-2100. World Data Center for Climate. CERA-DB "WR2010_EH5_1_A1B" Available online at: http://cera-www.dkrz.de/WDCC/ui/Compact.jsp?acronym=WR2010_EH5_1_A1B

Kreienkamp, F., Hübener, H., Linke, C., and Spekat, A. (2012). Good practice for the usage of climate model simulation results - A discussion paper. *Environ. Syst. Res.* 1:9. doi: 10.1186/2193-2697-1-9

Lautenschlager, M., Keuler, K., Wunram, C., Keup-Thiel, E., Schubert, M., Will, A., et al. (2009). *Climate Simulation with CLM, Scenario A1B run no.1, Data Stream 3: European region MPI-M/MaD*. Hamburg: World Data Center for Climate. doi: 10.1594/WDCC/CLM_A1B_1_D3

Lebon, E., Dumas, V., Pieri, P., and Schultz, H. R. (2003). Modelling the seasonal dynamics of the soil water balance of vineyards. *Funct. Plant Biol.* 30, 699–710. doi: 10.1071/FP02222

Löhnertz, O., Hoppmann, D., Emde, K., Friedrich, K., Schmanke, M., and Zimmer, T. (2004). *Die Standortkartierung der hessischen Weinbaugebiete*. Wiesbaden: Hessisches Landesamt für Umwelt und Geologie.

López-Lozano, R., Baret, F., Atauri, I. G. D. C., Lebon, E., and Tisseyre, B. (2011). 2D approximation of realistic 3D vineyard row canopy representation for light interception (fIPAR) and light intensity distribution on leaves (LIDIL). *Eur. J. Agron.* 35, 171–183. doi: 10.1016/j.eja.2011.06.005

López-Lozano, R., Baret, F., García De Cortázar-Atauri, I., Bertrand, N., and Casterad, M. A. (2009). Optimal geometric configuration and algorithms for LAI indirect estimates under row canopies: the case of vineyards. *Agric. Forest Meteorol.* 149, 1307–1316. doi: 10.1016/j.agrformet.2009.03.001

Louarn, G., Dauzat, J., Lecoeur, J., and Lebon, E. (2008b). Influence of trellis system and shoot positioning on light interception and distribution in two grapevine cultivars with different architectures: an original approach based on 3D canopy modelling. *Aust. J. Grape Wine Res.* 14, 143–152. doi: 10.1111/j.1755-0238.2008.00016.x

Louarn, G., Guedon, Y., Lecoeur, J., and Lebon, E. (2007). Quantitative analysis of the phenotypic variability of shoot architecture in two grapevine (*Vitis vinifera*) cultivars. *Ann. Bot.* 99, 425–437. doi: 10.1093/aob/mcl276

Louarn, G., Lecoeur, J., and Lebon, E. (2008a). A three-dimensional statistical reconstruction model of grapevine (*Vitis vinifera*) simulating canopy structure variability within and between cultivar/training system pairs. *Ann. Bot.* 101, 1167–1184. doi: 10.1093/aob/mcm170

Lu, P., Urban, L., and Ping, Z. (2004). Granier's Thermal Dissipation Probe (TDP) method for measuring sap flow in trees: theory and practice. *J. Integr. Plant Biol.* 46, 631–646.

Mabrouk, H., Carbonneau, A., and Sinoquet, H. (1997). Canopy Structure and radiation regime in grapevine. I. Spatial and angular distribution of leaf area in two canopy systems. *Vitis* 36, 119–123.

Malheiro, A. C., Santos, J. A., Fraga, H., and Pinto, J. G. (2010). Climate change scenarios applied to viticultural zoning in Europe. *Clim. Res.* 43, 163–177. doi: 10.3354/cr00918

Maraun, D., Wetterhall, F., Ireson, A. M., Chandler, R. E., Kendon, E. J., Widmann, M., et al. (2010). Precipitation downscaling under climate change: recent developments to bridge the gap between dynamical models and the end user. *Rev. Geophys.* 48:RG3003. doi: 10.1029/2009RG000314

McLeod, A. I. (2011). Kendall: Kendall rank correlation and Mann-Kendall trend test. R package version 2.2 Available online at: http://CRAN.R-project.org/package=Kendall

Modest, M. F. (2003). *Radiative Heat Transfer*. Oxford: Elsevier Science.

Morlat, R., Penavayre, M., Jacquet, A., Asselin, C., and Lemaitre, C. (1992). Influence des terroirs sur le fonctionnement hydrique et al photosynthèse de la vigne en millésime exceptionnellement sec (1990). Conséquence sur la maturation du raisin. *Int. J. Vine Wine Sci.* 26, 197–218.

Nakicenovic, N., Alcamo, J., and Davis, G. (2000). *Special Report on Emissions Scenarios. Intergovernmental Panel on Climate Change*. Cambridge: Cambridge University Press.

Ojeda, H., Andary, C., Kraeva, E., Carbonneau, A., and Deloire, A. (2002). Influence of pre- and postveraison water deficit on synthesis and concentration of skin phenolic compounds during berry growth of vitis vinifera cv. Shiraz. *Am. J. Enol. Vitic.* 53, 261–267.

Ojeda, H., Deloire, A., and Carbonneau, A. (2001). Influence of water deficits on grape berry growth. *Vitis* 40, 141–145.

Oren, R., Phillips, N., Ewers, B. E., Pataki, D. E., and Megonigal, J. P. (1999). Sap-flux-scaled transpiration responses to light, vapor pressure deficit, and leaf area reduction in a flooded Taxodium distichum forest. *Tree Physiol.* 19, 337–347. doi: 10.1093/treephys/19.6.337

Ortega-Farias, S., Carrasco, M., Olioso, A., Acevedo, C., and Poblete, C. (2007). Latent heat flux over cabernet sauvignon vineyard using the shuttleworth and wallace model. *Irrig. Sci.* 25, 161–170. doi: 10.1007/s00271-006-0047-7

Ortega-Farias, S., Poblete-Echeverría, C., and Brisson, N. (2010). Parameterization of a two-layer model for estimating vineyard evapotranspiration using meteorological measurements. *Agric. Forest Meteorol.* 150, 276–286. doi: 10.1016/j.agrformet.2009.11.012

Peak, D., and Mott, K. A. (2011). A new, vapour-phase mechanism for stomatal responses to humidity and temperature. *Plant Cell Environ.* 34, 162–178. doi: 10.1111/j.1365-3040.2010.02234.x

Pellegrino, A., Lebon, E., Voltz, M., and Wery, J. (2004). Relationship between plant and soil water status in vine (*Vitis vinifera* L.). *Plant Soil* 266, 129–142. doi: 10.1007/s11104-005-0874-y

Pellegrino, A., Lebon, E., Simonneau, T., and Wery, J. (2005). Towards a simple indicator of water stress in grapevine (Vitis vinifera L.) based on the differential sensitivities of vegetative growth components. *Aust. J. Grape Wine Res.* 11, 306–315. doi: 10.1111/j.1755-0238.2005.tb00030.x

Pfister, S., Koehler, A., and Hellweg, S. (2009). Assessing the environmental impacts of freshwater consumption in LCA. *Environ. Sci. Technol.* 43, 4098–4104. doi: 10.1021/es802423e

Pieri, P. (2010a). Modelling radiative balance in a row-crop canopy: row-soil surface net radiation partition. *Ecol. Model.* 221, 791–801. doi: 10.1016/j.ecolmodel.2009.11.019

Pieri, P. (2010b). Modelling radiative balance in a row-crop canopy: cross-row distribution of net radiation at the soil surface and energy available to clusters in a vineyard. *Ecol. Model.* 221, 802–811. doi: 10.1016/j.ecolmodel.2009.07.028

Pieri, P. (2012). "Changement climatique et culture de la vigne: l'essentiel des impacts," in Changement Climatique, Agriculture et forêt en France: Simulations d'impacts sur les principales espèces, eds N. Brisson and F. Levrault (Angers: Ademe Editions), 213–224.

Pieri, P., and Lebon, E. (2014). Modelling the future impacts of climate change on French vineyards. *J. Int. Sci. Vigne Vin.* (Special issue Laccave), 35–43.

Poblete-Echeverría, C., and Ortega-Farias, S. (2009). Estimation of actual evapotranspiration for a drip-irrigated Merlot vineyard using a three-source model. *Irrig. Sci.* 28, 65–78. doi: 10.1007/s00271-009-0183-y

Poni, S., Bernizzoni, F., Civardi, S., Gatti, M., Porro, D., and Camin, F. (2009). Performance and water-use efficiency (single-leaf vs. whole-canopy) of well-watered and half-stressed split-root Lambrusco grapevines grown in Po Valley (Italy). *Agric. Ecosyst. Environ.* 129, 97–106. doi: 10.1016/j.agee.2008.07.009

Poni, S., Rebucci, B., Magnanini, E., and Intrieri, C. (1996). Preliminary results on the use of a modified point quadrat method for estimating canopy structure of grapevine training systems. *Vitis* 35, 23–28.

Pou, A., Flexas, J., Alsina Mdel, M., Bota, J., Carambula, C., De Herralde, F., et al. (2008). Adjustments of water use efficiency by stomatal regulation during drought and recovery in the drought-adapted Vitis hybrid Richter-110 (*V. berlandieri x V. rupestris*). *Physiol. Plant* 134, 313–323. doi: 10.1111/j.1399-3054.2008.01138.x

Prieto, J. A., Louarn, G., Perez Peña, J., Ojeda, H., Simonneau, T., and Lebon, E. (2012). A leaf gas exchange model that accounts for intra-canopy variability by considering leaf nitrogen content and local acclimation to radiation in grapevine (*Vitis vinifera* L.). *Plant Cell Environ.* 35, 1313–1328. doi: 10.1111/j.1365-3040.2012.02491.x

R development core team. (2012). *R: A Language and Environment for Statistical Computing*. Vienna: R Foundation for Statistical Computing

Reindl, D. T., Beckman, W. A., and Duffie, J. A. (1990). Evaluation of hourly tilted surface radiation models. *Sol. Energy* 45, 9–17. doi: 10.1016/0038-092X(90)90061-G

Riou, C., Pieri, P., and Le Clech, B. (1994). Consommation d'eau de la vigne en conditions hydriques non limitantes. Formulation simplifiée de la transpiration. *Vitis* 33, 109–115.

Riou, C., Valancogne, C., and Pieri, P. (1989). Un modèle simple d'interception du rayonnement solaire par la vigne - vérification expérimentale. *Agronomie* 9, 441–450. doi: 10.1051/agro:19890502

Ritchie, J. T. (1972). Model for predicting evaporation from a row crop with incomplete cover. *Water Resour. Res.* 8, 1204–1213. doi: 10.1029/WR008i005p01204

Rockel, B., Will, A., and Hense, A. (2008). The Regional climate model COSMO-CLM (CCLM). *Meteorol. Z.* 17, 347–348. doi: 10.1127/0941-2948/2008/0309

Rogiers, S. Y., Hardie, W. J., and Smith, J. P. (2011). Stomatal density of grapevine leaves (*Vitis vinifera* L.) responds to soil temperature and atmospheric carbon dioxide. *Aust. J. Grape Wine Res.* 17, 147–152. doi: 10.1111/j.1755-0238.2011.00124.x

Santos, J. A., Malheiro, A. C., Pinto, J. G., and Jones, G. V. (2012). Macroclimate and viticultural zoning in Europe: observed trends and atmospheric forcing. *Clim. Res.* 51, 89–103. doi: 10.3354/cr01056

Schär, C. H., and Christensen, O. B. (2013). RT3_ETHZ-CLMHadCM3Q0. World Data Center for Climate. CERA-DB "RT3_ETHZ-CLMHadCM3Q0" Available online at: http://cera-www.dkrz.de/WDCC/ui/Compact.jsp?acronym=RT3_ETHZ-CLMHadCM3Q0

Schmid, J. (1997). "Xylemflussmessungen an Reben," in *Geisenheimer Berichte* (Geisenheim: Gesellschaft zur Förderung der Forschungsanstalt Geisenheim).

Schultz, H. R. (1995). Grape canopy structure, light microclimate and photosynthesis. 1. A two-dimensional model of the spatial distribution of surface area densities and leaf ages in two canopy systems. *Vitis* 34, 211–215.

Schultz, H. R. (2000). Climate Change and viticulture: a European perspective on climatology, carbon dioxide and UV-B effects. *Aust. J. Grape Wine Res.* 6, 2–12. doi: 10.1111/j.1755-0238.2000.tb00156.x

Schultz, H. R. (2003). Differences in hydraulic architecture account for near-isohydric and anisohydric behaviour of two field-grown *Vitis vinifera* L. cultivars during drought. *Plant Cell Environ.* 26, 1393–1405. doi: 10.1046/j.1365-3040.2003.01064.x

Schultz, H. R., and Lebon, E. (2005). Modeling the effect of climate change on grapevine water relations. *Acta Hortic.* 689, 71–78.

Schultz, H. R., and Jones, G. V. (2010). Climate induced historic and future changes in viticulture. *J. Wine Res.* 21, 137–145. doi: 10.1080/09571264.2010.530098

Schultz, H. R., and Stoll, M. (2010). Some critical issues in environmental physiology of grapevines: future challenges and current limitations. *Aust. J. Grape Wine Res.* 16, 4–24. doi: 10.1111/j.1755-0238.2009.00074.x

Shuttleworth, W. J., and Wallace, J. S. (1985). Evaporation from sparse crops – an energy combination theory. *Q. J. R. Meteorol. Soc.* 111, 839–855. doi: 10.1002/qj.49711146910

Sinclair, T. R., and Ludlow, M. M. (1986). Influence of soil water supply on the plant water balance of four tropical grain legumes. *Aust. J. Plant Physiol.* 13, 329–341. doi: 10.1071/PP9860329

Sinoquet, H., and Bonhomme, R. (1991). A theoretical analysis of radiation interception in a two-species plant canopy. *Math. Biosci.* 105, 23–45. doi: 10.1016/0025-5564(91)90047-M

Sinoquet, H., Thanisawanyangkura, S., Mabrouk, H., and Kasemsap, P. (1998). Characterization of the light environment in canopies using 3D digitising and image processing. *Ann. Bot.* 82, 203–212. doi: 10.1006/anbo.1998.0665

Soar, C. J., Speirs, J., Maffei, S. M., Penrose, A. B., McCarthy, M. G., and Loveys, B. R. (2006). Grape vine varieties Shiraz and Grenache differ in their stomatal response to VPD: apparent links with ABA physiology and gene expression in leaf tissue. *Aust. J. Grape Wine Res.* 12, 2–12. doi: 10.1111/j.1755-0238.2006.tb00038.x

Sonnentag, O., Hufkens, K., Teshera-Sterne, C., Young, A. M., Friedl, M., Braswell, B. H., et al. (2012). Digital repeat photography for phenological research in forest ecosystems. *Agric. Forest Meteorol.* 152, 159–177. doi: 10.1016/j.agrformet.2011.09.009

Tardieu, F., and Simonneau, T. (1998). Variability among species of stomatal control under fluctuating soil water status and evaporative demand: modelling isohydric and anisohydric behaviours. *J. Exp. Bot.* 49, 419–432. doi: 10.1093/jxb/49.Special_Issue.419

Tonietto, J., and Carbonneau, A. (2004). A multicriteria climatic classification system for grape-growing regions worldwide. *Agric. Forest Meteorol.* 124, 81–97. doi: 10.1016/j.agrformet.2003.06.001

Trambouze, W., and Voltz, M. (2001). Measurement and modeling of the transpiration of a Mediterranean vineyard. *Agric. Forest Meteorol.* 107, 153–166. doi: 10.1016/S0168-1923(00)00226-4

Uliarte, E. M., Schultz, H. R., Frings, C., Pfister, M., Parera, C. A., and Del Monte, R. F. (2013). Seasonal dynamics of CO_2 balance and water consumption of C3 and C4-type cover crops compared to bare soil in a suitability study for their use in vineyards in Germany and Argentina. *Agric. Forest Meteorol.* 181, 1–16. doi: 10.1016/j.agrformet.2013.06.019

Urhausen, S., Brienen, S., Kapala, A., and Simmer, C. (2011). Climatic conditions and their impact on viticulture in the Upper Moselle region. *Clim. Change* 109, 349–373. doi: 10.1007/s10584-011-0059-z

Valancogne, C., and Nasr, Z. (1993). "A heat balance method for measuring sap flow in small trees," in *Water Transport in Plants Under Climatic Stress*, eds M. Borghetti, J. Grace, and A. Raschi (Vallambrosa: Cambridge University Press), 166–173.

van Leeuwen, C., and Seguin, G. (1994). Incidences de l'alimentation en eau de la vigne, appreciée per l'etat hydrique du feuillage, sur le developpement de l'appareil végétatif et la maturation du raisin. *J. Vine Wine Sci.* 28, 81–110.

van Leeuwen, C., Pieri, P., and Vivin, P. (2010). "Comparison of three operational tools for the assessment of vine waterwater status: stem water potentialstem water potential, carbon isotope discriminationcarbon isotope discrimination measured on grapegrape sugar and water balance," in *Methodologies and Results in Grapevine Research*, eds S. Delrot, H. Medrano, E. Or, L. Bavaresco, and S. Grando (Dordrecht; Heidelberg; London; New York: Springer), 87–106.

Warrach-Sagi, K., Schwitalla, T., Wulfmeyer, V., and Bauer, H.-S. (2013). Evaluation of a climate simulation in Europe based on the WRF–NOAH model system: precipitation in Germany. *Clim. Dyn.* 41, 755–774. doi: 10.1007/s00382-013-1727-7

Webb, L. B., Whetton, P. H., and Barlow, E. W. R. (2007). Modelled impact of future climate change on the phenology of winegrapes in Australia. *Aust. J. Grape Wine Res.* 13, 165–175. doi: 10.1111/j.1755-0238.2007.tb00247.x

Webb, L. B., Whetton, P. H., and Barlow, E. W. R. (2011). Observed trends in winegrape maturity in Australia. *Glob. Change Biol.* 17, 2707–2719. doi: 10.1111/j.1365-2486.2011.02434.x

Webb, L. B., Whetton, P. H., Bhend, J., Darbyshire, R., Briggs, P. R., and Barlow, E. W. R. (2012). Earlier wine-grape ripening driven by climatic warming and drying and management practices. *Nat. Clim Change* 2, 259–264. doi: 10.1038/nclimate1417

Weeber, K.-W. (1993). *Die Weinkultur der Römer. Zürich: Artemis & Winkler Verlag*.

Williams, L. E., and Ayars, J. E. (2005). Grapevine water use and the crop coefficient are linear functions of the shaded area measured beneath the canopy. *Agric. Forest Meteorol.* 132, 201–211. doi: 10.1016/j.agrformet.2005.07.010

Williams, L. E., and Baeza, P. (2007). Relationships among ambient temperature and vapor pressure deficit and leaf and stem water potentials of fully irrigated, field-grown grapevines. *Am. J. Enol. Vitic.* 58, 173–181.

Williams, L. E., and Matthews, M. A. (1990). "Grapevine," in *Irrigation of Agricultural Crops*, eds B. A. Stewart and D. R. Nielsen (Madison, WI: ASA-CSSA-SSSA), 1019–1055.

Yin, X. (2013). Improving ecophysiological simulation models to predict the impact of elevated atmospheric CO(2) concentration on crop productivity. *Ann. Bot.* 112, 465–475. doi: 10.1093/aob/mct016

Yunusa, I. A. M., Walker, R. R., and Lu, P. (2004). Evapotranspiration components from energy balance, sapflow and microlysimetry techniques for an irrigated vineyard in inland Australia. *Agric. Forest Meteorol.* 127, 93–107. doi: 10.1016/j.agrformet.2004.07.001

Zhang, Y., Oren, R., and Kang, S. (2012). Spatiotemporal variation of crown-scale stomatal conductance in an arid *Vitis vinifera* L. cv. Merlot vineyard: direct effects of hydraulic properties and indirect effects of canopy leaf area. *Tree Physiol.* 32, 262–279. doi: 10.1093/treephys/tpr120

Conflict of Interest Statement: The authors declare that the research was conducted in the absence of any commercial or financial relationships that could be construed as a potential conflict of interest.

APPENDIX A

RADIATION PARTITIONING MODEL

The Monte Carlo simulation serves as a numerical experiment to solve the light partitioning inside the geometry described in Section Radiation partitioning model (**Figure 2**), where the shortwave radiation is expressed by a random sample of photons (Modest, 2003). The trace of each photon (ray trace) from emission until absorption or reflection back to the sky is followed by calculation of interaction sites, the corresponding probabilities for the possible interactions (transmittance, reflection, or absorption) and random numbers that decide which interactions took place. Therefore, the partitioning of radiation inside the canopy depends on the direction of the incoming radiation beam. This was modelled by a statistically adequate number of equally distributed photons between the rows, emitted between $-D/2 \leq x \leq D/2$, in defined interval steps and with a defined direction at the height $z = S + H$, where $S + H$ represents the distance between soil and upper foliage boundary (**Figure 2**). The interaction sites and possible travel distances inside the foliage were calculated by vector arithmetic in three dimensions. To follow the trace of a photon, it was assumed that absorption and reflection took only place at the bordering faces of the cuboid or the soil surface. Every absorption point of each photon was stored. Random numbers were also used to calculate the directions of diffuse reflections. The surfaces were treated as ideal diffuse reflectors. Literature values were chosen for the shortwave reflectivity (albedo, ρ_l) of leaves ($\rho_l = 0.22$) and the soil ($\rho_s = 0.18$) (Gates, 1980). No difference was made between green covered or bare soil surfaces at this stage.

To calculate the corresponding probabilities for an interaction of a photon with the grapevine foliage, the transmittance of the foliage was parameterized according to the Beer-Lambert law depending on the porosity (perpendicular to the vertical foliage walls) and the possible travel distance inside the cuboid (Sinoquet and Bonhomme, 1991). If the leaf area distribution is assumed to be homogenous inside the foliage, the porosity p can be expressed as:

$$I(x)/I_0 = p(x) \tag{A1}$$

where I is the (non-scattered) radiant flux density, I_0 is the unattenuated flux density and x is the distance the radiation travels in the foliage. The equivalent equation based on the Beer-Lambert law is:

$$I(x)/I_0 = e^{-kx}, \tag{A2}$$

where k is the extinction coefficient. For the porosity perpendicular to the side walls of the foliage $p_{\perp}$ and the corresponding width of the canopy L, Equation (A1) becomes:

$$I(L)/I_0 = p_{\perp} \tag{A3}$$

and the combination of Equations (A1–A3) results in:

$$\tau(x) = p(x) = \exp\left(\ln(p_{\perp})\frac{x}{L}\right) = p_{\perp}^{\frac{x}{L}}, \tag{A4}$$

where τ is the transmittance of the foliage which equals the porosity if the transmittance of single leaves is neglected. For single photons the porosity represents the probability for no interception inside the foliage, i.e., for transmittance (Sinoquet and Bonhomme, 1991). Since the sum of all probabilities for transmittance, reflection, and absorption is unity, it can be written as:

$$\tau + \rho_1(1 - \tau) + \alpha_v = 1, \tag{A5}$$

where the transmittance τ is determined by Equation (A4), $\rho_1(1 - \tau)$ is the probability that reflection occurs and α_v is the resulting probability for absorption at the grapevine canopy. In case of interaction at the soil surface, the transmittance is zero. The equation for the probabilities for interactions at the soil surface is:

$$\rho_s + \alpha_s = 1, \tag{A6}$$

where α_s is the absorptance of the soil surface.

For the purpose of this work only the partitioning between the foliage of the grapevines and the soil was of interest. If the incoming radiation direction is expressed in spherical coordinates (polar angle θ, azimuthal angle φ), the sum $N(\theta, \varphi)$ of all emitted photons from the direction θ, φ can be partitioned into photons absorbed by the grapevines (N_v), the soil (N_s), or reflected back to the sky (N_{vy}). Hence, the interception fractions for direct radiation for grapevines a_v, the soil a_s and the albedo ρ_{vy} of the vineyard are represented as:

$$a_v = \frac{N_v}{N(\theta, \varphi)}, a_s = \frac{N_s}{N(\theta, \varphi)}, \rho_{vy} = \frac{N_{vy}}{N(\theta, \varphi)} \tag{A7}$$

To calculate similar fractions for diffuse solar radiation, it has to be considered that the diffuse irradiance R_{dif} (in Wm^{-2}) received by a horizontal surface is the integral of the radiance L_e (in $\text{Wm}^{-2}\text{sr}^{-1}$) from a solid angle element $d\Omega$ over the hemisphere:

$$R_{dif} = Le \int_{2\pi} \cos\theta \, d\Omega, \tag{A8}$$

where $\cos\theta$ is the projection from the solid angle element $d\Omega$ into the horizontal and the radiance L_e is independent of the viewing direction, if the diffuse solar radiation is assumed to be isotropic. To calculate the amount of diffuse radiation which is intercepted by the foliage $R_{dif,v}$, the fractions of direct radiation have to be multiplied with the radiance L_e of the diffuse radiation and integrated over the hemisphere. Expressed in spherical coordinates it follows:

$$R_{dif,v} = R_{dif}a_{dif,v} = L_e \int_0^{2\pi} \int_0^{\pi/2} a_v(\theta, \varphi) \cos\theta \sin\theta \, d\theta \, d\varphi, \tag{A9}$$

where $d\Omega = \sin\theta \, d\theta \, d\varphi$ is the size of the solid angle element in spherical coordinates and $a_{dif,v}$ is the ratio of diffuse solar radiation which is intercepted by the grapevine canopy. To cover all directions of the radiation from the hemisphere, the numerical

experiment provides results for a discrete number of n equidistant elements for the intervals $0 < \theta < \pi/2$ and $0 < \varphi < 2\pi$ with the interval distances $\Delta\theta$ and $\Delta\varphi$. Therefore the diffuse fraction index for the foliage could be calculated with Equations (A8) and (A9) and the results of the simulation expressed as:

$$a_{dif,v} = \frac{R_{dif,v}}{R_{dif}} = \frac{\sum\limits_{i,j=1}^{n} a(\theta_i, \varphi_j) \cos\theta_i \sin\theta_i \Delta\theta \Delta\varphi}{n \sum\limits_{i=1}^{n} \cos\theta_i \sin\theta_i \Delta\theta \Delta\varphi}. \quad (A10)$$

The fractions for direct and diffuse solar radiation thus allow calculating the total radiation absorbed by the canopy R_v or the soil R_s:

$$R_v = a_{dif,v} R_{dif} + a_{dir,v} R_{dir} \quad (A11a)$$

$$R_s = a_{dif,s} R_{dif} + a_{dir,s} R_{dir} \quad (A11b)$$

APPENDIX B

ADAPTATION OF THE RADIATION PARTITIONING MODEL TO STEEP SLOPES

The partitioning of direct radiation inside the canopy depends on the incoming direction relative to the grapevine rows. Therefore, the position of the sun has to be expressed in a coordinate system which is fixed to the vineyard, the slope system K' (body-fixed frame). The orientation of K' with respect to a horizontal system K (space-fixed frame), can be described by Euler angles which also allow transforming a point from K to K'. The following process was adopted for vineyards with downhill row orientation which simplifies this transformation. The Cartesian coordinate axes of the K system (x, y, z) are defined so that the z axis corresponds to the vertical, y points to south and x to west on the northern hemisphere. The axes of the K' system (x', y', z') are set in order that z' corresponds to the normal of the slope system, y' points in the direction of the rows and x' is in the plane of the slope surface perpendicular to y'. If the grapevine rows run downhill (the normal case in German steep slope grape growing regions), and thus y' also points downhill, the position of the slope system K' could be defined by two rotations of the K system, with the result that the axes of the rotated system match the x', y', z' axes. The first rotation is around the z axis with the angle γ and corresponds to the aspect (orientation) of the vineyard. The second is around the x' axis (resulting from x-axis after the first rotation) with the angle β and corresponds to the slope of the vineyard. Positive rotation directions need to be respected.

The angles β and γ correspond to Euler angles and allow the calculation of the direction cosines, representing the elements of a rotation matrix (Bronstein et al., 1999) with which a point in x, y, z coordinates can be transformed to x', y', z' coordinates by:

$$x' = x \cos\gamma - y \cos\beta \sin\gamma + z \sin\beta \sin\gamma,$$
$$y' = x \sin\gamma + y \cos\beta \cos\gamma - z \sin\beta \cos\gamma, \quad (B1)$$
$$z' = y \sin\beta + z \cos\beta.$$

The position of the sun is described by the zenith angle θ_z (the angle between the vertical and the sun), and the solar azimuth angle γ_s (the angle between the projection of the line to the sun in the horizontal and south, Duffie and Beckman, 2006). To apply Equation (B1) to calculate the position of the sun in the K' system, θ_z and γ_s have to be transformed to x, y, z coordinates. The deducted x', y', z' coordinates could further be back transformed and expressed as angle of incidence θ (the angle between the sun and the normal of the vineyard) and as vineyard solar azimuth angle γ_v (the angle between the projection of the line to the sun in the plane of the vineyard surface and the direction of the rows), in analogy to θ_z and γ_s. Because of the similarity of θ_z and γ_s with spherical coordinates this is not outlined here.

APPENDIX C

ESTIMATING DIRECT AND DIFFUSE RADIATION COMPONENTS OF SOLAR RADIATION

We used a correlation between the solar global radiation and a clearness index as described in Duffie and Beckman (2006) to calculate the direct and diffuse radiation components of global radiation. The calculated regression coefficients based on measurements of global and diffuse radiation of the Geisenheim weather station from 2007 to 2012. The diffuse radiation component was measured with a pyranometer with a shading ring. The readings were corrected for the influence of the shading ring by applying correction factors as described by the manufacturer (Kipp and Zonen). For hourly data the correlation was:

$$\frac{R_{dif}}{R_{glob}} = \begin{cases} 1.0 - 0.065 k_t & (k_t \leq 0.22) \\ 1.2103 - 1.9287 k_t + 7.30 k_t^2 \\ -16.1542 k_t^3 + 10.0073 k_t^4 & (0.22 < k_t \leq 0.8) \\ 0.1675 & (k_t > 0.8) \end{cases}$$
$$\quad (C1)$$

and for daily data:

$$\frac{R_{dif}}{R_{glob}} = \begin{cases} 1.0 - 0.039 k_t & (k_t \leq 0.22) \\ 0.8501 + 2.4950 k_t - 12.2301 k_t^2 \\ +16.8298 k_t^3 - 8.7824 k_t^4 & (0.22 < k_t \leq 0.8) \\ 0.1727 & (k_t > 0.8) \end{cases}$$
$$\quad (C2)$$

where $k_t = R_{glob}/R_0$ is the clearness index, defined by the ratio of global radiation, R_{glob}, to extraterrestrial radiation, R_0, and R_{dif} is the diffuse radiation component.

frontiers in PLANT SCIENCE

The dynamic relationship between plant architecture and competition

E. David Ford*

School of Environmental and Forest Science, University of Washington, Seattle, WA, USA

In this review, structural and functional changes are described in single-species, even-aged, stands undergoing competition for light. Theories of the competition process as interactions between whole plants have been advanced but have not been successful in explaining these changes and how they vary between species or growing conditions. This task now falls to researchers in plant architecture. Research in plant architecture has defined three important functions of individual plants that determine the process of canopy development and competition: (i) resource acquisition plasticity; (ii) morphogenetic plasticity; (iii) architectural variation in efficiency of interception and utilization of light. In this review, this research is synthesized into a theory for competition based on five groups of postulates about the functioning of plants in stands. Group 1: competition for light takes place at the level of component foliage and branches. Group 2: the outcome of competition is determined by the dynamic interaction between processes that exert dominance and processes that react to suppression. Group 3: species differences may affect both exertion of dominance and reaction to suppression. Group 4: individual plants may simultaneously exhibit, in different component parts, resource acquisition and morphogenetic plasticity. Group 5: mortality is a time-delayed response to suppression. Development of architectural models when combined with field investigations is identifying research needed to develop a theory of architectural influences on the competition process. These include analyses of the integration of foliage and branch components into whole-plant growth and precise definitions of environmental control of morphogenetic plasticity and its interaction with acquisition of carbon for plant growth.

Keywords: stand structure, canopy structure, morphogenetic plasticity, resource acquisition

INTRODUCTION

Competition results in the preferential accrual of resources by one plant relative to its neighbors. How does plant architecture affect this process? Two characteristics of the subject determine the type of answers we can expect. First, competition and architectural development are interacting dynamic processes. As a plant grows, its architecture changes which in turn changes the surrounding environment so altering the resources available for both the plant and its neighbors—answers should encompass architectural effects on this dynamic process and not be restricted to static descriptions of plant form. Second, competition must be assessed in the way individuals develop within stands but explanation for how architecture affects the process requires understanding of details of plant growth—answers should encompass knowledge about both plant populations and plant growth processes and not be restricted to just one or other body of knowledge. The scope of this review is competition for light in even-aged single-species stands, such as crops and many types of naturally regenerated vegetation. Plant architecture refers to morphology and its associated physiology.

Section "The Dynamics of Stands Undergoing Competition" examines what needs to be explained about competition. The developmental sequence of single-species, even-aged stands

undergoing competition is described along with metrics that can be used for this description. There has been increasing realization that variation in the competition process may be related to differences in plant architecture. Suggestions are made why the relationship between architecture and competition is not explained by competition theories based on plant population dynamics.

Section "Plants as Competitors" discusses the properties of plants as competitors. These include: resource acquisition plasticity, which enables plants to maintain dominance; morphogenetic plasticity, which can reduce the impact of being shaded; and differences in the efficiency of interception and utilization of light that can affect both the degree of dominance found in a stand and its overall productivity.

Section "Development of Theory for the Effects of Plant Architecture on Competition" outlines components for theory defining competition as the result of interactions between architectural processes and describes how it can be used, developed, and tested.

Field measurements of stands and plants undergoing competition are being combined with use of models in the analysis of architectural effects on competition. In section "Architectural Models and Competition Dynamics," examples of such studies are

discussed that improve our understanding. Future directions are discussed in section "Conclusions".

THE DYNAMICS OF STANDS UNDERGOING COMPETITION

Most investigations into competition in whole stands have concentrated on describing the resulting population structure. Typically, investigators have sought generalizations, often implicitly, about structures that would apply to all stands and under all conditions (e.g., White, 1981). However, although there are common features, important variations have been found between species, and conditions of stand growth, that undermine construction of general theories of competition based on population studies (e.g., Weller, 1987).

Three general features observed in stands undergoing competition are: (i) emergence of dominants and suppressed individuals that sometimes die; (ii) development of spatial evenness in large and surviving plants; and (iii) general increase in the size of surviving plants as competition-induced mortality takes place. These features have been analyzed using three empirical descriptors: plant size–frequency distributions, spatial distribution of individuals, and plant size:density relationships during the self-thinning stage.

SIZE–FREQUENCY DISTRIBUTIONS

Size–frequency distributions of individuals within a stand are weak descriptors of competition because they do not identify the processes that contribute to stand development. As competition occurs, the frequency distribution of plant weights becomes right-skewed (**Figure 1B**), i.e., there are more smaller than large plants, originally described as log-normal by Koyama and Kira (1956). The right-skewed characteristic can be described by the Gini coefficient (Weiner and Solbrig, 1984): the differences between the weight of each of the n individuals, x, and all others are summed (numerator) and then averaged (denominator)

$$ G = \frac{\sum_{i=1}^{n} \sum_{j=1}^{n} |x_i - x_j|}{2n^2 \bar{x}} $$

G has a minimum of 0, when all individuals are equal, and a maximum of 1 in which all individuals but one have a value of 0.

This right-skewed distribution can be maintained through a considerable part of stand development. The inference made from this pattern, often implicit, is that large plants have greater growth and so are outcompeting smaller ones. However, the correct measurement to determine whether competition is occurring, and to assess its intensity, is the distribution of relative growth rate (RGR), weight weight^{-1} time^{-1}, in relation to plant size. This provides a measure of a plant's efficiency and distinguishes from size differences that can be perpetuated in the absence of competition. In stands undergoing competition, large plants have been found to have greater RGR (e.g., Ford, 1975). The interesting feature, though little studied, is the pattern of decline in RGR with decrease in plant size (Westoby, 1982) which could provide a measure of competition intensity. Degree of skewness is also limited as an indication of competition intensity because it can be affected
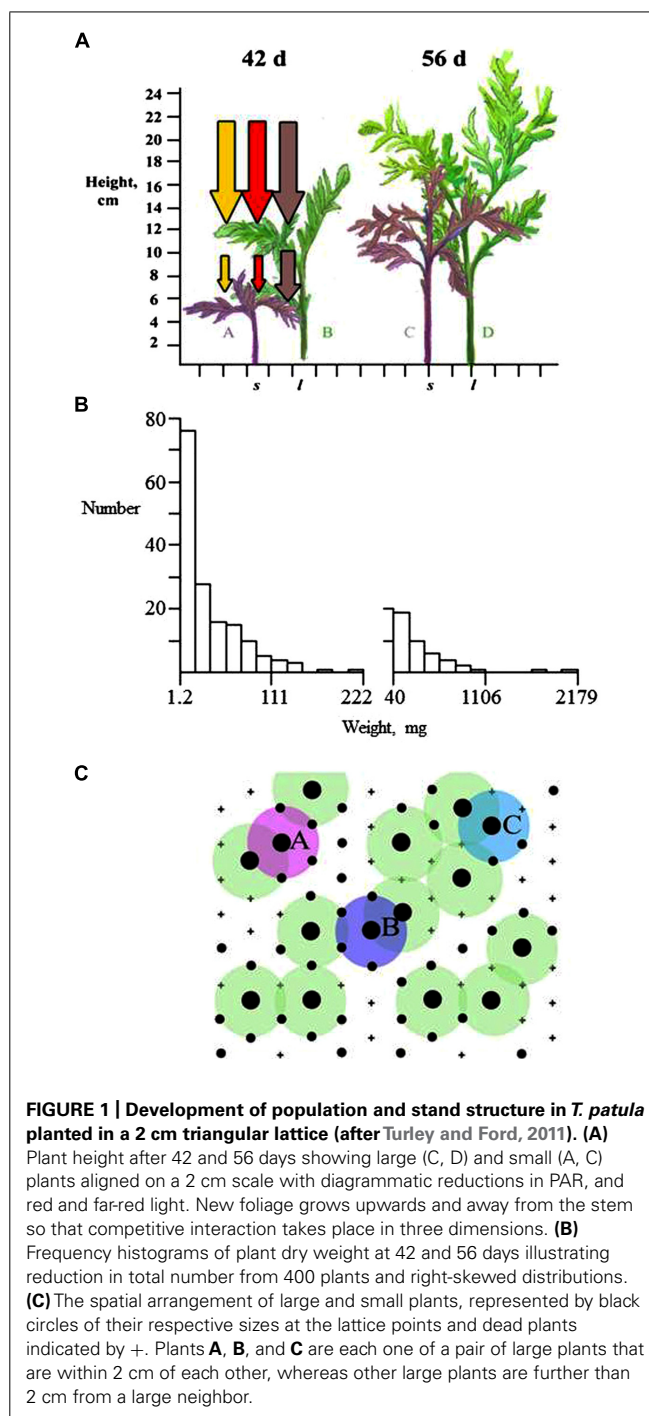
FIGURE 1 | Development of population and stand structure in *T. patula* planted in a 2 cm triangular lattice (after Turley and Ford, 2011**). (A)** Plant height after 42 and 56 days showing large (C, D) and small (A, C) plants aligned on a 2 cm scale with diagrammatic reductions in PAR, and red and far-red light. New foliage grows upwards and away from the stem so that competitive interaction takes place in three dimensions. **(B)** Frequency histograms of plant dry weight at 42 and 56 days illustrating reduction in total number from 400 plants and right-skewed distributions. **(C)** The spatial arrangement of large and small plants, represented by black circles of their respective sizes at the lattice points and dead plants indicated by +. Plants **A**, **B**, and **C** are each one of a pair of large plants that are within 2 cm of each other, whereas other large plants are further than 2 cm from a large neighbor.

by mortality, a time-delayed consequence of a plant being over-topped. As small plants die, the frequency distribution of plant size may actually become less skewed (e.g., Ford, 1975; Weiner and Thomas, 1986). The relative importance of differences in RGR and mortality in producing a particular frequency distribution cannot be distinguished from trends in the Gini coefficient alone (Wiegand et al., 2008).

A further difficulty in the interpretation of frequency distributions is that they have usually been applied to measures of

individual plant weight. Weight is the result of lifetime growth and so may have limited value as an indication of current status in a competition hierarchy. Nagashima (1999) suggests height may be more appropriate indicator of a plant's status in the canopy. For *Chenopodium album* he reported that the height ranks of plants were almost fixed 1–2 weeks after canopy closure when stand height was 10–20% of its final value. Nagashima (1999) proposed three phases in community stand height development: an early phase when plants with taller or closer neighbors elongate more rapidly; a short, second phase when competition between plants affects height growth; a third phase of ∼80% of stand growth when there was no change in plant height rank. This suggests a limited time in stand development when competition operates to affect establishment of a size hierarchy.

These three phases may not occur in all stands. Turley and Ford (2011) analyzed development of population structure of *Tagetes patula* using both weight and height. They showed, using a classification algorithm with the bivariate, height:weight distribution, the development of a bimodal plant size distribution with a distinct but relatively small group of dominant (large-sized) plants forming an upper canopy in the stand. These upper-canopy plants receive markedly greater illumination, and have greater RGR, than lower-canopy plants. Plants in the lower canopy do not die immediately on being over-topped and the number of plants in this mode can be three or four times that in the large-sized plant mode. In contrast to Nagashima's (1999) analysis suggesting stability in population structure, Turley and Ford (2011) found that a further bimodal distribution develops from within the initial one. This indicates that continued development of an upper canopy is a property of a stands of this species. There are multiple references in the literature to bimodality in size–frequency distributions found in different species (reviewed in Turley and Ford, 2011) but its definition can be difficult from just one measure of plant size.

SPATIAL STRUCTURE

In stands that have undergone competition large plants, or survivors, are spatially evenly distributed. This has been widely reported for many species and conditions of growth (Cooper, 1961; Ford, 1975; Kenkel, 1988) and indicates a process of spatial inhibition. It is the least controversial of structural properties reported for stands undergoing competition although it can take considerable time to develop to the point where it can be detected. Stoll and Bergius (2005) show the rate at which spatial inhibition develops can be affected by the intensity of competition.

Detection of spatial evenness for stands in which the initial distribution was either clumped or random, as might be expected in naturally regenerated stands or experiments using broadcast seeding, can be calculated using distance statistics (e.g., Kenkel, 1988; Bivand et al., 2013). However, the initial development of an even spatial distribution from within a clumped distribution may require more detailed analysis such as using the mark correlation function (Suzuki et al., 2008). For experiments using regularly spaced planting development of spatial evenness can be examined using lattice statistics (Bivand, 2009).

PLANT SIZE:DENSITY RELATIONSHIP

Yoda et al. (1963) proposed a simple summary for the development of a stand during the occurrence of competition-induced mortality, i.e., the phase of self-thinning. Plant numbers per unit area, N, decrease due to competition-induced mortality, while surviving plants increase in mean biomass, m, so that

$$\log m = \gamma \log N + \log K,$$

where K is a constant and Yoda et al. (1963) proposed that $\gamma = -3/2$. There was support for this relationship as a general result from some authors, e.g., White (1981), but through a detailed examination of available data, Weller (1987) showed there to be considerable variation. Weller suggests that a more appropriate formulation of the self-thinning relationship is

$$\log B = \beta \log N + \log K$$

where B is the stand biomass density (g m^{-2}), N is the plant density, individuals (m^{-2}), and β and K are constants. $\beta = -1/2$ corresponds to $\gamma = -3/2$. Weller (1987) examined data from a large number of stands. He found some values of β not significantly different from −0.5 but some markedly so and suggested variation may be related to functional differences between species. For example, for angiosperm trees more shade-tolerant species had steeper more negative thinning slopes than intolerants, while for gymnosperm trees more shade-tolerant species had shallower slopes.

It is unfortunate that research into self-thinning largely came to a standstill following Weller's (1987) demonstration that the self-thinning coefficient varies between species. Norberg (1988) provided an analysis of why the self-thinning slope is steeper for trees. He suggested that herbaceous plants grow with a pattern of geometric similarity, i.e., increments of branches have the same structure throughout growth. In contrast, trees have elastic similarity, i.e., branches are maintained with the same posture which requires increasing wood increment along existing branch structures, so that mean weight per plant increases more rapidly as additional space is occupied. However, this does not explain why there may be differences between shade-tolerant and -intolerant tree species suggested by Weller (1987; see also Zeide, 1985).

Important, but somewhat neglected, research by Carleton and Wannamaker (1987) suggests initial stand conditions affect the self-thinning process. In a post-fire, naturally regenerated stands of *Pinus mariana*, self-thinning occupied a distinct but limited period of stand development. While all stands went through a distinct self-thinning period, the steepness of the mortality slope was related to initial stand density and stands did not self-thin to the same final density. Stands of high initial density, ca. 194 stems per 0.01 ha, self-thinned to some 100 stems per 0.01 ha and stands with low initial density, ca. 65 stems per 0.01 ha, which is less than the final density of initial high-density stands, also showed self-thinning.

SUMMARY DESCRIPTION OF THE COMPETITION PROCESS IN STANDS AND POSSIBLE ARCHITECTURAL EFFECTS

The most informative result from stand investigations is that large plants and/or survivors show spatial inhibition. A simple

explanation is that two large plants cannot continue to grow at the same position, but in reality a complex process of spatial equalization of relative growth rates is likely required to produce this structure (Turley and Ford, 2011). Large plants are always likely to shade smaller neighbors but the crucial contest in development of spatial evenness is between neighboring large plants. The effect of competition experienced by a large-sized individual is likely to be greater when it has multiple large-sized plants as close neighbors. Plants A, B, and C (**Figure 1C**) have close contacts with another large plant and one of each pair is more likely to become suppressed than the other large plants represented in **Figure 1C**. As large plants decrease in number, the survivors would remain in a spatially even distribution. The process of resource acquisition plasticity (see section Plants as Competitors) is implicated in the asymmetric crown development that is likely to develop in these upper crowns. Spatial evenness seems to be ubiquitous where competition has occurred but differences in plant architecture could influence the rate at which crown interactions take place (Stoll and Bergius, 2005) and the depth of crown that might be involved.

The process outlined in **Figure 1** results in larger plants having higher RGR and can cause formation of a distinct upper canopy and a bimodal frequency distribution of plant weights and heights (**Figure 2**). Detection of these features requires precision in measurement and analysis, and a population of sufficient size to avoid type II statistical errors. Such analyses could be used to define the effects of architecture on stand structure and productivity. For example, Vega and Sadras (2003) explicitly suggest that high productivity is associated with lack of bimodality in size–frequency distributions. Modal analysis can be made using the methods of Fraley et al. (2012).

SOME POPULATION THEORY ON COMPETITION

Attempts have been made to classify the type of competitive interactions occurring between individuals within a stand. These have their origin in description of interactions between individuals represented as overlapping circles. Gates (1978) first suggested that one-sided competition, where the larger of two overlapping plants obtains all resources in the area of overlap, is sufficient to explain

the development of bimodal populations. This approach was continued by Gates et al. (1979) who calculated how differences in crown structure may affect the area of overlap, and division of resources in the overlap, between neighboring plants. Under conditions where smaller plants may have some effect on larger ones, but a lesser effect, then competition has been termed asymmetric (Weiner and Thomas, 1986; Weiner, 1990; Schwinning and Weiner, 1998). The principal objections to these approaches are that competition is a three-, rather than two-dimensional process (Reynolds and Ford, 2005) and that within a stand there may be different types of interactions. These objections would severely limit the effectiveness in using such models in analysis of architectural effects on competition.

PLANTS AS COMPETITORS

Three properties of plants may influence competition above ground as a 3-D process. (i) Resource acquisition plasticity, by which plants preferentially extend branches and/or foliage into regions where there are resources. (ii) Morphogenetic plasticity, by which plants respond to competition by changing their morphology, e.g., the increase in relative height growth of shaded plants. (iii) Architectural variation in interception and utilization of light: absorption of light by one plant obviously makes it unavailable for another and so will affect competition but efficiency of utilization of light in growth may also affect competition.

RESOURCE ACQUISITION PLASTICITY

Umeki (1995) showed preferential growth of crowns of *Xanthium canadense* in the direction of resources over a growing season (0.5 plants m^{-2}, mean plant final height 1.94 m, no mortality). Crown centers became significantly displaced from stem centers and as the population grew the spatial pattern of crown centers became regular. An index for neighborhood interference accounted for significant variation in plant RGR when calculated using crown center location, but not when calculated using stem location. Umeki (1997) developed a neighborhood model, i.e., representing plants in two dimensions, to calculate neighbor–neighbor effects. Crowns were represented as circular
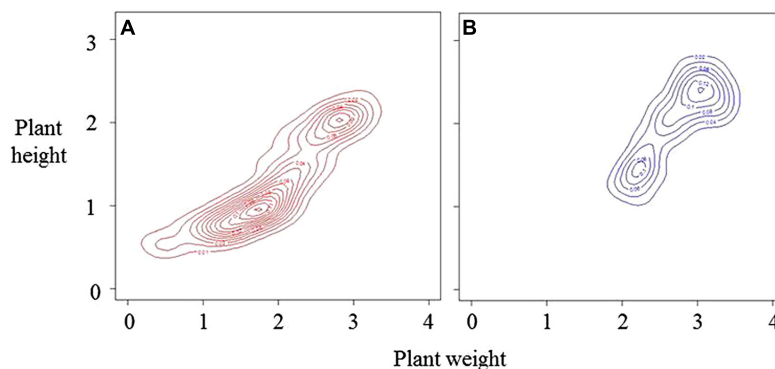

FIGURE 2 | Bivariate distributions of height and weight on the same arbitrary scales for a developing population over two time periods, A the younger stage, and B (based on Turley and Ford, 2011). The distributions are represented by density estimations using kernel smoothing (Wand and

Jones, 1995). Both distributions show distinct bimodality. At stage **A**, small-sized plants are the major mode. During the period of growth between **A** and **B**, some 60% of total plants died reducing the number of plants in the small-sized mode.

but with their centers moved relative to plant position to represent the asymmetry with the effect being calculated using a vector. The vector is based on the target plant's height in relation to the height, distance and direction of neighbors. Development of crown asymmetry produced larger survivorship, larger mean size, a more regular spatial pattern of survivors and less skewness in size distributions.

Crown asymmetry has also been found in tree species. Rouvinen and Kuuluvainen (1997) found two thirds of trees in a 150–200 y *Pinus sylvestris* forest in eastern Finland had asymmetric crowns. This asymmetry was positive toward the major direction of incoming radiation, but modified by competitive status so that trees with markedly asymmetric crowns were those with free growing space and close competitors in other directions. For *Acer saccharum* Brisson (2001) found neighbors to have a strong influence on orientation of crown asymmetry. The correlation between crown asymmetry and neighbors was greatest when only size and distance of the strongest neighbor was considered suggesting that this neighbor may have a disproportionate effect on crown symmetry of the target tree.

Koike (1989) suggests that shoots develop toward brighter light without there being a phototropic effect—the growth is due to utilization of the greater available resources. For crowns of two evergreen *Quercus* species, *Quercus acuta* and the more shade-tolerant *Q. gliva*, shoot production increased with increasing light received for both species. However, the critical level of light necessary for shoot production was that a shoot should receive ∼10% that of an open sky for *Q. gliva* and ∼30% for *Q. acuta*, but both the numbers of shoots produced and shoot length at higher light intensities was much greater for *Q. acuta*. For both species, shoot direction was significantly affected by geotropism. The finding that branches and foliage in the upper canopy respond to greater available resources is coherent with the finding that competition produces a spatially even distribution of large plants and survivors. It also suggests that branches do not provide resources to other parts of the plant that would restrict their own growth. This can be partially explained through the concept of branch autonomy (Sprugel et al., 1991).

Branch autonomy, with respect to carbon economy, implies that branches do not import carbon they use in growth but fix it locally on the branch. Consequently, sunlit branches that fix more carbon should grow more. In their review, Sprugel et al. (1991) note three general results: (i) old shaded branches do not import carbon—maintenance respiration alone is not a sufficiently strong sink to draw carbohydrates into a branch; (ii) the internal balance of sources and sinks is such that branches are self-supporting during growing seasons; (iii) branches are least autonomous when carbon reserves are involved—particularly when substantial reserves are stored in the main stem. Local supply of carbon on a branch through current photosynthesis can be sufficient to support periods of high growth, e.g., in shoot extension, so that storage carbohydrate may not be involved. Sprugel et al. (1991) note that bud formation is a crucial process in species with determinate growth since buds, once they start to grow, can draw carbon but that the formation of buds is unlikely to be limited by carbon availability since only small amounts are required.

Branch autonomy is a useful model for considering carbon economy of established branches within an existing crown but fails as a model for describing differences in branches between trees of different sizes within a canopy (Sprugel, 2002). Stoll and Schmid (1998) found that the growth of shaded branches was less in trees that were partially shaded than in trees that were completely shaded. Sprugel (2002) offers possible explanations for this phenomenon, one being that shaded foliage on dominant trees becomes water limited when sunlit branches elsewhere on the tree are strong sinks for water. Sprugel (2002) references evidence that vascular constrictions at the base of branches keep the water system of a branch somewhat isolated from the rest of the tree so that water flow will be directed to more illuminated branches. Boonman et al. (2007) demonstrated for foliage canopies of *Nicotiana tabacum* that cytokinin in the transpiration stream affects photosynthetic rate of foliage and when transpiration is reduced photosynthesis rate declines. If this result holds for trees, it may help to explain differences in branch growth on sunlit and shaded crowns.

Resource acquisition plasticity can have two consequences for competition dynamics. In the upper canopy, it may lead to preferential expansion of foliage into places where light is not utilized and so may be the driver for continuing development of dominant plants. The extent to which this may be constrained by plant architecture has not been studied in the context of competition dynamics. A second consequence may be in reduced growth, or even death, of foliage in the lower crowns of dominant plants, but at similar height the foliage of suppressed plants is not reduced. This may aid survival of suppressed plants.

MORPHOGENETIC PLASTICITY

Morphogenetic plasticity is the most studied plant architectural feature that may affect competition—largely due to wide interest in phytohormones. Selective absorption of red wavelengths (660 nm) by foliage relative to far-red wavelengths (735 nm; Smith, 1982; Franklin, 2008) results in decrease of the ratio of red to far red (R:FR) with increasing depth in a foliage canopy (e.g., Evers et al., 2007; Dauzat et al., 2008; Kahlen et al., 2008; Kahlen and Stützel, 2011a,b). This decrease can produce a number of morphological responses (e.g., Smith and Whitelam, 1997; Kahlen and Stützel, 2011a) mediated by the phytochrome photoreceptor system and frequently grouped together as the "shade avoidance" response (Franklin, 2008).

Morphogenetic plasticity is, primarily, a process of reaction to neighbors and may slow, or perhaps even halt, the progression toward suppression and death. Height growth is one of the most studied examples whereby plants increase height growth in response to decrease in R:FR in herbaceous plants (Ballaré et al., 1987, 1994; Ballaré and Scopel, 1997) but reduced tiller production in grasses also occurs at low R:FR (e.g., Evers et al., 2006). For *Impatiens capensis* Donohue and Schmitt (1999) suggest that primary responsive characters to changes in R:FR are increased internode elongation, decreased branch, flower, and node production, and increased meristem dormancy.

However, although effects of changes in R:FR can be demonstrated experimentally their actual effects on competition may

be restricted to limited conditions. Casal et al. (1986) showed a photosynthetically active radiation (PAR) requirement response to reduced R:FR decrease. They grew *Paspalum dilatatum* and *Lolium multiflorum*, grasses of the Argentinian pampas, at different densities (2.0–31.9 plants m^{-2} for *P. dilatatum*, 39.8–116.3 for *L. multiflorum*) and illuminated some individuals with red light at the plant base which stimulated tillering at low but not high densities. Casal et al. (1986) indicate that limits for tillering are established by: (i) insufficient PAR in very dense canopies, which may result in reduced resources for growth; (ii) insufficiently low R:FR in sparse canopies (see also Monaco and Briske, 2001). An exception to the lack of an R:FR effect at low plant densities may be where FR is reflected horizontally so that R:FR is reduced by an increase in FR by reflection from neighbors rather than by a decrease in R through absorption of vertical beams (Ballaré et al., 1988). This effect may enable anticipation of canopy competition.

There is dispute whether height growth stimulation produced by decrease in R:FR has a cost in terms of reduced biomass growth in other parts of the plant. Maliakal et al. (1999) working with *I. capensis* and Ballaré et al. (1991) with *Amaranthus quitensis* both report that stimulation of height growth does not cause a reduction in root or leaf growth. On the other hand, Vermeulen et al. (2008a) found through experimental manipulation of R:FR, an increase in petiole length and petiole mass for *Potentilla reptans* but decrease in root, stolon, and total biomass. They also report that petiole length can be limited by the productive capacity of plants. Direct application of gibberellic acid to stems of *Phaseolus vulgaris* produced the expected increase in stem elongation but a concomitant reduction in total mass, pod number, and pod mass (Cipollini and Schultz, 1999).

Whether there is a carbon cost to R:FR-induced height growth could be important in considering its possible effect on competition. Dudley and Schmitt (1996) manipulated R:FR supplied to seedlings of *I. capensis* to produce stem-elongated and non-elongated plants. These seedlings were transplanted to within both high- (plants 3 cm apart) and low- (20 cm apart) density arrays. Lifetime fitness was calculated as number of reproductive structures produced over the lifetime of the plant. Elongated plants were more fit at high density and non-elongated plants at low density. Dudley and Schmitt (1996) suggested the advantage of elongated plants at high density was that greater height resulted in greater light capture, while their disadvantage at low density may be the result of the additional carbon cost of increased height. In a comparison of eight genotypes of *P. reptans* grown in a mixture to form single-species stands, Vermeulen et al. (2008b) found that genotypes with relatively more leaves in the top layer of the canopy were, on average, more efficient in light capture per unit leaf weight.

Photomorphogenetic-induced height increase can change plant population structures through increasing survival of smaller plants. However, the extent of this effect on the competition process, as a whole, is likely affected by the conditions of growth, particularly spacing, and the genetic structure of the population. We need to know the balance between change in R:FR in relation to PAR level for particular instances and to define how this relationship may change as the plant stand increases in height and total foliage amount. Interestingly, Dudley and Schmitt (1995) showed that while populations of *I. capensis* from more open conditions, where there was likely considerable competition for light, showed photomorphogenetic-induced height growth, populations from more shaded conditions did not. Schmitt (1997) cites additional examples of similar ecotypic variation. Certainly, we can anticipate limitation to the effect that a decrease in R:FR may have in rescuing the growth of over-topped plants since we know that small plants do die due to the effects of competition.

ARCHITECTURAL VARIATION IN INTERCEPTION AND UTILIZATION OF LIGHT

Much research has been conducted into variation in plant structure on light absorptance but primarily with a standpoint of examining the efficiency of whole canopies rather than possible effects on competition within a stand (Niinemets, 2010). However, there are reasonable grounds for considering that architectural variation found between competing plants may influence competition through their effects on interception and utilization of light, e.g., Bendix et al. (2010). Leaf angle and the spatial distribution of leaf biomass can be affected by plant density (Vandenbussche et al., 2005; van Zanten et al., 2010) as well as leaf orientation, e.g., in maize (Drouet and Moulia, 1997) and cucumber (Kahlen et al., 2008). Some rosette species show hyponastic leaf growth in response to crowding, i.e., where leaves bend upwards, which can reduce the impact of competition: Pierik et al. (2003) planted hyponasty loss-of-function transgenic plants along with wild-type *Nicotiana tabacum* at the rosette stage of development and demonstrated that the transgenic was outcompeted.

Anten and Hirose (1998) calculated light absorption by individual plants in natural monospecific stands of *X. canadense*, a fast-growing, shade-intolerant annual. Dominant plants absorbed more light both per unit leaf area (Φ_{area}) and per unit mass (Φ_{mass}) and that the greater Φ_{area} more than compensated for the lower leaf area ratio of dominant plants. They concluded that the greater Φ_{mass} of dominant plants is quantitative evidence that success in competing for light is disproportionally related to the size of shoots. The proportion of mass in leaf lamina, the leaf mass ratio (LMR), decreased with increasing height but solitary plants had higher LMR than competing plants of the same height. Anten and Hirose (1998) concluded that LMR is not determined by biomechanical constraints but results from a plastic shift in allocation in response to competition.

From the perspective of competition, the production of foliage has two functions: certainly one is production of photosynthate for growth but the other can be simply shading neighbors even if there is no net gain in photosynthesis to the producing plant. Trends in development of *Zea mays* hybrids provide an example where reduced competition may contribute to an increased in total crop yield. Commercial hybrids have been selected, and commercially planted, in the central corn belt of the United States (Duvick et al., 2004) at increasingly closer spacing from ~30,000 plants ha^{-1} in the 1930s to ~75,000 plants ha^{-1} or higher by the 1990s. Production has increased markedly over this period and while a number of phenotypic characters have

changed (Duvick et al., 2004) whole canopy efficiency (yield per ground area) has increased. Ford et al. (2008) compared the major hybrid used in the 1960s with that in the 1990s and found the 1990 hybrid had smaller leaves. Maize leaves are curved and Ford et al. (2008) found less curvature and more uprightness for the 1990 hybrid compared with that for the 1960 hybrid and so, potentially a reduced competitive influence. Interestingly, experimental manipulation of foliage of the same 1960s hybrid, by tying leaves into a more upright position, produced an increase in yield (Pendleton et al., 1968). Curvature is a plastic character in response to plant density and while Ford et al. (2008) found both hybrids had less curvature at higher planting density the effect was greatest for the 1990 hybrid. Fellner et al. (2003, 2006) show that this plasticity is related to an interaction between light quality and auxin particularly in the development of the leaf auricle.

How can a decrease in leaf size and an increase in leaf inclination increase productivity of a whole stand and do these changes reduce competition between individuals? Generally, increased leaf inclination from the horizontal will reduce incident quantum flux density on the leaf surface although the exact effect depends upon sun angle, foliage inclination, and the azimuth between sun and plane of the laminar surface. The effect of more upright foliage may be more appropriately thought of as reducing the duration of high incident quantum flux density.

Lateral extension of uppermost leaves may reduce light received by neighbors, but that light may be intercepted by the larger plant at intensities in excess of the light saturation point of the photosynthesis curve. An increase in inclination of these leaves, and reduction in their size, may reduce total light intercepted but not necessarily the total amount of whole-plant photosynthesis since uppermost leaves may still receive light close to the light saturation point of photosynthesis for considerable periods and more light will reach lower, more shaded, foliage. Reduced exposure of foliage to high irradiance may reduce the possibility of photo-damage and/or high evaporative demand on the foliage, e.g., Falster and Westoby (2003) for sclerophyllous plants.

Conifers also have consistent modifications to foliage in response to differences in ambient light levels. In the *Pinacea* foliage, needles are clumped around the supporting shoot at higher light levels and more spread out at lower levels and this is measured by the silhouette to area ratio (STAR), e.g., Stenberg et al. (2001) for *P. sylvestris*. In the *Cupressaceae*, which has foliage in fronds, there are multiple variations in foliage and branch structure as light varies, e.g., Edelstein and Ford (2003) for *Thuja plicata*.

In summary, although investigations of plants as competitors have shown the importance of considering competition as a 3-D and not 2-D process we still lack investigations of canopy formation, particularly of the effects of differences in resource acquisition plasticity. The three features of plants as competitors (resource acquisition plasticity, morphogenetic plasticity, architectural variation in interception and utilization of light) should not be considered separately although the history of the subject shows that they have been—which is not surprising given the details of the research required.

DEVELOPMENT OF THEORY FOR THE EFFECTS OF PLANT ARCHITECTURE ON COMPETITION

Competition theory based on studies of populations and stands has been challenged and found wanting. This is not surprising. Competition can affect the component parts of plants differently (sec Plants as Competitors) and the effect on the individual, as a whole, results from the integration of many such interactions. The size of an individual is only an approximate indication of competitive status and can neither be used to indicate the component interactions that will occur nor how their effects may be integrated.

Nevertheless, studies of stands undergoing competition provide essential descriptions of what needs to be explained. They show that the process has multiple effects on stand structure in the numbers of plants that survive or reproduce, the distribution of plant sizes, and the spatial distribution of individuals. These effects are interrelated but the relationships may vary between species and conditions of growth. Unfortunately, some research into the properties of plants as competitors has selected just one component of stand development as an indicator of competition. This can lead to a biased view of the process as a whole and inadequate understanding of the role of particular properties.

This section outlines a theory for analyzing the dynamics of architectural effects on competition. However, prior to that it is necessary to define what the theory should be able to explain both in general terms and in details of stand development.

WHAT SHOULD THE THEORY BE ABLE TO EXPLAIN?

There are considerable challenges in establishing a relationship between plant architecture and competition. Plant morphology is diverse and this presents us with a conundrum. If competition for light is ubiquitous then why has there not been evolution for an obviously successful architecture? Niklas (1997) suggests the requirement to conserve water reduced phenotypic options available to the earliest land plants. However, once this adaptive hurdle was overcome the next requirement was to achieve effective performance of multiple functions simultaneously—such as maximizing both light interception and reproductive success and ensuring mechanical stability—which took place where plants were growing together in communities. This increased the number of phenotypic options that had equivalent relative fitness. A system with a single defined task has fewer alternative designs compared to that for systems with manifold tasks which may be globally efficient yet comparatively poor at doing any one task. This implies there are multiple answers to the apparently simple question of what makes an effective competitor and a theory for the effects of plant architecture on competition should be required to show how different combinations of features may have similar results.

Population- and stand-level studies illustrate that the intensity of competition and the results it produces change over time. For practical purposes, this requires that investigations and studies should be assessed on rates of change rather than outcomes at a single point in time. Consider a study that compares plants with different architectures, e.g., the pioneering study by Geber (1989) which compared effects of differences in

morphology between two species of *Polygonum* on competition. We can ask:

1. Is there a difference in the rate with which spatial inhibition develops? An advantage of this test is that spatial inhibition is the most reliable indication that competition has occurred. Disadvantages are that spatial inhibition may take considerable stand development before it is apparent and that use of distance statistics requires care (Loosmore and Ford, 2006).

2. Are there differences in the relationship between plant size and RGR? An advantage of this test is that it is likely to indicate competition at an early stage in stand development. Disadvantages are that, generally, calculation of RGR requires repeated measurements of plants which can be difficult in stands of many plants and that we have little background information about the distribution of RGR of different components of plants, e.g., height, weight, foliage area.

3. Are there differences in rates of change in the frequency distributions of plant sizes? Some difficulties of using frequency distributions have already been discussed. Use of the bivariate plant height: plant weight distribution has the advantage of providing more information about stand structure than univariate distributions.

In practice, competition has multiple effects and more than one metric should be used. Techniques for multi-criteria assessment are discussed by Reynolds and Ford (1999) specifically for competition; Ford and Kennedy (2011) for FSPMs; Kennedy and Ford (2012) as a general strategy of investigation.

STRUCTURE FOR A THEORY TO INVESTIGATE THE EFFECTS OF PLANT ARCHITECTURE ON COMPETITION

Five groups of postulates are required to analyze the effects of differences in architecture on competition. These are given in general terms here and specific postulates would need to be developed for particular questions.

Group 1

Competition for light takes place at the level of foliage and foliated axes rather than whole plants—save for small plants that have only a single foliated axis.

This is the foundation postulate for attempts to explain competition through architecture and provides a clear distinction from population or whole-plant-based theories. It ensures that explanations for differences that we may see in competition will be sought in differences in the processes of plant growth. A corollary is that the effects on the whole plant depend upon integration of affects across all foliage and foliated shoots (see Group 4). Section "Architectural Models and Competition Dynamics," on modeling illustrates the importance, and difficulty, of explaining how this integration in the growth of the whole plant takes place.

Group 2

The outcome of competition is determined by interaction between two processes:

- *Exertion of dominance* through growth of foliage or a foliated axis that intercepts light that would otherwise could be utilized by neighboring foliage and;

- *Reaction to shading* through changing form and/or physiological characteristics.

This postulate is fundamental to determination of the dynamics of the competition process. Exertion of dominance can occur through resource acquisition plasticity and may be affected by efficiency of interception and utilization of received PAR. Reaction to shading can be through morphogenetic plasticity. Both process *Exertion of dominance* and *Reaction to shading* may occur on different parts of the same plant (see Group 4) and the results for plant growth and/or survival depend upon the integration of effects. It is important that studies claiming to define competition as some result of a particular architecture should define both processes. We have many studies (see Plants as Competitors) demonstrating that one or the other of these processes occur but their effects on the competition process require analysis of both components in the dynamic system.

The implication of specifying competition in this way is that the primary process is the exertion of dominance and that morphogenetic plasticity is a *reaction* to that but does not halt it or stop its effects completely. So we can expect to see stand structural characteristics that indicate competition has occurred even in roseate plants such as *Arabidopsis* (e.g., Stoll and Bergius, 2005). The intensity of competition might be considered as the extent to which *Exertion of dominance* exceeds *Reaction to shading*. The rate at which these two processes proceed may change during stand development. This is the central group of postulates that defines the work to be done to develop understanding of architectural effects on competition because it indicates the dynamics of interaction.

Group 3

Architectural properties of a species determine both *Exertion of dominance* and *Reaction to shading*.

Comparative analysis of species seems to be an important approach to analyze the effects of architecture on competition. Research has shown (see Plants as Competitors) that plant species exhibit different responses to being crowded but analysis of architectural effects on competition requires that exertion of dominance and responses to shade be quantified simultaneously.

Group 4

For an individual plant, the outcome of competition depends upon integration of effects of *Exertion of dominance* and *Reaction to shading* across the component foliage and foliated shoots.

Individual plants may simultaneously exhibit, in different parts, both resource acquisition plasticity, differences in interception and utilization of PAR, and forms of morphogenetic plasticity depending on their size, modularity of construction and architecture. In Section "Architectural Models and Competition Dynamics," the importance of understanding the integration of plant growth is illustrated.

Group 5

Mortality is a time-delayed response to suppression. It is an important result of competition, particularly in dense stands or those where competition persists for long periods as in stands of trees.

However, it is not generally studied in relation to architectural effects.

ARCHITECTURAL MODELS AND COMPETITION DYNAMICS

Simulating competition provides an excellent test for functional–structural plant models (FSPMs; Godin and Sinoquet, 2005) because it requires effective representation of plants as conditions change. Two types of problems have been encountered: how to represent the integration of plant function and how to define precise relationships for operation of morphogenetic plasticity.

INTEGRATION OF WHOLE-PLANT FUNCTION

Trees are interesting subjects for the study of plant competition. Their size and longevity raise questions about how effects of different parts of trees and how the effect of such competition is integrated in the growth of the whole tree.

Sorrensen-Cothern et al. (1993) investigated the extent to which morphogenetic plasticity affected competition. They simulated competition for light in a young stand of dense, naturally regenerated *Abies amabilis*. The model simulated growth of each individual tree in annual height and branch, including foliage increments, and the 3-D spatial location of branch and foliage was calculated.

Light was considered in contiguous vertical columns and absorption depended upon the total leaf area density and its interception characteristics that had morphogenetic plasticity depending on whether the tree was classified as a "sun," "intermediate," or "shade" individual, according to its relative height in the stand. No direct calculation of photosynthesis was made but a conversion efficiency, which varied between the three trees classes, was applied to the light absorbed to give a surrogate variable for photosynthate. The accounting system for the penetration and absorption of light, represented in vertical columns, allowed for spatial variability of light to have an effect on growth.

Height and individual branch increments were estimated through parameters applied respectively to the sum of the surrogate variable for the whole tree and the branch being considered. Branches grew as expanding fans of foliage with foliage density depending on the light level at each point within the branch, i.e., for the relevant 10 cm × 10 cm × 10 cm section. Model parameters were calculated using an extended sensitivity analysis.

When no plasticity was incorporated into the model, suppressed trees lost the structure found in empirical investigations. It was essential to incorporate plasticity in the amount of light absorbed per unit foliage as well as foliage survival in relation to light level to simulate observed changes in crown apex angles of suppressed trees, and correct crown lengths and to simulate the frequency distribution of tree heights and mortality.

In a subsequent uncertainty assessment of the model, Reynolds and Ford (1999) found it important to assign the plastic characteristics of foliage based on the local light level rather than based on classification of complete trees as sun, intermediate, or shade. The effectiveness of this model depended upon the interaction between resource acquisition plasticity and morphogenetic plasticity. Resource acquisition plasticity occurred because of the modular construction so that branches extended and grew into areas of greater illumination. This occurred through the depth of the canopy.

To simulate tree mass, further architectural information is required, particularly details on the structure of the tree body, i.e., the development of branches by increasing order, and representation of how branches thicken. Sievänen et al. (2008) developed LIGNUM (Perttunen et al., 1996) parameterized for *P. sylvestris* based on growth of successive metamers (Room et al., 1994) each comprising a woody pipe in the modular segment (node plus internode) terminated with apical and axillary meristems and covered with needles. LIGNUM was designed and. Wood increment to the body of the tree was calculated using the pipe-model theory (Shinozaki et al., 1964) which specified that the amount of foliage carried on a shoot section was matched by the cross-sectional area of sapwood of the shoot and that this cross-sectional area was propagated down through all more proximal shoots, branches, and the trunk. Based on empirical investigation, the sapwood area per unit foliage requirement declined with increasing branching order. The length, radius, and amount of foliage on new shoots were in proportions derived from empirical investigations. Segments became shorter as branching order increased. The length, and consequently other dimensions, was determined by the availability of photosynthate. After considering respiration losses, the photosynthate available for growth was considered in one pool and all of it distributed to growth.

The model simulated growth and development of trees over four decades giving effective 3-D images. However, Sievänen et al. (2008) noted a number of discrepancies from expected quantities. Generally, branch diameters and branch lengths were greater than expected, and the number of surviving branches was greater. Branch mortality in the model only occurred close to the base of the live crown, whereas field studies showed it to be distributed over more of the crown length. Increasing the density of trees in the plot decreased tree diameter as expected. An interesting result was that increase in foliage density along shoots caused lower photosynthesis per unit mass. Shoot extension was greater with lower foliage mass which increased both photosynthesis, by decreasing crowding, and production of woody material.

Sievänen et al. (2008) commented that considering the resources available for growth in one pool may not be appropriate. If resources are low then all growing segments grow less so that, for example, a branch producing less than it consumes in respiration decreases the growth of branches that produce a surplus. This does not agree with branch autonomy (Sprugel et al., 1991). Sievänen et al. (2008) noted that the larger dimensions of branches produced by the model than found in measurements may be due to inadequacy in the light model component or application of the pipe model.

Competition for a number of species (*Fagus sylvatica*, Letort et al., 2008; *Pinus tabulaeformis*, Guo et al., 2012) have been studied using the GREENLAB model (Yan et al., 2004) which comprises a formal grammar to describe plant structure. Mathieu et al. (2009) presented a version where increment to the plant body

depends upon the ratio of biomass produced to demand from new meristems. The plant grew as a collection of sinks competing for allocation of photosynthate. Net photosynthate production was calculated from radiation interception which depended upon a calibrated radiation use efficiency and a coefficient related to the projected ground surface area of the plant. Biomass was stored in a common pool and distributed among new and existing organs according to calculated sink values. Distribution to the cambium was computed according to the pipe-model theory. A feedback between growth and development was included whereby the number of branches and the composition of growth units depended upon the ratio of the increment pool of biomass/plant demand which is the sum of all sinks in the current growth cycle.

Plants were simulated in a homogenous stand and competition was the result of shading which affects biomass increment and, as plant density increases, a greater priority in allocation was given to height growth. Mathieu et al. (2009) discussed four issues. First, organogenesis may not be strictly controlled by the ratio of available biomass to demand. Second, the inability of the model to reproduce the spatially heterogeneous expression of plasticity, which they comment cannot be neglected in large trees. Third, the hypothesis of a common pool of photosynthate may not be adequate. Fourth, in some instances the supply of photosynthate may be regulated by demand.

CANOPY DEVELOPMENT, LIGHT INTERCEPTION, AND COMPETITION

Models that simulate penetration of light into canopies based on absorption, reflection, and transmission for individual structural elements of the canopy particularly that of Chelle and Andrieu (1998) have stimulated research into canopy development and competition. When combined with a model for detailed geometry of the foliage canopy estimates can be made of light conditions at the organs of individual plants and their light-dependent growth. In the two cases reviewed here, the investigators reported advances in understanding provided by modeling as well as improvements they consider should be made to models.

From empirical investigations with spring wheat Evers et al. (2006) reported that the probability of tiller appearance decreased earlier in crop development at higher population density. Their simulation study (Evers et al., 2007) was designed to investigate the form of the relationship between R:FR and the relative extension of a tiller bud. Evers et al. (2007) used an architectural model, ADEL-wheat (Fournier et al., 2003) calibrated for spring wheat (Evers et al., 2006, 2007) and the nested radiosity light interception model (NR) of Chelle and Andrieu (1998). ADEL-wheat simulates production and growth from a given initial planting of phytometer units comprising a leaf (blade and sheath) inserted on a node, an internode, and a tiller bud. ADEL-wheat calculates leaf size and shape, basal angle, and curvature, and blade and tiller azimuth angles. Each leaf is defined by a set of polygons with coordinates that establish their position in space. This geometry was interfaced to NR which calculates irradiance on, and energy absorbed by, each simulated plant organ.

Evers et al. (2007) hypothesized that the growth of tiller buds was arrested when R:FR received fell below a threshold value. Tiller bud extension was represented in ADEL-wheat by an exponential growth function

$$L = L_0 e^{F.RFR_p.t},$$

where L is the bud length, L_0 is the initial bud length, RER_p is the potential relative extension rate $(^oCd)^{-1}$, t is the thermal time (^oCd) since the initiation of the bud. F was a function of R:FR so that F decreased as R:FR decreased and three forms were examined, a threshold value and curvilinear or linear decrease.

Simulations were conducted for a range of initial planting for which the time course of numbers of tillers.plant^{-1} had been measured in field experiments. Evers et al. (2007) noted that a threshold function with an R:FR value of 0.8–0.9 was required to simulated both a comparable tillering rate to field data and a final tiller number to that found experimentally. This was considerably higher than found in measurements and they suggest this may be due to use of a higher above canopy R:FR, 1.2, than is actually found under natural conditions.

Dauzat et al. (2008) combined the modeling strategy of using an architectural and a light penetration model with analysis of canopy structure using the 3-D Fastrack digitizer (Polhemus Inc., Sinoquet and Rivet, 1997). They studied growth of cotton at three densities, 1, 2, and 4 plants m^{-2}. They anticipated that greater morphogenetic plasticity would occur at higher planting densities and investigated the effects of these changes on crop efficiency in intercepting light over a growing season. Measurements were made of crop cover, time courses of plant height growth, and leaf area.

They observed that morphogenetic plasticity varied with plant density and stage of development of the stand with a transition between increasing internode lengths in the lower part of the stem and decreasing internode lengths in the upper part. Dauzat et al. (2008) suggested that while the pattern of increasing internode lengths early in development was consistent with decreasing R:FR this was counteracted by plant carbon limitations during the latter phase. They noted that internode length and leaf area increment decreased simultaneously. The transition between the two phases occurred when average leaf irradiance decreased below 60% of incident PAR.

CONCLUSION

Although it seems intuitively obvious that plant architecture should affect competition for light between plants we have little knowledge about the effects that different architectural features may have on the competition process. Not surprisingly, pioneering studies that demonstrated such effects (Ellison and Rabinowitz, 1989; Geber, 1989) used plants with large contrasts. Niklas (1997) description of how multiple plant forms may have arisen suggests that obtaining an understanding of competition effects may be a considerable challenge. Nevertheless, explaining competition effects is one of the important challenges faced by FSPMs because of the range of information that must be integrated into a model.

Much research into competition has been conducted with a standpoint of population biology and such work enables us to define some effects of competition on stands and individual plants. However, it has not provided an analytical framework for analysis

of the effects of architecture on the process. Studies of plant functioning in stands undergoing competition have shown interesting responses to changes in the environment as a stand develops. However, the assessment of effects on competition in such work has typically been limited to measurements that only give a partial representation of the competition process and interactions between different aspects of physiology and morphology have largely been ignored.

Section "Development of Theory for the Effects of Plant Architecture on Competition," of this review outlines a basic structure of a theory for analyzing the influences that architecture may have on competition and how such a theory may be assessed. The research reviewed here was conducted on multiple species growing under different conditions. The proposed theory is a synthesis from this wide ranging work. Postulates for two groups of ideas are central. Group I—that competition for light takes place at the level of foliage and foliated axes—defines competition as a local event within the canopy. To a considerable extent, it tallies with theories of plant growth based on modular development of plants and branch and foliage reiteration. Use of this postulate in models for competition would reorient how such models are constructed.

Group II defines the outcome of competition as determined by the interaction between the exertion of dominance, particularly through resource acquisition plasticity, and reaction to shading through changing form and/or physiological characteristics. This suggests it is essential to study *interactions* between these processes rather than just one or another. The pioneering work of Casal et al. (1986) did this, at least to the extent of showing the importance of a certain level of PAR being necessary for a response to changes in R:FR. It was unfortunate that this duality in approach was not continued as it led to larger claims being made for the importance of morphogenetic plasticity than are warranted. The field study of Dauzat et al. (2008) showing a change over time in the control of internode length, from R:FR to carbohydrate limitation reinforces the need for this approach.

Work with tree species illustrates that considerable development of the Group 4 postulates on integration of plant growth is essential. Although it seems reasonable that competition for light should be accounted at the level of foliage and the foliage-bearing structure, understanding and representing how such units are sustained requires considerable work. The idea of a whole-plant carbon pool and the pipe-model theory for addition of wood need to be replaced and this suggests that further research is required into the interactions between carbohydrate metabolism and the structures produced for water conduction.

Section "Development of Theory for the Effects of Plant Architecture on Competition" illustrates the value of models, when combined with field investigations. Laboratory-based investigations present us with possibilities that certain processes may be important—but the experimental conditions under which they are established may not reflect those found in developing stands. Stand conditions do need to be documented carefully.

REFERENCES

Anten, N. P. R., and Hirose, T. (1998). Biomass allocation and light partitioning among dominant and subordinate individuals in *Xanthium canadense* stands. *Ann. Bot.* 82, 665–673. doi: 10.1006/anbo.1998.0729

Ballaré, C. L., Sanchez, R. A., Scopel, A. L., Casal, J. J., and Ghersa, C. M. (1987). Early detection of neighbour plants by phytochrome perception of spectral changes in reflected sunlight. *Plant Cell Environ.* 10, 551–557. doi: 10.1111/1365-3040.ep11604091

Ballaré, C. L., Sanchez, R. A., Scopel, A. L., and Ghersa, C. M. (1988). Morphological responses of *Datura ferox* L. seedlings to the presence of neighbours. Their relationships with canopy microclimate. *Oecologia* 76, 288–293. doi: 10.1007/BF00379965

Ballaré, C. L., Scopel, A., Jordan, E., and Vierstra, R. D. (1994). Signalling among neighboring plants and the development of size inequalities in plant populations. *Proc. Natl. Acad. Sci. U.S.A.* 91, 10094–10098. doi: 10.1073/pnas.91.21.10094

Ballaré, C. L., Scopel, A. L., and Sánchez, R. A. (1991). On the opportunity cost of the photosynthate invested in stem elongation reactions mediated by phytochrome. *Oecologia* 86, 561–567. doi: 10.1007/BF00318323

Ballaré, C. L., and Scopel, A. L. (1997). Phytochrome signalling in plant canopies: testing its population-level implications with photoreceptors mutants of *Arabidopsis. Funct. Ecol.* 11, 441–450.

Bendix, J., Silva, B., Roos, K., Göttlicher, D. O., Rollenbeck, R., Nauss, T., et al. (2010). Model parameterization to simulate and compare the PAR absorption potential of two competing plant species. *Int. J. Biometeorol.* 54, 283–295. doi: 10.1007/s00484-009-0279-3

Bivand, R. (2009). "Package 'spdep'," in *R Core Team (2012) R: A Language and Environment for Statistical Computing.* Vienna: R Foundation for Statistical Computing.

Bivand, R., Pebesma, E., and Gómez-Rubio, V. (2013). *Applied Spatial Data Analysis with R*, 2nd Edn, New York, NY: Springer. doi: 10.1007/978-1-4614-7618-4

Boonman, A., Prinsen, E., Gilmer, F., Schurr, U., Peeters, A. J. M., Voesenek, L. A. C. J., et al. (2007). Cytokinin import rate as a signal for photosynthetic acclimation to canopy light gradients. *Plant Physiol.* 143, 1841–1852. doi: 10.1104/pp.106.094631

Brisson, J. (2001). Neighborhood competition and crown asymmetry in *Acer saccharum. Can. J. For. Res.* 31, 2151–2159. doi: 10.1139/x01-161

Carleton, T. J., and Wannamaker, B. A. (1987). Mortality and self-thinning in postfire black spruce. *Ann. Bot.* 59, 621–628.

Casal, J. J., Sanchez, R. A., and Deregibus, V. A. (1986). The effect of plant density on tillering: the involvement of R/FR ratio and the proportion of radiation intercepted per plant. *Environ. Exp. Bot.* 26, 365–371. doi: 10.1016/0098-8472(86)90024-9

Chelle, M., and Andrieu, B. (1998). The nested radiosity model for the distribution of light within plant canopies. *Ecol. Model.* 111, 75–91. doi: 10.1016/S0304-3800(98)00100-8

Cipollini, D. F., and Schultz, J. C. (1999). Exploring cost constraints on stem elongation in plants using phenotypic manipulation. *Am. Nat.* 153, 236–242. doi: 10.1086/303164

Cooper, C. F. (1961). Pattern in ponderosa pine forests. *Ecology* 42, 493–499. doi: 10.2307/1932235

Dauzat, J., Clouvel, P., Luquet, D., and Martin, P. (2008). Using virtual plants to analyse the light-foraging efficiency of a low-density cotton crop. *Ann. Bot.* 101, 1153–1166. doi: 10.1093/aob/mcm316

Donohue, K., and Schmitt, J. (1999). The genetic architecture of plasticity to density in *Impatiens capensis. Evolution* 53, 1377–1386. doi: 10.2307/2640884

Drouet, J. L., and Moulia, B. (1997). Spatial re-orientation of maize leaves affected by initial plant orientation and density. *Agric. For. Meteorol.* 88, 85–100. doi: 10.1016/S0168-1923(97)00047-6

Dudley, S., and Schmitt, J. (1995). Genetic differentiation between open and woodland *Impatiens capensis* populations in morphological responses to simulated foliage shade. *Funct. Ecol.* 9, 655–666. doi: 10.2307/2390158

Dudley, S. A., and Schmitt, J. (1996). Testing the adaptive plasticity hypothesis: density-dependent selection on manipulated stem length in *Impatiens capensis*. *Am. Nat.* 147, 445–465. doi: 10.1086/285860

Duvick, D. N., Smith, J. S. C., and Cooper, M. (2004). "Long-term selection in a commercial hybrid maize breeding program," in *Plant Breeding Reviews 24 (Part 2), Long Term Selection: Crops, Animals, and Bacteria*, ed. J. Janick (New York: John Wiley & Sons), 109–151.

Edelstein, Z. R., and Ford, E. D. (2003). Branch and foliage morphological plasticity in old-growth *Thuja plicata*. *Tree Physiol.* 23, 649–662. doi: 10.1093/treephys/23.10.649

Ellison, A. M., and Rabinowitz, D. (1989). Effects of density and emergence time on size hierarchy formation in populations of leafed and leafless peas (*Pisum sativum* L.). *Am. J. Bot.* 76, 427–436. doi: 10.2307/2444613

Evers, J. B., Vos, J., Andrieu, B., and Struik, P. C. (2006). Cessation of tillering in spring wheat in relation to light interception and red: far-red ratio. *Ann. Bot.* 97, 649–658. doi: 10.1093/aob/mcl020

Evers, J. B., Vos, J., Chelle, M., Andrieu, B., Fournier, C., and Struik, P. C. (2007). Simulating the effects of localized red:far-red ratio on tillering in spring wheat (*Triticum aestivum*) using a three-dimensional virtual plant model. *New Phytol.* 176, 325–336. doi: 10.1111/j.1469-8137.2007.02168.x

Falster, D. S., and Westoby, M. (2003). Leaf size and angle vary widely across species: what consequence for light interception? *New Phytol.* 158, 509–525. doi: 10.1046/j.1469-8137.2003.00765.x

Fellner, M., Ford, E. D., and Van Volkenburgh, E. (2006). Development of erect leaves in a modern maize hybrid is associated with reduced responsiveness to auxin and light of young seedlings in vitro. *Plant Signal. Behav.* 1, 204–211. doi: 10.4161/psb.1.4.3106

Fellner, M., Horton, L. A., Cocke, A. E., Stephens, N. R., Ford, E. D., and Van Volkenburgh, E. (2003). Light interacts with auxin during leaf elongation and leaf angle development in young corn seedlings. *Planta* 216, 366–376. doi: 10.1007/s00425-002-0881-7

Ford, E. D. (1975). Competition and stand structure in some even-aged plant monocultures. *J. Ecol.* 63, 311–333. doi: 10.2307/2258857

Ford, E. D., Cocke, A., Horton, L., Fellner, M., and Van Volkenburgh, E. (2008). Estimation, variation and importance of leaf curvature in *Zea mays* hybrids. *Agric. For. Meteorol.* 148, 1598–1610. doi: 10.1016/j.agrformet.2008.05.015

Ford, E. D., and Kennedy, M. C. (2011). Assessment of uncertainty in functional-structural plant models. *Ann. Bot.* 108, 1043–1053. doi: 10.1093/aob/mcr110

Fournier, C., Andrieu, B., Ljutovac, S., and Saint-Jean, S. (2003). "ADEL-wheat: a 3D architectural model of wheat development," in *International Symposium on Plant Growth Modeling, Simulation, Visualization, and their Applications*, eds B. G. Hu and M. Jaeger (Beijing: Tsinghua University Press), 54–63.

Fraley, C., Raftery, A. E., Murphy, T., and Scruga, L. (2012). *MCLUST Version 4 for R: Normal Mixture Modeling for Model-Based Clustering, Classification, and Density Estimation*, Technical Report, No. 597. Seattle, WA: Department of Statistics, University of Washington.

Franklin, K. A. (2008). Shade avoidance. *New Phytol.* 179, 930–944. doi: 10.1111/j.1469-8137.2008.02507.x

Gates, D. J. (1978). Bimodality in even-aged plant monocultures. *J. Theor. Biol.* 71, 525–540. doi: 10.1016/0022-5193(78)90323-5

Gates, D. J., O'Connor, A. J., and Westcott, M. (1979). Partitioning the union of disks in plant competition models. *Proc. Roy. Soc. A Math. Phys.* 367, 59–79. doi: 10.1098/rspa.1979.0076

Geber, M. A. (1989). Interplay of morphology and development on size inequality: a Polygonum greenhouse study. *Ecol. Monogr.* 59, 267–288. doi: 10.2307/1942602

Godin, C., and Sinoquet, H. (2005). Functional–structural plant modelling. *New Phytol.* 166, 705–708. doi: 10.1111/j.1469-8137.2005.01445.x

Guo, H., Lei, X., Counède, P.-H., and Letort, V. (2012). Characterization of the effects of inter-tree competition on source-sink balance in Chinese pine trees with the GreenLab model. *Trees Struct. Funct.* 26, 1057–1067. doi: 10.1007/s00468-012-0683-x

Kahlen, K., and Stützel, H. (2011a). Modelling photo-modulated internode elongation in growing glasshouse cucumber canopies. *New Phytol.* 190, 697–708. doi: 10.1111/j.1469-8137.2010.03617.x

Kahlen, K., and Stützel, H. (2011b). Simplification of a light-based model for estimating final internode length in greenhouse cucumber canopies. *Ann. Bot.* 108, 1055–1063. doi: 10.1093/aob/mcr130

Kahlen, K., Wiechers, D., and Stützel, H. (2008). Modelling leaf phototropism in a cucumber canopy. *Funct. Plant Biol.* 35, 876–884. doi: 10.1071/FP08034

Kenkel, N. C. (1988). Pattern of self-thinning in Jack pine: testing the random mortality hypothesis. *Ecology* 69, 1017–1024. doi: 10.2307/1941257

Kennedy, M. C., and Ford, E. D. (2012). Using multi-criteria analysis of simulation models to understand complex biological systems. *Bioscience* 61, 994–1004. doi: 10.1525/bio.2011.61.12.9

Koike, F. (1989). Foliage-crown development and interaction in *Quercus gilva* and *Q. acuta*. *J. Ecol.* 77, 92–111. doi: 10.2307/2260919

Koyama, H., and Kira, T. (1956). Intraspecific competition among higher plants. VIII Frequency distribution of individual plant weight as affected by the interaction between plants. *J. Inst. Polytech. Osaka City Univ. Ser. D* 7, 73–94.

Letort, V., Counède, P.-H., Mathieu, A., de Reffye, P., and Constant, T. (2008). Parametric identification of a functional-structural tree growth model and application to beech trees (*Fagus sylvatica*). *Funct. Plant Biol.* 35, 951–963. doi: 10.1071/FP08065

Loosmore, N., and Ford, E. D. (2006). Statistical inference using the G or K point pattern spatial statistics. *Ecology* 87, 1925–1931. doi: 10.1890/0012-9658(2006)87[1925:SIUTGO]2.0.CO;2

Maliakal, S. K., McDonnell, K., Dudley, S. A., and Schmitt, J. (1999). The effects of red to far-red ratio and plant density on biomass allocation and gas exchange in *Impatiens capensis*. *Int. J. Plant Sci.* 160, 723–733. doi: 10.1086/314157

Mathieu, A., Counède, P.-H., Letort, V., Barthélémy, D., and de Reffye, P. (2009). A dynamic model of plant growth with interactions between development and functional mechanisms to study plant structural plasticity related to trophic competition. *Ann. Bot.* 103, 1173–1186. doi: 10.1093/aob/mcp054

Monaco, T. A., and Briske, D. D. (2001). Contrasting shade avoidance responses in two perennial grasses: a field investigation in simulated sparse and dense canopies. *Plant Ecol.* 156, 173–182. doi: 10.1023/A:1012617014417

Nagashima, H. (1999). The process of height-rank determination among individuals and neighbourhood effects in *Chenopodium album* L. stands. *Ann. Bot.* 83, 501–507. doi: 10.1006/anbo.1999.0848

Niinemets, U. (2010). A review of light interception in plant stands from leaf to canopy in different plant functional types and in species with varying shade tolerance. *Ecol. Res.* 25, 693–714. doi: 10.1007/s11284-010-0712-4

Niklas, K. J. (1997). Adaptive walks through fitness landscapes for early vascular plants. *Am. J. Bot.* 84, 16–25. doi: 10.2307/2445878

Norberg, R. A. (1988). Theory of growth geometry of plants and self-thinning of plant populations: geometric similarity, elastic similarity, and different growth modes of plant parts. *Am. Nat.* 131, 220–256. doi: 10.1086/284787

Pendleton, J. W., Smith, G. E., Winter, S. R., and Johnston, T. J. (1968). Field investigations of the relationship of leaf angle in corn (*Zea mays* L.) to grain yield and apparent photosynthesis. *Agron. J.* 60, 422–424. doi: 10.2134/agronj1968.00021962006000040027x

Perttunen, J., Sievänen, R., Nikinmaa, E., Salminen, H., Saarenmaa, H., and Väkeva, J. (1996). LIGNUM: a tree model based on simple structural units. *Ann. Bot.* 77, 87–98. doi: 10.1006/anbo.1996.0011

Pierik, R., Visser, E. J. W., De Kroon, H., and Voesenek, L. A. C. J. (2003). Ethylene is required in tobacco to successfully compete with proximate neighbours. *Plant Cell Environ.* 26, 1229–1234. doi: 10.1046/j.1365-3040.2003.01045.x

Reynolds, J. H., and Ford, E. D. (1999). Multi-criteria assessment of ecological process models. *Ecology* 80, 538–553. doi: 10.1890/0012-9658(1999)080[0538:MCAOEP]2.0.CO;2

Reynolds, J. H., and Ford, E. D. (2005). Improving competition representation in theoretical models of self-thinning: a critical review. *J. Ecol.* 93, 362–372. doi: 10.1111/j.1365-2745.2005.00976.x

Room, P. M., Maillette, L., and Hanan, J. S. (1994). Module and metamer dynamics and virtual plants. *Adv. Ecol. Res.* 25, 105–157. doi: 10.1016/S0065-2504(08)60214-7

Rouvinen, S., and Kuuluvainen, T. (1997). Structure and asymmetry of tree crowns in relation to local competition in a natural mature Scots pine forest. *Can. J. For. Res.* 27, 890–902. doi: 10.1139/x97-012

Schmitt, J. (1997). Is photomorphogenis shade avoidance adaptive? Perspectives from population biology. *Plant Cell Environ.* 20, 826–830. doi: 10.1046/j.1365-3040.1997.d01-96.x

Schwinning, S., and Weiner, J. (1998). Mechanisms determining the degree of size asymmetry in competition among plants. *Oecologia* 113, 447–455. doi: 10.1007/s004420050397

Shinozaki, K., Yoda, K., Hozumi, K., and Kira, T. A. (1964). A quantitative analysis of plant form – the pipe model theory. I. Basic analysis. *Jpn. J. Ecol.* 14, 978–105.

Sievänen, R., Perttunen, J., Nikinmaa, E., and Kaitaniemi, P. (2008). Towards extension of a single tree functional-structural model of Scots pine to stand level: effect of the canopy of randomly distributed, identical trees on development of tree structure. *Funct. Plant Biol.* 35, 964–975. doi: 10.1071/FP08077

Sinoquet, H., and Rivet, P. (1997). Measurement and visualization of the architecture of an adult tree basede on a three-dimensional digitising device. *Trees Struct. Funct.* 11, 265–270. doi: 10.1007/s004680050084

Smith, H. (1982). Light quality, photoperception, and plant strategy. *Annu. Rev. Plant Physiol.* 33, 481–518. doi: 10.1146/annurev.pp.33.060182.002405

Smith, H., and Whitelam, G. C. (1997). The shade avoidance syndrome: multiple responses mediated by multiple phytochromes. *Plant Cell Environ.* 20, 840–844. doi: 10.1046/j.1365-3040.1997.d01-104.x

Sorrensen-Cothern, K. A., Ford, E. D., and Sprugel, D. G. (1993). A model of competition incorporating plasticity through modular foliage and crown development. *Ecol. Monogr.* 63, 277–304. doi: 10.2307/2937102

Sprugel, D. G. (2002). When branch autonomy fails: Milton's law of resource availability and allocation. *Tree Physiol.* 22, 1119–1124. doi: 10.1093/treephys/22.15-16.1119

Sprugel, D. G., Hinckley, T. M., and Schaap, W. (1991). The theory and practice of branch autonomy. *Annu. Rev. Ecol. Syst.* 22, 309–334. doi: 10.1146/annurev.es.22.110191.001521

Stenberg, P., Palmroth, S., Bond, B. J., Sprugel, D. G., and Smolander, H. (2001). Shoot structure and photosynthetic efficiency along the light gradient in a Scots pine canopy. *Tree Physiol.* 21, 805–814. doi: 10.1093/treephys/21.12-13.805

Stoll, P., and Bergius, E. (2005). Pattern and process: competition causes regular spacing of individuals within plant populations. *J. Ecol.* 93, 395–403. doi: 10.1111/j.0022-0477.2005.00989.x

Stoll, P., and Schmid, B. (1998). Plant foraging and dynamic competition between branches of *Pinus sylvestris* in contrasting light environments. *J. Ecol.* 86, 934–945. doi: 10.1046/j.1365-2745.1998.00313.x

Suzuki, S. N., Kachi, N., and Suzuki, J.-I. (2008). Development of a local size hierarchy causes regular spacing of trees in an even-aged Abies forest: analyses using spatial autocorrelation and the mark correlation function. *Ann. Bot.* 102, 435–441. doi: 10.1093/aob/mcn113

Turley, M. C., and Ford, E. D. (2011). Detecting bimodality in plant size distributions and its significance for stand development and competition. *Oecologia* 167, 991–1003. doi: 10.1007/s00442-011-2048-3

Umeki, K. (1995). Importance of crown position and morphological plasticity in competitive interaction in a population of *Xanthium canadense*. *Ann. Bot.* 75, 259–255. doi: 10.1006/anbo.1995.1019

Umeki, K. (1997). Effect of crown asymmetry on size-structure dynamics of plant populations. *Ann. Bot.* 79, 631–641. doi: 10.1006/anbo.1996.0388

Vandenbussche, F., Pierik, R., Millenaar, F. F., Voesenek, L. A. C. J., and Van Der Straeten, D. (2005). Reaching out of the shade. *Curr. Opin. Plant Biol.* 8, 462–468. doi: 10.1016/j.pbi.2005.07.007

van Zanten, M., Pons, T. L., Janssen, J. A. M., Voesenek, L. A. C. J., and Peters, A. J. M. (2010). On the relevance and control of leaf angle. *Crit. Rev. Plant Sci.* 29, 300–316. doi: 10.1080/07352689.2010.502086

Vega, C. R. C., and Sadras, V. O. (2003). Size-dependent growth and the development of inequality in maize, sunflower and soybean. *Ann. Bot.* 91, 795–805. doi: 10.1093/aob/mcg081

Vermeulen, P. L., Anten, N. P. R., Schieving, F., Werger, M. J. A., and During, H. J. (2008a). Height convergence in response to neighbour growth: genotypic differences in the stoloniferous plant *Potentilla reptans*. *New Phytol.* 177, 688–697. doi: 10.1111/j.1469-8137.2007.02301.x

Vermeulen, P. J., Stuefer, J. F., During, H. J., and Anten, N. P. R. (2008b). Leaf investment and light partitioning among leaves of different genotypes of the clonal plant *Potentilla reptans* in a dense stand after 5 years of competition. *Ann. Bot.* 102, 935–943. doi: 10.1093/aob/mcn185

Wand, M. P., and Jones, M. C. (1995). *Kernel Smoothing*. Boca Raton: Chapman & Hall. doi: 10.1007/978-1-4899-4493-1

Weiner, J. (1990). Asymmetric competition in plant populations. *Trends Ecol. Evol.* 5, 360–364. doi: 10.1016/0169-5347(90)90095-U

Weiner, J., and Solbrig, O. T. (1984). The meaning and measurement of size hierarchies in plant populations. *Oecologia* 61, 334–336. doi: 10.1007/BF00379630

Weiner, J., and Thomas, S. C. (1986). Size variability in plant monocultures. *Oikos* 47, 211–222. doi: 10.2307/3566048

Weller, D. E. (1987). A reevaluation of the -3/2 power rule of plant self-thinning. *Ecol. Monogr.* 57, 23–43. doi: 10.2307/1942637

Westoby, M. (1982). Frequency distributions of plant size during competitive growth of stands: the operation of distribution-modifying-functions. *Ann. Bot.* 50, 733–735.

White, J. (1981). Generalization of self-thinning of plant populations. *Nature* 268:373. doi: 10.1038/268373a0

Wiegand, K., Saltz, D., Ward, D., and Levin, S. A. (2008). The role of size inequality in self-thinning: a pattern-oriented simulation model for arid savannas. *Ecol. Model.* 210, 431–445. doi: 10.1016/j.ecolmodel.2007.08.027

Yan, H., Kang, M., de Reffye, P., and Dingkuhn, M. (2004). A dynamic, architectural plant model simulating resource-dependent growth. *Ann. Bot.* 93, 591–602. doi: 10.1093/aob/mch078

Yoda, K., Kira, T., Ogawa, H., and Hozumi, K. (1963). Self-thinning in overcrowded pure stands under cultivated and natural conditions. *J. Biol. Osaka City Univ.* 14, 107–129.

Zeide, B. (1985). Tolerance and self-tolerance of trees. *For. Ecol. Manag.* 13, 149–166. doi: 10.1016/0378-1127(85)90031-3

Conflict of Interest Statement: The author declares that the research was conducted in the absence of any commercial or financial relationships that could be construed as a potential conflict of interest.

frontiers in
PLANT SCIENCE

Optimizing illumination in the greenhouse using a 3D model of tomato and a ray tracer

Pieter H. B. de Visser[1]*, Gerhard H. Buck-Sorlin[2] and Gerie W. A. M. van der Heijden[3]†

[1] Department of Greenhouse Horticulture, Wageningen University and Research Centre, Wageningen, Netherlands
[2] Institut de Recherche en Horticulture et Semences, AGROCAMPUS OUEST, Angers, France
[3] Biometris, Wageningen University and Research Centre, Wageningen, Netherlands

Reduction of energy use for assimilation lighting is one of the most urgent goals of current greenhouse horticulture in the Netherlands. In recent years numerous lighting systems have been tested in greenhouses, yet their efficiency has been very difficult to measure in practice. This simulation study evaluated a number of lighting strategies using a 3D light model for natural and artificial light in combination with a 3D model of tomato. The modeling platform GroIMP was used for the simulation study. The crop was represented by 3D virtual plants of tomato with fixed architecture. Detailed data on greenhouse architecture and lamp emission patterns of different light sources were incorporated in the model. A number of illumination strategies were modeled with the calibrated model. Results were compared to the standard configuration. Moreover, adaptation of leaf angles was incorporated for testing their effect on light use efficiency (LUE). A Farquhar photosynthesis model was used to translate the absorbed light for each leaf into a produced amount of carbohydrates. The carbohydrates produced by the crop per unit emitted light from sun or high pressure sodium lamps was the highest for horizontal leaf angles or slightly downward pointing leaves, and was less for more upward leaf orientations. The simulated leaf angles did not affect light absorption from inter-lighting LED modules, but the scenario with LEDs shining slightly upward (20°) increased light absorption and LUE relative to default horizontal beaming LEDs. Furthermore, the model showed that leaf orientation more perpendicular to the string of LEDs increased LED light interception. The combination of a ray tracer and a 3D crop model could compute optimal lighting of leaves by quantification of light fluxes and illustration by rendered lighting patterns. Results indicate that illumination efficiency increases when the lamp light is directed at most to leaves that have a high photosynthetic potential.

Keywords: photosynthesis, greenhouse crop, HPS, LED, light distribution, LUE

INTRODUCTION

The spatial distribution of assimilation lights in greenhouse horticulture, especially in countries with a deficiency in natural sunlight, is a controversially debated topic (Hovi-Pekkanen and Tahvonen, 2008; Trouwborst et al., 2010; de Visser and Buck-Sorlin, 2011). However, there is general agreement that lamp type, density, positioning and orientation with respect to plant orientation are important and that an optimization of these factors can help improve crop light interception and thus reduce energy costs. Finding the optimal solution experimentally is nearly impossible due to the large number of possible combinations and the high financial, and time investment per experiment. Computer-aided design coupled with 3D modeling of plants and light distribution could be a more rapid and cost-effective solution in order to test the effect of possible lamp configurations in the greenhouse on crop light interception. Software tools (e.g., computer aided design – CAD) that enable 3D visualization of objects in a 3D scene, including the simulation of the trajectories of light rays using ray tracing methods, are well established and tested. Commonly used methods to simulate light distribution in plant

canopies are Monte Carlo ray tracing (Veach, 1997) and nested radiosity (Chelle and Andrieu, 1998). The exponential increase in computing power also allowed the further development of simple crop models into more elaborate versions, so-called functional-structural plant models (FSPM; Vos et al., 2010). FSPM refers to a paradigm for the description of a plant by creating a (usually object-oriented) computer model of its structure and selected physiological and physical processes, at different hierarchical levels: organ, plant individual, canopy (a stand of plants), and in which the processes are modulated by the local environment. With respect to greenhouse crops FSPMs for tomato (Sarlikioti et al., 2011a,b), cut rose (Buck-Sorlin et al., 2011) cucumber (Kahlen et al., 2008; Kahlen and Stützel, 2011; Wiechers et al., 2011) and *chrysanthemum* (de Visser et al., 2007) have been devised. Although in greenhouse practice a small number of 3D models of greenhouse structure including lamps are available, the model by de Visser et al. (2012) is to our knowledge the only one that considers the greenhouse interior (lamps, slabs) as well as the 3D structure and physiology of the plants. The reported model simulates the light distribution of natural (diffuse and direct)

daylight and artificial light within a realistic 3D representation of a crop.

de Visser et al. (2012) simulated some energy saving light strategies by optimization of position of local LED lights in the crop, but the options of lamps with specific angles to better illuminate the leaves at angles changing with age were not addressed. Moreover, answers are needed on effects of leaves oriented toward the path, as raised by Sarlikioti et al. (2011b) and whether leaf positions are equally important for High-pressure sodium (HPS) and LED lamps. With the upcoming technology of LEDs as a (partial) alternative for HPS lamps, growers have an instrument to adapt the angles of the LED modules to account for local leaf angles. The 3D modeling can be used to find promising set-ups of LED lighting in a tomato crop that may result in increased light absorption and crop growth, concomitantly supporting a more energy saving lighting strategy.

MATERIALS AND METHODS

The GroIMP interactive modeling platform, initially developed and described by Kniemeyer (2008) and maintained by the University of Göttingen (Germany), was used for the simulations. A virtual greenhouse was constructed within GroIMP on basis of an existing greenhouse compartment at the Improvement Center, Bleiswijk, The Netherlands, by explicitly considering the positions, shapes and optical properties of all its constituting objects (see

below) in a 3D scene. The light distribution at a given time step was then computed by the GroIMP radiation model, which is based on an inversed Monte Carlo path tracer, similar to the one used by Cieslak et al. (2008). Sunlight was modeled as a direct and a diffuse component, depending on the 10-year average recorded outside light level. Diffuse light came from a sky object consisting of 72 directional lights arranged in a hemisphere around the greenhouse, whilst direct sun light was provided by a single directional light. The power of both light sources, as well as the position of the sun was a function of latitude, day of year, and time of day (Goudriaan and van Laar, 1994).

Optical properties of all greenhouse objects as well as leaves entailed reflection, transmission and absorption of the fraction of photosynthetic radiation (PAR) generated by a light source, and were measured on subsamples with a Lambda 1050 spectrophotometer (Perkin-Elmer Inc) coupled to a snap-in light integrating sphere.

Net photosynthesis was simulated for each leaflet on the basis of absorbed light, air temperature and CO_2 according to Kim and Lieth (2003), with a leaf-age-depended value for Jmax, the potential rate of electron transport (in μmol electrons m^{-2} s^{-1}). Measured light-response curves (3 heights in the crop, $n = 3$, 10 PAR levels from 0 to 2000 μmol m^{-2} s^{-1}, measured with a Licor 6400 by gas exchange) at 700 ppm CO_2 (annual average in greenhouse air) for winter and summer were used to calibrate
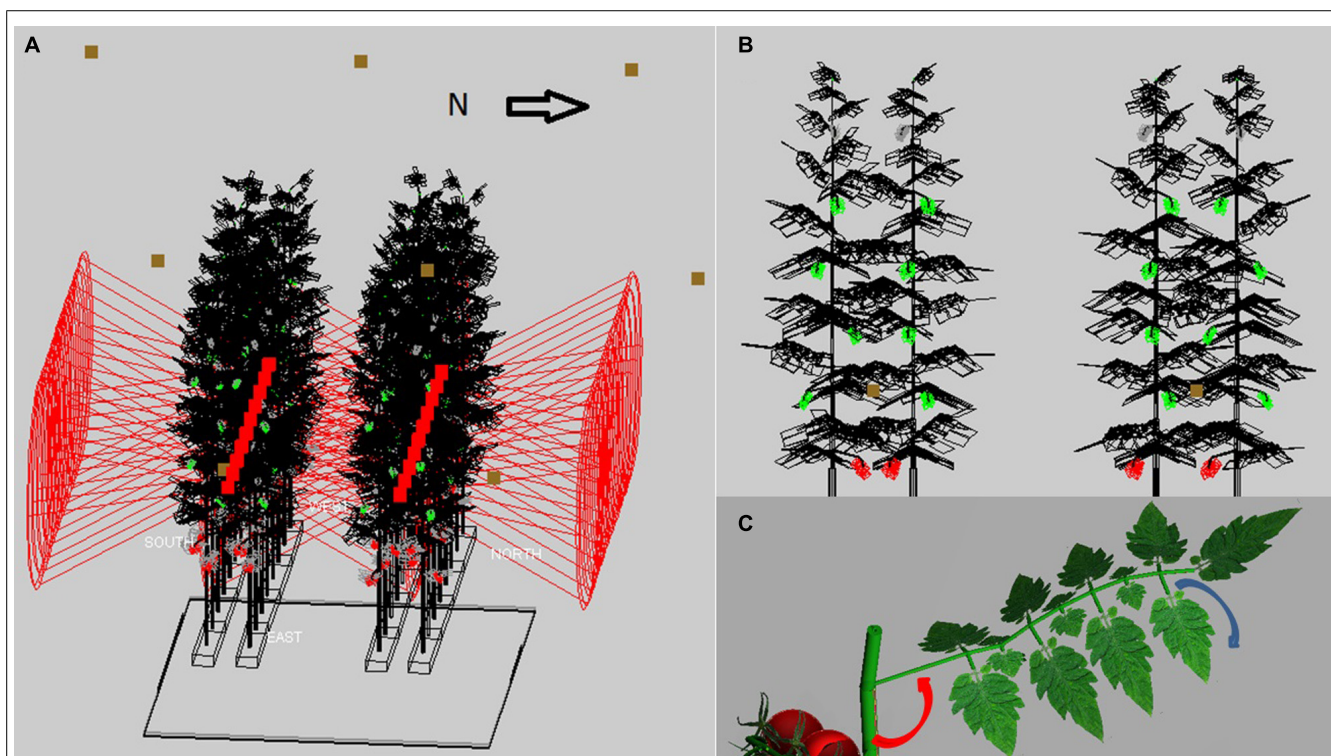

FIGURE 1 | The modeled 3D scene of the tomato crop: (A) A crop of 32 plants (wireframe with black leaves, green unripe trusses and red ripe trusses) on two double rows of slabs at 0.8 m above the floor, with LED (red squares) inside the double row at 2.4 m height and HPS lamps (brown squares) at 1.5 m above the crop, (B) cross-section of four plants with leaf angles increasing with height (LED position at brown square), (C) rendered image of a single leaf with its rachis at a specific angle (red arrow) with the main stem, and consisting of leaflets that hang down by 30−50° (see blue arrow) relative to the horizontal.

parameters f (spectral correction factor, dimensionless) and Jmax in the photosynthesis model by reducing least square differences between modeled and observed photosynthesis.

The virtual greenhouse consisted of a glass roof, side walls, floor, energy-saving screen, gutters, assimilation lamps, and a crop consisting of static virtual plants (**Figure 1A**). The light pattern emitted by the HPS lamps of 1000 W concisely matched (per 10° interval) that of a SON-T in a wide angle reflector (data from Hortilux ©), see Buck-Sorlin et al. (2009) for details. The HPS lamps were placed in a grid of 6 m (in row direction) × 2.5 m (across rows) at 1.5 m above top of the crop. The emission pattern of LED light was simulated using simple, horizontally shining spotlights which had an opening angle similar to what has been measured on the 150 cm, commercially available, production module RB (data from Philips ©), and emitted PAR was calibrated to 60 μmol m^{-2} s^{-1} greenhouse. The strings with LEDs were at a height of 2.1 m above the ground, LEDs were 40 cm horizontally apart within each double plant row and placed in row direction. Ca. 3 leaves were situated below the LEDs which is regularly occurring in practice. The crop was represented as a static structure, corresponding to measurements on a tomato crop cv. Kommeet in our research facilities in Bleiswijk, The Netherlands: for the HPS and LED scenarios in winter, as measured on six plants on January 11th in 2011, for the sunlight scenarios in summer in another crop as measured on August 9th in 2011. The average value and its variation of leaf angles, length, width, internode length, and phyllotaxis were measured with ruler and protractor. The data were incorporated in GroIMP as average values per phytomer and the associated random variation, using a set of growth rules that created 32 (summer) or 36 (winter) phytomers per plant, of which eight were trusses and the rest consisted of leaves (**Figure 1B**). Each leaf was composed of 15 leaflets of a fixed geometry, yet their size increased in proportion to the length of the terminal leaflet of the composite leaf (**Figure 1C**). The modeled scene of 4 by 3.2 m ground area consisted of 32 plants with their lowest leaf oriented at a random azimuthal direction, an observed phyllotaxis of 130° between leaves, leaf angle of 90° (i.e., horizontal position) for lowest leaves and becoming slightly higher, maximizing at 130° for upper leaves (**Figures 1B,C**). Plants were placed on slabs at 0.8 m above the floor, and pairs of slabs, with internal distance 0.4 m, were divided by a path, giving 1.6 m distance from center to center between slab pairs (**Figure 1A**). On a slab, plants were 0.4 m apart, and had only one stem without a split. Crop density was 2.5 stems per m^2 ground floor; the top of the canopy was situated at maximally 4.5 m above the floor. Plant rows were oriented east-west as observed. An infinite canopy was simulated by placing perfect mirrors around the scene.

SCENARIOS

Based on the above described default setup, different scenarios were examined to gain insight in the influence of plant architecture and light source specifics on crop light absorption and photosynthesis:

(1) Leaves were tilted by angles of +30% of default (i.e., from default 90 to 117° (lowest leaves) and from 130 to 169° (upper leaves), 0 and -30% (runs a, b, and c) relative to default, combined

with different light sources: (1.1) daily course on June 21st of 10-year averaged sun light (70% direct, 30% diffuse), (1.2) HPS top light (130 μmol m^{-2} s^{-1} PAR), (1.3) LED inter-lighting (60 μmol m^{-2} s^{-1} PAR)

(2) Leaves were forced to orientate toward the path (2a) or parallel to the slab (2b), combined with LED inter-lighting. Each of the leaf directions is imposed with a uniform continuous random variation between −10° and +10° in the horizontal plane, i.e., left and right of the main leaf direction.

(3) Inter-lighting with LED modules illuminating the plants at different angles [LEDs heading from upward by 30° (scenario 3a) to downward −30° (3f) in steps of 10°]

Each scenario was replicated five times, and at each run leaf angles were randomly varied in vertical direction between −10° and +10° of the measured angle, and each plant was turned around its axis randomly between −180 and +180°. Each run took ca. 10 s on a standard PC. Apart from percentage of emitted light per light source absorbed by the crop, per scenario the average net photosynthesis per MJ absorbed or emitted PAR light, referred to as light use efficiency (LUE) in its most usual unit, is calculated. Analysis of variance and t-test for differences were carried out in GenStat, 16th Edition.

RESULTS

The tomato leaves reflected and transmitted 8 and 3% of PAR light, respectively. The greenhouse floor reflected on average ca. 40% of PAR light and the white plastic 75%. For the relatively small area of stem surface we assumed similar optics as for leaves.

With the 3D structure of the measured crop, results of the scenarios on leaf angles showed an effect of maximally 3% relative to the control for most situations (**Table 1**). In the control situation, the rachis of mature leaves has an almost horizontal position (see indicated angle in **Figure 1C**), and the attached leaflets hung down by another 30–50°. Modeling a larger angle of the rachis relative to the main stem (scenario 1.1a) made the leaves point a little upward, which was detrimental for light interception (**Table 1**; **Figure 2**). Leaves that pointed more downward (scenario 1.1.c) did not increase light absorption of sun light compared to default, horizontal leaves. Averaged over the day, this scenario, however, showed absorption to decrease 2% around noon and increase 2% in morning and afternoon relative to default. For sun light the leaf angle changes, similar to light absorption, only decreased LUE for steeper leaves (scenario 1.1.a). The day average of LUE for absorbed light was relatively low as compared to other scenarios, and despite 20% higher photosynthetic potential in summer, due to the higher light levels which at noon (at 1400 μmol PAR m^{-2} s^{-1}) resulted in light saturation.

For winter the measured crop structure had similar leaf angles, yet smaller LAI (2.7 vs. 3.4), longer internodes (0.11 vs. 0.08 m on average) and a 20% lower maximum photosynthesis relative to summer, and was used for HPS and LED scenarios. For HPS lighting, raising the leaves from −30 to +30% from default, decreased light absorption but hardly affected LUE (**Table 1**). The latter means that between these leaf angle scenarios the light-absorbing leaves all have a similar leaf age and thus similar photosynthetic

Table 1 | Light absorption (% of input) and light use efficiency (LUE) per unit absorbed or emitted light per mentioned light source of the tomato crop for the different scenarios. Within each group (1.1, 1.2, 1.3, 2, or 3) letters behind a mean indicate a significant difference between scenarios ($p < 0.05$). DM, dry matter.

Scenario	Property	Value changed	Light absorption (% of input)	LUE (g DM MJ^{-1} absorbed PAR)	LUE (g DM MJ^{-1} emitted PAR)
			Sunlight (30% diffuse)[#]		
1.1.a	Leaf	+30%	90.2 ± 0.06a	3.08 ± 0.06	2.77 ± 0.05a
1.1.b	angle	0	93.1 ± 0.06b	3.10 ± 0.06	2.86 ± 0.05b
1.1.c		−30%	93.7 ± 0.06b	3.07 ± 0.06	2.90 ± 0.05b
			HPS lamps only		
1.2.a		+30%	85.8 ± 0.8a	4.22 ± 0.07	3.62 ± 0.05
1.2.b		0	87.3 ± 0.6b	4.21 ± 0.06	3.67 ± 0.06
1.2.c		−30%	88.0 ± 0.3b	4.15 ± 0.06	3.65 ± 0.05
			LED inter-lighting only		
1.3.a		+30%	93.7 ± 0.5	4.08 ± 0.06a	3.82 ± 0.06a
1.3.b		0	94.1 ± 0.5	4.09 ± 0.06a	3.84 ± 0.05a
1.3.c		−30%	93.5 ± 0.5	3.56 ± 0.05b	3.33 ± 0.05b
			LED inter-lighting only		
2.a	Leaf	Toward path	96.0 ± 0.4a	3.11 ± 0.11a	2.98 ± 0.09a
2.b	direction	Parallel to slab	94.1 ± 0.3b	3.64 ± 0.05b	3.43 ± 0.04b
			LED inter-lighting only		
3.a	LED light direction	+30°	92.0 ± 0.8a	3.98 ± 0.13a	3.66 ± 0.12a
3.b		+20°	95.5 ± 0.2b	4.14 ± 0.14a	3.95 ± 0.13b
3.c		+10°	94.5 ± 0.5ab	3.97 ± 0.06ab	3.75 ± 0.06ab
3.d		0°	94.1 ± 0.5ab	4.09 ± 0.07ab	3.84 ± 0.05ab
3.e		−10°	86.8 ± 0.7c	3.38 ± 0.06b	2.93 ± 0.05c
3.f		−20°	81.3 ± 1.0d	3.13 ± 0.06c	2.54 ± 0.04d
3.g		−30°	78.8 ± 1.3e	2.48 ± 0.05d	1.95 ± 0.04e

[#]*For sunlight scenarios a measured summer crop structure was used instead of the default winter structure*

potential. On the contrary, for the LED scenarios with horizontal and steeper leaves (scenarios 1.3.a,b) the increased absorption did not increase but lighting more upper leaves were illuminated as shown by increased LUE relative to down-hanging leaves (scenario 1.3.c).

Leaves oriented to the path (scenario 2.a) had only 2% more interception than leaves oriented toward the slab (**Table 1**), yet utilization per MJ emitted light was lower than leaves oriented parallel to the row and slab (scenario 2.b).

Directing LEDs more upward up to 20° (scenario 3.b) resulted in higher absorption of LED light by the crop and the highest LUE per MJ emitted light of all scenarios. In this scenario no increased loss of light to the sky was simulated since the LEDs were positioned rather low in the crop. Pointing the light more downward did dramatically decrease light interception (only 78% of input at scenario 3.g) and led to less photosynthesis due to the lower performance of the lower leaves (**Table 1**).

The light model computed considerable horizontal differences in light intensity within the crop. For HPS lamps without plants, the visual rendering seemed to indicate large intensity differences in the area between lamps as shown by illumination of a horizontal plane (**Figure 3**), yet the sensed light level showed only modest differences (**Figure 4**). When plants are introduced in the model, the sensed light level between positions in and outside the plant row were large (**Figure 4**). Also for LEDs, after light penetration through the plant, hardly any light remained to illuminate the neighboring row (data not shown), suggesting each double plant row should contain a LED module for homogeneous illumination.

DISCUSSION

A 3D model of light including leaf photosynthesis has seldom been used to predict effect of artificial light on LUE of the crop (Delepoulle et al., 2008; de Visser and Buck-Sorlin, 2011). The present, unique model indicates that HPS lamps result in a higher photosynthesis per unit absorbed light than LEDs. This is caused by the higher LUE of upper leaves, catching more light for HPS than for LEDs. Yet, per emitted MJ, LED lighting is more efficient than HPS lighting due to a higher fraction of absorbed light. Apart from HPS lamps illuminating the upper
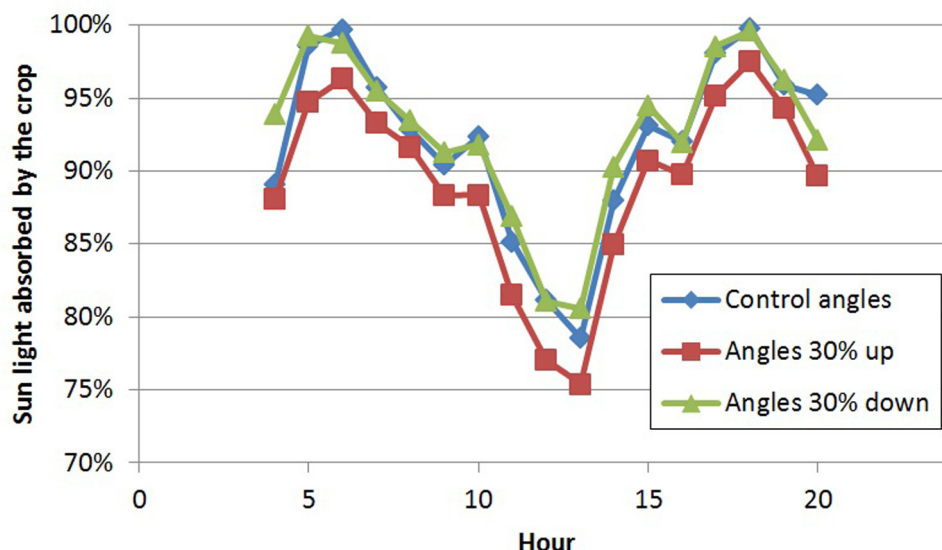
FIGURE 2 | Diurnal pattern of light absorption (% of incoming radiation) by the crop on day 180 for three scenarios of leaf angles.
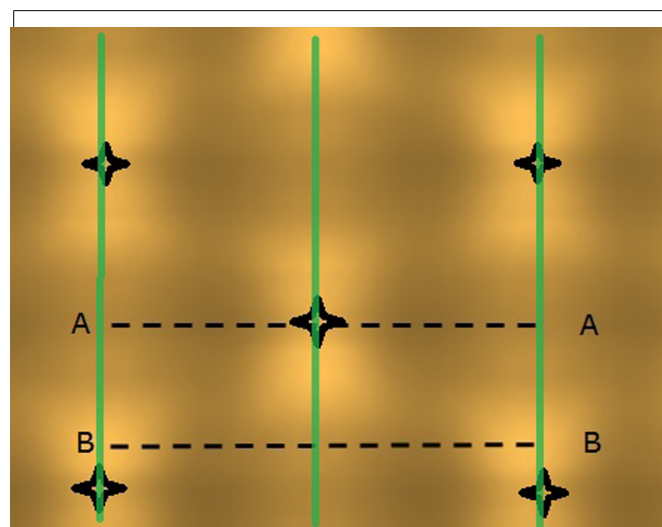

FIGURE 3 | Projected light pattern of HPS lamps without plants, on a horizontal plane at 2.5 m distance from the lamps, with sensor trajectories (A – A and B – B) indicated by dashed lines, lamp positions are shown by star-like symbols, and the double plant rows by green lines.

FIGURE 4 | Computed light intensity (W per sensor with 6 cm radius) at the trajectories of Figure 3, with and without light intercepting plants (plant positions indicated by arrows). For this simulation the HPS lamps had an arbitrary light output of 1000 W m^{-2}.

leaves with high photosynthetic capacity, an additional advantage of HPS relative to LED is that they combine PAR and heat radiation, thus supporting both assimilate supply by photosynthesis and temperature driven organ development. Despite the efficiency of LED light interception, their PAR emission should be accompanied by a certain level of heating, reducing their energy-saving advantages. Only a 3D model incorporating energy balance calculations can fully estimate the energy efficiency of a LED strategy.

Tilting the leaves upward decreased light interception of the downward light from sun and HPS lamps, but not for LEDs. Very probably leaves have less surface exposed to the sun, alike more erect leaves in arid, sunny climates that prevent excess light heating the leaves. The decreased light interception did not affect LUE because still the same leaves were illuminated, at similar photosynthetic potential. In contrast, light interception was not affected for LEDs when leaf angles were changed. Yet, when down by −30%, the lowest leaves were illuminated more which resulted in a lower computed LUE due to lower photosynthetic capacity of these leaves. The winter crop structure was different from summer structure in terms of internode length and leaf area, but not

in terms of leaf angles. We expect that the longer internodes in winter do result in a wider spread of LED light.

The turning of leaves predominantly toward the path slightly increased LED light interception relative to default leaf positions, whereas leaves predominantly oriented parallel to the rows did not alter light interception relative to default. Leaves may orient toward LED light or turn away at too high light level (e.g., Trouwborst et al., 2011), thus impacting the interception of LED light.

For LEDs, the beaming angle had a strong effect on light absorption and LUE. The highest light interception was modeled at 20° up from horizontal position, and a significant decrease from 0° toward −30° angle due to loss to the ground. This effect may have been lower if the LEDs were positioned higher in the crop, showing the sensitivity of our results to the particular situation of LED placement and crop architecture. Placement of LEDs should be carefully planned, taking into consideration the given plant structure. A similar conclusion was drawn by Sarlikioti et al. (2011b) who observed strong effects of plant structure on light interception, in particular for internode lengths and leaf shape. The same authors found that leaves orientate themselves toward the path to intercept more light (Sarlikioti et al., 2011a), which agrees to our findings of a modest 2% light interception increase relative to orientation parallel to the plant row, as calculated for LED light.

Optimal lighting of leaves is driven by a combination of spatial emission pattern and crop characteristics such as structure and optical properties. We did not test the effect of the emitted light spectrum and its transformation (selective absorption, transmission, and reflection) as the light rays pass through the canopy. A recent extension of GroIMP, the GPUFlux light model (van Antwerpen et al., 2011), is a spectral Monte Carlo light tracer, which offers this possibility. The light tracer utilizes available computing resources through OpenCL. For each object, the model either computes a fully discretized absorption spectrum or several integrated weighted spectra, which are subsequently used in a photosynthesis model.

An important factor in optimization of light use is the positioning of light sources close to leaves with highest photosynthetic potential. It is standard practice that lamp power is accommodated such that the light level on nearby leaves is not at a saturating level but still in the linear trajectory of the light-response of photosynthesis. This is now also accommodated for LED modules when using interlighting, resulting in an average supplement of about 60 μmol PAR m^{-2} s^{-1} greenhouse. Whether this light amount will not lead to deleterious, high light levels on nearby leaves could be verified using the present model, ultimately leading to an advice to, e.g., use lower intensities and save energy. Yet, leaves can adapt their photosynthetic properties in response to their history of perceived local light, resulting, e.g., in sun-adapted leaves with high amounts of Rubisco and a high photosynthetic capacity. In a high-wired and dense crop, leaves normally decrease their photosynthetic capacity as well as their compensation point following adaptation to decreasing levels of perceived light lower in the canopy (Trouwborst et al., 2011). However, prolonged high light levels on aging cucumber leaves halted the decrease of photosynthetic capacity (Hovi-Pekkanen and Tahvonen, 2008). This is also aimed at with LED interlighting, yet this has to be confirmed

experimentally. Maintenance of photosynthetic capacity would be another advantage of interlighting, adding to the lower light losses as shown in this study.

The computer graphical representation of tomato leaves that we used in our model was a combination of textured cylinders (petioles and rachies) and flat boxes (leaflets). This was clearly a simplification as tomato leaflets are in reality variously convexly or concavely curved surfaces: such curved surfaces will increase diffuse reflection and probably lead to better LUE in a dense canopy. Such an effect can at present not be considered by our model, but the representation of leaves as complexly curved surfaces is technically possible (Gerhard Buck-Sorlin and Michael Henke, unpublished work).

In conclusion, based on the present simulation study we would be able to give the following, tentative, recommendations to improve the efficacy of assimilation light in the greenhouse: LEDs should be preferred over HPS as the light interception efficiency is bigger; the crop's LUE for HPS is higher than for LED due to lighting a higher fraction of leaves with higher photosynthetic capacity; light interception of LED interlighting is increased if LEDs are sufficiently high above the greenhouse floor and pointing slightly upward, thereby avoiding loss of light to the ground.

REFERENCES

Buck-Sorlin, G. H., Hemmerling, R., Vos, J., and de Visser, P. H. B. (2009). "Modelling of spatial light distribution in the greenhouse: description of the model," in *Proceedings of the Third International Symposium on Plant Growth Modeling, Simulation, Visualization and Applications*, Beijing. doi: 10.1109/PMA.2009.45

Buck-Sorlin, G. H., Visser, P. H. B., de Henke, M., Sarlikioti, V., Heijden, G. W. A. M., van der Marcelis, L. F. M., et al. (2011). Towards a functional–structural plant model of cut-rose: simulation of light environment, light absorption, photosynthesis and interference with the plant structure. *Ann. Bot.* 108, 1121–1134. doi: 10.1093/aob/mcr190

Chelle, M., and Andrieu, B. (1998). The nested radiosity model for the distribution of light within plant canopies. *Ecol. Model.* 111, 75–91. doi: 10.1016/S0304-3800(98)00100-8

Cieslak, M., Lemieux, C., Hanan, J., and Prusinkiewicz, P. (2008). Quasi-Monte Carlo simulation of the light environment of plants. *Funct. Plant Biol.* 35, 837–849. doi: 10.1071/FP08082

Delepoulle, S., Renaud, C., and Chelle, M. (2008). "Improving light position in a growth chamber through the use of a genetic algorithm," in *Artificial Intelligence Techniques for Computer Graphics, Studies in Computational Intelligence*, Vol. 159/2008 (Berlin: Springer), 67–82.

de Visser, P. H. B., and Buck-Sorlin, G. H. (2011). *Modelling Spatial Light Distribution in Crops (in Dutch)*. GTB report 1104. Wageningen, UR Greenhouse Horticulture, Netherlands.

de Visser, P. H. B., Buck-Sorlin, G. H., van der Heijden, G. W. A. M., and Marcelis, L. F. M. (2012). A 3D model of illumination, light distribution and crop photosynthesis to simulate lighting strategies in greenhouses. *Acta Hortic.* 956, 195–200.

de Visser, P. H. B., Heijden, G. W. A. M., van der Heuvelink, E., Carvalho, S. M. P. (2007). "Functional-structural modelling of chrysanthemum," in *Functional-Structural Plant Modelling in Crop Production*, eds J. Vos, L. F. M. Marcelis, P. H. B. de Visser, P. C. Struik, and J. B. Evers (Dordrecht: Springer), 199–208. doi: 10.1007/1-4020-6034-3_17

Hovi-Pekkanen, T., and Tahvonen, R. (2008). Effects of interlighting on yield and external fruit quality in year-round cultivated cucumber. *Sci. Hortic.* 761, 183–191.

Goudriaan, J., and van Laar, H. H. (1994). *Modelling Potential Crop Growth Processes.* Dordrecht: Kluwer Academic Publishers. doi: 10.1007/978-94-011-0750-1

Kahlen, K., and Stützel, H. (2011). Modelling photo-modulated internode elongation in growing glasshouse cucumber canopies. *New Phytol.* 190, 697–708. doi: 10.1111/j.1469-8137.2010.03617.x

Kahlen, K., Wiechers, D., and Stützel, H. (2008). Modelling leaf phototropism in a cucumber canopy. *Funct. Plant Biol.* 35, 876–884. doi: 10.1071/FP 08034

Kim, S-H., and Lieth, J. H. (2003). A coupled model of photosynthesis, stomatal conductance and transpiration for a rose leaf (*Rosa hybrida* L.). *Ann. Bot.* 91, 771–781. doi: 10.1093/aob/mcg080

Kniemeyer, O. (2008). *Design and Implementation of a Graph Grammar Based Language for Functional-Structural Plant Modelling.* Doctoral dissertation, Fakultät für Mathematik, Naturwissenschaften und Informatik, Brandenburg University of Technology, Cottbus.

Sarlikioti, V., Visser, P. H. B., and de Marcelis, L. F. M. (2011a). Exploring the spatial distribution of light absorption and photosynthesis of canopies by means of a functional-structural plant model. *Ann. Bot.* 107, 875–883. doi: 10.1093/aob/mcr006

Sarlikioti, V., Visser, P. H. B., de Buck-Sorlin, G. H., and Marcelis, L. F. M. (2011b). How plant architecture affects light absorption and photosynthesis in tomato: towards an ideotype for plant architecture using a functional-structural plant model. *Ann. Bot.* 108, 1065–1073. doi: 10.1093/aob/m cr221

Trouwborst, G., Hogewoning, S. W., Harbinson, J., and Ieperen, W. van. (2011). The influence of light intensity and leaf age on the photosynthetic capacity of leaves within a tomato canopy. *J. Hortic. Sci. Biotechnol.* 86, 403–407.

Trouwborst, G., Oosterkamp, J., Hogewoning, S. W., Harbinson, J., and Ieperen, W. van. (2010). The responses of light interception, photosynthesis and fruit yield of cucumber to LED-lighting within the canopy. *Physiol. Plant.* 138, 289–300. doi: 10.1111/j.1399-3054.2009.01333.x

van Antwerpen, D., van der Heijden, G. W. A. M., Marcelis, L. F. M., de Visser, P. B., Buck-Sorlin, G. H., and Jansen E. (2011). "High performance spectral light transport model for agricultural applications," in *Proceedings of the ACM SIGGRAPH/EUROGRAPHICS Conference on High Performance Graphics 2011*, eds C. Dachsbacher, W. Mark, and J. Pantaleoni (Vancouver: Eurographics Association).

Veach, E. (1997). *Robust Monte Carlo Methods for Light Transport Simulation.* Ph.D. Dissertation, Stanford University, Standford. Available at: http://graphics.stanford.edu/papers/veach_thesis/

Vos, J., Evers, J. B., Buck-Sorlin, G. H., Andrieu, B., Chelle, M., and de Visser, P. H. B. (2010). Functional–structural plant modelling: a new versatile tool in crop science. *J. Exp. Bot.* 61, 2101–2115. doi: 10.1093/jxb/erp345

Wiechers, D., Kahlen, K., and Stützel, H. (2011). Dry matter partitioning models for the simulation of individual fruit growth in greenhouse cucumber canopies. *Ann. Bot.* 108, 1075–1084. doi: 10.1093/aob/mcr150

Meeting present and future challenges in sustainable horticulture using virtual plants

Gerhard Buck-Sorlin * and *Mickaël Delaire*

Agro Campus OUEST Centre d'Angers, Institut de Recherche en Horticulture et Semences, Institut National d'Horticulture et de Paysage, UMR 1345, Angers, France
*Correspondence: gerhard.buck-sorlin@agrocampus-ouest.fr

THE PURPOSE OF MODELS AND THE MODELING EXERCISE

In order to better understand the significance of models in practical horticulture we have to put ourselves into the position of the horticulturist (orchard grower, consultant …) and appreciate first of all some skepticism toward modeling. This does not necessarily mean a downright refusal to use models: on the contrary, it is often the result of an initial keen interest coupled with high expectations in modeling as such, frequently followed by disillusionment that the high hopes were not satisfied; that *the* model as a response to very specific problems and questions does not exist; that the models offered were remote from practice, unreliable, or too complicated to use. The special case of orchards as perennial production systems, poses a further challenge, for two reasons. Firstly, a rapidly increasing complexity: if considered it renders the model difficult to parameterize, intransparent and expensive; if, on the other hand, it is neglected it is fair to question the model's added value compared to the extensive experience of a grower. Secondly, a perennial production system represents the integral of a unique combination of location and history of production, and the interaction between the genotype with the local environment, making a generalization more difficult than for annual crops. So, what should be done about it? First of all, models are tools, equivalent to other experimental tools, not ultimate purposes: it is up to the researcher to get this message across to the user, to remove any misunderstandings regarding models as "perfect solutions" delivering "absolute answers," and to lower exaggerated hopes. Next, a common language between the researcher and the practitioner must be found, because in practice wires get crossed, not only with respect to the technicalities of the modeling approach but also with respect to the goals of the modeling exercise. Despite that, modelers and people from practice do actually pursue the same goal: trying to integrate the complex information (measured and observed) about a given system, in order to obtain a result (admittedly, opinions as to what is an acceptable result diverge, ranging from a decision-support tool to a publication...).

THE "TRUE" CHALLENGES OF MODELING

In order to advance modeling as a scientific technique and to render its products more accessible to practice—in other words to come down the ivory tower of theoretical biology and applied mathematics in which many biological models and their authors reside—it is important to communicate the true challenges of modeling (which go beyond the predictions coming out of the black box of the model). The three principal challenges are:

- To design models as tools of information exchange between the different types of experts and practitioners of a horticultural sector (e.g., orcharding). Using the formalism developed to construct the model it must be possible to confront the different implicit representations of the stakeholders and to further let these representations evolve using a co-construction approach (similar to developing the Wikipedia), considering at the same time representations added from the "outside" (by scientists) and those belonging to the stakeholders working in practice. In this respect it is crucial that the modelers provide communication tools that permit to state explicitly and simply the conceptual bases of the formalism used to construct the model. This type of models is usually referred to as decision-support tools (DST), but actually DST is a too general and too advanced term for them as DST can also be derived from scientific and pedagogic models (**Figure 1**). We will instead call them prototype tools as they allow us to integrate and structure different knowledge types about a particular system into a simplified representation that serves as a first step toward developing either true DSTs or scientific tools. A prototype tool, like the prototype of a new car, can thus be conceived as an early version of the model, in which the boundaries, elements, behavior and levels of the system are already roughly specified.
- To design models as systems analysis tools which permit to capture emergent phenomena and predetermined breaking points. The computational capacity, available thanks to progress in hardware technology allows testing an infinite diversity of scenarios and combinations of potential actions. This type of models could be termed scientific tools.
- To design educational models which convey textbook knowledge in a visual and dynamic form in order to serve as teaching material in university courses, e-learning, or as instructions for orchard workers (e.g., technique
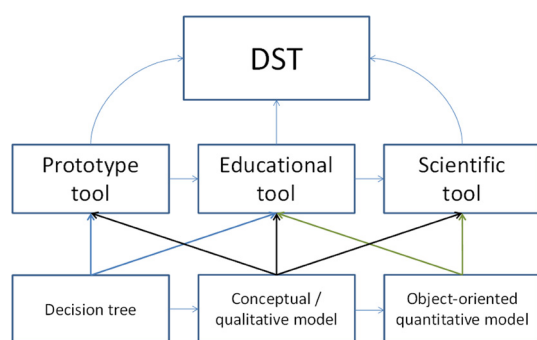
FIGURE 1 | Typology of models used in horticulture. DST, Decision Support Tool. For explanations see text.

and consequences of pruning and shoot bending). We will term this type educational tool.

All of the three types can be developed into DSTs (**Figure 1**), depending on the level of prior knowledge of the user, the design of the model and the modeling paradigm used (e.g., a decision tree, a conceptual model, or an object-oriented model), and the kind of decision-support envisaged (e.g., initial orchard design, prediction of fruit quality, scheduling of pest control measures as part of integrated biological production…).

An additional challenge for biological modeling is the change of scale, i.e., the integration from a lower to a higher scale, and the differentiation from a higher to a lower scale. Integration of knowledge from the gene to the field, or even to the production region or the natural ecological zone is fanciful among plant scientists and this despite the lack of a clear methodology. From the shelter of their disciplines (genetics, physiology, ecophysiology, agronomy, ecology), scientists hypothesize that modeling might be the best choice to try to simplify the complexity encountered at each level and at the transgression from one level to the next. Accordingly, models have been developed to document the knowledge of a certain discipline and at a certain hierarchical scale. However, the concepts and tools to scale up and down, let alone to integrate "horizontally," i.e., to meaningfully link two or more disciplines (beyond the use of a common database…), are still in their infancy.

WHAT TYPE OF MODELING?

Different approaches to crop modeling have been developed in the past (Vos et al., 2010). The most recent approach among them, functional-structural plant modeling or "virtual plants" currently seems the most promising, especially in horticulture which distinguishes itself from agriculture by its enormous genetic and structural diversity (cultures and production methods) and a high technological investment (see greenhouse horticulture). FSPM refers to a paradigm for the description of a plant by creating a computer model of its structure and selected physiological and physical processes, at different hierarchical levels: organ, plant individual, canopy, and in which the processes are modulated by the local environment (Buck-Sorlin, 2013). Within the modeling paradigm of FSPM there exist types and gradations along the following opposite pairs: descriptive versus explanatory, stochastic versus deterministic, or dynamic versus static. From a programming paradigm point of view the most meaningful criterion is the one which distinguishes procedural, object-oriented, and rule-based approaches. Independent of the paradigm chosen in the end, all approaches have in common that they serve to represent a complex reality by decomposing, modularizing and simplifying it into (arguably) atomic units, in order to make it easier to handle, to understand, and to anticipate changes. The method of decomposition necessarily is often biased and depending on the eye and the intention of the observer, thence the importance of fixing the objectives of the model ahead of the actual modeling

exercise. On the other hand, a deliberate effort can be made to approach the description of the system in an "objective" way, i.e., trying to be independent of any intention or subjective bias (knowing fully well, of course, that this is only possible as an approximation since all system descriptions are ultimately subjective). It is in this respect useful to make a distinction between procedural and object-oriented modeling: In procedural modeling (equivalent to classical crop modeling: applied in horticulture and agriculture since more than forty years) the available information is structured according to a chain of more or less concrete processes; ultimate aims of the model are fixed beforehand and the process of knowledge acquisition (and subsequent use in the model) is deductive and top-down. Contrary to this, in object-oriented modeling the available information is structured around objects (their traits and relations to each other) that have been identified a priori as relevant and/or characteristic, and in which knowledge acquisition is inductive and bottom-up.

THE NOTION OF STRUCTURE IN FSPM

Though perfectly clear to everyone involved in research on FSPM, the idea of structure in Functional-Structural Plant Models regularly leads to misunderstandings outside the community. *Structure* in an FSPM, especially with respect to woody plants, corresponds to plant architecture, more precisely at the organ and plant individual level, not more and not less. This notion of architecture comprises the topology and the geometry of plant organs in relative and absolute coordinates and also helps to improve the definition of the interfaces with the microenvironment, which latter is both surrounding and being modified by the architecture of the plant (part) located inside it. The precise description of organ location and orientation by topology and geometry is the basis for quantitatively modeling the transport of carbon, water and minerals between sources and sinks. Many FSPM exist that have implemented the process chain from light interception to photosynthesis, assimilate distribution and growth in terms of organs extension or increase in biomass. On the other hand, FSPMs which also consider the feedback of a change in

architecture (organogenesis by bud break) on, e.g., photosynthesis rate are rare.

A MULTI-SCALE OBJECT-ORIENTED FSPM OF THE APPLE PRODUCTION SYSTEM

Heterogeneity, within the tree and in different years, in apple (*Malus × domestica*) fruit production poses a number of challenges: fruit quality and number (fruit load) can vary as a function of genotype, climate, or an interaction between these factors. Previous experimental work conducted by the ecophysiology team at Angers has shown that the carrying branch or limb is an apt experimental system for the investigation of these phenomena if certain key variables at the next lower (organ) and next higher (plant) scale are considered at the same time.

We have recently started to create a prototype model of the apple limb, in order to improve our knowledge about the role of plant architecture for the formation of fruit quality. This model is object-oriented and covers three hierarchical, consecutive scales: organ, branch, and plant; a number of physiological processes is defined for each organ (e.g., photosynthesis, growth, respiration…); transport of sugar, water and minerals will be defined at the organ level using rules that apply rate equations to pairs of topologically joined organs (leaf–internode, internode–internode, internode–petiole,

petiole–fruit), whilst the equations will be integrated in parallel with an embedded ODE solver (Hemmerling, 2012). At the level of the organ type "fruit" a modification of the "Virtual Fruit" model (Génard et al., 2007) will be employed. Since we are interested in the production (quantity and quality) of a given year, without having to reconstruct the history of the tree at each simulation run, we devised an initiation rule which at the start of each run puts in place the initial (measured) plant architecture as encountered in spring before bud break, of that year.

OUTLOOK

The modeling exercise described here is exemplary for many modeling projects in horticulture, independently of whether these are departing from existing modules or from scratch. In the first place a conceptual model is elaborated and then qualitatively validated. Existing modules that have been parameterized for a certain fruit (e.g., peach) eventually need to be reparameterized, as in the Virtual Fruit model, where also a partial rewriting of the equations is necessary to make it applicable for apple. After proper calibration of modules (this can be done by doing sensitivity analyses under standard conditions), the latter can be tentatively combined, recalibrated and eventually validated using an external data set, with the ultimate aim to obtaining a model which can predict fruit quality

as a function of the genotype and a specific production environment.

REFERENCES

Buck-Sorlin, G. H. (2013). "Functional-structural plant modeling," in *Encyclopedia of Systems Biology*, eds W. Dubitzky, O. Wolkenhauer, K. Cho, and H. Yokota (New York, NY: Springer), 778–781. doi: 10.1007/978-1-4419-9863-7

Génard, M., Bertin, N., Borel, C., Bussières, P., Gautier, H., Habib, R., et al. (2007). Towards a virtual fruit focusing on quality: modelling features and potential uses. *J. Exp. Bot.* 58, 917–928. doi: 10.1093/jxb/erl287

Hemmerling, R. (2012). *Extending the Programming Language XL to Combine Graph Structures with Ordinary Differential Equations*. Ph.D. thesis, Georg-August-University Göttingen, 189.

Vos, J., Evers, J. B., Buck-Sorlin, G. H., Andrieu, B., Chelle, M., and de Visser, P. H. B., (2010). Functional-structural plant modelling: a new versatile tool in crop science. *J. Exp. Bot.* 61, 2102–2115. doi: 10.1093/jxb/erp345

Advantages
of publishing
in Frontiers

OPEN ACCESS

Articles are free to read,
for greatest visibility

COLLABORATIVE PEER-REVIEW

Designed to be rigorous
– yet also collaborative,
fair and constructive

85

FAST PUBLICATION

Average 85 days from
submission to publication
(across all journals)

COPYRIGHT TO AUTHORS

No limit to article
distribution and re-use

TRANSPARENT

Editors and reviewers
acknowledged by name
on published articles

SUPPORT

By our Swiss-based
editorial team

IMPACT METRICS

Advanced metrics
track your article's impact

GLOBAL SPREAD

5'100'000+ monthly
article views
and downloads

LOOP RESEARCH NETWORK

Our network
increases readership
for your article